UNIVERSITY OF SOUTHAMPTON

System Identification of the Hydrodynamic Characteristics of Underwater Vehicles

By

Maaten Furlong

Thesis for the degree of Doctor of Engineering

FACULTY OF ENGINEERING, SCIENCE AND MATHEMATICS
SCHOOL OF ENGINEERING SCIENCES,
FLUID-STRUCTURE INTERACTION RESEARCH GROUP

March 2005

UNIVERSITY OF SOUTHAMPTON

ABSTRACT

FACULTY OF ENGINEERING, SCIENCE AND MATHEMATICS
SCHOOL OF ENGINEERING SCIENCES,
FLUID-STRUCTURE INTERACTION RESEARCH GROUP

Doctor of Engineering

System Identification of the Hydrodynamic Characteristics of Underwater Vehicles

Maaten Furlong

Accurate physics based simulations of Autonomous Underwater Vehicles (AUVs) and submarines require precise knowledge of the physical loads on the vehicle. Of these loads the hydrodynamic component is the most challenging to determine. One common method of representing these loads is to use hydrodynamic coefficients. These coefficients are commonly determined from captive model testing, which is expensive. However, in theory these coefficients can be found from free swimming trials. This thesis documents research undertaken, in collaboration with QinetiQ, to determine whether the hydrodynamic coefficients in a set of non-linear submarine equations can be determined from free swimming trials data.

Two coefficient identification procedures are described. The first, a non-linear approach attempts to find a set of coefficients reproduced the manoeuvring submarine's path. The second, a linear approach recasts the identification task into a linear algebra problem which can be solved using standard techniques.

When tested using simulated data both approaches indicated that accurate submarine track identification is not equivalent to correct submarine hydrodynamic coefficient identification. This arises from two causes. First, it was discovered that the coefficients were not unique, and thus there are an infinite number of different coefficient sets which produce the same manoeuvre. Secondly, it was found that the manoeuvre always identified an ill-conditioned set of coefficients; that is small deviations in the manoeuvre produced large deviations in the identified coefficient values.

Due to these issues, the results of the research suggest that it is not possible to determine the non-linear hydrodynamic coefficients of a submarine or AUV from free swimming manoeuvre data.

Contents

Abstract ii

Table of Contents iii

List of Tables x

List of Figures xiii

Acknowledgements xx

Nomenclature xxi

Glossary xxv

Author's Declaration xxvi

1 Introduction 1

1.1 Background 1

1.2 Scope of the EngD Research 2

1.3 Scope of the Hydrodynamic Coefficient Identification Research 4

1.4 Layout of the Thesis 5

2 Mathematical Modelling of Underwater Vehicle Dynamics 7

2.1 Rotation Between the Body and Fixed Coordinate Frames 7

2.1.1 The Euler Angle Representation of Rotation 8

2.1.2 Problems with the Euler Angle Representation 12

2.1.3 Calculating the Euler Angle Update Matrix 14

2.1.4 Using the Euler Angle System for UV Modelling 17
2.2 Rigid Body Dynamics 18
2.3 Conclusions 19

3 Modelling the Forces and Moments on Underwater Vehicles 20
3.1 Introduction 20
3.2 Sources of the Loads on an Underwater Vehicle 21
3.3 Calculating the Hydrostatic Forces and Moments — $\boldsymbol{g}(\boldsymbol{\eta})$ 23
3.3.1 Determining the Hydrostatic Forces in the Body Fixed Coordinate Frame 24
3.3.2 Determining the Hydrostatic Moments in the Body Fixed Coordinate Frame 24
3.4 Methods of Estimating the Hydrodynamic Forces and Moments . . . 26
3.5 Modelling the Forces and Moments Using Computational Fluid Dynamics 26
3.5.1 Calculating the Added Mass 27
3.6 Hydrodynamic Coefficients Method 33
3.6.1 The Basic Approach 34
3.6.2 Modern Submarine Equations 36
3.6.3 Modelling AUVs Using Submarine Equations 37
3.6.4 Free Running Model Tests 41
3.7 Modelling Propeller Thrust and Torque 44
3.7.1 Modelling K_T and K_Q 47
3.7.2 Determining the Propulsion Data 48
3.8 Conclusions 50

4 System Identification of Hydrodynamic Coefficients 51
4.1 Introduction 51
4.2 The QinetiQ Task 52
4.3 The QinetiQ Submarine Equations 54
4.4 Addressing the QinetiQ Task 54
4.4.1 The Linear Procedure to Identify $\boldsymbol{\xi}$ 55
4.4.2 The Non-linear Procedure to Identify $\boldsymbol{\xi}$ 57
4.4.3 Analysis of the Two Approaches 61

4.5 The System Identification Manoeuvres 62
4.5.1 Problems with Real Underwater Vehicle Manoeuvres 62
4.5.2 Defining a UV Manoeuvre 64
4.5.3 Determining Sufficiently 'Rich' Identification Manoeuvres . . . 64
4.6 The Chosen Standard UV Test Manoeuvres 65
4.6.1 Description of Horizontal Motion Manoeuvre 66
4.6.2 Description of Vertical Motion Manoeuvre 68
4.6.3 Description of Coupled Motion Manoeuvre 70
4.7 Conclusions 72

5 Creating the Generic Submarine Simulation **73**
5.1 Introduction 73
5.2 Simulation Requirements 74
5.3 The Submarine Equations of Motion 75
5.3.1 Expressing the Motion Equations in Terms of Fossen's Notation 76
5.4 Converting the Motion Equations into a Form Appropriate for Simulation 81
5.4.1 Calculating $\dot{\boldsymbol{\nu}}$ 82
5.4.2 Calculating $\dot{\boldsymbol{s}}_{\mathbf{v}}$ 83
5.5 Selection of Integration Routines 83
5.5.1 Accuracy, Efficiency and Stability of Integration Routines . . . 83
5.5.2 Errors in Numerical Integration Routines 84
5.5.3 The Chosen Approach: The 4^{th}-order Runge-Kutta Method 86
5.6 Creating the UV Simulation Code 87
5.6.1 Three Versions of the Generic Submarine Simulation 88
5.7 Testing and Validating the Simulation Code 89
5.8 Comparing the Matlab and QinetiQ's SubHov Simulations 90
5.8.1 Specification of Manoeuvre Used in Comparative Studies . . . 91
5.8.2 Comparison of the Predictions 92
5.9 The Accuracy of the Matlab Simulation 97
5.10 Conclusions 100

6 Assessment of the Uniqueness of the Hydrodynamic Coefficients 101

6.1 Introduction 101

6.2 The Horizontal Manoeuvre Rank Analysis 103

6.2.1 The Causes of the Reduced Rank of the $\boldsymbol{A}_Y$ Matrix 104

6.2.2 The Causes of the Reduced Rank of the $\boldsymbol{A}_N$ Matrix 106

6.3 The Vertical Manoeuvre Rank Analysis 109

6.3.1 The Causes of the Reduced Rank of the $\boldsymbol{A}_Z$ Matrix 110

6.3.2 The Causes of the Reduced Rank of the $\boldsymbol{A}_M$ Matrix 111

6.4 The Coupled Manoeuvre Rank Analysis 112

6.4.1 The Causes of the Reduced Rank of the $\boldsymbol{A}_Y$ Matrix 113

6.4.2 The Causes of the Reduced Rank of the $\boldsymbol{A}_Z$ Matrix 114

6.4.3 The Causes of the Reduced Rank of the $\boldsymbol{A}_M$ Matrix 115

6.4.4 The Causes of the Reduced Rank of the $\boldsymbol{A}_N$ Matrix 117

6.5 Conclusions 120

7 Building and Testing the Non-linear Parameter Identification Procedure 121

7.1 Introduction 121

7.2 Implementing the Non-Linear Parameter Identification Procedure in Matlab 122

7.2.1 The Cost Function Routine 123

7.2.2 Overview of the Optimization Routine 125

7.3 Assumptions Made During the Non-Linear Identification Procedure Testing 129

7.4 The Tests Performed 132

7.5 Horizontal Manoeuvre Results 132

7.5.1 Horizontal Manoeuvre Track Convergence 133

7.5.2 Horizontal Manoeuvre Coefficient Convergence 137

7.5.3 Optimization Routine Performance — Horizontal Manoeuvre 139

7.5.4 Horizontal Manoeuvre Testing Conclusions 143

7.6 Vertical Manoeuvre Results 144

7.6.1 Vertical Manoeuvre Track Convergence 144

7.6.2 Vertical Manoeuvre Coefficient Convergence 147
7.6.3 Optimization Routine Performance — Vertical Manoeuvre 150
7.6.4 Vertical Manoeuvre Testing Conclusions 153
7.7 Coupled Test Results 153
7.7.1 Coupled Manoeuvre Track Convergence 154
7.7.2 Coupled Manoeuvre Coefficient Convergence 157
7.7.3 Optimization Routine Performance — Coupled Manoeuvre . . 161
7.7.4 Coupled Manoeuvre Testing Conclusions 164
7.8 Analysis of the Ill-Conditioning Phenomenon 165
7.8.1 Coefficient Cost Function Contribution 166
7.8.2 Coefficient Error Cancellation 172
7.8.3 Ill-conditioning Conclusions 175
7.9 Conclusions 175

8 Converged Coefficient Manoeuvre Prediction 177
8.1 Introduction 177
8.2 Designing the UVi Test Manoeuvres 179
8.3 Coefficient Manoeuvre Prediction Test Procedure 182
8.4 Coefficient Manoeuvre Prediction Results 184
8.4.1 The Effect of the Manoeuvre on the Prediction Performance . 188
8.5 Analysing the Range in Prediction Accuracy Produced by the Identified Coefficients 191
8.5.1 The Converged Coefficient Results 197
8.6 Conclusions 202

9 The Linear Parameter Identification Procedure 204
9.1 Introduction 204
9.1.1 The INS System 205
9.1.2 The ADCP 205
9.1.3 Available Autosub State Information 206
9.1.4 Applications of INS and ADCP Data 207
9.2 Linear Form of the Booth et al. Equations 207

9.3 Solving the Linear System Using Linear Programming Techniques . . 208
9.3.1 Testing the Linear Programming Approach 210
9.3.2 Results of the Linear Programming Investigation 211
9.4 The Linear Algebra Approach 217
9.4.1 Applications of the Linear Algebraic Approach 219
9.5 Comparison of the Two Linear Approaches 224
9.6 Ill-conditioning of the Linear Approach 224
9.7 Conclusions 228

10 Conclusions **230**
10.1 Further Works 234

APPENDICES **241**

A Calculating the Euler Angle Update Matrix **242**

B Quaternion Representation of Rotation **245**
B.1 Quaternion Fundamentals 245
B.2 Rotation Using Quaternions 249
B.3 Using Quaternions for UV Modelling 253

C Alternative Propulsion Models **255**
C.1 The NPS AUV II propulsion model 255
C.2 The Fossen Two Parameter Propulsion Model 257
C.3 The Booth et al. Propulsion Model 258

D The Booth et al. Submarine Equations **259**
D.1 The Booth et al. Submarine Equations 260
D.1.1 The Propulsion Model 263
D.2 The Modified Booth et al. Equations — Horizontal Sub-problem . . . 266
D.2.1 Assumptions Used in the Horizontal Motion Model 266
D.2.2 Equations of Motion — Horizontal Case 267
D.3 The Modified Booth et al. Equations — Vertical Sub-problem 268
D.3.1 Assumptions Used in the Vertical Motion Model 268
D.3.2 Equations of Motion — Vertical Case 268

E Inputs to the Matlab Submarine Simulation **270**

E.1 The UV Mechanical Coefficient Vector — $\boldsymbol{m}$ 270

E.2 The UV Propulsion Coefficient Vector — $\boldsymbol{n}$ 270

E.3 The UV Hydrodynamic Coefficient Vector – $\boldsymbol{\xi}$ 271

E.4 Comparison Between SubHov and the Matlab Simulations 272

F Coefficient Prediction Results **279**

F.1 The Manoeuvre Prediction Surfaces 280

F.2 The Predicted Manoeuvre Cost Functions 283

F.3 The Worst Predicted Manoeuvres 286

G Presented Paper **287**

List of Tables

1 Comparison of simulation time for the standard horizontal manoeuvre. 89

2 Maximum differences between SubHov and the Matlab simulation for three submarines performing the comparison manoeuvre. 95

3 Maximum differences between SubHov simulating the comparison manoeuvre with a 0.01s time step and SubHov simulating the same manoeuvre with 1.0s and 0.1s time steps. 96

4 Variation of cost function for each submarine undertaking the three standard manoeuvres using different times steps. 98

5 Maximum positional difference for each submarine undertaking the three standard manoeuvres using different times steps. 99

6 Horizontal manoeuvre rank analysis. 104

7 Vertical manoeuvre rank analysis. 110

8 Fully coupled case rank analysis. 113

9 The dimensions of the null spaces, $\mathcal{N}(\boldsymbol{A})$'s, for the coupled manoeuvre, and the causes of the rank reductions. 113

10 Summary of the horizontal manoeuvre convergence results — submarine 1. 134

11 Summary of the horizontal manoeuvre convergence results — submarine 2. 135

12 Summary of the horizontal manoeuvre convergence results — submarine 3. 136

13 Summary of the optimization routine efficiency — horizontal manoeuvre, submarine 1. 140

14 Summary of the optimization routine efficiency — horizontal manoeuvre, submarine 2. 141
15 Summary of the optimization routine efficiency — horizontal manoeuvre, submarine 3. 142
16 Summary of the vertical manoeuvre convergence results — submarine 1.145
17 Summary of the vertical manoeuvre convergence results — submarine 2.145
18 Summary of the vertical manoeuvre convergence results — submarine 3.146
19 Summary of the optimization routine efficiency — vertical manoeuvre, submarine 1. 151
20 Summary of the optimization routine efficiency — vertical manoeuvre, submarine 2. 151
21 Summary of the optimization routine efficiency — vertical manoeuvre, submarine 3. 152
22 Summary of the coupled manoeuvre convergence results — submarine 1.154
23 Summary of the coupled manoeuvre convergence results — submarine 2.155
24 Summary of the coupled manoeuvre convergence results — submarine 3.156
25 Summary of the optimization routine performance — coupled manoeuvre, submarine 1. 162
26 Summary of the optimization routine performance — coupled manoeuvre, submarine 2. 163
27 Summary of the optimization routine efficiency — coupled manoeuvre, submarine 3. 164
28 Maximum absolute error associated with the differences produced by the X'_{vv}, X'_{vr} & X'_{rr} hydrodynamic coefficients. 174
29 The manoeuvre prediction summary results for the identified coefficients of submarines 1–3. 184
30 Spread of the cost function value for the converged coefficient sets — submarine 1, with the corresponding maximum positional error in metres presented within parentheses. 194
31 Spread of the cost function value for the converged coefficient sets — submarine 2, with the corresponding maximum positional error in metres presented within parentheses. 195

32 Spread of the cost function value for the converged coefficient sets — submarine 3, with the corresponding maximum positional error in metres presented within parentheses. 196

33 Manoeuvre data available for Autosub and its source. 206
34 Time in seconds to solve for the different coefficient sets using linear programming techniques — horizontal manoeuvre. 213
35 Time in seconds to solve for the different coefficient sets using linear programming techniques — vertical manoeuvre. 214
36 Time in seconds to solve for the different coefficient sets using linear programming techniques — coupled manoeuvre. 217
37 Time in seconds to solve for the different coefficient sets using linear algebra techniques — horizontal manoeuvre 220
38 Time in seconds to solve for the different coefficient sets using linear algebra techniques — vertical manoeuvre 222
39 Time in seconds to solve for the different coefficient sets using linear algebra techniques — coupled manoeuvre 223

List of Figures

1 An example of the xyz Euler angle rotation sequence. 9
2 A mechanical example of the xyz Euler rotation sequence. 13
3 A mechanical example of the xyz Euler rotation sequence with the UV rotated to show gimbal lock. 14
4 Comparison of the added mass of an ellipsoid and Munk's method normalized with the volume of a sphere of radius r. 31
5 Comparison of the normalized added-inertias of a cruciform plate, a flat plate and a finned cylinder. 33
6 Lawnmower survey performed by Autosub 24/08/04 of the North-West coast of Greenland. 38
7 First turn of the lawnmower survey. 39
8 Non-dimensional Autosub and submarine 1 turning manoeuvre comparison. 40
9 Schematic of a propeller operating in open water. 45
10 Outline of the QinetiQ question 53
11 Schematic of the linear parameter identification procedure. 56
12 Schematic of the non-linear parameter identification scheme. 58
13 Example of local and global maxima and minima 60
14 The horizontal manoeuvre rudder angle time history. 67
15 The $x - y$ positional time history of the three submarines performing the horizontal manoeuvre. 68
16 The vertical manoeuvre stern dive-plane angle time history. 69
17 The $x - z$ positional time history of the three submarines performing the vertical manoeuvre. 70

18 The coupled manoeuvre control-plane time histories. 71
19 The positional time history of the three submarines performing the coupled manoeuvre. 72

20 Block diagram of a manoeuvre implemented in SubHov 75
21 Inputs to the generic simulation code 87
22 The control plane angle time history for submarine 1 performing the SubHov comparison manoeuvre. 92
23 Comparison of the SubHov and Matlab simulation positional time history. 93
24 Plot of x and x error. 93
25 Plot of u and u error. 94

26 Horizontal Manoeuvre showing the relationship between v & r 108
27 Results of the sign(v)/sign(r)) analysis for the three test submarines . 119

28 Overview of the cost function and optimization routine. 124
29 Example of the cost function reduction during a parameter identification test. 128
30 Track convergence results for the horizontal manoeuvre — submarine 1. 134
31 Track convergence results for the horizontal manoeuvre — submarine 2. 135
32 Track convergence results for the horizontal manoeuvre — submarine 3. 136
33 Coefficient convergence for the horizontal manoeuvre — submarine 1. 138
34 Coefficient convergence for the horizontal manoeuvre — submarine 2. 138
35 Coefficient convergence for the horizontal manoeuvre — submarine 3. 139
36 Optimization routine efficiency results for the horizontal manoeuvre — submarine 1. 140
37 Optimization routine efficiency results for the horizontal manoeuvre — submarine 2. 141
38 Optimization routine efficiency results for the horizontal manoeuvre — submarine 3. 142
39 Track convergence results for the vertical manoeuvre — submarine 1. 144
40 Track convergence results for the vertical manoeuvre — submarine 2. 145
41 Track convergence results for the vertical manoeuvre — submarine 3. 146
42 Coefficient convergence for the vertical manoeuvre — submarine 1. . 148

43 Coefficient convergence for the vertical manoeuvre — submarine 2. . 148
44 Coefficient convergence for the vertical manoeuvre — submarine 3. . 149
45 System performance results for the vertical manoeuvre — submarine 1. 150
46 System performance results for the vertical manoeuvre — submarine 2. 151
47 System performance results for the vertical manoeuvre — submarine 3. 152
48 Track convergence results for the coupled manoeuvre — submarine 1. 154
49 Track convergence results for the coupled manoeuvre — submarine 2. 155
50 Track convergence results for the coupled manoeuvre — submarine 3. 156
51 Converged force coefficient for the coupled manoeuvre — submarine 1. 158
52 Converged moment coefficient for the coupled manoeuvre — submarine 1.158
53 Converged force coefficient for the coupled manoeuvre — submarine 2. 159
54 Converged moment coefficient for the coupled manoeuvre — submarine 2.159
55 Converged force coefficient for the coupled manoeuvre — submarine 3. 160
56 Converged moment coefficient for the coupled manoeuvre — submarine 3.160
57 System performance results for the coupled manoeuvre — submarine 1. 162
58 System performance results for the coupled manoeuvre — submarine 2. 163
59 System performance results for the coupled manoeuvre — submarine 3. 164
60 Cost functions for assigned coefficients corresponding to 25% of true value — horizontal manoeuvre. 168
61 Cost functions for assigned coefficients corresponding to 99% of true value — horizontal manoeuvre. 168
62 Cost functions for assigned coefficients corresponding to 25% of true value — vertical manoeuvre. 169
63 Cost functions for assigned coefficients corresponding to 99% of true value — vertical manoeuvre. 169
64 Cost functions for assigned force coefficients corresponding to 25% of true value — coupled manoeuvre. 170
65 Cost functions for assigned force coefficients corresponding to 99% of true value — coupled manoeuvre. 170
66 Cost functions for assigned moment coefficients corresponding to 25% of true value — coupled manoeuvre. 171
67 Cost functions for assigned moment coefficients corresponding to 99% of true value — coupled manoeuvre. 171

68 The relationship between v^2 and r^2 for the horizontal test manoeuvre performed by submarine 1. 173
69 The relationship between v^2 and r^2 for the horizontal test manoeuvre performed by submarine 1. 174

70 Description of the control plane dynamics. 180
71 Example of the first 200 seconds of a random test manoeuvre. 182
72 The prediction test manoeuvre produce by submarine 1. 183
73 Surface showing the maximum positional error for submarine 1 as a function of $\hat{\boldsymbol{\xi}}^*$ and prediction manoeuvre — coefficient view. 185
74 Surface showing the maximum positional error for submarine 1 as a function of $\hat{\boldsymbol{\xi}}^*$ and prediction manoeuvre — manoeuvre view. 186
75 Surface showing the cost functions for submarine 1 as a function of $\hat{\boldsymbol{\xi}}^*$ and prediction manoeuvre — coefficient view. 187
76 The predicted manoeuvre cost functions (ε's) sorted by average ε — submarine 1. 188
77 The predicted manoeuvre cost functions (ε's) sorted by average ε, with the five largest varying coefficient sets highlighted — submarine 1. . . 190
78 The predicted manoeuvre cost functions (ε's) sorted by average ε, with the five smallest varying coefficient sets highlighted — submarine 1. . 190
79 Cost function distribution produced using three selected converged hydrodynamic coefficient sets and the upper and lower calibration levels — submarine 1. 194
80 Cost function distribution produced using three selected converged hydrodynamic coefficient sets and the upper and lower calibration levels — submarine 2. 195
81 Cost function distribution produced using three selected converged hydrodynamic coefficient sets and the upper and lower calibration levels — submarine 3. 196
82 Positional time history of the worst coefficient set performing the worst manoeuvre — submarine 1. 198
83 The best, worst and middle performing converged force coefficients — submarine 1. 199

84 The best, worst and middle performing converged moment coefficients — submarine 1. 199
85 The best, worst and middle performing converged force coefficients — submarine 2. 200
86 The best, worst and middle performing converged moment coefficients — submarine 2. 200
87 The best, worst and middle performing converged force coefficients — submarine 3. 201
88 The best, worst and middle performing converged moment coefficients — submarine 3. 201
89 Coefficient convergence results produced using the linear programming procedure — horizontal manoeuvre. 212
90 Coefficient convergence results produced using the linear programming procedure — vertical manoeuvre. 214
91 Force coefficient convergence results produced using the linear programming procedure — coupled manoeuvre. 215
92 Moment coefficient convergence results produced using the linear programming procedure — coupled manoeuvre. 216
93 Coefficient convergence results produced using the linear algebra procedure — horizontal manoeuvre. 220
94 Coefficient convergence results produced using the linear algebra procedure — vertical manoeuvre. 221
95 Force coefficient convergence results produced using the linear algebra procedure — coupled manoeuvre. 222
96 Moment coefficient convergence results produced using the linear algebra procedure — coupled manoeuvre. 223
97 Linear algebra estimated force coefficient values for submarine 1 calculated from the 100 prediction manoeuvres. 226
98 Linear algebra estimated moment coefficient values for submarine 1 calculated from the 100 prediction manoeuvres. 227
99 The accuracy with which each identified coefficient set reproduce its identification manoeuvre. 228

100 Vector and reference frame rotation about the x-axis by angle ϕ. . . . 250

101 Plot of the errors associated with the x value. 272
102 Plot of the errors associated with the y value. 273
103 Plot of the errors associated with the z value. 273
104 Plot of the errors associated with the ϕ value (roll). 274
105 Plot of the errors associated with the θ value (pitch). 274
106 Plot of the errors associated with the ψ value (yaw). 275
107 Plot of the errors associated with the u value. 275
108 Plot of the errors associated with the v value. 276
109 Plot of the errors associated with the w value. 276
110 Plot of the errors associated with the p value. 277
111 Plot of the errors associated with the q value. 277
112 Plot of the errors associated with the r value. 278

113 Surface showing the maximum positional error for submarine 2's as a function of $\hat{\boldsymbol{\xi}}^*$ and prediction manoeuvre — coefficient view. 280
114 Surface showing the maximum positional error for submarine 2' as a function of $\hat{\boldsymbol{\xi}}^*$'s and prediction manoeuvre — manoeuvre view. 280
115 Surface showing the cost functions for submarine 2's as a function of $\hat{\boldsymbol{\xi}}^*$'s and prediction manoeuvre — coefficient view 281
116 Surface showing the maximum positional error for submarine 3's as a function of $\hat{\boldsymbol{\xi}}^*$ and prediction manoeuvre — coefficient view. 281
117 Surface showing the maximum positional error for submarine 3' as a function of $\hat{\boldsymbol{\xi}}^*$'s and prediction manoeuvre — manoeuvre view. 282
118 Surface showing the cost functions for submarine 3's as a function of $\hat{\boldsymbol{\xi}}^*$'s and prediction manoeuvre — coefficient view 282
119 The predicted manoeuvre ε's sorted by average ε — submarine 2. . . 283
120 The predicted manoeuvre ε's sorted by average ε, with the five highest varying coefficient sets highlighted — submarine 2. 283
121 The predicted manoeuvre ε's sorted by average ε, with the five lowest varying coefficient sets highlighted — submarine 2. 284
122 The predicted manoeuvre ε's sorted by average ε — submarine 3. . . 284

123 The predicted manoeuvre ε's sorted by average ε, with the five highest varying coefficient sets highlighted — submarine 3. 285
124 The predicted manoeuvre ε's sorted by average ε, with the five lowest varying coefficient sets highlighted — submarine 3. 285
125 Positional time history of the worst coefficient set performing the worst manoeuvre — submarine 2. 286
126 Positional time history of the worst coefficient set performing the worst manoeuvre — submarine 3. 286

Acknowledgements

I would like to thank my academic supervisor Professor Grant Hearn for his support and encouragement during the EngD. Working with Grant has taught me much. I would also like to thank my industrial supervisor Dr Miles Pebody and the Autosub team in general for their help and putting up with me asking 'what does this bit do?' for the n^{th} time.

I would also like to thank Professor Sandor Veres, Professor Eric Rogers and Peter Butterworth of QinetiQ for their words of advice while working on the submarine coefficient identification problem.

I also owe a debt of gratitude to Anne Donohue of the EngD centre without whose encouragement I would not have come to Southampton.

Finally, it wouldn't have been nearly as much fun doing the EngD without my friends in Southampton who have made the time spent here an enjoyable, if slightly drunken, experience. Cheers!

Nomenclature

$\boldsymbol{A_X}$, $\boldsymbol{A_Y}$, $\boldsymbol{A_Z}$	Matrices associated with determination of hydrodynamic coefficients associated with X, Y and Z forces reported in the linear formulation of identification problem linear coefficients	
$\boldsymbol{A_K}$, $\boldsymbol{A_M}$, $\boldsymbol{A_N}$	Matrices associated with determination of hydrodynamic coefficients associated with K, M and N moments reported in the linear formulation of identification problem linear coefficients	
$\boldsymbol{A_X^*}$, $\boldsymbol{A_Y^*}$, $\boldsymbol{A_Z^*}$	Matrices associated with determination of hydrodynamic coefficients associated with X, Y and Z forces reported in the linear programming of identification problem linear coefficients	
$\boldsymbol{A_K^*}$, $\boldsymbol{A_M^*}$, $\boldsymbol{A_N^*}$	Matrices associated with determination of hydrodynamic coefficients associated with K, M and N moments reported in the linear programming of identification problem linear coefficients	
$\boldsymbol{A}$	General matrix for linear model $\boldsymbol{Ax} = \boldsymbol{b}$	
$\boldsymbol{b}$	General vector for linear model $\boldsymbol{Ax} = \boldsymbol{b}$	
$\boldsymbol{b_X}$, $\boldsymbol{b_Y}$, $\boldsymbol{b_Z}$	Column vector used with $\boldsymbol{A_X}$, $\boldsymbol{A_Y}$ and $\boldsymbol{A_Z}$ respectively	
$\boldsymbol{b_K}$, $\boldsymbol{b_M}$, $\boldsymbol{b_N}$	Column vector used with $\boldsymbol{A_K}$, $\boldsymbol{A_M}$ and $\boldsymbol{A_N}$ respectively	
B	Buoyancy of UV	[N]
ΔB	Net buoyancy of UV represented by $(B - mg)$	[N]
$\boldsymbol{c}$	Control input vector $[\delta R, \delta B, \delta S, n]$ at an instant in time	
$\boldsymbol{c}$	Constraints on linear and non-linear optimization problems	
$\boldsymbol{d}(\boldsymbol{\nu})$	Hydrodynamic damping forces and moments vector	
$\boldsymbol{d_{rb}}(\boldsymbol{\nu})$	Coriolis and centripetal terms for rigid body motions	
D	Propeller diameter	[m]
f	general function	
$\boldsymbol{f}$	Linear programming function	

f_X	Hydrodynamic X force function	[N]
$\boldsymbol{f}_B$	Buoyancy force in body axis	[N]
$\boldsymbol{f}_G$	Gravitational force in body axis	[N]
g	Acceleration due to gravity	[m·s^{-2}]
$\boldsymbol{g}(\boldsymbol{\eta})$	Hydrostatic loads vector	
I_{XX}, I_{YY}, I_{ZZ}	Moments of inertia with respect to the body fixed axis	
I_{XY}, I_{YZ}, I_{ZX}	Products of inertia with respect to the body fixed axis	
J	Advance coefficient for propeller	
$\boldsymbol{J}_1(\boldsymbol{\eta}_2)$	Body to inertial axis rotation matrix	
$\boldsymbol{J}_2(\boldsymbol{\eta}_2)$	Euler angle update matrix	
$\boldsymbol{J}(\boldsymbol{\eta}_2)$	General update matrix	
$K_Q(J)$	Non-dimensional propeller torque coefficient	
$K_T(J)$	Non-dimensional propeller thrust coefficient	
K, M, N	Roll, pitch and yaw moments on UV	[Nm]
K_n, M_n, N_n	Propeller induced poll, pitch and yaw moments	[Nm]
l	Length of UV	[m]
m	Mass of UV	[kg]
$\boldsymbol{m}$	Vector of mechanical UV coefficients	
$\boldsymbol{M}$	General rotation matrix	
$\boldsymbol{M}_A$	Added mass matrix	
$\boldsymbol{M}_{rb}$	Rigid body mass matrix	
n	Rotation rate of propeller	[rps]
$\boldsymbol{N}$	Matrix of vehicle position and attitude at every time step in a manoeuvre generated using the correct hydrodynamic coefficients	
$\hat{\boldsymbol{N}}$	Matrix of estimated vehicle position and attitude throughout a manoeuvre generated using the estimated hydrodynamic coefficients	
$\mathcal{N}(\boldsymbol{A})$	The null space of matrix $\boldsymbol{A}$	
$\mathbf{q}$, $\mathbf{p}$	General quaternions	
$\mathbf{q}^*$	Quaternion conjugate	
$\mathbf{q}^{-1}$	Quaternion inverse	
Q	Torque on the propeller	[Nm]

$\boldsymbol{r}_G$	Vector to the centre of gravity $[x_G, y_G, z_G]$	[m]
$\boldsymbol{r}_B$	Vector to the centre of buoyancy $[x_B, y_B, z_B]$	[m]
$\boldsymbol{R}_x^\phi$, $\boldsymbol{R}_y^\theta$, $\boldsymbol{R}_z^\psi$	Euler angle component rotation matrices	
$\boldsymbol{s}_\mathbf{v}$	State vector of the submarine $=[\boldsymbol{\eta}^T, \boldsymbol{\nu}^T]^T$	
$\boldsymbol{s}_\mathbf{v}^{(0)}$	Initial UV state vector at the start of a manoeuvre	
t	time	[s]
Δt	Simulation time step size	[s]
T	Thrust produced by the propeller	[N]
$\boldsymbol{T}_\mathbf{c}$	Matrix of the control inputs ($\boldsymbol{c}$) during a manoeuvre	
u, v, w	Linear velocities in the body fixed axes	[m·s^{-1}]
V_A	Speed of advance of a propeller	[m·s^{-1}]
x, y, z	Position of the the UV in inertial coordinate system	[m]
x_b, y_b, z_b	The body fixed axis system	
x_B, y_B, z_B	The position of the centre of buoyancy	[m]
x_G, y_G, z_G	The position of the centre of gravity	[m]
x_i, y_i, z_i	The inertial axis system	
X, Y, Z	Forces acting on the UV in the body axis system	[N]
X_n, Y_n, Z_n	Propeller induces forces in the body axis	[N]
α_1, α_2, α_3	Coefficients used in the $K_T(J)$ models	
β_1, β_2	Coefficients used in the $K_Q(J)$ model	
δR, δB, δS	Rudder, bow and stern dive-plane angles	[rad]
ϵ	The eccentricity of an ellipsoid of revolution	
ε	A scalar value measuring the error between $\hat{\boldsymbol{N}}$ and $\boldsymbol{N}$	
$\varepsilon^{(n)}$	The scalar error produced by the $\hat{\boldsymbol{\xi}}^{(n)}$ coefficient set	
ε_{lp}	The scalar error to minimize within the linear programming system	
$\boldsymbol{\varepsilon}_N$	Measurement 'noise' on the manoeuvre data	
$\boldsymbol{\eta}$	$[\boldsymbol{\eta}_1^T, \boldsymbol{\eta}_2^T]^T$	
$\boldsymbol{\eta}_1$	$[x, y, z]^T$	[m]
$\boldsymbol{\eta}_2$	$[\phi, \theta, \psi]^T$	[rad]
$\tilde{\boldsymbol{\eta}}$	Noise ($\boldsymbol{\varepsilon}_N$) corrupted $\boldsymbol{\eta}$	
ν	Cross-flow velocity $\nu = \sqrt{v^2 + w^2}$	[m·s^{-1}]

$\boldsymbol{\nu}_1$	$[u, v, w]^T$	[m·s^{-1}]
$\boldsymbol{\nu}_2$	$[p, q, r]^T$	[rad·s^{-1}]
$\boldsymbol{\xi}$	The hydrodynamic coefficient vector	
$\hat{\boldsymbol{\xi}}$	Estimate of the hydrodynamic coefficient vector	
$\hat{\boldsymbol{\xi}}^{(n)}$	The n^{th} estimate of $\hat{\boldsymbol{\xi}}$ produced by the non-linear parameter identification procedure	
$\hat{\boldsymbol{\xi}}^*$	The identified estimate of $\hat{\boldsymbol{\xi}}$	
$\hat{\boldsymbol{\xi}}^X, \hat{\boldsymbol{\xi}}^Y, \hat{\boldsymbol{\xi}}^Z$	The estimated X, Y, Z force related coefficient of the UV	
$\hat{\boldsymbol{\xi}}^K, \hat{\boldsymbol{\xi}}^M, \hat{\boldsymbol{\xi}}^N$	The estimated K, YM, N moment related coefficient of the UV	
ρ	Density of sea water	
τ	Combined thrust and control induced loads vector	
$\boldsymbol{\tau}_c$	Control induced loads vector	
$\boldsymbol{\tau}_d$	Disturbances induced loads vector	
$\boldsymbol{\tau}_n$	Propeller induced loads vector	
∇	Displacement of the UV	[m^3]
∇x	The grad function of x	
$\|\|\boldsymbol{x}\|\|_\infty$	The infinity norm of $\boldsymbol{x}$ =max$_i$ $\|\boldsymbol{x}_i\|$	

Glossary

AUV	Autonomous Underwater Vehicle
UV	Underwater Vehicle
CFD	Computational Fluid Dynamics
SOC	Southampton Oceanography Centre
OED	Ocean Engineering Division (of SOC)
UnRANS	Unsteady Reynolds Averaged Navier Stokes
RANS	Reynolds Averaged Navier Stokes
PMM	Planar Motion Mechanism
LP	Linear Programming
SQP	Sequential Quadratic Programming
GPS	Global Positioning System
INS	Inertial Navigation System
ADCP	Acoustic Doppler Current Profilers

DECLARATION OF AUTHORSHIP

I, **Maaten Furlong**

declare that the thesis entitled

"System Identification of the Hydrodynamic Characteristics of Underwater Vehicles"

and the work presetned in it are my own. I confirm that:

- this was done wholly or mainly while in cadidature for a research degree at this University;
- where any part of this thesis has previously been submitted for a degree or any other qualification at this University or any other institution, this has been clearly stated;
- where I have consulted the published work of others, this is always clearly attributed;
- where I have quoted from the work of others, the source is always given. With the exception of such quotations, this thesis is entirely my own work;
- I have acknowledged all main sources of help;
- where the thesis is based on work done by myself jointly with others, I have made clear exactly what was done by others and what I have contributed myself;
- part of this work has been published, see Furlong et al. (2003).

Signed:.. [redacted] .....

Date:..4/3/5.....

Chapter 1

Introduction

1.1 Background

Southampton Oceanography Centre (SOC) is the UK's leading centre for research in marine and earth sciences. As part of the SOC role of providing first rate facilities for marine research the Ocean Engineering Division (OED) of SOC has been involved in the research and development of autonomous underwater vehicles (AUV) since the late 1980s. As part of this work the Autosub AUV, described by Millard et al. (1997), was developed. This AUV is designed as a sensor platform for scientific exploration of the world's oceans. In 1996 Autosub had its first trial in Southampton's Empress Dock adjacent to SOC. Since these early tests Autosub has been continually upgraded and deployed in over 365 missions of up to 50 hours duration and 262km in length. The most recent deployments have involved surveying the arctic ice shelves off the coast of Greenland.

The vehicle is 7m in length and 0.9m in diameter and is of torpedo shape. It displaces approximately 3 tonnes and is powered by a single propeller. Control is provided by vertical and horizontal tail planes. The vehicle is required to fiy through the water to maintain control. Its configuration is known as a fiight style AUV.

As part of the further development of Autosub a need for a dynamic simulation of the vehicle was identified. The simulation would fill the niche between information

gathered through simple steady state analysis that cannot deal with complex dynamics problems such as obstacle avoidance and that produced from testing of the real vehicle. The latter is very expensive and time consuming. Once created the simulation could be used to rapidly test 'what if' scenarios and analyse alternative control strategies, obstacle avoidance algorithms and explore the flight envelope of the vehicle. The simulation would also provide insight into the actual flight characteristics of Autosub while manoeuvring. The initial goal of the EngD research was to develop a simulation of Autosub that would accurately reproduce the motions of the vehicle.

1.2 Scope of the EngD Research

The initial research involved surveying the state of the art in AUV and submarine simulations techniques. Due to the similarity between flight style AUVs and submarines this thesis considers them together as Underwater Vehicles (UVs). It became clear from the survey that creating an accurate dynamic UV model is a non-trivial task. Although, the problem has been widely researched and a general method has been established, accurately determining the hydrodynamic loads on the vehicle is still a considerable challenge. This challenge arises because no one has yet found a method of solving the Navier-Stokes equations for general hull forms subject to arbitrary motions. These equations describe the pressure and velocity of the water on the outer hull of the vehicle and, from this the loads can be determined. Likewise the empirical determination of the loads has its own set of difficulties. The hydrodynamic loads on an UV are a non-linear function of the linear and angular, velocities and accelerations of the vehicle. Thus, to be able to map this function experimentally would require that a test be performed for every combinations of the 12 different velocities and accelerations. Hence, even if the hydrodynamic loads were only evaluated at a small number of values for each velocity and acceleration the total number of tests required to cover every combination is impractically large. Therefore, generating a look-up table that maps the non-linear hydrodynamic load function to the vehicle's motion it is not practical. Thus, approximations for the hydrodynamic loads are used when modelling UVs.

These approximations range in complexity from using CFD to get an approximate solutions to the Navier-Stokes equations to modelling the UV as a collection of simple well tested shapes and estimating the interaction between the shapes. However, the most common approach is to use a set of equations that are thought to approximate the actual non-linear hydrodynamic load function. The equations are based on the work of Abkowitz (1969) and use a multivariate Taylor series expansion along with the an understanding of the underlying physics to determine their form. The form of the equations is independent of the modelled submarine. The dynamics of each submarine are captured through a finite set of hydrodynamic coefficients, which when combined with the governing equations approximate the hydrodynamic loads on the UV. The advantage of the approach is that it is only necessary to determining the hydrodynamic coefficients, a relatively simple task, to approximate the hydrodynamic loads. Although it is possible to determine some of these coefficients analytically it is more accurate to measure them through extensive captive model tests. Unfortunately, the expense involved is usually beyond the budget of AUV builders, hence less accurate methods are employed.

From the survey of UV simulations it was decided that the most appropriate hydrodynamic load model for Autosub would use a set of non-linear hydrodynamic coefficient equations. However, the cost of determining the hydrodynamic coefficients was beyond the budget of the project. So, an inexpensive alternative method of accurately determining the coefficients was desired. At the same time the School of Engineering Sciences at the University of Southampton was involved in a contract with QinetiQ Haslar to investigate methods of determining hydrodynamic coefficients from free swimming submarine trials data. If this was successful then the technique could be used to determine the hydrodynamic coefficients of Autosub from the large library of Autosub missions data. As the contract was in its early stages the research effort put into modelling Autosub was added to the project to help facilitate the development of the coefficient identification procedure. One side benefit of this collaboration was that the knowledge of submarine modelling possessed by the QinetiQ personnel could be used to inform the modelling of Autosub.

1.3 Scope of the Hydrodynamic Coefficient Identification Research

The goal of QinetiQ's identification procedure was to determine the hydrodynamic coefficients used in their submarine equations, described in Booth et al. (1980), from submarine inputs (control plane angles and propeller rpm) and outputs (position and attitude) generated during manoeuvring. However, there is an implicit question associated with the identification procedure, that being: is it possible to determine the hydrodynamic coefficient from the input and output data? Whilst it is possible to calculate the UV outputs from a knowledge of the UV inputs and the hydrodynamic coefficients it is not necessary for the process to be reversible and for the coefficients to be determined from the inputs and outputs. Initially the question of identification was posed in terms of identifying a set of coefficient so that target track and predicted track matched. The identification problem was then recast in terms of identifying the hydrodynamic coefficients derived using captive model tests. This added extra complexity to the problem as it is possible to have a manoeuvre which can be produced by two or more distinct sets of coefficients. Hence, determining the correct values can only be performed using a manoeuvre that can only be produced using the towing tank derived coefficients.

The research involved two distinct but related areas. The first looked at trying to answer whether it is possible to accurately identify the hydrodynamic coefficient values from manoeuvre data, and the second involved developing techniques that would efficiently determine the correct coefficient values. Two different approaches were used to identify the hydrodynamic coefficients. The first, non-linear approach was designed to identify a set of coefficients that would reproduced the target manoeuvre. This only required the UV inputs and the position and attitude outputs as specified by QinetiQ. The procedure required an optimization routine and the routine used was written by Professor Veres of the University of Southampton, see Veres (2003). The second, a linear approach uses the UV attitude, velocity and acceleration data as well as the inputs to identify the coefficients. The submarine manoeuvres used to identify the coefficients were simulated using captive model testing derived hydrodynamic coefficient values for real submarines. Simulated data was used as it allowed

rapid testing of alternate manoeuvres and the accuracy of the converged coefficients could be easily determined.

To avoid tuning the system identification process the hydrodynamic coefficients of three submarines of quite different form and hydrodynamic coefficients were selected to be identified.

1.4 Layout of the Thesis

The thesis comprises 10 chapters and naturally partitioned into two parts.

The first part (Chapters 2–3) is a survey of the state of the art of UV simulations. This describes the general framework used in modelling UVs and then discusses how the loads on the vehicle are determined. The second part of the thesis (Chapters 4–9) describes the hydrodynamic coefficient identification research. The remaining chapters of the thesis are outlined next.

Chapter 2 describes the two coordinate systems used in modelling UVs. It explains why they are needed and details the mathematics involved in using the two coordinate system approach. It also outlines the rigid body dynamics equations required when using an UV fixed coordinate system.

Chapter 3 explains how the loads applied to the UV are determined. It outlines how the total load arises from many sources and the methods used in determining these individual components.

Chapter 4 introduces two alternative hydrodynamic coefficient identification procedures and then describes the difficulties involved in determining a suitable candidate identification manoeuvre. The manoeuvres chosen to identify the coefficients are explained. The choices made allow investigation of simplified versions of the fully coupled non-linear motion equations as well as the complete fully coupled motion equations.

Chapter 5 addresses the creation of the general UV simulations used with the identification procedures described. It starts by discussing how the submarine equations were rearranged into a form suitable for simulation. It then outlines the three simulation versions created and describes their validation and testing. The chapter concludes by outlining the accuracy with which the simulation approximates the submarine equations.

Chapter 6 demonstrates that the coefficients of the test submarines are not-unique and that there are an infinite number of sets of coefficients that will produce the same manoeuvres.

Chapter 7 describes the implementation of the non-linear identification procedure and outlines the testing use to identify the submarine coefficients. It describes: the accuracy with which the identified manoeuvre reproduces the target manoeuvre; the accuracy with which the hydrodynamic coefficients are identified; and the speed and general performance of the non-linear procedure.

Chapter 8 discusses the accuracy with which the coefficients identified in Chapter 7 predict other manoeuvres. After discussing the process by which the random test manoeuvres are generated the accuracy with which the identified coefficients predict these test manoeuvres is addressed.

Chapter 9 investigates how the linear coefficient identification procedure can be used to determine the coefficients and presents the results of the associated numerical testing.

Chapter 10 presents and discusses the conclusions that can be drawn from the reported research and the implications for identifying the hydrodynamic coefficients from free swimming UVs. The chapter ends by discussing further testing that could be carried out and outlines other potential techniques for creating a simulation from trials data.

Chapter 2

Mathematical Modelling of Underwater Vehicle Dynamics

2.1 Rotation Between the Body and Fixed Coordinate Frames

The position and attitude of the vehicle are defined in the inertial coordinate system, whereas the vehicle velocity and body rotation rates are defined in the body coordinate system. To update the position and attitude information within the simulation procedure it is necessary to know the rates of change of position and attitude. These rates of change are calculated from the velocity and body rotation rates using relationships described in the following sections. The rate of change of position is related to the velocity through a simple coordinate rotation. This rotation can be performed by pre-multiplying the velocity vector by the required unique rotation matrix. The rate of change of attitude is harder to calculate. The relationship depends upon how the attitude is defined. The attitude definition also dictates how the rotation matrix is calculated.

There are two principal methods of defining the attitude and thereby calculating the rotation operator for an UV; these are the *Euler angle* method and the *quaternion* approach. The Euler angle approach has been used by Feldman (1979) and Booth

et al. (1980) and the Quaternion has been used by Prestero (2001a) and Fjellstad and Fossen (1994) to represent attitude in their respective UV simulations.

When comparing the two approaches, the Euler angle method uses a more intuitive representation (typically giving angles of roll, pitch and yaw), however there are problems with the method. The main criticism being the presence of singularities in the Euler angle update matrix. These singularities occur, for the commonly used aerospace sequence, when the pitch (θ) equals $\pm 90°$. However, it is highly unlikely (and undesirable) for the AUVs and submarines considered to have a pitch of $\pm 90°$. Thus, in this case, the singularities can be ignored. Alternatively the singularities can be avoided by truncating the Euler angles so that pitch never equals $\pm 90°$, as described in Cooke et al. (1992). In contrast the quaternion representation uses hyper-complex numbers to represent rotation. This is less intuitive but does not have the problems with singularities associated with the Euler angle approach.

After some consideration of which approach would be most appropriate for use in this thesis, the Euler angle method was chosen. Although the quaternion approach is mathematically superior, the Euler angle method was already used by the Booth et al. (1980) submarine equations whose study forms a large part of the research undertaken and therefore using the quaternion approach would require reformulating the Booth et al. (1980) equations with little benefit.

A description of how the Euler angle method represents rotation and how this can subsequently be used to define the rate of change of position and attitude is discussed next. For completeness the details of the quaternion approach are given in Appendix B

2.1.1 The Euler Angle Representation of Rotation

Rotation of a vector can be accomplished by pre-multiplication of the vector by a suitable square matrix. The set of matrices that produce rotation are known as the special orthogonal (SO) group. The three dimensional rotation matrices are known as $SO(3)$. All SO matrices $\boldsymbol{C}$ have the following properties:

$$\boldsymbol{C}\boldsymbol{C}^T = \boldsymbol{C}^T\boldsymbol{C} = \boldsymbol{I} \quad \text{and} \qquad Det(\boldsymbol{C}) = 1.$$

The Euler angle based $SO(3)$ matrix required to produce any rotation in three dimensional space are generated by three separate rotations about 3 orthogonal axes. As an example assume that the rotation was first about the z-axis, then the y_1-axis and finally the x_2-axis as indicated in Figure 1(a), (b) and (c) respectively. In Figure 1 the rotated axis systems are offset from the origin to aid the presentation. The figure shows the first rotation of ψ about z rotates xyz to $x_1y_1z_1$. The second rotation of θ about y_1 rotates $x_1y_1z_1$ to $x_2y_2z_2$. The third rotation of ϕ about x_2 transforms the axes $x_2y_2z_2$ to $x_3y_3z_3$.

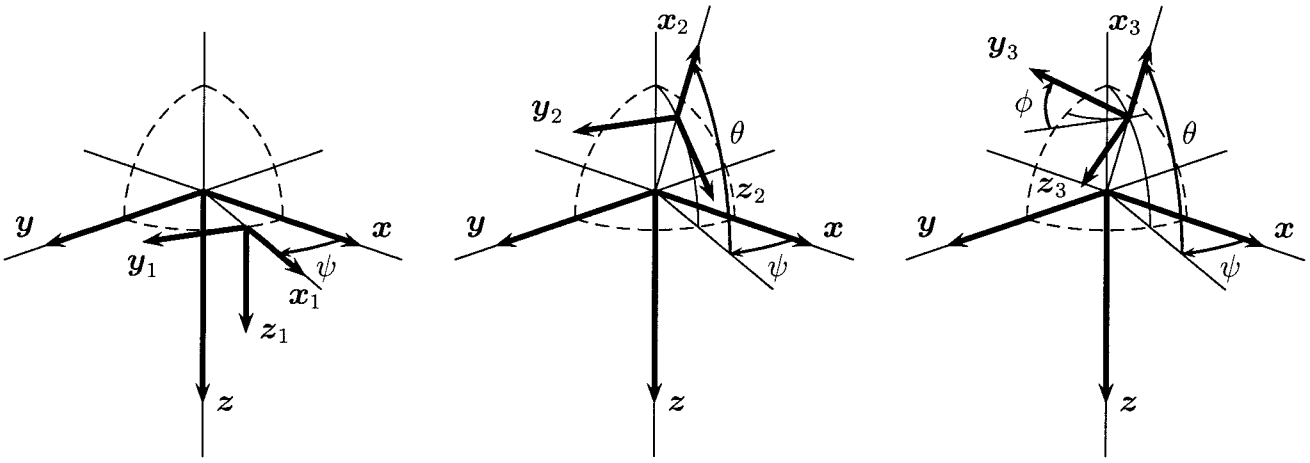

(a) Rotation about the z-axis by ψ

(b) Rotation about the y_1-axis by θ

(c) Rotation about the x_2-axis by ϕ

Figure 1: An example of the xyz Euler angle rotation sequence.

This xyz Euler angle convention is used in many naval applications. It defines the rotation from the inertial fixed frame *to the* body fixed coordinate frame. This rotation can be achieved mathematically by multiplying the matrices defining the rotation about x_2, y_1 and z. Thus, letting:

$$\boldsymbol{R}_x^{\phi} = \begin{bmatrix} 1 & 0 & 0 \\ 0 & \cos(\phi) & \sin(\phi) \\ 0 & -\sin(\phi) & \cos(\phi) \end{bmatrix},$$

$$\boldsymbol{R}_y^{\theta} = \begin{bmatrix} \cos(\theta) & 0 & -\sin(\theta) \\ 0 & 1 & 0 \\ \sin(\theta) & 0 & \cos(\theta) \end{bmatrix}$$

and

$$\boldsymbol{R}_z^{\psi} = \begin{bmatrix} \cos(\psi) & \sin(\psi) & 0 \\ -\sin(\psi) & \cos(\psi) & 0 \\ 0 & 0 & 1 \end{bmatrix}.$$

The rotation matrix is,

$$\begin{bmatrix} x_3 \\ y_3 \\ z_3 \end{bmatrix} = \boldsymbol{R}_x^{\phi}\boldsymbol{R}_y^{\theta}\boldsymbol{R}_z^{\psi} \begin{bmatrix} x \\ y \\ z \end{bmatrix}$$

or, in the notation of Fossen this may be written as,

$$\begin{bmatrix} x_B \\ y_B \\ z_B \end{bmatrix} = \boldsymbol{J}_1^{-1}(\boldsymbol{\eta}_2) \begin{bmatrix} x_I \\ y_I \\ z_I \end{bmatrix}$$

where,

$$\boldsymbol{J}_1^{-1}(\boldsymbol{\eta}_2) = \boldsymbol{R}_x^{\phi}\boldsymbol{R}_y^{\theta}\boldsymbol{R}_z^{\psi}$$

$$\boldsymbol{\eta}_2 = [\phi, \theta, \psi]^T.$$

As it is necessary to transform from the *body* coordinate frame to the *inertial* coordinate frame the inverse of $\boldsymbol{J}_1^{-1}(\boldsymbol{\eta}_2)$ must be found. The inverse $\boldsymbol{J}_1(\boldsymbol{\eta}_2)$ will undo the rotation performed by $\boldsymbol{J}_1^{-1}(\boldsymbol{\eta}_2)$. Changing the sign of the angle used in the Euler

angle rotations and performing the rotations in the reverse order will produce the inverse. Mathematically this is expressed through the identity,

$$\boldsymbol{I} = \left(\boldsymbol{R}_z^{-\psi}\boldsymbol{R}_y^{-\theta}\boldsymbol{R}_x^{-\phi}\right)\left(\boldsymbol{R}_x^{\phi}\boldsymbol{R}_y^{\theta}\boldsymbol{R}_z^{\psi}\right).$$

Alternatively, using the stated properties of the SO group,

$$\boldsymbol{J}_1(\boldsymbol{\eta}_2) = \left(\boldsymbol{J}_1^{-1}(\boldsymbol{\eta}_2)\right)^T = \left(\boldsymbol{R}_x^{\phi}\boldsymbol{R}_y^{\theta}\boldsymbol{R}_z^{\psi}\right)^T = \boldsymbol{R}_z^{\psi T}\boldsymbol{R}_y^{\theta T}\boldsymbol{R}_x^{\phi T}.$$

Multiplying the transposed matrices gives,

$$\boldsymbol{J}_1(\boldsymbol{\eta}_2) = \begin{bmatrix} c\psi \cdot c\theta & -s\psi \cdot c\phi + c\psi \cdot s\theta \cdot s\phi & s\psi \cdot s\phi + c\psi \cdot c\phi \cdot s\theta \\ s\psi \cdot c\theta & c\psi \cdot c\phi + s\phi \cdot s\theta \cdot s\psi & -c\psi \cdot s\phi + s\theta \cdot s\psi \cdot c\phi \\ -s\theta & c\theta \cdot s\phi & c\theta \cdot c\phi \end{bmatrix} \tag{1}$$

with c and s denoting cosine and sine respectively.

Trailing vs. Fixed Axis Rotation

The Euler angle system described in the previous section is known as a 'trailing axis rotation' system. Here the θ rotation is about y_1 not y. However, it is possible to use a fixed axis to define the rotation (therefore the rotation of θ would be about y not y_1) and specify the temporal order of the rotation. Interestingly, using a zyx temporal order for the fixed axis rotations produces the same rotation matrix $\boldsymbol{M}$ as the xyz rotation sequence of the trailing axis system. Thus, the fixed axis rotation is the same as that of a trailing axis but the rotation order is reversed. This effect occurs in all Euler angle sequences and is discussed in Craig (1986) and McGhee et al. (2000). However, in this thesis the more common trailing axis rotation approach is adopted.

Euler Angle Systems

The xyz rotation sequence previously defined is known as the *aerospace sequence* and is commonly used in naval applications. However, it is not unique. The only specific requirement for the Euler angle definition is that the rotations should be about three

orthogonal axes in which each successive rotation axis should not be coincident with the immediately previous rotation axis. Thus, zxz (but not xzz) is a legitimate definition of an Euler angle system and is in fact quite commonly used in other fields. This requirement leads to 12 possible Euler angle systems, these are:

$$\begin{array}{cccccc} xyz & xzy & yxz & yzx & zxy & zyx \\ xyx & xzx & yxy & yzy & zxz & zyz \end{array}$$

Whilst, not all of these systems are in common use, there is also no single accepted standard system for all fields of study. Thus care must be taken to match the given Euler angles to the appropriate Euler rotation sequence.

2.1.2 Problems with the Euler Angle Representation

There are a number of problems inherent in the Euler angle representation of rotation. The first is that the resulting rotation matrix does not have a unique set of Euler angles. For example using the xyz rotation system rotating with $\phi = 180°$, $\theta = 0°$ and $\psi = 180°$ results in the same rotation matrix as using $\phi = 0°$, $\theta = 180°$ and $\psi = 0°$. Thus, to extract the Euler angles from a rotation matrix is not possible, because the representation is ambiguous.

A more serious problem with the representation occurs when trying to update the current Euler angles from the body rotational velocities (p, q, r). At certain body orientations two of the Euler angle rotation axes become coincident, thus an axis of rotation is lost. When this occurs certain body rotations cannot update the Euler angles and the system breaks down. In mechanical gyros this phenomenon is known as *gimbal lock* and in the mathematical representation singularities occur in the Euler angle update matrix.

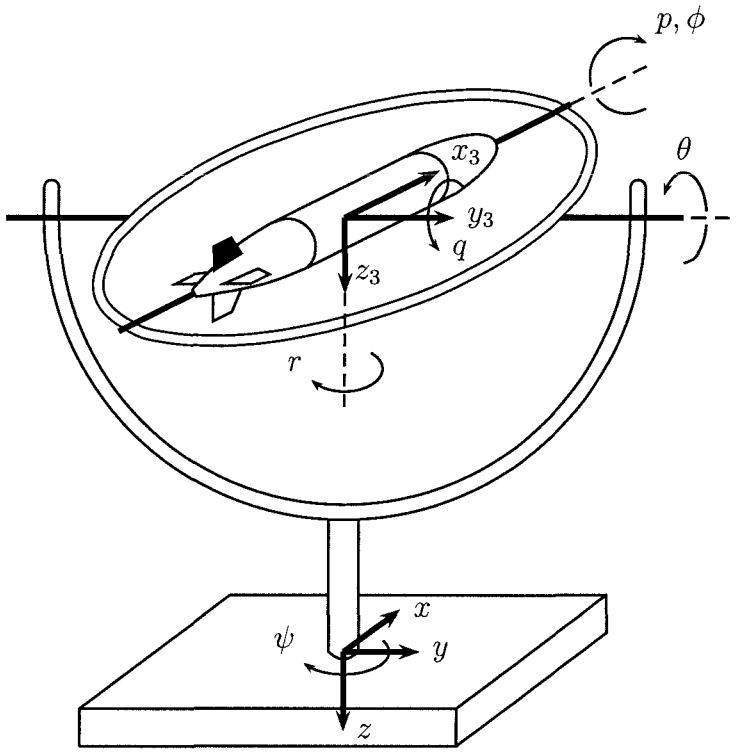

Figure 2: A mechanical example of the xyz Euler rotation sequence.

Gimbal lock can be illustrated using the mechanical example illustrated in Figures 2 & 3. Consider a gimballed model of a UV where the model is connected nose and tail to an inner ring, as illustrated in Figure 2. This inner ring is connected in turn to an outer ring at right angles to the connection to the UV and inner ring. The outer ring is then allowed to rotate about the base. This setup will allow the model to assume any orientation relative to the base and mechanically represents the xyz Euler angle system. When the inner ring is rotated by $\pm 90°$ the UV model will point vertically upwards as indicated in Figure 3. This will cause the rotation of the UV model about the inner ring and rotation of the outer ring about the base to be coincident. Therefore an axis of rotation is lost. If in this position the UV model was rotated in yaw, represented by r in Figure 3, it would be restrained by the rings, as rotation in this axis is not possible. Hence gimbal lock occurs.

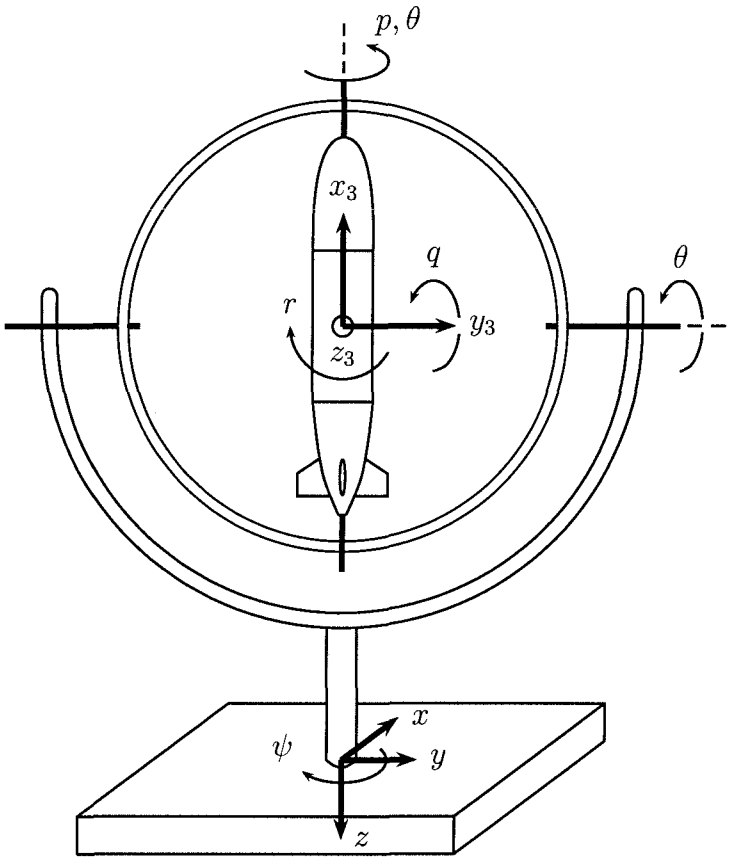

Figure 3: A mechanical example of the xyz Euler rotation sequence with the UV rotated to show gimbal lock.

To show the same phenomenon in the mathematical representation it is necessary to define the Euler angle update matrix.

2.1.3 Calculating the Euler Angle Update Matrix

Although rotation rates can be represented by a vector it is not possible to transform the vector in the body fixed coordinate system to the inertial coordinate system to get the Euler angle update rates. This is because each Euler angle rates describe rotation rates in different coordinate systems (eg '$x_1y_1z_1$', '$x_2y_2z_2$' and '$x_3y_3z_3$' illustrated in Figure 1). Hence the transformation matrix used to calculate the Euler angle rates from the body rates does not belong to $SO(3)$. However, the body rates are related to the rates of change of the Euler angles through a transformation matrix, hence one

may write,

$$\begin{bmatrix} p \\ q \\ r \end{bmatrix} = \boldsymbol{J}_2^{-1}(\boldsymbol{\eta}_2) \begin{bmatrix} \dot{\phi} \\ \dot{\theta} \\ \dot{\psi} \end{bmatrix}, \quad \text{where} \quad \boldsymbol{J}_2^{-1}(\boldsymbol{\eta}_2) \notin SO(3).$$

However, as previously mentioned, at certain Euler angles the matrix $\boldsymbol{J}_2^{-1}(\boldsymbol{\eta}_2)$ is singular and therefore $\boldsymbol{J}_2(\boldsymbol{\eta}_2)$ does not exist. At these points it is not possible to update the Euler angles from the body rotations.

The matrices $\boldsymbol{J}_2^{-1}(\boldsymbol{\eta}_2)$ and $\boldsymbol{J}_2(\boldsymbol{\eta}_2)$ can be determined as follows, as described in Fossen (1994):

Defining

$$\boldsymbol{\nu}_2 = \begin{bmatrix} p \\ q \\ r \end{bmatrix} \qquad \text{and} \qquad \boldsymbol{\eta}_2 = \begin{bmatrix} \phi \\ \theta \\ \psi \end{bmatrix}$$

leads to

$$\boldsymbol{\nu}_2 = \boldsymbol{J}_2^{-1}(\boldsymbol{\eta}_2)\dot{\boldsymbol{\eta}}_2.$$

Remembering that the rotation matrix from the inertial to the body fixed frame was defined by

$$\boldsymbol{R}_x^{\phi}\boldsymbol{R}_y^{\theta}\boldsymbol{R}_z^{\psi}.$$

Thus, $\dot{\phi}$ will produce a pure rotation about the body x_2 axis, as illustrated in Figure 1(b) & (c) and thus

$$\begin{bmatrix} p \\ 0 \\ 0 \end{bmatrix} = \begin{bmatrix} \dot{\phi} \\ 0 \\ 0 \end{bmatrix}.$$

Likewise, $\dot{\theta}$ will produce a rotation about the y_1 axis as shown in Figure 1(a) & (b). However, as this rotation rate is defined in the $x_z y_2 z_2$ axis system it needs to be rotated to the body axis to be given in terms of body rates. Therefore,

$$\begin{bmatrix} 0 \\ q \\ r \end{bmatrix} = \boldsymbol{R}_x^{\phi} \begin{bmatrix} 0 \\ \dot{\theta} \\ 0 \end{bmatrix}$$

Extending the idea it follows that,

$$\boldsymbol{\nu}_2 = \begin{bmatrix} \dot{\phi} \\ 0 \\ 0 \end{bmatrix} + \boldsymbol{R}_x^{\phi} \begin{bmatrix} 0 \\ \dot{\theta} \\ 0 \end{bmatrix} + \boldsymbol{R}_x^{\phi} \boldsymbol{R}_y^{\theta} \begin{bmatrix} 0 \\ 0 \\ \dot{\psi} \end{bmatrix} = \boldsymbol{J}_2^{-1}(\boldsymbol{\eta}_2)\dot{\boldsymbol{\eta}}_2.$$

Noting that

$$\boldsymbol{R}_x^{\phi} = \begin{bmatrix} 1 & 0 & 0 \\ 0 & c\phi & s\phi \\ 0 & -s\phi & c\phi \end{bmatrix} \qquad \text{and} \qquad \boldsymbol{R}_y^{\theta} = \begin{bmatrix} c\theta & 0 & -s\theta \\ 0 & 1 & 0 \\ s\theta & 0 & c\theta \end{bmatrix}$$

then

$$\boldsymbol{R}_x^{\phi} \boldsymbol{R}_y^{\theta} = \begin{bmatrix} 1 & 0 & 0 \\ 0 & c\phi & s\phi \\ 0 & -s\phi & c\phi \end{bmatrix} \cdot \begin{bmatrix} c\theta & 0 & -s\theta \\ 0 & 1 & 0 \\ s\theta & 0 & c\theta \end{bmatrix} = \begin{bmatrix} c\theta & 0 & -s\theta \\ s\phi \cdot s\theta & c\phi & s\phi \cdot c\theta \\ c\phi \cdot s\theta & -s\phi & c\phi \cdot c\theta \end{bmatrix}.$$

By substituting and expansion of terms in the expression for $\boldsymbol{\nu}_2$ leads to,

$$\boldsymbol{J}_2^{-1}(\boldsymbol{\eta}_2) = \begin{bmatrix} 1 & 0 & -s\theta \\ 0 & c\phi & s\phi \cdot c\theta \\ 0 & -s\phi & c\phi \cdot c\theta \end{bmatrix}.$$

If $\theta = \pm 90°$ then,

$$\boldsymbol{J}_2^{-1}(\boldsymbol{\eta}_2) = \begin{bmatrix} 1 & 0 & \mp 1 \\ 0 & c\phi & 0 \\ 0 & -s\phi & 0 \end{bmatrix}$$

and the matrix $\boldsymbol{J}_2^{-1}(\boldsymbol{\eta}_2)$ is singular as $\det\left(\boldsymbol{J}_2^{-1}(\boldsymbol{\eta}_2)\right) = 0$, therefore $\boldsymbol{J}_2(\boldsymbol{\eta}_2)$ does not exist for the indicated values of θ.

For other values of θ the matrix $\boldsymbol{J}_2(\boldsymbol{\eta}_2)$ can be shown to have the form,

$$\boldsymbol{J}_2(\boldsymbol{\eta}_2) = \begin{bmatrix} 1 & s\phi \cdot t\theta & c\phi \cdot t\theta \\ 0 & c\phi & -s\phi \\ 0 & s\phi/c\theta & c\phi/c\theta \end{bmatrix}, \tag{2}$$

as presented in Appendix A.

Changing the Euler angle sequence does not remove the singularities it merely changes the orientation at which they occur. In fact it is not possible to create an Euler angle system that does not produce these singularities. As Fossen (1994) states, " ...no continuous three parameter description can be both global and without singularities".

2.1.4 Using the Euler Angle System for UV Modelling

To complete the picture of how Euler angles can be used to model a UV's motion it is necessary to combine the preceding section. The requirement for the UV model is to transform the body fixed linear velocities into the inertial frame and to use the body fixed angular velocities to update the vehicles attitude. Using the xyz Euler angle sequence typical in naval architecture this proceeds as follows:

First, from Equation (1) the body fixed velocities (u, v, w) are related to the inertial velocities $(\dot{x}, \dot{y}, \dot{z})$ by,

$$\begin{bmatrix} \dot{x} \\ \dot{y} \\ \dot{z} \end{bmatrix} = \boldsymbol{J}_1(\boldsymbol{\eta}_2) \begin{bmatrix} u \\ v \\ w \end{bmatrix}.$$

Second, from Equation (2) the body rotation rates (p, q, r) define the rate of change of the Euler angles $(\dot{\phi}, \dot{\theta}, \dot{\psi})$ as follows,

$$\begin{bmatrix} \dot{\phi} \\ \dot{\theta} \\ \dot{\psi} \end{bmatrix} = \boldsymbol{J}_2(\boldsymbol{\eta}_2) \begin{bmatrix} p \\ q \\ r \end{bmatrix}.$$

These two equations can be combined into a large matrix, which when written in Fossen's notation becomes,

$$\dot{\boldsymbol{\eta}} = \boldsymbol{J}(\boldsymbol{\eta}_2)\boldsymbol{\nu},$$

with,

$$\boldsymbol{\eta} = [x, y, z, \phi, \theta, \psi]^T,$$

$$\boldsymbol{\nu} = [u, v, w, p, q, r]^T$$

and

$$\boldsymbol{J}(\boldsymbol{\eta}_2) = \begin{bmatrix} \boldsymbol{J}_1(\boldsymbol{\eta}_2) & 0_{3\times3} \\ 0_{3\times3} & \boldsymbol{J}_2(\boldsymbol{\eta}_2) \end{bmatrix}.$$

This completes how Euler angles can be used to model the relationship between the body axis velocities and rotation rates, and the inertial axis velocities and attitude change for a manoeuvring UV.

2.2 Rigid Body Dynamics

It is necessary to be able to calculate the acceleration of the UV in the body fixed coordinate system. As this coordinate system moves and rotates with the body it does not form an inertial frame of reference and so Newton's second law cannot be directly applied. To calculate the accelerations in the body coordinate system it is necessary to take account of the rotation of the coordinate system. This problem can be tackled using either Newtonian or Lagrangian mechanics.

The commonly used *Newton-Euler* equations of motion for rigid body dynamics in the body fixed reference system assume the general form:

$$m[\dot{u} - vr + wq - x_G(q^2 + r^2) + y_G(pq - \dot{r}) + z_G(pr + \dot{q})] = X$$

$$m[\dot{v} - wp + ur - y_G(r^2 + p^2) + z_G(qr - \dot{p}) + x_G(qp + \dot{r})] = Y$$

$$m[\dot{w} - uq + vp - z_G(p^2 + q^2) + x_G(rp - \dot{q}) + y_G(rq + \dot{p})] = Z$$

$$I_{XX}\dot{p} + (I_{ZZ} - I_{YY})qr - (\dot{r} + pq)I_{ZX} + (r^2 - q^2)I_{YZ} + (pr - \dot{q})I_{XY} + m[y_G\dot{w} - uq + vp) - z_G(\dot{v} - wp + ur)] = K$$

$$I_{YY}\dot{q} + (I_{XX} - I_{ZZ})rp - (\dot{p} + qr)I_{XY} + (p^2 - r^2)I_{ZX} + (qp - \dot{r})I_{YZ} + m[z_G(\dot{u} - vr + wq) - x_G(\dot{w} - uq + vp)] = M$$

$$I_{ZZ}\dot{r} + (I_{YY} - I_{XX})pq - (\dot{q} + rp)I_{YZ} + (q^2 - p^2)I_{XY} + (rq - \dot{p})I_{ZX} + m[x_G(\dot{v} - wp + ur) - y_G(\dot{u} - vr + wq)] = N$$

where,

X, Y, Z	–	Represent the external forces
K, M, N	–	Represent the external moments
u, v, w	–	Represent the linear velocities
p, q, r	–	Represent the body rotation rates
x_G, y_G, z_G	–	Represent the xyz coordinates of the centre of gravity

All variables are measured in the body fixed coordinate system.

This standard formulation can be found in many source, such as Abkowitz (1969), ?, Booth et al. (1980), and Fossen1994, and can be calculated from first principles using techniques described in graduate mechanics books.

2.3 Conclusions

This chapter has looked in detail at how dynamic models of UVs are created. It gave an overview of the process describing: the need for a world (inertial) and body reference frame; how the moving body reference frame would require rigid body dynamics to calculate the acceleration in it; the various forces and moments applied to the body. This was followed by a more detailed examination of how the rotation between the reference frames could be achieved. Here the Euler angle and Quaternion representation were compared. This then lead to the final section describing the rigid-body dynamic equations used to calculate the acceleration of a UV in the body fixed rotating reference frame.

The modelling described so far has not considered how the forces $[X, Y, Z]$ and moment $[K, M, N]$ on the UV are determined, Chapter 3 considers this in detail. It describes the complexity of determining these forces and moments and also outlines methods for their estimation.

Chapter 3

Modelling the Forces and Moments on Underwater Vehicles

3.1 Introduction

The previous chapter described how the dynamics of UVs can be modelled, but to create a simulation of a UV it is necessary to be able to estimate the forces and moments it experiences. This chapter describes the source of the forces $[X,Y,Z]$ and moments $[K,M,N]$, and outlines how they can be approximated. At a simple level the forces and moments on an UV can be attributed to:

- The weight of the vehicle.
- The pressure distribution over the surface of the body (pressure drag).
- The fluid shear force distribution over the surface of the body (skin friction drag).

By integrating the hydrostatic and hydrodynamic pressure acting over the surface of the body and including the influence of the distribution of the weight of the vehicles the total force and moment can be determined. Unfortunately, it is not possible to analytically determine the pressure and shear force distributions for an arbitrary

shaped vehicle as this requires the solution of the Navier-Stokes equations. The quality of Navier-Stokes solvers is currently insufficient to determine the actual flow about an arbitrary body. So considerable time and effort has been invested in finding alternative methods of describing the forces and moments acting on an UV. The first stage is to analyse the sources of the loads on an UV.

3.2 Sources of the Loads on an Underwater Vehicle

It is known that the pressure and shear forces and moments experienced by a UV arise from a number of separate sources. Analyzing and approximating the contribution associated with each mechanisms produces a method of tackling the problem. The contributions can be divided into the following qualitative categories:

Hydrostatic (or restoration) forces and moments. The hydrostatic forces and moments can be simply determined using the principle of Archimedes. For a fully submerged UV, the problem simply becomes one of transforming the forces generated by the weight and buoyancy into the body axes of the UV. The equations describing the hydrostatic forces and moments are given in Section 3.3.

Hydrodynamic forces and moments. The hydrodynamic forces and moments experienced by a vessel are generated by its movement through the water. The forces and moments are a function of both the UV's velocity and acceleration. The total hydrodynamic force is usually sub-divided into the components that are governed by and in-plane with the velocity and acceleration components as follows:

- *Velocity forces and moments — Pressure and skin friction drag.*
  The pressure drag comes from incomplete pressure recovery at the rear of an UV. The skin friction drag is produced by the shear layer of water flowing over the skin of the UV. Both of the effects are due to the viscosity of the water and are dependent, in the steady state, on the speed of the UV. This is often termed the hydrodynamic damping.

- *Acceleration forces and moments — Added Mass.*
  When a body is accelerated in a fluid the force required for a given acceleration is greater than one would expect from the body's mass; thus the body acts as though it has a larger mass. This extra mass is termed the *added mass* of the vehicle. The apparent increase in mass occurs because when the body accelerates it also accelerates the surrounding fluid. The phenomenon is primarily an inviscid effect, and thus can be calculated using potential flow theory. The actual added mass value depends upon the shape of the body, the direction of the acceleration and the frequency of the accelerations. However, in an unbounded fluid, as can be assumed for deeply submerged UVs, the added-mass becomes independent of frequency.

Control forces and moments. The control forces and moments are usually produced by control planes in UVs. These require flow over the plane that causes lift which is subsequently used to control the UVs attitude. Although these forces and moments are technically generated from *hydrodynamic* effects they are considered separately to simplify the analysis.

Propulsion forces and moments. The propulsion forces and moments are produced by the main propulsion system. This is usually a propeller in UVs and extensive work has been compiled regarding propulsion models.

By summing the loads associated with each contribution defined above the total forces and moments can be determined. Using a notation system similar to that of Fossen this summation can be written as:

$$\begin{bmatrix} X \\ Y \\ Z \\ K \\ M \\ N \end{bmatrix} = \boldsymbol{g}(\boldsymbol{\eta}) + \boldsymbol{d}(\boldsymbol{\nu}) + \boldsymbol{M}_A\dot{\boldsymbol{\nu}} + \boldsymbol{\tau}_c + \boldsymbol{\tau}_n.$$

The different components on the right hand side of the above identity are defined as follows:

$\boldsymbol{g}(\boldsymbol{\eta})$ — Hydrostatic force and moments vector

$\boldsymbol{d}(\boldsymbol{\nu})$ — Hydrodynamic damping vector

$\boldsymbol{M}_A$ — Added mass matrix

$\boldsymbol{\tau}_c$ — Control forces and moments vector

$\boldsymbol{\tau}_n$ — Propulsions forces and moments vector

The hydrostatic loads and vehicle weight are easily determined as described in the following section. However, the remaining coefficients are far more challenging to determine. The methods used to calculate the loads are discussed in the subsequent sections.

3.3 Calculating the Hydrostatic Forces and Moments — $\boldsymbol{g}(\boldsymbol{\eta})$

The hydrostatic (or restoration) forces and moments are generated by the forces due to the mass of the vessel (weight) and the force from the displaced water (buoyancy). These forces act at the centre of gravity (x_G, y_G, z_G) and the centre of buoyancy (x_B, y_B, z_B) of the vessel. As the forces act vertically in the inertial coordinate system they need to be transformed into the body coordinate system to calculate the body fixed forces and moments.

The hydrostatic forces are:

mg — Weight of UV

$B = \rho g \nabla$ — Buoyancy of UV

Here ∇ denotes the displaced volume of the UV.

As the inertial z-axis is positive downwards the buoyancy force is negative.

3.3.1 Determining the Hydrostatic Forces in the Body Fixed Coordinate Frame

The transformation of the forces from the world to the body coordinate system can be accomplished using the rotation matrix $\boldsymbol{M}$ described in Section 2.1.1. Thus,

$$\boldsymbol{f}_G = \boldsymbol{M} \begin{bmatrix} 0 \\ 0 \\ mg \end{bmatrix} \quad \text{and} \quad \boldsymbol{f}_B = \boldsymbol{M} \begin{bmatrix} 0 \\ 0 \\ -B \end{bmatrix}$$

where, $\boldsymbol{f}_G$ and $\boldsymbol{f}_B$ represent the gravitational and buoyancy force in the body fixed coordinate system and $\boldsymbol{M}$ is the matrix of rotation from the inertial to the body fixed coordinate frame.

The forces in the body fixed coordinate frame are therefore defined as:

$$\begin{bmatrix} X_{Hs} \\ Y_{Hs} \\ Z_{Hs} \end{bmatrix} = \boldsymbol{f}_G + \boldsymbol{f}_B = \boldsymbol{M} \begin{bmatrix} 0 \\ 0 \\ mg - B \end{bmatrix}.$$

3.3.2 Determining the Hydrostatic Moments in the Body Fixed Coordinate Frame

The moments in the body fixed coordinate frame generated by the hydrostatic forces can be calculated using the vector cross product of the body fixed forces $\boldsymbol{f}_G$ & $\boldsymbol{f}_B$ and their associated points of action at the centres of gravity and buoyancy respectively. This is expressed mathematically as:

$$\begin{bmatrix} K_{Hs} \\ M_{Hs} \\ N_{Hs} \end{bmatrix} = \boldsymbol{r}_G \times \boldsymbol{f}_G + \boldsymbol{r}_B \times \boldsymbol{f}_B$$

$$= \boldsymbol{r}_G \times \boldsymbol{M} \begin{bmatrix} 0 \\ 0 \\ mg \end{bmatrix} + \boldsymbol{r}_B \times \boldsymbol{M} \begin{bmatrix} 0 \\ 0 \\ -B \end{bmatrix}$$

subject to

$$\boldsymbol{r}_G = [x_G, y_G, z_G]^T \quad \text{— centre of gravity,}$$
$$\boldsymbol{r}_B = [x_B, y_B, z_B]^T \quad \text{— centre of buoyancy.}$$

The Hydrostatic Forces and Moments Vector — $\boldsymbol{g}(\boldsymbol{\eta})$

To calculate the forces and moments in the body reference frame it is necessary to know the terms in the rotation matrix $\boldsymbol{M}$. One choice for $\boldsymbol{M}$ is the rotation matrix $\boldsymbol{J}_1^{-1}(\boldsymbol{\eta}_2)$ defined by the xyz Euler angle representation commonly used in naval applications. The matrix $\boldsymbol{J}_1^{-1}(\boldsymbol{\eta}_2)$ describes the rotation from the inertial to the body fixed coordinate system and can be determined from the transpose of $\boldsymbol{J}_1(\boldsymbol{\eta}_2)$ given in Section 2.1.1. Thus,

$$\boldsymbol{J}_1^{-1}(\boldsymbol{\eta}_2) = \boldsymbol{J}_1(\boldsymbol{\eta}_2)^T = \begin{bmatrix} c\psi \cdot c\theta & s\psi \cdot c\theta & -s\theta \\ -s\psi \cdot c\phi + c\psi \cdot s\theta \cdot s\phi & c\psi \cdot c\phi + s\phi \cdot s\theta \cdot s\psi & c\theta \cdot s\phi \\ s\psi \cdot s\phi + c\psi \cdot c\phi \cdot s\theta & -c\psi \cdot s\phi + s\theta \cdot s\psi \cdot c\phi & c\theta \cdot c\phi \end{bmatrix}.$$

Therefore, the hydrostatic force and moment vector becomes,

$$\begin{bmatrix} X_{Hs} \\ Y_{Hs} \\ Z_{Hs} \\ K_{Hs} \\ M_{Hs} \\ N_{Hs} \end{bmatrix} = \begin{bmatrix} -(mg - B)s\theta \\ (mg - B)c\theta \cdot s\phi \\ (mg - B)c\theta \cdot c\phi \\ (y_G mg - y_B B)c\theta \cdot c\phi - (z_G mg - z_B B)c\theta \cdot s\phi \\ -(z_G mg - z_B B)s\theta - (x_G mg - x_B B)c\theta \cdot c\phi \\ (x_G mg - x_B B)c\theta \cdot s\phi + (y_G mg - y_B B)s\theta \end{bmatrix}.$$

Using Fossen's notation the hydrostatic forces and moments are written as the vector:

$$\boldsymbol{g}(\boldsymbol{\eta}) = [X_{Hs}, Y_{Hs}, Z_{Hs}, K_{Hs}, M_{Hs}, N_{Hs}]^T,$$

and

$$\boldsymbol{\eta} = [x, y, z, \phi, \theta, \psi].$$

As the xyz Euler angle sequence is common in naval applications the presented form of the hydrostatic forces and moments appear in the governing equations of Feldman (1979) and Booth et al. (1980).

3.4 Methods of Estimating the Hydrodynamic Forces and Moments

Determining the remaining forces and moments is a challenge. There are two basic approaches that can be used. The first uses our understanding of the underlying physics of fluids to analytical solve the fluid flow problem. As stated earlier, the Navier-Stokes equations in general cannot be solved, but simplifying assumptions can be made that make the problem tractable. This results in computational fluid dynamics coupled with potential flow solutions. The other possibility is to use experimental data to determine the load on a vehicle. This approach can be either direct using a scaled model or the actual UV, or indirect whereby the results of tests for similar UVs or components are used to estimate the loads. In general analytical and empirical approaches are used in combination to estimate the hydrodynamic loads.

A survey of the literature revealed three different approaches to modelling UVs. These are discussed in the following sections.

3.5 Modelling the Forces and Moments Using Computational Fluid Dynamics

As computational fluid dynamics (CFD) techniques and computing power have improved over the last 5-10 years, it is now becoming possible to use analytical techniques to model the hydrodynamic forces and moments on a UV. By combining these forces and moments with a UV dynamic model, it is possible to tackle the UV manoeuvring problem. However, attempts at using CFD (both viscous and inviscid solvers) for manoeuvring are in the early stages of research, Bertram (2000).

Research work on modelling submarine manoeuvres has been reported in Pankajakshan et al. (2002). In this case, an Unsteady Reynolds Averaged Navier Stokes (UnRANS) solver was used for computing the unsteady fluid flow, and was linked with a quaternion based dynamic model of a submarine. The estimated forces and

moments acting on the hull, propeller, and hydroplanes were calculated by integrating the approximated pressure and shear forces over the body of the vehicle. Various tests were performed for slow manoeuvres using the UnRANS code, and the results were validated against a free swimming model submarine. Good agreement between the simulation and the experimental trials were reported.

However, the model of the submarine used was of a relatively simple streamlined shape, and although good agreement was shown with this vehicle it is not clear whether the code would produce the same level of agreement with a submarine of more complex shape.

This technique has the advantage of calculating the forces and moments associated with the added mass, the hydrodynamic damping, the control plane position, and the propeller thrust all in one physics based model. However, there are still many theoretical and practical problems that need to be solved before the approach becomes either common place or widespread. The main practical problem involves the computational effort required to perform the simulation. For example, Pankajakshan et al. (2002) states that when modelling the submarine and propeller a simulation time step of 0.001s was required. This took one hour of computation time on a Cray T3E-900 to advance the solution 0.03 seconds. Thus, even for parallelized super-computers the simulation takes many hundreds of hours. The key theoretical issues are associated with automatic mesh generation, modelling turbulence, and modelling flow separation. Substantial difficulties with all these areas still remain, and are current areas of research in the CFD community; see Bertram (2000) for an overview.

The next section provides an alternative method of calculating the hydrodynamic damping, added mass, and propulsion loads required for simulating Autosub.

3.5.1 Calculating the Added Mass

As has been stated the added-mass concept is primarily an inviscid fluid effect. It stems from the energy required to change the flow velocity of the fluid produced by a change in UV's velocity. For a deeply submerged UV the fluid can be treated as unbounded and as such the added mass is dependent solely on the shape of the

vehicle, the density of the fluid, and the direction of the acceleration.

As the added-mass is an inviscid effect it can be accurately calculated using potential flow theory. However, calculating the potential flow for an arbitrary shape is not straightforward, but the added mass can be simply estimated by assuming the vehicle is comparable in shape to a standard form for which an analytic solution is available. For slender bodies the local flow over a section is approximately 2-dimensional, thus the 2-dimensional added-mass for the section can be determined. By integrating the 2-dimensional added masses over the length of the body the 3-dimensional added mass can be calculated. This approach is known as strip theory, see Newman (1977).

Although the added-mass is an acceleration dependent force, due to the rotating nature of the local axis system the Coriolis and centripetal forces and moments need to be taken into account. The forces and moments can be represented by

$$\boldsymbol{C}(\boldsymbol{\nu})\boldsymbol{\nu}$$

Where $\boldsymbol{C}(\boldsymbol{\nu})$ represents the Coriolis and centripetal matrix described by Fossen (1994), and can be calculated from the added mass and inertia matrix $\boldsymbol{M}_A$.

Simplifications to the added mass matrix

The UVs for which the component build up method is applied tend to be streamlined torpedo shape vehicles, and as such can be considered as a body of revolution with cruciform tail fins (e.g. as Autosub). These UV have port-starboard and top-bottom symmetry, and under these conditions Prestero (2001b) states that the added mass matrix reduces to:

$$\boldsymbol{M}_A = \begin{bmatrix} X_{\dot{u}} & 0 & 0 & 0 & 0 & 0 \\ 0 & Y_{\dot{v}} & 0 & 0 & 0 & Y_{\dot{r}} \\ 0 & 0 & Z_{\dot{w}} & 0 & Z_{\dot{q}} & 0 \\ 0 & 0 & 0 & K_{\dot{p}} & 0 & 0 \\ 0 & 0 & M_{\dot{w}} & 0 & M_{\dot{q}} & 0 \\ 0 & N_{\dot{v}} & 0 & 0 & 0 & N_{\dot{r}} \end{bmatrix}.$$

Each element of the matrix is denoted using the standard SNAME naming convention.

The number of coefficient can be further reduced by noting that the vehicle has rotational symmetry, that is the shape can be rotated through 90° without changing form. Combining this with the fact that $\boldsymbol{M}_A$ is symmetrical, see Newman (1977), it follows that,

$$Y_{\dot{v}} = Z_{\dot{w}}, \qquad M_{\dot{w}} = N_{\dot{v}} = Z_{\dot{q}} = Y_{\dot{r}} \quad \text{and} \quad M_{\dot{q}} = N_{\dot{r}}$$

Hence, it is only necessary to find five added-mass values for the described torpedo shaped AUVs. Methods of estimating the added-mass coefficients are discussed in the following sections.

Calculating $Y_{\dot{v}}$, $N_{\dot{v}}$ and $N_{\dot{r}}$

The values of $Y_{\dot{v}}$, $N_{\dot{v}}$ and $N_{\dot{r}}$ have been estimated using strip theory by Prestero (2001b) for Remus and by Bø (2004) for Maya. In both cases the vehicles are decomposed into circular and finned sections. The finned sections are composed of a circular inner sections with four equally spaced fins radiating outwards. The two-dimensional radial added-mass values for these sections are given by Blevins (1993). For a circle the radial added-mass per unit length is,

$$\rho\pi r^2,$$

and for a finned section the radial added-mass is,

$$\rho\pi r^2 \left(1 - \frac{a^2}{r^2} + \frac{a^4}{r^4}\right);$$

where a is the radius of the circular inner section.

Following from this if m_{c_i} and m_{f_j} are the masses of the ith circular and jth finned sections respectively, and l_{c_i} and l_{f_j} are the associated distances from the origin, it then follows that:

$$\begin{aligned}
Y_{\dot{v}} &= \sum_i m_{c_i} + \sum_j m_{f_j} \\
N_{\dot{v}} &= \sum_i m_{c_i} \cdot l_{c_i} + \sum_j m_{f_j} \cdot l_{f_j} \\
N_{\dot{r}} &= \sum_i m_{c_i} \cdot l_{c_i}^2 + \sum_j m_{f_j} \cdot l_{f_j}^2
\end{aligned}$$

Calculating $X_{\dot{u}}$

As the vehicles to be analysed tend to be torpedo shaped the assumption of a slender form used by strip theory becomes invalid when estimating the surge added-mass and an alternative approach needs to be used. The general approach is to ignore the fins on the airship as they are assumed to contribute little to the added mass in the surge direction and to approximate the body to that of a known 3-dimensional form.

Munk (1923) estimated the $X_{\dot{u}}$ added mass for an airship by first assuming the ends were adequately modelled by a point source in nose and tail, and then assumed that the nose and tail were sufficiently far apart to negate any interaction between them. Thus, the airship was modelled as a Rankine ovoid with sufficient distance between the source and sink so that they did not significantly infiuence each other. The resultant total kinetic energy of the fiuid (T) was given as:

$$T = \frac{1}{6}\pi r^3 V^2 \rho.$$

Where, r is the maximum radius of the airship, V is the forward speed of the airship and ρ is the density of air. From this it follows that the added mass is:

$$X_{\dot{u}} = \frac{1}{6}\pi r^3 \rho.$$

This is equivalent $\frac{1}{4}$ of the mass of a sphere of radius equal to the maximum radius of the airship.

An alternative approach is to model the UV as an ellipsoid of revolution. The 'end-on' added-mass for this shape can be calculated analytically. Lamb (1932) gives the kinetic energy (T) of the fluid displaced by an ellipsoid of revolution with length l and radius r moving 'end-on' as,

$$2T = \frac{\alpha_0}{2-\alpha_0} \cdot \frac{4}{3} l r^2 \rho \cdot U^2.$$

Where,

$$\alpha_0 = \frac{2(1-\epsilon^2)}{\epsilon^3}\left(\frac{1}{2}\ln\frac{1+\epsilon}{1-\epsilon} - \epsilon\right),$$

and, ϵ is the eccentricity of the ellipsoid and is given by,

$$\epsilon^2 = 1 - \frac{r^2}{l^2}.$$

Thus, the added mass becomes,

$$X_{\dot{u}} = \frac{\alpha_0}{2 - \alpha_0} \cdot \frac{4}{3}\pi l r^2 \rho.$$

To give and idea of the differences between the methods Figure 4 shows the data for the normalized added-mass calculated using both approaches as a function of length to diameter ratio. The added-mass is normalized using a sphere of radius r equal to the maximum radius of the UV.

For Autosub the length to diameter ratio is about 7.8 and thus the two approaches give very similar results.

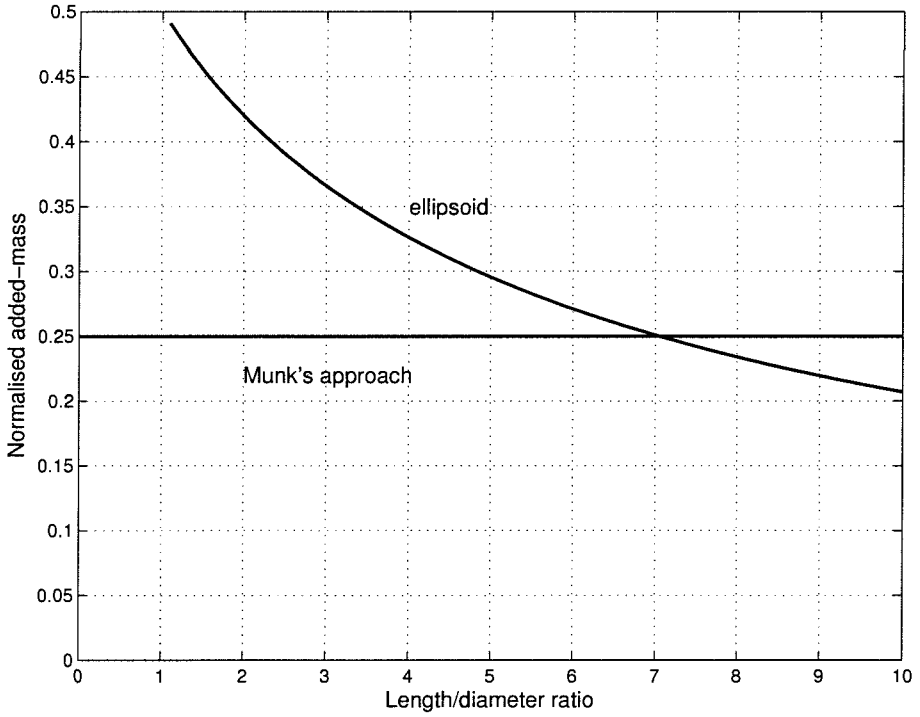

Figure 4: Comparison of the added mass of an ellipsoid and Munk's method normalized with the volume of a sphere of radius r.

Calculating $K_{\dot{q}}$

To calculate the added-inertia $K_{\dot{q}}$ of a torpedo shaped UV only requires the consideration of the finned section, as the body of revolution is assumed to have no added-inertia. Typically added-inertias can be calculated using the two-dimensional forms given in Blevins (1993) and Newman (1977), unfortunately, these authors do not give the added-inertia for a cylinder with cruciform fins. However, $K_{\dot{q}}$ has been approximated by Prestero (2001b) who assumed a simple cruciform section and hence ignored the presence of the inner cylindrical section, and by Bø (2004) who assumed a circular section with two fins, thus ignoring the second set of fins. From Newman (1977) the two approaches give the following added-inertias:

$$\begin{aligned} \text{Cruciform section} &\quad — \quad \frac{2}{\pi}\rho r^4 \\ \text{Finned cylinder} &\quad — \quad \rho a^2 \left[\frac{2\alpha^2 - \alpha \sin 4\alpha + \frac{1}{2}\sin^2 2\alpha}{\pi \sin^4 \alpha} - \frac{\pi}{2} \right]. \end{aligned}$$

Where,

$$\sin\alpha = \frac{2ar}{a^2 + r^2}, \qquad \frac{\pi}{2} < \alpha < \pi$$

and a is the radius of the inner circular section.

The results of the added-inertia calculated for the two methods are shown in Figure 5 along with the added-inertia of a plate (this is $\frac{1}{8}\pi\rho r^4$, see Newman (1977)). The figure shows that the added-inertias of the flat plate and the finned cylinder are reasonably similar for a/r ratios of 0.5 or less; above this value the added-inertias differ markedly. Assuming that the a cruciform finned cylinder behaves similarly to a flat plate finned cylinder counterpart the simple cruciform would give a estimate for the added inertia when a/r is 0.5 or less.

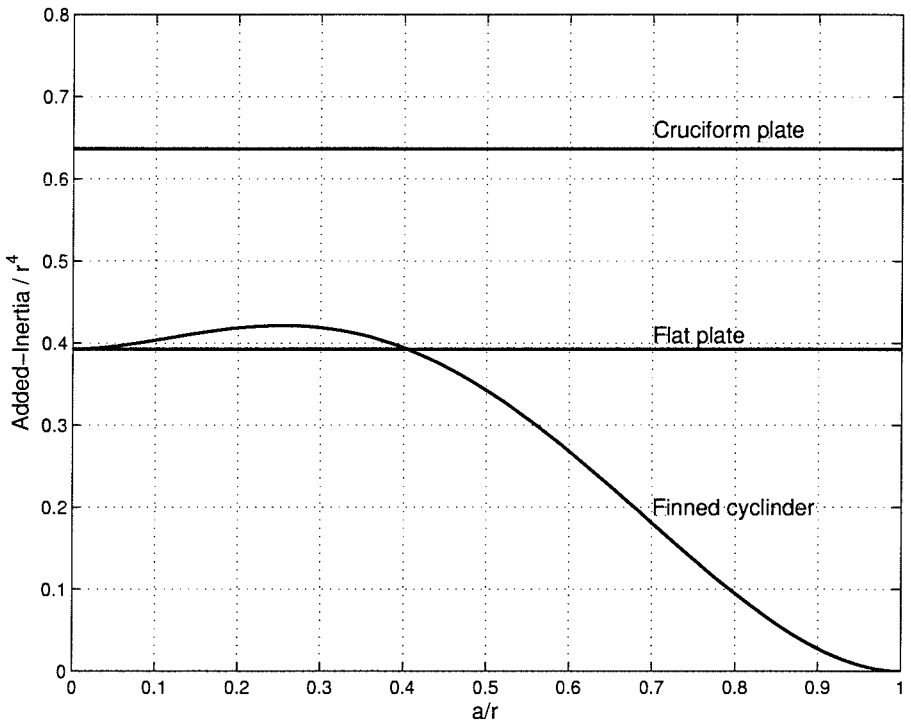

Figure 5: Comparison of the normalized added-inertias of a cruciform plate, a flat plate and a finned cylinder.

This completes how the added-masses and added-inertias of a torpedo shaped UV can be calculated for the component build up method.

3.6 Hydrodynamic Coefficients Method

In theory the hydrodynamic loads for a UV can be determined through experimentation. One can assume that the loads are dependent solely on the velocities and accelerations of the vehicle at any specific time instant (this is not strictly true as there is a time dependency in fluid flow, and so the current loads depend upon the time history of the vehicle, however as UVs accelerate slowly it is possible to ignore the effects and assume the system is in a quasi steady state). Also, if one ignores the effect of the control plane and propulsion system, the hydrodynamic loads will be some function f of $\boldsymbol{\nu}$ and $\dot{\boldsymbol{\nu}}$.

One possible method of determining the function f which describes the characteristics

of the forces and moment is to measure the loads experimentally for every possible motion. To make this approach viable one could investigate a fixed finite number of situations for each motion, covering the values of interest, and then test every combination of these motions. These results could then be interpolated to provide an estimate of the loads for any motion in the range of interest. As an example, if each motion was measured at 10 different values the process would required 10^{12} tests, as there are 12 velocities and accelerations to consider. Whilst this approach might be theoretically sound, the process is unworkable in practice.

However, the basic approach does have merit, but what is required is a method of approximating the loads that does not require the huge volume of testing implied above. If one was only interested in the loads produced within a small region of all the motions, for example small deviations about a straight, level, constant speed flight for a UV, it is possible to use a truncated multivariate Taylor series expansion to model the velocity and acceleration dependencies of the loads in this small region. The experimental testing would then be limited to determining the derivatives associated with the truncated Taylor series. This is the basis for the *Hydrodynamic Coefficient Method* proposed by Abkowitz (1969).

The Abkowitz method, and extensions to it, have been used extensively in the modelling of ocean going vehicles. A more detailed discussion of the procedure is presented next.

3.6.1 The Basic Approach

The basic approach outlined by Abkowitz assumes that the hydrodynamic loads are dependent upon:

- The vessels linear velocity – $\boldsymbol{\nu}_1$
- The vessels linear acceleration – $\dot{\boldsymbol{\nu}}_1$
- The vessels angular velocity – $\boldsymbol{\nu}_2$
- The vessels angular acceleration – $\dot{\boldsymbol{\nu}}_2$

- The control plane angles associated with rudder, bow and stern planes – δR, δB, δS

Thus, the X force in the x direction could be represented in the form:

$$F_X = f_X(\boldsymbol{\nu}_1, \boldsymbol{\nu}_2, \dot{\boldsymbol{\nu}}_1, \dot{\boldsymbol{\nu}}_2, \delta R, \delta S, \delta B)$$

It is not necessary to have these control planes, there are used here merely for illustration of a general submarine. No dependence upon the propulsion system is assumed as it is assume that the propulsion system will be kept in the same state as used for the reference motion.

This function f_X describing the X component of the hydrodynamic force component is then assumed to be sufficiently differentiable over the range of motion values of interested. Therefore, the function f_X can be decomposed using a multi-variate Taylor series expansion. By truncating the series and assuming that only small deviations from some reference motion (straight, level, constant speed flight for UVs) then a reasonable approximation to the X force component is generated.

The number of terms in the force equation generated by the truncated Taylor series can be reduced by noting the symmetries of the vehicle (usually $x - y$ plane). The terms can be further reduced using a knowledge of the physical phenomena being modelled. Reducing the coefficient count is necessary, as the number of terms in the truncated Taylor series quickly become unmanageable as the order of the approximation increases.

Hydrodynamic load equations truncated after the first derivative, generating a linear model, are used in stability analysis. However, the accuracy of the predictions for manoeuvring is limited as large deviations from the reference motion can generate large errors. Truncating the load equations later produces non-linear equations. These require more testing to determine the derivatives but the resulting equations approximate the loads better in more severe manoeuvres.

The approach described produces general force and moment equations for any vessel. However, within the equations are a number of unknown derivatives that must be specified to allow the equations to described the forces and moments for a specific

vehicle. These coefficients are classically known as hydrodynamic derivatives as they represent the partial differentials of the hydrodynamic loads, at the reference motion, an example being,

$$\frac{\partial f_X}{\partial u}.$$

This is the partial derivative of the force in the x direction with respect to the forward velocity u.

As there are a large number of terms in the force and moment approximations, using the partial differential notation is cumbersome therefore a separate notation was developed by SNAME. Here the above partial derivative would be written as X'_u, where X represents the force function f_X and the subscript u defines the variable of differentiation. Using this notation greatly simplifies writing the equations. It is also common practise to non-dimensionalise the derivatives.

For submarines the non-linear models developed using the classic approach have been modified to try and reduce the number of derivatives that need to be determined without sacrificing the accuracy of the modelled hydrodynamic loads. This approach is discussed next.

3.6.2 Modern Submarine Equations

More recent non-linear submarine equations, for example those described by Feldman (1979) and Booth et al. (1980), cannot be derived using a Taylor series expansion. The non-linear submarine equations are initially based on the Taylor series approach, but are then modified to reduce the coefficient count whilst adding the terms apparently ad hoc to increase the accuracy of the simulation.

One of the differences in the submarines equations is that they only use 2^{nd} order coefficients. Using a Taylor series the 2^{nd} order coefficients such as K'_{pp} produce an *even* function, that is, the sign of the moment (in this case) is independent of the sign of p. Thus, K'_{pp} has to be zero as otherwise it would imply that the hydrodynamic damping would produce a moment in the same axis as the direction of roll, a physically impossible phenomenon. However, this inherent problem is overcome in the submarine

equations by using $K'_{p|p|}$. As this is not a hydrodynamic derivative as it cannot be derived using the Taylor series, in this thesis these pseudo derivatives will be called *hydrodynamic coefficients.* Using these hydrodynamic coefficients in preference to the hydrodynamic derivatives allows the number of coefficients to be reduced as it is not necessary to use third order derivatives to increase the accuracy of *odd* functions.

The equations are systematically modified using other similar concepts to produce a more useful set of equations approximating the force and moments. Unfortunately the reasoning behind each coefficient's inclusion or exclusions is not readily available, thus it is not possible to derive the equations from first principles or explain how the equations were arrived at. However, as these equations are in common use in the simulation of submarines, and have been used to model AUVs, they were considered to be appropriate for creating the dynamic simulation of Autosub. However, the determination of the coefficients for Autosub stills needs to be addressed. Techniques for determining the coefficients are discussed next.

3.6.3 Modelling AUVs Using Submarine Equations

The submarine equations are designed to model naval submarines considerably faster and large than flight style AUVs. UK submarines vary in length from 83m for the Swiftsure class to 150m for the Vanguard class, and have a maximum submerged speeds in excess of 30 knots (15 $\text{m}\cdot\text{s}^{-1}$), as given by Sharpe (1996). Comparing this to Autosub with a length of 7m and a maximum submerged speed of 2 $\text{m}\cdot\text{s}^{-1}$, it is clear that Autosub operates at completely different speed and length scales. However, when one considers the manoeuvres produced by Autosub they are similar in form to those of the submarines.

Autosub mission typically involve long periods of straight and level flight followed by brief periods of sharp turning. This is illustrated in Figure 6 where Autosub is performing a lawnmower survey off the North-West Coast of Greenland — mission 367.

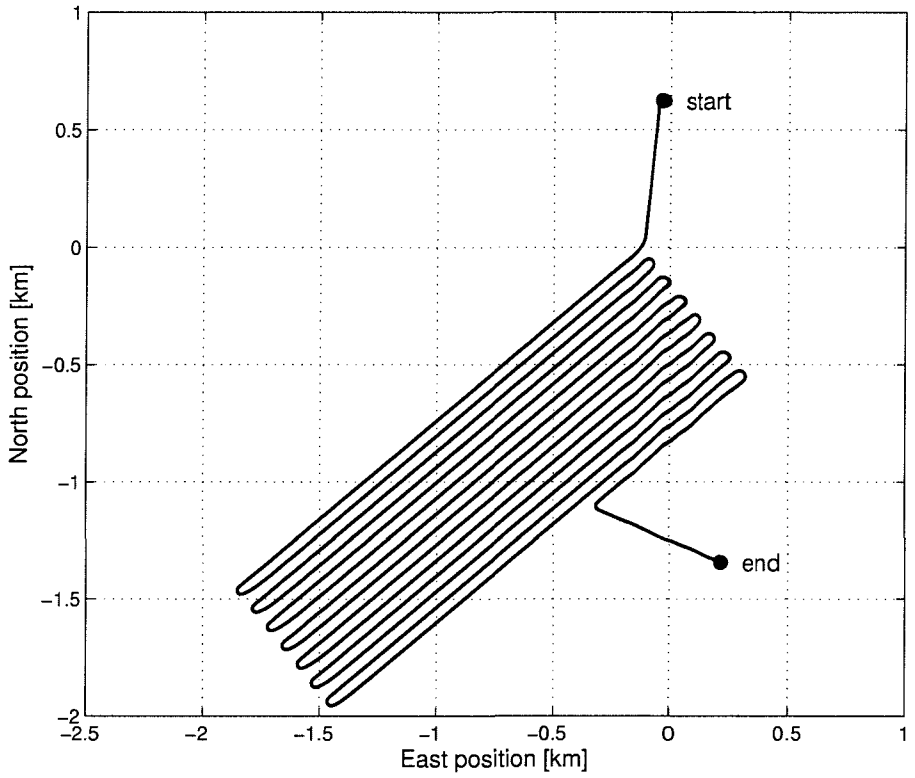

Figure 6: Lawnmower survey performed by Autosub 24/08/04 of the North-West coast of Greenland.

At the end of each survey leg the rudder is moved to $\pm 15°$ to turn the vehicle quickly onto the next track. The first turn of the lawnmower search is shown in more detail in Figure 7.

In Figure 7 a cross represents each recorded data point. The figure does not show a complete 180° turn, as Autosub's turning circle is smaller than the separation distance between the survey legs, so the final stages of the turn involve Autosub manoeuvring to join the next survey leg.

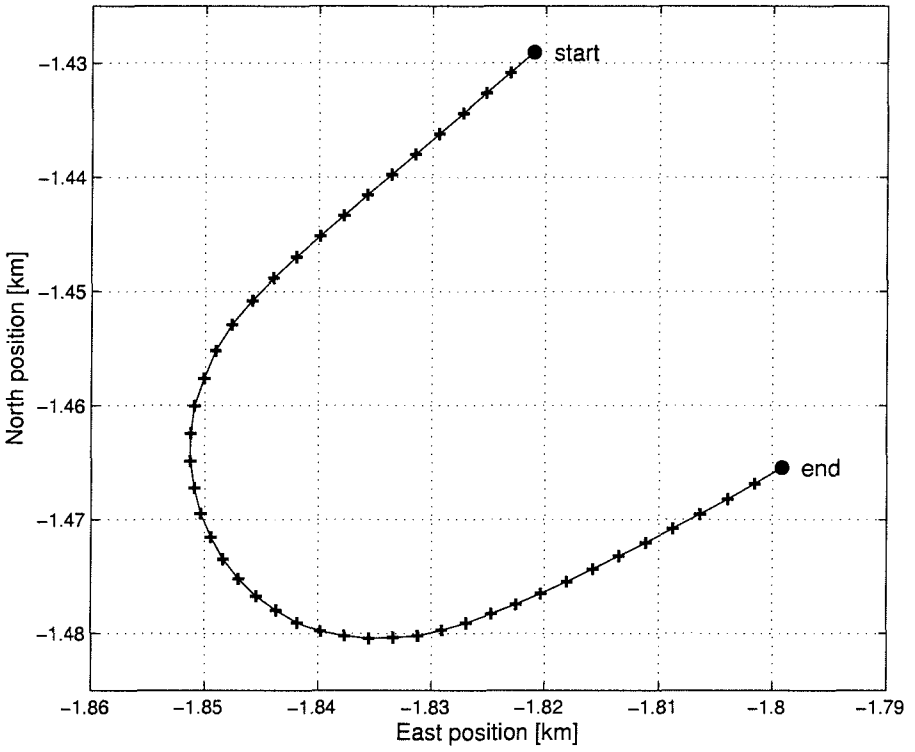

Figure 7: First turn of the lawnmower survey.

To compare this manoeuvre to that performed by a submarine, it needs to be non-dimensionalised. This is traditionally done using the vehicle length.

A comparison of this turn with that of submarine 1 travelling at $7.5\text{m}\cdot\text{s}^{-1}$ performing a turning circle manoeuvre with a 15° rudder angle is shown in Figure 8. In this figure the Autosub manoeuvre has been rotated so that the initial path of the manoeuvre lies along the figure's X-axis. When the Autosub track passes through the 0,0 point the rudder is applied. The Autosub path has also been corrected to remove the effect of the measured current.

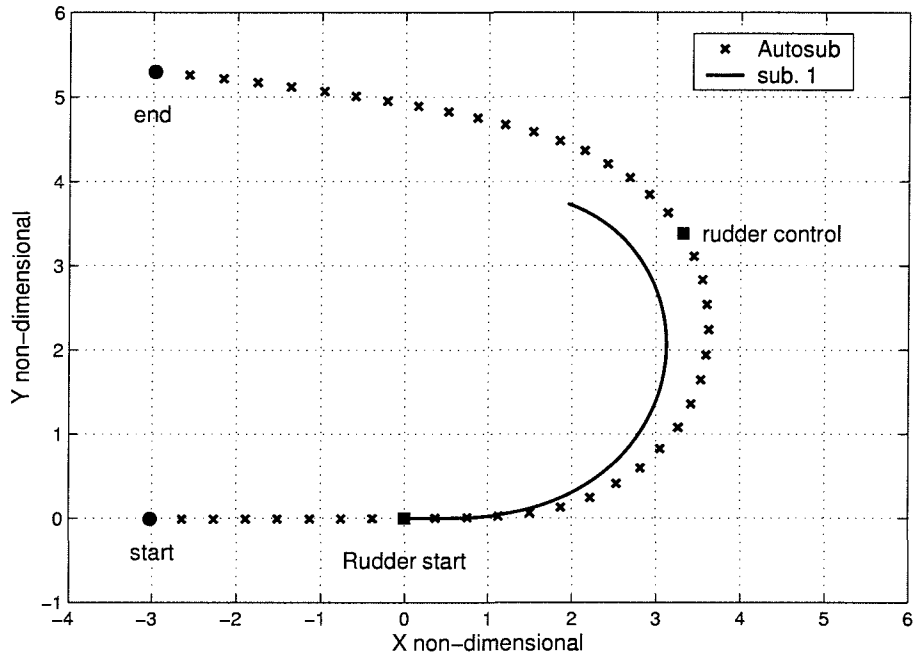

Figure 8: Non-dimensional Autosub and submarine 1 turning manoeuvre comparison.

During the initial part of the Autosub manoeuvre the rudder is controlled around 0°, this occurs between the 'start' and 'rudder start' marks on the plot. At the 'rudder start' point the rudder is moved to 15° and held constant until the 'rudder control' point. From here to the end of the manoeuvre the rudder is automatically adjusted so that Autosub smoothly joins the next survey leg. The submarine 1 manoeuvre follows the same basic pattern as that for Autosub except that the rudder is held at 15° after it has been applied.

Comparing the simulated manoeuvre of submarine 1 and the track of Autosub, it is clear that submarine 1 turns more quickly for a given angle of attack. However, the difference is not that substantial and further investigation revealed that a very good match between the Autosub and submarine 1 occurred when a rudder angle of 12° was applied to the submarine.

So although submarines and AUVs operate at different length and time scales, they produce similar non-dimensional manoeuvres, thus the submarine equations will be valid when used at the appropriate length and time scales for Autosub.

3.6.4 Free Running Model Tests

An alternative to forced captive model tests is to use free running model trials to identify the hydrodynamic coefficients. Here a scale model of the vessel (or the vessel itself) runs through a series of controlled manoeuvres, and the relevant control plane angle and vehicle motion information is recorded. This data can then be used to identify the vehicle's hydrodynamic coefficient values using system identification techniques. Considerable research has been performed into the identification of ship hydrodynamic coefficient values. This research started in the early 1970s and continues to date. Less research has been undertaken into the identification of underwater vehicle hydrodynamic coefficients, but with the growing interest in and use of AUV since the early 1990's activity in this area has increased. An introductory overview of the procedure for system identifying ship hydrodynamic coefficient values can be found in Lewis (1989a); while Fossen (1994) contains information on ship and UV system identification techniques. A brief discussion of the relevant ship and underwater vehicle research follows.

The ship identification problem is primarily concerned with determining the coefficients relating to the steering dynamics of the craft. To simplify the problem it is assumed that the heave, pitch and roll of the vehicle do not have an effect on the steering dynamics and hence can be decoupled from the full six-degree of freedom problem. The simplified coupled two-dimensional, surge-sway-yaw problem has been investigated extensively. Both linear and non-linear motion equations have been studied.

Åström and Källström (1976) considered the identification of the coefficient values associated with the linear dynamic equations for ships. The research showed that it was impossible to identify all the hydrodynamic derivatives in the model as the added-mass and added-inertia coefficients acted like the real masses and inertias. This coupling made the coefficients non-unique and hence unidentifiable. However, by specifying the added masses and inertias the remaining coefficients become unique and can therefore be identified. This added-mass issue also occurs in the non-linear equations of motion, and all subsequent identification procedures assume that the added-mass values are known.

Källström and Åström (1981) reviewed the research examining identification of ship steering dynamics. The work considered the non-linear equations of motion for ships attributed to Norrbin (1970). When identifying the hydrodynamic coefficient values associated with this model (excluding the specified added-mass coefficients) it was shown that the remaining coefficient values could not be accurately identified even though accurate path information was reproduced.

Haddara and Wang (1999) discussed the difficulty of identifying non-linear hydrodynamic coefficients from input-output records, when describing research into identification of the coefficients associated with the non-linear ship equations described in Lewis (1989a). The identification problems stemmed from coefficient error cancellation; that is errors in several coefficients cancel, thus making it a difficult to identify the correct coefficient values from input-output data. Haddara and Wang (1999) proposed a solution by calculating the linear hydrodynamic coefficient values using methods attributed to Clarke et al. (1983), and then training a neural network to model the forces and moments associated with the non-linear terms. The approach was tested using a simulated ship performing a $\pm 35°$ zig-zag manoeuvre. Once trained the resulting neural network was combined with the linear coefficients model and the resulting model was shown to produced accurate manoeuvring predictions for a 20° zig-zag, a 25° turning circle and a 20° Dieudonné spiral manoeuvre. The results suggest the procedure had accurately capture the dynamics of the simulated vessel. Regression analysis was then used to determine the hydrodynamic coefficient values associated with the neural network model and the full set of coefficients identified. The coefficients identified had values that were a poor match to the true coefficient values.

Yoon and Rhee (2003) used a different approach to identify the coefficient values. The method involved a two stage process to identify the non-linear hydrodynamic coefficient values of a third order model (again excluding the specified added-mass coefficients as before) using noisy manoeuvring data. The first stage of the procedure involved using an Extended Kalman Filter and modified Bryson-Frazier smoother to filter the motion data to determine the best estimate of the ship motions. The second stage used the processed data to generate regression matrices. The hydrodynamic coefficients were then calculated from these regression matrices using a least-squares

error approach. The identification procedure was used to identify the coefficients of a simulated ship performing a 35° turning circle and a ±20° zig-zag manoeuvre. The identified coefficients accurately reproduced a manoeuvre generated using a 10° (PRBS) rudder command, however the coefficients were poorly identified. Correlation analysis of the regression matrices showed that the hydrodynamic coefficients were highly correlated and hence difficult to identify.

The results of the ship identification testing show that it is not possible to identify the hydrodynamic coefficients of the two-dimensional surge-sway-yaw motion equations without specifying the added-mass hydrodynamic coefficients. The results also suggest that it is extremely difficult to identify the non-linear coefficient values due to the correlation between the different coefficients, as these correlations results in the error cancellation effect.

As stated, identification of the hydrodynamic coefficients for UVs has been less thoroughly researched. Marco and Healey (1998) have identified a simplified model of the surge motion coefficients for the Naval Postgraduate School (NPS) AUV Phenoix, and Ridao et al. (2001) have reported identifying the coefficients for a simple decoupled set of hydrodynamic load equations for the GARBI AUV. However, no research has been found in the literature that applied system identification techniques to determine all the coefficients used in a set of non-linear submarine equations of the type described in Feldman (1979).

If identification of the hydrodynamic coefficients used in a set of non-linear submarine equations was possible then the approach could be easily used on Autosub. This may require that specific *identification manoeuvres* are performed during deployments of Autosub at sea or it may be possible to use the extensive library of Autosub manoeuvres from previous deployments.

As has been highlighted in the ship identification research one of the issues with using system identification techniques is the possibility of identifying a set coefficient values that are different from the true captive model derived values. The identified coefficients may reproduce the identification manoeuvre accurately but may not reproduce other manoeuvres with the same fidelity. Thus, it is important to try and identify the captive model testing derived coefficient values.

Both the Component Build up Method and the hydrodynamic coefficient approach do not, of themselves, model the propulsion loads applied to UV. Possible propulsion models, suitable for UVs, are discussed in the following section.

3.7 Modelling Propeller Thrust and Torque

Propulsion modelling is a well researched area of naval architecture. Overviews of this topic are given in Lewis (1989b) and Bertram (2000), whilst Breslin and Andersen (1994) lays out the subject in more detail. The following sections briefly summarize the propeller modelling methods applied to UVs.

When modelling the propulsion system of an UV the factors of interest are the forces and moments applied to the vehicle by the propulsion system. Thus, it is necessary to know the force and moment vector,

$$\boldsymbol{\tau}_n = [X_n, Y_n, Z_n, K_n, M_n, N_n]^T$$

at any given instant in time.

It is usual to calculate the loads produced by a propeller in isolation. The loads are then calculated with the propeller moving forward relative to the water. This produces the *open water* performance. The propeller is assumed to produce a thrust (T) parallel to the axis of rotation of the propeller and a torque (Q) about the axis of rotation as illustrated in Figure 9.

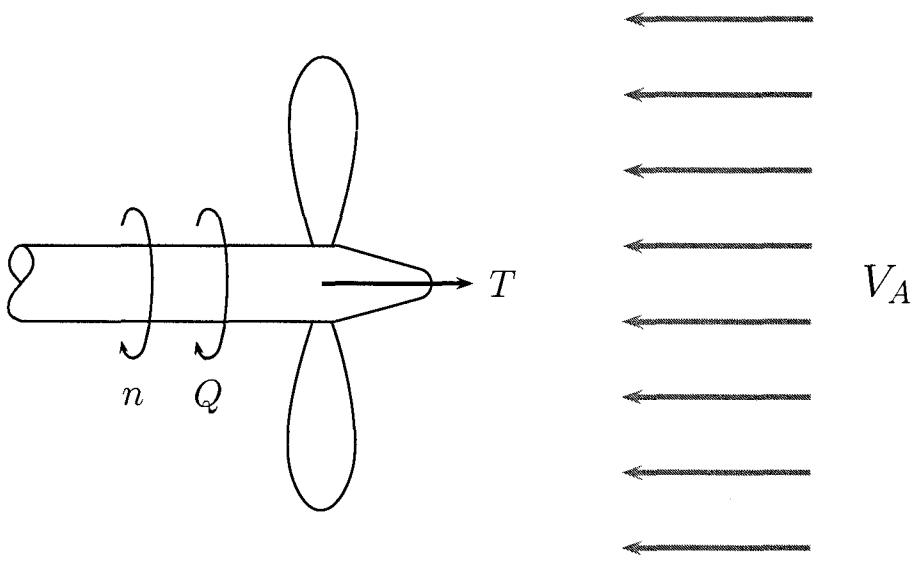

Figure 9: Schematic of a propeller operating in open water.

These open water results are usually expressed non-dimensionally using the following coefficients:

$$K_T(J) = \frac{T}{\rho n^2 D^4} \tag{3}$$
$$K_Q(J) = \frac{Q}{\rho n^2 D^5}$$
$$J = \frac{V_A}{nD}$$

Subject to the following notation:

- n — Propeller revolutions rate [rps].
- D — Propeller diameter [m].
- V_A — Speed of advance of the propeller [m·s^{-1}].
- J — Propeller advance coefficient, a non-dimensional velocity.

The open water performance for a propeller cannot be directly used to determine the performance when installed on an UV as two mechanisms affect the open water performance. The first mechanism is known as the *thrust deduction* factor. The thrust deduction factor describes how the open water thrust of a propeller is apparently

reduced when installed on a vehicle. This thrust reduction can be explained by the reduction in pressure at the rear of the vehicle caused by the increased flow produced by the propeller. This drop in pressure at the rear of the vehicle produces an increase in pressure drag on the body and this must be overcome by the thrust produced by the propeller. Hence, the propeller thrust is seen to be reduced. This thrust reduction factor is simply modelled as a multiplicative correction factor, namely,

$$R_T = (1 - t)T \tag{4}$$

where,

R_T — bare hull resistance of ship (N)

T — open water thrust of the ship (N)

t — thrust deduction factor for ship subject.

The second factor affect the open water performance of a propeller arises from the concept of a *Wake fraction.* This wake fraction describes the relationship between the flow speed into the propeller and the speed of advance of the ship. When a vehicle is advancing forward the mean flow into the propeller is less than the advance speed of the vehicle. This reduction in flow speed into the propeller is due to the boundary layer surrounding the vehicle. Thus, the open water speed of advance for the propeller can be calculated from the vehicle advance speed using a wake faction. This is done using the following expressions:

$$w_T = \frac{V - V_A}{V} = 1 - \frac{V_A}{V} \tag{5}$$

or

$$V_A = (1 - w_T)V.$$

With additional parameters defined as

$w_T =$ Taylor wake fraction.

$V =$ Ship speed.

$V_A =$ Average water velocity into the propeller disc.

Combining Equations (3), (4) and (5) the thrust from the installed propulsion system is

$$T_r = (1-t)\rho n^2 D^4 K_T\left(J'\right)$$

with

$$J' = \frac{(1-w_T)\,V}{nD} \equiv (1-w_T)\,J.$$

In this case T_r and J' are the effective thrust on the vehicle and the modified advance coefficient.

Thus for this quasi-steady state model of the propulsion system thrust, it is necessary to have knowledge of the thrust coefficient K_T. Several different approximations of the function have been used in modelling UVs and are discussed in Section 3.7.1

Once the open water thrust (T) and torque (Q) for the propeller have been determined, it is necessary to describe these in terms of $\boldsymbol{\tau}_n$. To do this it is necessary to express T and Q in the body fixed axis of the UV. If the main propulsion system comprises a single screw propeller with the thrust direction parallel to the x axis and acting through the origin of the body coordinate system, as is the case with Autosub, then the forces and moment vector becomes,

$$\boldsymbol{\tau}_n = [T, 0, 0, Q, 0, 0]^T = [X_n, 0, 0, K_n, 0, 0]^T.$$

This describes the general model of the propulsion system for Autosub. But to create the specific $\boldsymbol{\tau}_n$ it is necessary to determine K_T, K_Q, w_T and t. However, before considering the methods of determining the data various formulae outlined in the UV literature to describe K_T and K_Q are discussed.

3.7.1 Modelling K_T and K_Q

In standard submarine simulations it is common to equate the value of K_T and K_Q to J dependent polynomials. Three different models, as outlined in Appendix C, have

been identified in the literature, for K_T, these are:

$$K_T = \alpha_1 \qquad \text{— given by Healey and Lienard (1993).}$$

$$K_T = \alpha_1 + \alpha_2 J \qquad \text{— given by Fossen (1994).}$$

$$K_T = \alpha_1 + \alpha_2 J + \alpha_3 J^2 \qquad \text{— given by Booth et al. (1980).}$$

The propulsion model presented in Healey and Lienard (1993) is for the Naval Postgraduate School (NPS) AUV II vehicle. This AUV has twin propellers and the torque produced by the propellers cancel and hence are not modelled. Thus, K_Q for the model is zero. Fossen (1994) and Booth et al. (1980) both use the same propeller torque model, that is,

$$K_Q = \beta_1 + \beta_2 J.$$

By assuming that K_T and K_Q are of a polynomial form simplifies the UV simulation procedure as the thrust and torque can be easily calculated for any advance ratio. Methods of determining the associated K_T and K_Q coefficients used in the propulsion model are considered next.

3.7.2 Determining the Propulsion Data

The open water values of K_T and K_Q can be found experimentally from model testing in a circulating water tunnel or a towing tank. In these tests the thrust and torque are measured for a given water flow into the propeller (V_A) known as the *speed of advance* and a given propeller rotation rate (n) usually measured in revolutions per second. From this testing of the steady state performance it is possible to create a mapping of the functions of K_T and K_Q against J. The measured data can then be fitted to one of the polynomial models described previously. Alternatively the coefficients can be determined analytically using techniques such as blade element theory and CFD. These analytical techniques are generally less accurate than model experiments.

The wake fraction can be measured for the bare hull of a vessel by using pitot tubes, particle image velocimetry (PIV) and such like. This information gives the *nominal* wake fraction. This nominal wake fraction needs to be modified when the propeller is added, as the propulsion system modifies the wake behind the vehicle, thereby

creating the *effective* wake fraction. This effective wake fraction can be calculated by measuring the thrust or torque at a given speed of advance of a ship and then comparing the thrust or torque to the open water results to determine J for the propeller. By comparing the J value into the propeller and the ship speed of advance, a wake fraction can be determined. The wake fraction is assumed to be constant throughout the speed range. As this is not necessarily so the wake fraction should be calculated for the reference motion of the vehicle to model the propeller thrust and torque accurately over this range.

The thrust reduction factor can be found using self propulsion trials. Here the propeller is installed on the vehicle and the propeller rpm at self propulsion for a given vehicle speed of advance is found. Using this information, the wake fraction and the open water results it is possible to determine the thrust deduction factor for the propeller.

The advantage in using this approach is that once the open water characteristics of a propeller have been found using that propeller on a different vehicle only requires the thrust reduction factor and the wake fraction. As determining this data is relatively simple the propulsion characteristics of the propeller vehicle system are easily found. However, if only the propulsion characteristic for a given propeller vehicle system are required and the open water characteristic of the propeller have not been characterized then describing the propulsion system as above is overly complex.

An alternative method of defining the propulsion characteristics is to ignore the thrust reduction factor and wake fraction concepts and to measure the K_T and K_Q values when applied to the vehicle. For example, the values of the α's and β's used in the Booth et al. (1980) model are determined from acceleration and deceleration trials of the actual submarine. Trials such as this are relatively simple to carry out on Autosub and hence would be a relatively straightforward way of determining the propulsion characteristics for Autosub. However, care would need to be taken when performing these tests as although Autosub logs all the appropriate manoeuvre data, the logging process is not designed to accurately record vehicle motions. Also, to determine K_T would requires a knowledge of the added-mass and hydrodynamic damping in the X force direction. Despite these challenges this form of testing would be well suited to

Autosub.

3.8 Conclusions

This chapter has reviewed how the loads on an UV can be modelled. It started by describing how the loads arise and then outlined the various sources of loads that makeup the total load on the UV. It was shown how the hydrostatic loads can be determined analytically. Thereafter methods of determining the remaining hydrodynamic and propulsion loads were presented. Three separate methods of modelling the hydrodynamic loads were described, these were CFD, the Component Build-up Method, and then the hydrodynamic coefficient method. The hydrodynamic coefficient method was considered to have the best accuracy; it was decide to use a set of non-linear submarine equations to model Autosub. These equations would require the hydrodynamic coefficient associated with Autosub to be determined. As there were not sufficient funds to determine the coefficients using captive model testing it was decided to attempt to system identify the coefficients using submarine trials data. The method for identifying these coefficients is outlined in the next chapter.

Chapter 4

System Identification of Hydrodynamic Coefficients

4.1 Introduction

Having considered the modelling of the motion simulation of an UV and elected to follow the naval architectural practice of using hydrodynamic coefficient based estimations of the external forces and moments, the problem of determining the coefficients had to be addressed. In this case serendipity played an important role. Whilst methods other than experimental captive model testing were being considered, as described in Chapter 3, exchanges regarding collaborative research between the Ship Science department of the University of Southampton and QinetiQ (Haslar) were under discussion. One particular task was to use system identification software developed within the University of Southampton to identify the hydrodynamic coefficients of submarines from a knowledge of the path traversed and the time histories of the different control surfaces. It seemed logical that if one could successfully system identify the hydrodynamic coefficients of submarines then the method ought to be transferable to torpedo shaped AUVs such as Autosub.

A number of potential benefits were recognized within the proposed collaborative research, namely:

- The system identification approach could potentially use the large library of Autosub's manoeuvres to predict the coefficients or could perform special identification manoeuvre during deployments at sea. Both options were inexpensive thus were within the budget of the project. Whereas the funds required to identify the coefficient using captive model testing were not available.
- QinetiQ's knowledge of submarine modelling could be used to inform the modelling of Autosub. Also, the submarine governing equations used by QinetiQ (similar in form to the equations in Feldman (1979)) could be used to simulate Autosub. These governing equations are well developed and have been used to model the Naval submarines for the last two decades.
- Sets of Hydrodynamic coefficients for real submarines were available to test the performance of the identification procedure.

As these benefits were considerable it was decided to proceed with the collaborative research.

This chapter outlines the identification task posed by QinetiQ, discusses the submarine equations used and then outlines possible approaches to the QinetiQ task. Following this, the role of the manoeuvres selected for the determination of the identification procedure is considered. The chapter concludes by discussing the standard manoeuvres used to test the identification procedure.

4.2 The QinetiQ Task

The task posed by QinetiQ was:

> Can the hydrodynamic coefficients used to simulate a submarine be determined from a knowledge of submarine positional & attitude time history and the control time history for a manoeuvre, when these measurements are subject to noise and the submarine is subject to disturbances?

This task is represented graphically in Figure 10.

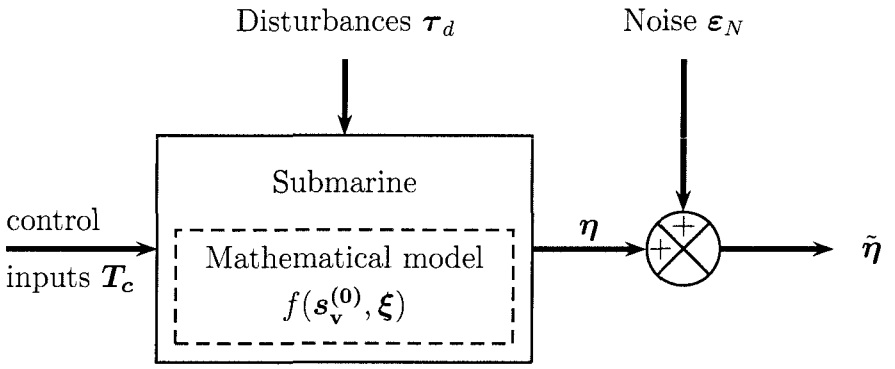

Figure 10: Outline of the QinetiQ question

Figure 10 shows the control inputs to the submarine or simulation as $\boldsymbol{T_c}$ and the disturbance input as $\boldsymbol{\tau_d}$. Within the model the starting condition of the submarine at the beginning of the manoeuvre are described by $\boldsymbol{s_v^{(0)}}$ and the hydrodynamic coefficients by $\boldsymbol{\xi}$. The position and attitude output from the submarine or simulation at a given time instant is $\boldsymbol{\eta}$. This is subject to noise $\boldsymbol{\varepsilon_N}$, which produce a final output $\tilde{\boldsymbol{\eta}}$. Letting,

$$\boldsymbol{N} = [\tilde{\boldsymbol{\eta}}(0), \tilde{\boldsymbol{\eta}}(t_1), \tilde{\boldsymbol{\eta}}(t_2), ...\tilde{\boldsymbol{\eta}}(t_n)]^T,$$

the QinetiQ task becomes,

> Given $\boldsymbol{N}$ and $\boldsymbol{T_c}$ for a manouevre can you find the submarine hydrodynamic coefficients $\boldsymbol{\xi}$?

As was discussed in Section 3.6.4 research has be undertaken to identify of hydrodynamic coefficients of UVs. However, this research has only considered simplified hydrodynamic coefficient models. The identification of the coefficients for a fully coupled six degree of freedom UV model has not been found in the consulted literature.

4.3 The QinetiQ Submarine Equations

The submarine equations used by QinetiQ are essentially those attributed to Booth et al. (1980). The equations describing the hydrodynamic forces and moments are reproduced in Appendix D. The equations use the standard 'Newton-Euler' formulation of the rigid body dynamics reported in Section 2.2. They also use the xyz Euler angle system to define the attitude of the UV. Thus, the rotation matrix $\boldsymbol{J}_1(\boldsymbol{\eta}_2)$ and the Euler angle update matrix $\boldsymbol{J}_2(\boldsymbol{\eta}_2)$ derived in Section 2.1.1 are used by the governing equations.

The equations describe a 'classical' naval submarine with a single screw propeller, bow & stern dive-planes, and a rudder. The vehicle control inputs are the propeller rpm (n), rudder angle (δR), bow dive-plane angle (δB), and stern dive-plane angle (δS).

4.4 Addressing the QinetiQ Task

To determine the hydrodynamic coefficients used in the Booth et al. (1980) equations from a submarine's positional and attitude time history $\boldsymbol{N}$ with no measurement error and its control input history $\boldsymbol{T_c}$ is challenging. This is because simulation output $\boldsymbol{\eta}$ at any time instant is related to the hydrodynamic coefficients ($\boldsymbol{\xi}$) through an integrated set of non-linear coupled differential equation (see Appendix D). Thus, there is no obvious analytical approach to solving the problem.

However, two potential techniques were identified. The first technique involved tackling the non-linear problem head on by trying to identify a set of hydrodynamic coefficients $\hat{\boldsymbol{\xi}}$ (an estimate of $\boldsymbol{\xi}$) that would reproduce the target (*identification*) manoeuvre $\boldsymbol{N}$. The second involved reforming the Booth et al. (1980) equations into a linear system, and then using either Linear Programming (LP) or linear algebra techniques to determine $\hat{\boldsymbol{\xi}}$. It was important that $\hat{\boldsymbol{\xi}} = \boldsymbol{\xi}$ for the techniques as, although a set of coefficients $\hat{\boldsymbol{\xi}} \neq \boldsymbol{\xi}$ may produce the same manoeuvre, it is not necessarily the case that the identified coefficients $\hat{\boldsymbol{\xi}}$ would provide acceptable predictions for all other manoeuvres.

The linear and non-linear approaches are outlined in the following sections.

4.4.1 The Linear Procedure to Identify ξ

Although the Booth et al. (1980) submarine equations are coupled, non-linear differential equations when used to predict the position and attitude of an UV, they can be rearranged so that the hydrodynamic coefficients can be solved in a linear fashion. This is demonstrated using the equation governing the acceleration along the x-axis. The rigid body accelerations, or the left hand side of the equations of motion, are,

$$m\left[\dot{u} - vr + wq - X_G(q^2 + r^2) + Y_G(pq - \dot{r}) + Z_G(pr + \dot{q})\right] = X,$$

and the force model used in the Booth et al. (1980) equations is,

$$\begin{aligned} X = & \frac{1}{2}\rho l^2 \left(X'_{uu}u^2 + X'_{vv}v^2 + X'_{ww}w^2\right) \\ & + \frac{1}{2}\rho l^3 \left(X'_{\dot{u}}\dot{u} + X'_{vr}vr + X'_{wq}wq\right) \\ & + \frac{1}{2}\rho l^4 \left(X'_{qq}q^2 + X'_{rr}r^2 + X'_{rp}rp\right) \\ & + \frac{1}{2}\rho l^2 u^2 \left(X'_{uu\delta\delta R}\delta R^2 + X'_{uu\delta\delta B}\delta B^2 + X'_{uu\delta\delta S}\delta S^2\right) \\ & + (B - mg)\sin\theta \\ & + X_n. \end{aligned}$$

These two equations can be combined and expressed in a matrix form as,

$$\frac{1}{2}\rho l^2 \left[u^2, v^2, w^2, \cdots, u^2\delta S^2\right] \begin{bmatrix} X'_{uu} \\ X'_{vv} \\ X'_{ww} \\ \vdots \\ X'_{uu\delta\delta S} \end{bmatrix} = \begin{bmatrix} m\left[\dot{u} - vr + wq - \cdots + Z_G(pr + \dot{q})\right] \\ -(B - mg)\sin\theta - X_n \end{bmatrix}.$$

So provided that the UV's attitude ($\boldsymbol{\eta}_2$), velocity ($\boldsymbol{\nu}$), acceleration ($\dot{\boldsymbol{\nu}}$) and control input ($\boldsymbol{T_c}$) are sampled at various times during a manoeuvre, a set of linear equations

can be created for the manoeuvre with each equations representing one sample period. These equations can be combined into the following matrix equation,

$$\boldsymbol{A}\boldsymbol{\xi}_X = \boldsymbol{b}. \tag{6}$$

Here,

$\boldsymbol{A}_X$ — The matrix of hydrodynamic coefficient multipliers.

$\boldsymbol{\xi}_X$ — The column vector of 'X' hydrodynamic coefficients.

$\boldsymbol{b}_X$ — The column vector of 'constant' terms.

As each row of the $\boldsymbol{A}_X$ matrix and the $\boldsymbol{b}_X$ vector represent one time sample period, the matrix equation (6) forms an over determined set of linear equations. The equation can be solved using least squares techniques or reformulated into a linear programming (LP) problem and solved using LP techniques.

An overview of the basic procedure is represented in Figure 11. The inputs to the submarine are the control input time history, $\boldsymbol{T_c}$, and $\boldsymbol{s}_{\mathbf{v}}^{(0)}$ is the initial state vector of the submarine, $\boldsymbol{s}_{\mathbf{v}}^{(0)}$.

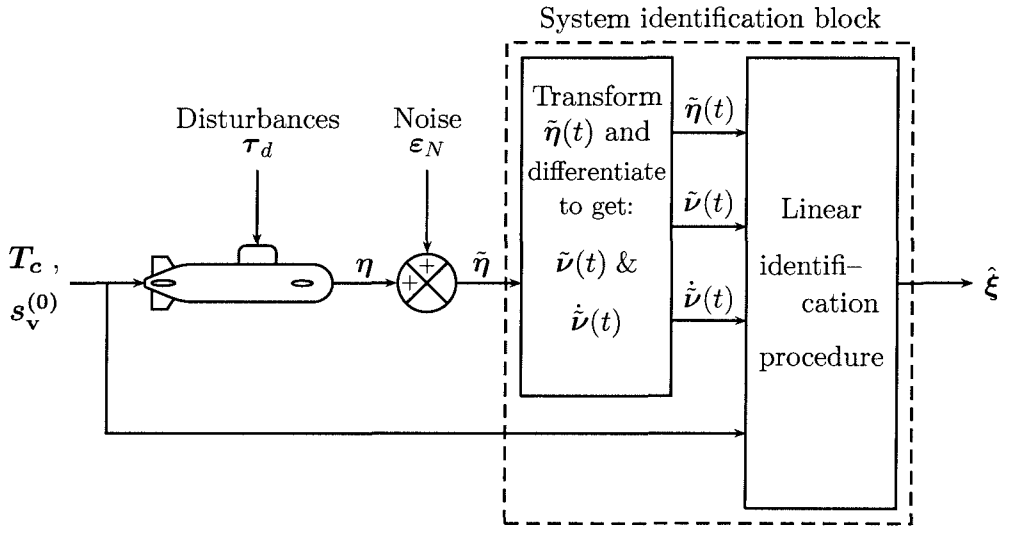

Figure 11: Schematic of the linear parameter identification procedure.

The principal problem with this approach is accurately determining $\boldsymbol{\nu}$ and $\dot{\boldsymbol{\nu}}$ from

$\tilde{\boldsymbol{\eta}}$ at each time step. This can be done by transforming the values of $\tilde{\boldsymbol{\eta}}$ into the local axis system and then double differentiating. However, the presence of the noise would lead to substantial errors in the calculated velocities and accelerations. For this reason it was initially decided that this technique was not appropriate to address the QinetiQ task. However, what was not initially appreciated was the fact that the QinetiQ task was subtly different to the Autosub problem as the instrumentation of Autosub is such that the attitude, velocities and acceleration are known and hence the stated criticisms of the approach are not justifiable for the Autosub case. The reasons for these differences and the performance of the linear approaches are discussed in detail in Chapter 9, whereas Chapter 6 address the uniqueness of the hydrodynamic coefficients by examining the rank of the influence matrix $\boldsymbol{A}_X$.

4.4.2 The Non-linear Procedure to Identify $\boldsymbol{\xi}$

The non-linear approach tries to identify the hydrodynamic coefficients $\boldsymbol{\xi}$ directly and is represented graphically in Figure 12. This figure shows the basic outline of the procedure and identifies the key steps involved.

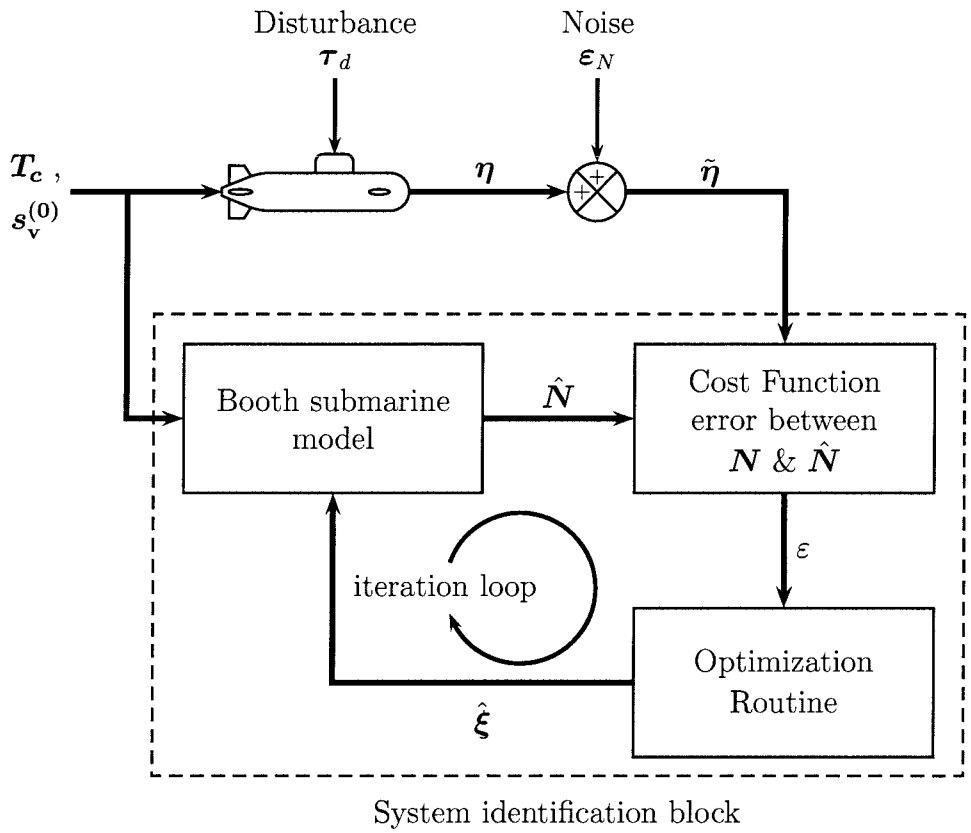

Figure 12: Schematic of the non-linear parameter identification scheme.

In this figure $\boldsymbol{T_c}$ represents the control input time histories for the manoeuvre performed by the real and simulated submarines, and $\boldsymbol{s_v^{(0)}}$ represents the initial state vector of the submarine and simulation. The simulation output $\hat{\boldsymbol{N}}$ represents the simulated manoeuvre time history produced using the latest estimate of the hydrodynamic coefficient vector $\hat{\boldsymbol{\xi}}$.

The basic procedure for determining the set of hydrodynamic coefficient is,

1. Initially estimate the hydrodynamic coefficient vector $\hat{\boldsymbol{\xi}}$.
2. Run the simulation with the estimated coefficient $\hat{\boldsymbol{\xi}}$ and determine the UV path $\hat{\boldsymbol{N}}$.
3. Compare the estimated path $\hat{\boldsymbol{N}}$ and the target path $\boldsymbol{N}$ to form a scalar quantity ε representing the error between the two paths using a defined cost function.

4. Use the optimization routine to estimate a new hydrodynamic coefficient set $\hat{\boldsymbol{\xi}}$ that reduces the path error ε.

5. Repeat steps 2–4 until some convergence conditions have been satisfied.

6. Output the final estimate of hydrodynamic coefficient $\hat{\boldsymbol{\xi}}$.

There are three key areas in defining this identification approach, they are the selection of the manoeuvre used for the identification ($\boldsymbol{T_c}$), the optimization routine used and the cost function used to measure the error between $\boldsymbol{N}$ and $\hat{\boldsymbol{N}}$.

The selection of the manoeuvre is considered in more detail in Section 4.5. The cost function and optimization routine are outlined next.

The Cost Function used in the Non-linear Identification Procedure

The purpose of the cost function was to produce a scalar metric (ε) of the closeness of the estimated manoeuvre $\hat{\boldsymbol{N}}$ to the target manoeuvre $\boldsymbol{N}$. The constraints for this cost function form were that it should be minimal when $\hat{\boldsymbol{N}}$ equalled $\boldsymbol{N}$ and should increase as $\hat{\boldsymbol{N}}$ moved further from $\boldsymbol{N}$. The chosen method of producing this was to use the sum of the squares of the errors between $\boldsymbol{N}$ and $\hat{\boldsymbol{N}}$.

The $\boldsymbol{N}$ and $\hat{\boldsymbol{N}}$ matrices are both sized $n \times 6$. The columns of $\boldsymbol{N}$ contain the known positions x, y & z (in metres) and attitudes ϕ, θ & ψ (here measured in degrees), with each row corresponding to a different point in time. Whereas the columns of $\hat{\boldsymbol{N}}$ represent the estimated positions $\hat{x}$, $\hat{y}$ & $\hat{z}$ and attitudes $\hat{\phi}$, $\hat{\theta}$ & $\hat{\psi}$. Thus, the cost function can be written as,

$$\varepsilon = \sum_{i=1}^{n} [\hat{x}(t_i) - x(t_i)]^2 + [\hat{y}(t_i) - y(t_i)]^2 + \cdots + \left[\hat{\psi}(t_i) - \psi(t_i)\right]^2.$$

This cost function is manoeuvre dependent. It is not appropriate to compare the cost function values between manoeuvres as the value only gives the relative level of agreement between $\boldsymbol{N}$ and $\hat{\boldsymbol{N}}$ for a specific manoeuvre.

The Optimization Routine used in the Non-linear Identification Procedure

The optimization routine was required to adjust $\hat{\boldsymbol{\xi}}$ to minimize the value of ε. There are many different non-linear optimization routines available but no particular routine has been found to be optimal in all applications, for an overview of the subject see Fletcher (1987). Broadly the routines can be broken into *local* and *global* optimizers. The local optimizers are designed to find the minimum or maximum point in a local area, whereas the global optimizers are designed to find the global maximum. This is illustrated in Figure 13.

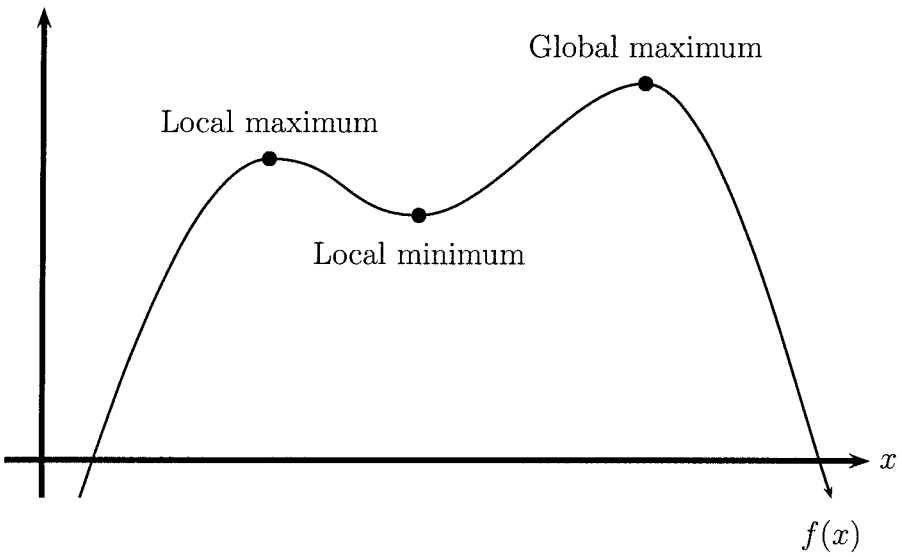

Figure 13: Example of local and global maxima and minima

As local optimizers are quicker at finding a solution, and as it was felt that the problem domain would not have many local optima, the optimization routine was chosen to be a local optimizer. As part of the QinetiQ identification team Professor Veres of the University of Southampton had implemented a Sequential Quadratic Programming (SQP) procedure in Matlab, this is an advanced local optimizer that has shown good performance in solving constrained non-linear problems. It was decided to use this code as the optimization routine. This, restricted the implementation of the motion simulation code to the Matlab computing environment. Although Matlab is somewhat slow in execution, it allows rapid code development so Matlab would have been an

appropriate choice even without this restriction. The details of the SQP procedure are outlined in Section 7.2.

4.4.3 Analysis of the Two Approaches

The detailed implementation and testing of the two approaches are discussed in Chapter 7 for the non-linear approach and Chapter 9 for the linear approach.

Both coefficient identification approaches require a UV output $\boldsymbol{N}$ and UV inputs $\boldsymbol{T_c}$ & $\boldsymbol{s_v^{(0)}}$ to work. As real submarine data is time consuming and expensive to acquire it was decided to used simulated data to generate $\boldsymbol{N}$ from $\boldsymbol{T_c}$ & $\boldsymbol{s_v^{(0)}}$. This had the advantage that the data was not subject to noise or disturbances. But, it did require creation of a general submarine simulation with applications based on realistic submarine coefficients to produce $\boldsymbol{N}$.

It was thought that using only one set of submarine coefficients $\boldsymbol{\xi}$ to produce the manoeuvres could lead to 'tuning' of the system identification procedure to the selected vehicle, so data for three submarines was supplied by QinetiQ. Thus, for any trial manoeuvre ($\boldsymbol{T_c}$, $\boldsymbol{s_v^{(0)}}$) the appropriate submarine output ($\boldsymbol{N}$) could be produced for all three submarines.

The question of whether the Booth et al. (1980) equations accurately reproduce real submarine manoeuvres for a given input time history was not addressed because it was thought that being able to identify the coefficients from simulated data was a necessary, but not sufficient, condition to being able to identify the coefficients from real submarine data. So testing the relatively simple case using simulated manoeuvres would give an appreciation of the suitability of the technique for identifying the coefficients of real UVs.

Selection of the manoeuvre used to identify the unknown hydrodynamic coefficients is considered in detail next.

4.5 The System Identification Manoeuvres

To perform the system identification to identify the hydrodynamic coefficients $\boldsymbol{\xi}$, it is necessary for the UV to perform a manoeuvre. The nature of this manoeuvre will define how well the coefficients can be identified. For example if the manoeuvre only involved forward motion at constant speed with no control input it would only be possible to determine the drag on the vehicle and hence only the X'_{uu} term. Therefore, this manoeuvre is not suitable for general identification purposes, and a more complex manoeuvre is required.

Generally for the manoeuvre to be useful it needs to be sufficiently 'rich' in information to stimulate all the dynamic characteristics of the UV. The concept of 'richness' is useful in qualitatively describing the properties of an ideal manoeuvre, but it is difficult to specify how to design a 'rich' manoeuvre. The selection of a suitable manoeuvre for the identification procedures is thus a non-trivial task. Some of the complexities are considered next.

4.5.1 Problems with Real Underwater Vehicle Manoeuvres

In captive model testing all UV motions are controlled; this simplifies the identification of the hydrodynamic coefficient values. However, for real UV manoeuvres the motions of the vehicle depend upon the forces and moments applied. These forces and moments tend to produce coupled vehicle motions. As an example, when considering a turning circle it is not possible to generate a yaw rate (r) without inducing a sway motion (v). Thus, due to this coupling it is impossible to produce an arbitrary motion for the submarine style UVs considered.

The effect of this close coupling of UV motions in a manoeuvre is to couple the coefficients linked with these motions. This, coefficient coupling can in turn lead to error cancellation when trying to identify the coefficients. For example, the X force comprise the coefficients X'_{vv} and X'_{rr}, thus a good approximation of the X force can be produced when errors in X'_{vv} are cancelled by errors in X'_{rr}. This error cancellation effect makes the identification of the coefficients difficult. The errors can be cancelled

in two ways, these are:

Partial Error Cancellation. Here errors in one coefficient are almost completely cancelled by errors in the coupled coefficients. This error cancellation means that certain large changes in the coefficient values only produce small changes in the UV positional time histories. As the mapping from the coefficients $\boldsymbol{\xi}$ to the positional time history $\boldsymbol{N}$, is assumed to be an injective function (i.e. one to one) it is also possible to consider the mapping from the manoeuvre time history $\boldsymbol{N}$ back to the hydrodynamic coefficients $\boldsymbol{\xi}$. When the mapping is viewed $\boldsymbol{N} \mapsto \boldsymbol{\xi}$ the partial error cancellation means that very small changes (or errors) in $\boldsymbol{N}$ can produce very large changes (or errors) in $\boldsymbol{\xi}$. The phenomenon of small errors in the input data creating large errors in the output data is known as *ill-conditioning.* As we are attempting to map from the manoeuvre time histories $\boldsymbol{N}$ to the hydrodynamic coefficients $\boldsymbol{\xi}$ any manoeuvre which exhibits this property will be described as *ill-conditioned* within this thesis .

Complete Error Cancellation. Under certain circumstances the coupling between the different motions will produce complete error cancellation. In this case the system becomes *under-determined.* That is, it is not possible to identify all the coefficients, only the relationships between them as an infinite number of sets of coefficients will produce the same manoeuvre. The set of possible coefficient values can be represented geometrically by a line, plane or hyper-plane in a hyper-dimensional space where each dimension represents a coefficient value.

Although the hydrodynamic coefficients can be identified via captive model testing; the motions used cannot be reproduced by free swimming UVs. Thus, due to the error cancellation described, it is not certain whether it is possible to produce a free swimming manoeuvre that is 'rich' enough to identify all the coefficients accurately. It maybe possible to produce a manoeuvre from which a set of hydrodynamic coefficients can be identified which adequately predicts the motions of the UV, but establishing that this set of coefficients will predict every manoeuvre is extremely difficult.

4.5.2 Defining a UV Manoeuvre

Before a more detailed discussion of manoeuvres is possible it is necessary to have a definition for a manoeuvre. For the purposes of this thesis a manoeuvre can be defined by a starting condition $\left(\boldsymbol{s}_{\mathbf{v}}^{(0)}\right)$, and a time history of the control inputs $(\boldsymbol{T_c})$, thus,

$$\text{manoeuvre} = (\boldsymbol{s}_{\mathbf{v}}^{(0)}, \boldsymbol{T_c})$$

where,

$$\begin{aligned}
\boldsymbol{s}_{\mathbf{v}}^{(0)} &= [\boldsymbol{\eta}^T, \boldsymbol{\nu}^T]^T && \text{— The UV's state vector at } t = 0. \\
\boldsymbol{\eta}^T &= [x, y, z, \phi, \theta, \psi] && \text{— The position and attitude vector.} \\
\boldsymbol{\nu}^T &= [u, v, w, p, q, r] && \text{— The linear and angular velocity vector.} \\
\boldsymbol{T_c} &= [\boldsymbol{c}^{(0)}, \boldsymbol{c}^{(t_1)}, \cdots, \boldsymbol{c}^{(t_n)}] && \text{— The UV control input time history.} \\
\boldsymbol{c}^{(t)} &= [\delta R, \delta B, \delta S, n]^T && \text{— The UV control input at time } t.
\end{aligned}$$

Here δR, δB and δS are the rudder, bow-plane and dive-plane angles at the various time intervals, and n is the propeller rpm. Using this description all manoeuvres can be described by the associated initial vehicle state, $\boldsymbol{s}_{\mathbf{v}}^{(0)}$, and the control time history, $\boldsymbol{T_c}$.

This description does not put any restrictions on possible manoeuvres. However, real submarines have: maximum and minimum hydroplane angles; maximum hydroplane slew rates; maximum and minimum forward and reverse propeller speed, etc. Thus, some physical restrictions apply to real UV manoeuvres.

Even though restrictions apply there are still an infinite number of possible manoeuvres that can be described.

4.5.3 Determining Sufficiently 'Rich' Identification Manoeuvres

As was mentioned in the beginning of Section 4.5 there are definitely manoeuvres that are not 'rich' enough to identify all the coefficients. Also, there are an infinite number of possible manoeuvres that can be performed by an UV. It is not certain that

any of these manoeuvres will allow complete identification of the coefficients. This poses a problem as we cannot test every manoeuvre to see which are good or bad at identifying the coefficients. As there is no clear way of ascertaining the performance of a manoeuvre without testing it, it was decide to design several standard manoeuvres based on practical ship manoeuvres performed (zig-zag, spiral) and use these for the identification tests. These standard manoeuvres are described in detail in the following sections.

4.6 The Chosen Standard UV Test Manoeuvres

Due to the unknown nature of the identification task, it was considered that reducing the fully coupled equations of motion to simpler sub-problems would be useful during the initial development of the identification technique. The idea being it is easier to learn to crawl before attempting to walk. To this end three separate cases were identified, these were:

The horizontal sub-problem. Here motion was restricted to the horizontal plane only. Thus, only the velocities u, v and r were possible. In this case only a small sub-set of 25 coefficients played a contributing part, so only these 25 coefficients were identified.

The vertical sub-problem. Here motion was restricted to the vertical plane, and only the velocities u, w and q were permitted. Consequently only 32 coefficients associated with the vertical motion were identified.

The fully coupled problem. This is the complete identification problem. No motions were restricted and all 101 hydrodynamic coefficients were identified.

The horizontal and vertical sub-problem manoeuvres were produced using the full submarine simulation (described in Appendix D). However, all the coefficients associated with the unused forces were set to zero. Also all coefficients involving the unused motions were set to zero. Finally all 'mechanical' coupling coefficients (e.g.

z_G for the horizontal case) were set to zero. This allowed the full simulation to be used for the two sub-problems.

After some discussion with QinetiQ standard manoeuvres for all three cases were developed. These standard manoeuvres, although generated from an intuition of what would represent a 'rich' manoeuvre, have no theoretical justification. The three test submarines all use the same standard $\boldsymbol{T_c}$ & $\boldsymbol{s_v^{(0)}}$, but due to their different coefficients the paths produced are substantially different. This caused depth problems with some submarines, as shown later, but allowed the manoeuvres to be compared for the different submarines.

The three inputs $\boldsymbol{T_c}$ & $\boldsymbol{s_v^{(0)}}$ for the standard manoeuvres and the manoeuvre paths $\boldsymbol{N}$s for the three test submarines are illustrated in the following sections.

4.6.1 Description of Horizontal Motion Manoeuvre

The chosen horizontal manoeuvre was a spiral performed over 600 seconds of simulated time. The rudder angle used to generate the spiral is given in Figure 14. The resultant UV paths are illustrated in Figure 15. The rudder angle time histories, although stepped in appearance, include the rudder dynamics as the rudder changes from one angle to another.

No scale is given on the path figure as the performance of the submarines is considered to be sensitive.

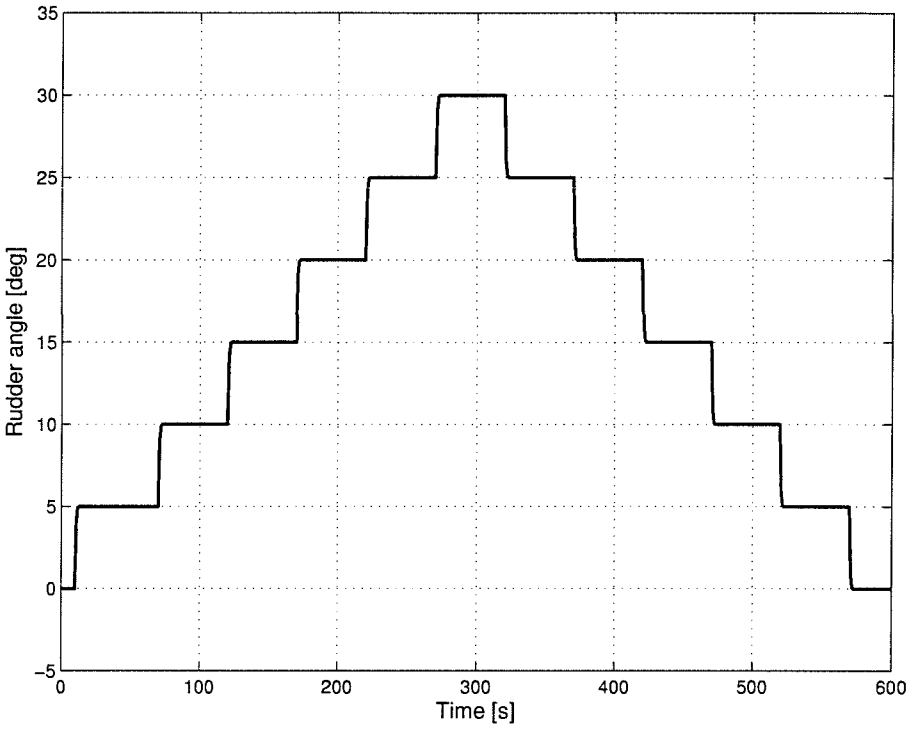

Figure 14: The horizontal manoeuvre rudder angle time history.

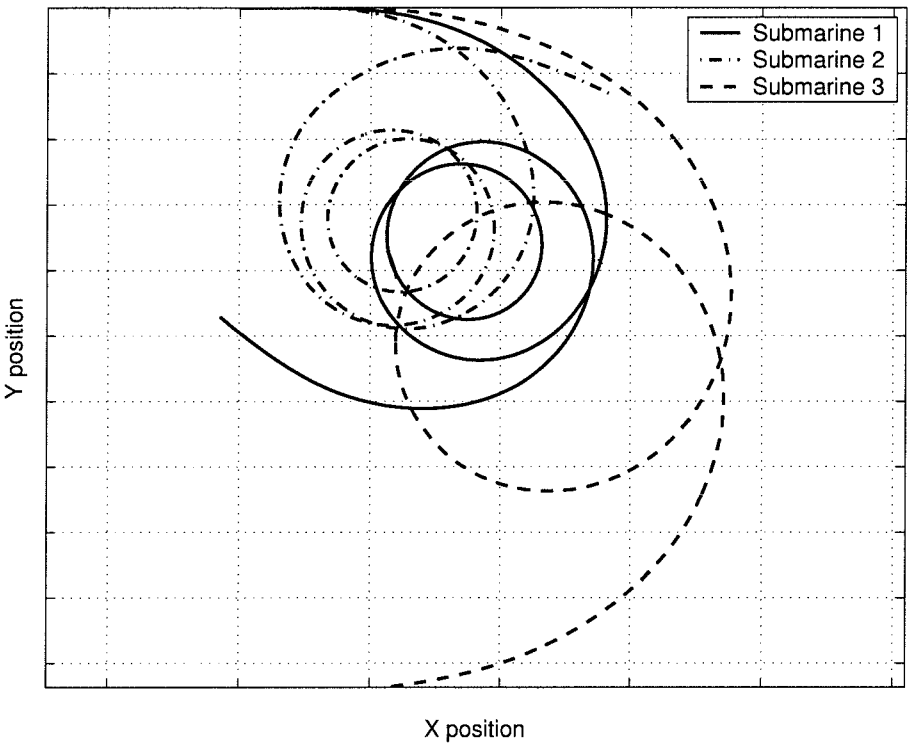

Figure 15: The $x - y$ positional time history of the three submarines performing the horizontal manoeuvre.

4.6.2 Description of Vertical Motion Manoeuvre

The choice of potential vertical manoeuvres was more restricted than the horizontal case due to the limited depth envelope of the submarine. That is, the submarine path must lie between the free surface and the maximum service depth. For this reason the chosen vertical manoeuvre is based on the horizontal 'zig-zag' manoeuvre. This allowed the depth of the submarine to be controlled to lie within the depth envelope.

The stern dive-plane time history, shown in Figure 16, was found using submarine 1. This was done as follows: First, after 10 seconds of straight and level flight, the rear dive plane (δS) was set to 5° and once the submarine pitched down to -5° the dive plane was set to -5°. This cycle of ±5° was repeated three times and on the fourth repeat the dive plane was set to 0° and the vehicle was left to stabilize. The full manoeuvre lasts 350 seconds. As only the stern dive-planes were used in the manoeuvre none of the bow dive-planes coefficients can be identified.

The submarine paths are given in Figure 17. Although the depth is measured positively downwards the data is displayed in the more intuitive orientation, with increasing depth going from top to bottom of the page. The figure shows that submarine 3 dives deeper than submarines 1 or 2. Although this may break the service depth of the submarine it was accepted so that the same manoeuvre control input could be compared on the different submarines.

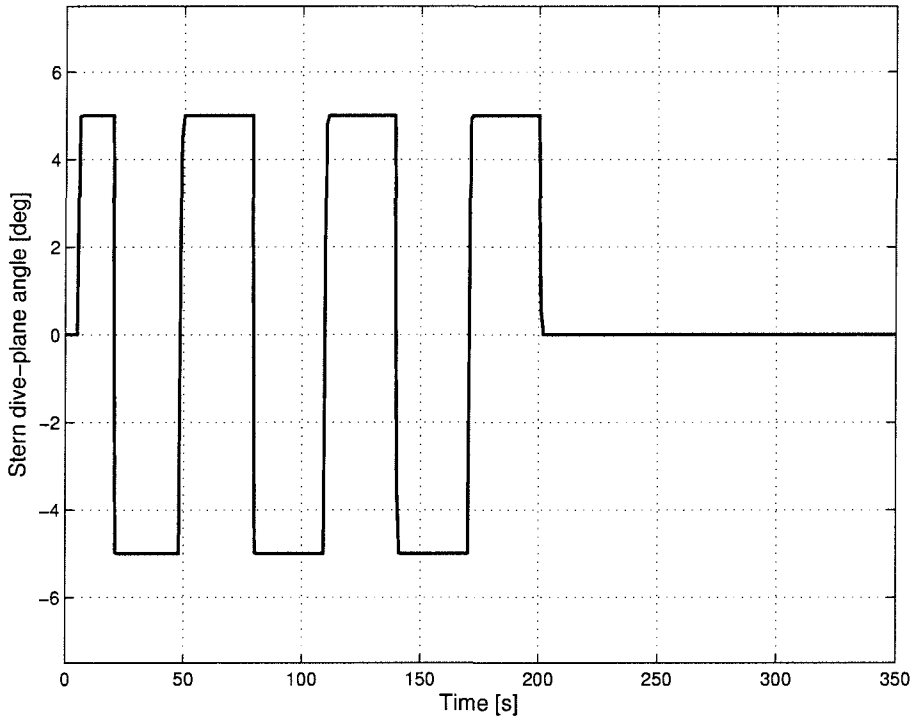

Figure 16: The vertical manoeuvre stern dive-plane angle time history.

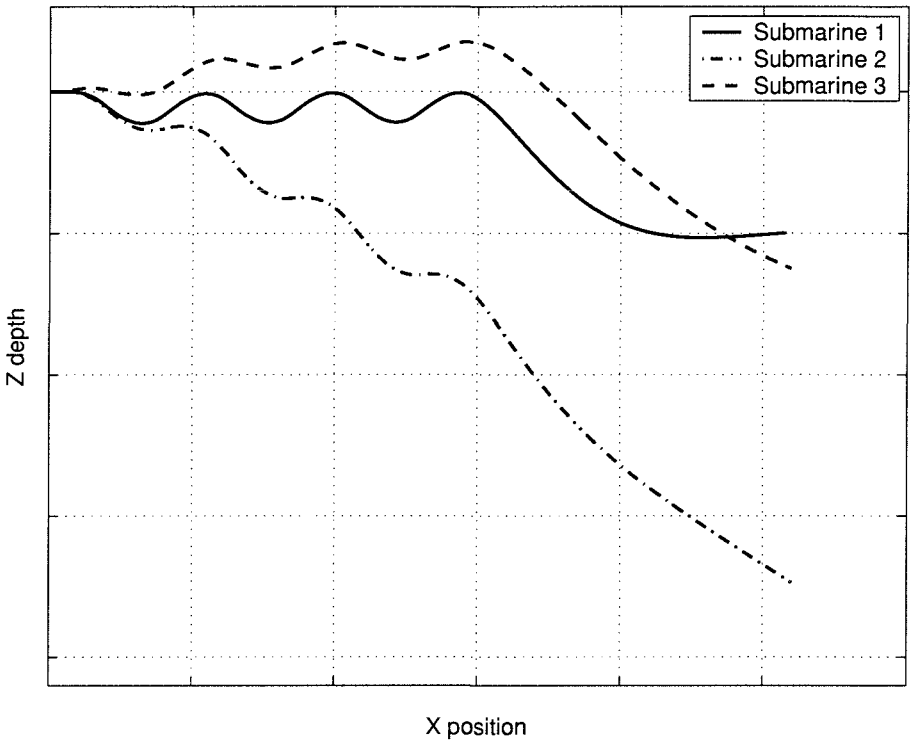

Figure 17: The $x - z$ positional time history of the three submarines performing the vertical manoeuvre.

4.6.3 Description of Coupled Motion Manoeuvre

The coupled manoeuvre is based on submarine 1 performing the horizontal spiral manoeuvre. Due to the coupling between the horizontal and vertical planes the manoeuvre produces vertical and horizontal motions. However, due to the large depth change experienced by submarine 1 during this manoeuvre the stern dive-planes were used to control the depth. The bow-planes were not used, and hence the manoeuvre is not able to determine the bow-plane related coefficients. The depth control was necessary as the submarine was breaking the free surface. The stern dive plane angle was generated by trial and error to produce reasonable depth control. The stern dive-plane time history was determined for submarine 1, and once established was used on submarines 2 & 3. Thus, the depth was only controlled for submarine 1. The control plane time histories are shown in Figure 18, and the three submarine paths produced by the manoeuvre are shown in Figure 19.

The depth of submarine 3, shown in Figure 19, is not well controlled and the submarine dives excessively deep. Although this, in all likelihood, exceeds the maximum service depth for the submarine, the issue was ignored in the simulations so that the manoeuvre input could be compared for the different submarines.

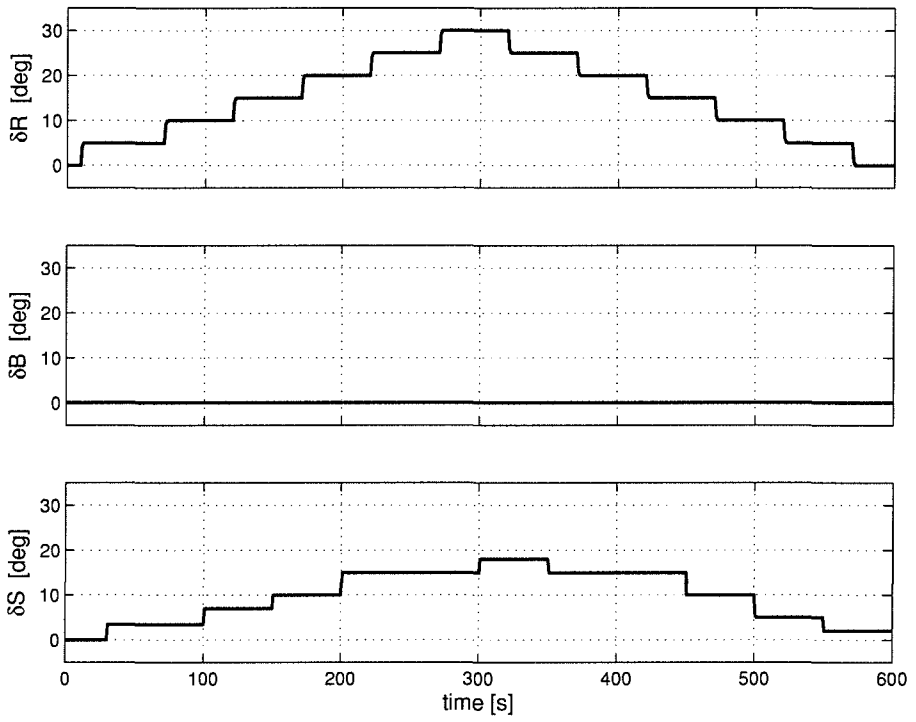

Figure 18: The coupled manoeuvre control-plane time histories.

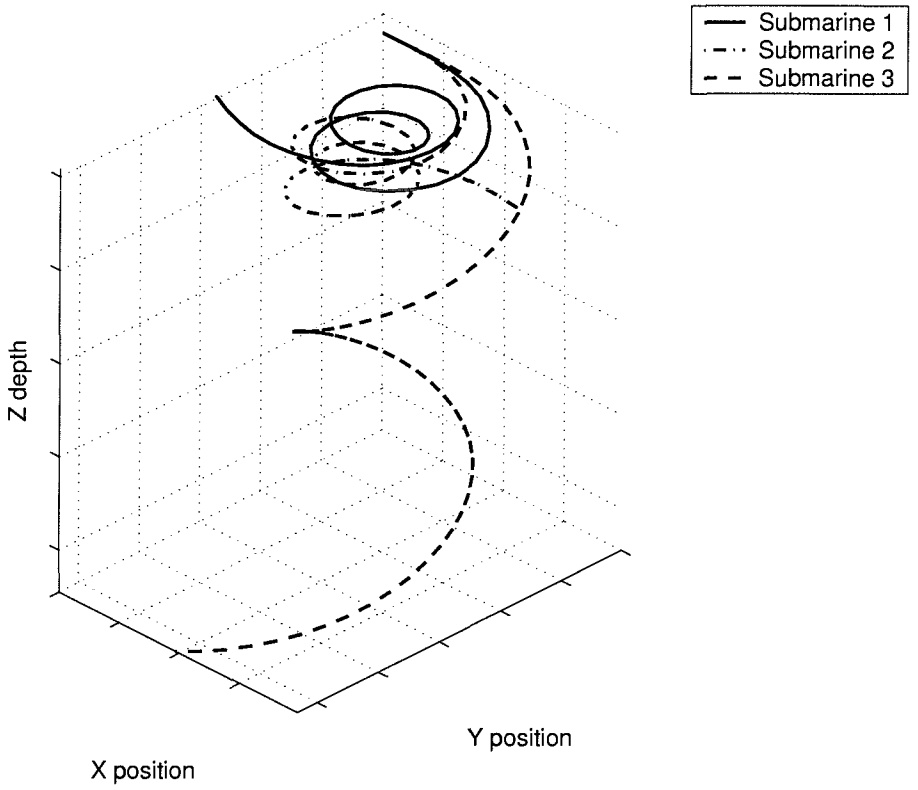

Figure 19: The positional time history of the three submarines performing the coupled manoeuvre.

4.7 Conclusions

The manoeuvres presented in Figures 15, 17 and 19 represented simulated horizontal plane, vertical plane and fully coupled motions. These figures and the control plane angles given in Figures 14, 16 and 18 essentially provide the data required to use the non-linear identification strategy given in Figure 12 to address the QinetiQ task defined at the beginning of this chapter.

The simulations just described were produced using the Matlab based UV motion simulation developed for the identification procedure. The development and testing of the UV motion simulation is discussed in the next chapter.

Chapter 5

Creating the Generic Submarine Simulation

5.1 Introduction

This chapter describes the implementation of the QinetiQ submarine equations into a generic simulation used with the system identification techniques discussed in Chapter 4. The work undertaken with QinetiQ required the use of their general submarine equations produced by Booth et al. (1980), the submarine model is described in detail in Appendix D.

The simulations described in this chapter were designed to work with the system identification procedures. The simulations generate a vehicle path ($\boldsymbol{N}$) from a known control input time history ($\boldsymbol{T_c}$). The simulation was not designed to react to the environment as the complete control time history was input prior to commencement of the simulation. Therefore the simulation cannot react to new conditions, and thus it is not possible to use as a general Autosub simulation. However, it is straightforward to create a separate simulation using the same governing equations that is suitable for modelling Autosub's motions.

The system identification simulation described was well suited for generating vehicles paths that could be used to test the system identification strategy and was ideal for

addressing the QinetiQ system identification task.

The chapter first describes some of the requirements needed to generate the Matlab UV simulation. Thereafter it discusses the submarine equations and describes how they can be represented in the notation similar to that used by Fossen. The method of generating the simulation is described and includes how the submarine equations are rearranged for implementation in the simulation. The features of alternative integration routines are considered and the chosen routine is described. Having established the approach required to produced the simulation, the implementation within the Matlab computing environment is described. The chapter concludes by describing the validation testing performed on the simulations.

5.2 Simulation Requirements

QinetiQ provided a series of manoeuvres ($\boldsymbol{N}$) and control input time histories ($\boldsymbol{T_c}$) to test the system identification procedure. The manoeuvres were simulated by QinetiQ's in house submarine simulation SubHov using coefficients only known to QinetiQ. This enabled blind testing of the identification procedure.

Unfortunately it was not possible to integrate the SubHov software into the identification procedure as the identification procedure had to be able to call the simulation at will and then receive the results. As SubHov did not allow this interface a simulation with this capability had to be created. This simulation had to produce outputs 'identical' to SubHov.

The problem with reproducing SubHov's output was that the input to the software was cascaded through a series of sub-models as shown in Figure 20.

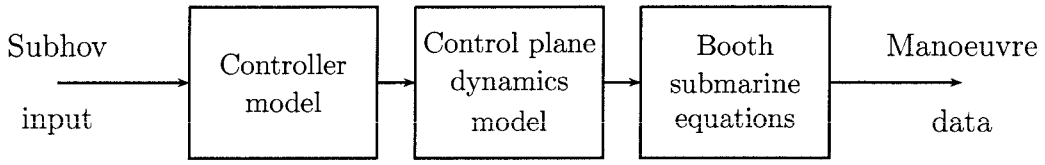

Figure 20: Block diagram of a manoeuvre implemented in SubHov

However, it was not possible to recreate the complete SubHov model as no specific information was available on the controller or the dive-plane dynamics models.

But as SubHov outputs the control plane positions at fixed time intervals (0.1s default) throughout the manoeuvre the control plane time history ($\boldsymbol{T_c}$) could be determined. Hence using the control plane time history ($\boldsymbol{T_c}$) allowed SubHov manoeuvre to be recreated in the SI simulation. A consequence of this was that the input was determined at a set time step (Δt). This has a direct effect on the simulation time integration routines described in Section 5.5.

Along with the control plane time history $\boldsymbol{T_c}$ being set at fixed time intervals it was also necessary for the positional time history $\boldsymbol{N}$ to be determined at fixed time intervals so that the earlier defined cost function could be calculated (see Section 4.4.2).

Thus both the input and output of the simulation had to be determined at a fixed time step.

5.3 The Submarine Equations of Motion

The full Booth et al. (1980) submarine equations are described in Appendix D and the propulsion model is also analysed in Appendix C.

5.3.1 Expressing the Motion Equations in Terms of Fossen's Notation

It is possible to rewrite the Booth et al. (1980) equations using a notation similar to that outlined by Fossen (1994). This is done, as in Chapter 2, to maintain a consistent notation format. Using this notation the governing equations can be written as,

$$\boldsymbol{M}_{rb}\dot{\boldsymbol{\nu}} + \boldsymbol{d}_{rb}(\boldsymbol{\nu}) = \boldsymbol{M}_{A}\dot{\boldsymbol{\nu}} + \boldsymbol{d}(\boldsymbol{\nu}) + \boldsymbol{g}(\boldsymbol{\eta}) + \boldsymbol{\tau}.$$

Here,

$\boldsymbol{M}_{rb}$— Is a matrix of the rigid body acceleration terms.

$\boldsymbol{d}_{rb}(\boldsymbol{\nu})$— A vector of the rigid body velocity terms.

$\boldsymbol{M}_{A}$— A matrix of the hydrodynamic added mass coefficients.

$\boldsymbol{d}(\boldsymbol{\nu})$— A vector of the hydrodynamic damping coefficients.

$\boldsymbol{g}(\boldsymbol{\eta})$— A vector of the hydrostatic forces and moments.

$\boldsymbol{\tau} = \boldsymbol{\tau}_c + \boldsymbol{\tau}_n$— A vector of the control forces and moments.

$\boldsymbol{\nu} = [u, v, w, p, q, r]^T$.

The associated force and moment vectors are defined in the following sections.

The rigid body acceleration matrix — $\boldsymbol{M}_{rb}$

The rigid body acceleration matrix is defined as,

$$\boldsymbol{M}_{rb} = \begin{bmatrix} m & 0 & 0 & 0 & mz_G & -my_G \\ 0 & m & 0 & -mz_G & 0 & mx_G \\ 0 & 0 & m & my_G & -mx_G & 0 \\ 0 & -mz_G & my_G & I_{XX} & -I_{XY} & -I_{ZX} \\ mz_G & 0 & -mx_G & -I_{XY} & I_{YY} & -I_{YZ} \\ -my_G & mx_G & 0 & -I_{ZX} & -I_{YZ} & I_{ZZ} \end{bmatrix}.$$

This matrix when multiplied by $\dot{\boldsymbol{\nu}}$ forms the rigid body dynamic acceleration vector. These terms can be readily reconciled with the equations laid out in Section 2.2.

The rigid body dynamics velocity vector — $\boldsymbol{d}_{rb}(\boldsymbol{\nu})$

This vector represents the forces and moments associated with the velocity terms of the rigid body dynamics model. The rigid body dynamics equations were described earlier in Section 2.2. The vector is defined as,

$$\boldsymbol{d}_{rb}(\boldsymbol{\nu}) = \begin{bmatrix} m\left[-vr + wq - x_G(q^2 + r^2) + y_G(pq) + z_G(pr)\right] \\ m\left[-wp + ur - y_G(r^2 + p^2) + z_G(qr) + x_G(qp)\right] \\ m\left[-uq + vp - z_G(p^2 + q^2) + x_G(rp) + y_G(rq)\right] \\ (I_{ZZ} - I_{YY})qr - (pq)I_{ZX} + (r^2 - q^2)I_{YZ} + (pr)I_{XY} \\ \qquad +m\left[y_G\left(-uq + vp\right) - z_G\left(-wp + ur\right)\right] \\ (I_{XX} - I_{ZZ})rp - (qr)I_{XY} + (p^2 - r^2)I_{ZX} + (qp)I_{YZ} \\ \qquad +m\left[z_G\left(-vr + wq\right) - x_G\left(-uq + vp\right)\right] \\ (I_{YY} - I_{XX})pq - (rp)I_{YZ} + (q^2 - p^2)I_{XY} + (rq)I_{ZX} \\ \qquad +m\left[x_G\left(-wp + ur\right) - y_G\left(-vr + wq\right)\right] \end{bmatrix}.$$

The added-mass matrix — $\boldsymbol{M}_A$

The added-mass matrix when multiplied by $\dot{\boldsymbol{\nu}}$ represents the hydrodynamic reactions of the UV with the surrounding fluid. When the matrix is multiplied by $\dot{\boldsymbol{\nu}}$ the result is a force and moment vector. The added-mass matrix is defined as

$$\boldsymbol{M}_A = \begin{bmatrix} \frac{1}{2}\rho l^3 X'_{\dot{u}} & 0 & 0 & 0 & 0 & 0 \\ 0 & \frac{1}{2}\rho l^3 Y'_{\dot{v}} & 0 & \frac{1}{2}\rho l^4 Y'_{\dot{p}} & 0 & \frac{1}{2}\rho l^4 Y'_{\dot{r}} \\ 0 & 0 & \frac{1}{2}\rho l^3 Z'_{\dot{w}} & 0 & \frac{1}{2}\rho l^4 Z'_{\dot{q}} & 0 \\ 0 & \frac{1}{2}\rho l^4 K'_{\dot{v}} & 0 & \frac{1}{2}\rho l^5 K'_{\dot{p}} & 0 & \frac{1}{2}\rho l^5 K'_{\dot{r}} \\ 0 & 0 & \frac{1}{2}\rho l^4 M'_{\dot{w}} & 0 & \frac{1}{2}\rho l^5 M'_{\dot{q}} & 0 \\ 0 & \frac{1}{2}\rho l^4 N'_{\dot{v}} & 0 & \frac{1}{2}\rho l^5 N'_{\dot{p}} & 0 & \frac{1}{2}\rho l^5 N'_{\dot{r}} \end{bmatrix}.$$

The hydrodynamic damping vector — $\boldsymbol{d}(\boldsymbol{\nu})$

This hydrodynamic damping vector represents the fluid dynamic damping associated with the vehicle. The fluid dynamic damping is difficult to model as it is a complex phenomenon, thus the terms involve in the model are numerous and the model complex. The vector is described by

$$\boldsymbol{d}(\boldsymbol{\nu}) = \left[X_d, Y_d, Z_d, K_d, M_d, N_d\right]^T.$$

The associated descriptions for each of the force and moment components of $\boldsymbol{d}(\boldsymbol{\nu})$ are respectively:

$$\begin{aligned} X_d = &\frac{1}{2}\rho l^2 \left(X'_{uu}u^2 + X'_{vv}v^2 + X'_{ww}w^2\right) \\ &+ \frac{1}{2}\rho l^3 \left(X'_{vr}vr + X'_{wq}wq\right) \\ &+ \frac{1}{2}\rho l^4 \left(X'_{qq}q^2 + X'_{rr}r^2 + X'_{rp}rp\right) \end{aligned}$$

$$\begin{aligned} Y_d = &\frac{1}{2}\rho l^2 \left(Y'_{uu}u^2 + Y'_{uv}uv + Y'_{vw}vw + Y'_{v\nu}v\nu\right) \\ &+ \frac{1}{2}\rho l^3 \left(Y'_{up}up + Y'_{ur}ur + Y'_{vq}vq + Y'_{wp}wp + Y'_{wr}wr\right) \\ &+ \frac{1}{2}\rho l^3 \left(Y'_{v\nu|\frac{r}{v}|}v\nu\left|\frac{r}{v}\right|\right) \\ &+ \frac{1}{2}\rho l^4 \left(Y'_{p|p|}p|p| + Y'_{pq}pq + Y'_{qr}qr\right) \end{aligned}$$

$$\begin{aligned} Z_d = &\frac{1}{2}\rho l^2 \left(Z'_{uu}u^2 + Z'_{uw}uw + Z'_{vv}v^2\right) \\ &+ \frac{1}{2}\rho l^2 \left(Z'_{w\nu}w\nu + Z'_{u|w|}u|w| + Z'_{|w\nu|}|w\nu|\right) \\ &+ \frac{1}{2}\rho l^3 \left(Z'_{uq}uq + Z'_{vp}vp + Z'_{vr}vr\right) \\ &+ \frac{1}{2}\rho l^3 \left(Z'_{w\nu|\frac{q}{w}|}w\nu\left|\frac{q}{w}\right|\right) \\ &+ \frac{1}{2}\rho l^4 \left(Z'_{pp}p^2 + Z'_{rr}r^2 + Z'_{rp}rp\right) \end{aligned}$$

$$
\begin{aligned}
K_{d_{hd}} &= \frac{1}{2}\rho l^3 \left(K'_{uu}u^2 + K'_{uv}uv + K'_{vw}vw\right) \\
&+ \frac{1}{2}\rho l^3 \left(K'_{v\nu}v\nu\right) \\
&+ \frac{1}{2}\rho l^4 \left(K'_{up}up + K'_{ur}ur + K'_{vq}vq + K'_{wp}wp + K'_{wr}wr\right) \\
&+ \frac{1}{2}\rho l^5 \left(K'_{qr}qr + K'_{pq}pq + K'_{p|p|}p|p|\right)
\end{aligned}
$$

$$
\begin{aligned}
M_d &= \frac{1}{2}\rho l^3 \left(M'_{uu}u^2 + M'_{uw}uw + M'_{vv}v^2\right) \\
&+ \frac{1}{2}\rho l^3 \left(M'_{w\nu}w\nu + M'_{u|w|}u|w| + M'_{|w\nu|}|w\nu|\right) \\
&+ \frac{1}{2}\rho l^4 \left(M'_{uq}uq + M'_{vr}vr + M'_{vp}vp\right) \\
&+ \frac{1}{2}\rho l^4 \left(M'_{q\nu}q\nu\right) \\
&+ \frac{1}{2}\rho l^5 \left(M'_{pp}p^2 + M'_{rr}r^2 + M'_{pr}pr + M'_{q|q|}q|q|\right)
\end{aligned}
$$

$$
\begin{aligned}
N_d &= \frac{1}{2}\rho l^3 \left(N'_{uu}u^2 + N'_{uv}uv + N'_{vw}vw\right) \\
&+ \frac{1}{2}\rho l^3 \left(N'_{v\nu}v\nu\right) \\
&+ \frac{1}{2}\rho l^4 \left(N'_{up}up + N'_{ur}ur + N'_{wp}wp + N'_{wr}wr + N'_{vq}vq\right). \\
&+ \frac{1}{2}\rho l^4 \left(N'_{r\nu}r\nu + N'_{u|r|\delta R}u|r|\delta R\right) \\
&+ \frac{1}{2}\rho l^5 \left(N'_{pq}pq + N'_{qr}qr + N'_{r|r|}r|r|\right)
\end{aligned}
$$

The hydrostatic force vector — $\boldsymbol{g(\eta)}$

The hydrostatic force and moment vector was defined previously in Section 3.3 and is repeated here for clarity.

$$\boldsymbol{g}(\boldsymbol{\eta}) = \begin{bmatrix} -(mg-B)s\theta \\ (mg-B)c\theta s\phi \\ (mg-B)c\theta c\phi \\ (y_G mg - y_B B)c\theta c\phi - (z_G mg - z_B B)c\theta s\phi \\ -(z_G mg - z_B B)s\theta - (x_G mg - x_B B)c\theta c\phi \\ (x_G mg - x_B B)c\theta c\phi + (y_G mg - y_B B)s\theta \end{bmatrix}.$$

The control force vector – $\boldsymbol{\tau}$

The control vector represents the forces and moments exerted by the hydroplane and the propulsion system. The vector can be broken down into the following terms,

$$\boldsymbol{\tau} = \boldsymbol{\tau}_c + \boldsymbol{\tau}_n,$$

where the control forces and moments from the fins, $\boldsymbol{\tau}_c$, are modelled by

$$\boldsymbol{\tau}_c = \frac{1}{2}\rho l^2 u^2 \begin{bmatrix} X'_{uu\delta\delta R}\delta R^2 + X'_{uu\delta\delta B}\delta B^2 + X'_{uu\delta\delta S}\delta S^2 \\ Y'_{uu\delta R}\delta R \\ Z'_{uu\delta B}\delta B + Z'_{uu\delta S}\delta S \\ l \cdot K'_{uu\delta R}\delta R \\ l \cdot (M'_{uu\delta B}\delta B + M'_{uu\delta S}\delta S) \\ l \cdot N'_{uu\delta R}\delta R \end{bmatrix} + \frac{1}{2}\rho l^3 \begin{bmatrix} 0 \\ Y'_{u|r|\delta R}u|r|\delta R \\ Z'_{u|q|\delta S}u|q|\delta S \\ 0 \\ l \cdot M'_{u|q|\delta S}u|q|\delta S \\ l \cdot N'_{u|r|\delta R}u|r|\delta R \end{bmatrix}.$$

This can be found from an analysis of the governing equations presented in Appendix D.

The propulsion forces and moments, $\boldsymbol{\tau}_n$, are modelled by

$$\boldsymbol{\tau}_n = \begin{bmatrix} X_n \\ 0 \\ 0 \\ K_n \\ 0 \\ 0 \end{bmatrix}$$

as described in Section 3.7.

5.4 Converting the Motion Equations into a Form Appropriate for Simulation

The goal of the simulation is to produce a positional time history of the submarine ($\boldsymbol{N}$). Thus, the Booth et al. (1980) equations have to be rearranged so that the acceleration can be calculated at any time point. The approach to converting the equations of motion into a form that can be integrated to form a positional time history is based on work described in McGhee et al. (2000). The basic approach is to describe the UV motion through a state vector defined by

$$\boldsymbol{s}_{\mathbf{v}} = [x, y, z, \phi, \theta, \psi, u, v, w, p, q, r]^T.$$

The vehicles control inputs are defined in vector form as

$$\boldsymbol{c} = [\delta R, \delta S, \delta B, n]^T.$$

To simulate the UV motion it is necessary to find the first time differential of the state vector. This can be done from a knowledge of the current state and the control inputs. Hence, it is necessary to find the function f in,

$$\dot{\boldsymbol{s}}_{\mathbf{v}} = f(\boldsymbol{s}_{\mathbf{v}}, \boldsymbol{c}). \tag{7}$$

Using Fossen's notation $\boldsymbol{s}_{\mathbf{v}}$ can be represented as,

$$\boldsymbol{s}_{\mathbf{v}} = \begin{bmatrix} \boldsymbol{\eta} \\ \boldsymbol{\nu} \end{bmatrix}.$$

Thus, the first differential of the state vector $\boldsymbol{s}_{\mathbf{v}}$ can be broken down into finding f_1 and f_2 for the expressions:

$$\dot{\boldsymbol{\eta}} = f_1(\boldsymbol{\eta}, \boldsymbol{\nu}, \boldsymbol{c})$$
$$\dot{\boldsymbol{\nu}} = f_2(\boldsymbol{\eta}, \boldsymbol{\nu}, \boldsymbol{c}).$$

It was shown in Section 2.1.4 using the xyz Euler angle sequence, that:

$$\dot{\boldsymbol{\eta}} = \boldsymbol{J}(\boldsymbol{\eta}_2)\boldsymbol{\nu},$$

where,

$$\boldsymbol{J}(\boldsymbol{\eta}_2) = \begin{bmatrix} \boldsymbol{J}_1(\boldsymbol{\eta}_2) & 0_{3\times3} \\ 0_{3\times3} & \boldsymbol{J}_2(\boldsymbol{\eta}_2) \end{bmatrix}.$$

The matrices $\boldsymbol{J}_1(\boldsymbol{\eta}_2)$ and $\boldsymbol{J}_2(\boldsymbol{\eta}_2)$ are described in Section 2.1.1 and Section 2.1.3 respectively.

Thus,

$$f_1(\boldsymbol{\eta}, \boldsymbol{\nu}, \boldsymbol{c}) = \boldsymbol{J}(\boldsymbol{\eta}_2)\boldsymbol{\nu}.$$

To calculate the function f_2 is more complex.

5.4.1 Calculating $\dot{\boldsymbol{\nu}}$

The governing dynamic equations of the Booth et al. (1980) model can be written in the notation previously described, as

$$\boldsymbol{M}_{rb}\dot{\boldsymbol{\nu}} + \boldsymbol{d}_{rb}(\boldsymbol{\nu}) = \boldsymbol{M}_A\dot{\boldsymbol{\nu}} + \boldsymbol{d}(\boldsymbol{\nu}) + \boldsymbol{g}(\boldsymbol{\eta}) + \boldsymbol{\tau}.$$

The equation can then be rearranged to give

$$[\boldsymbol{M}_{rb} - \boldsymbol{M}_A]\,\dot{\boldsymbol{\nu}} = \boldsymbol{d}(\boldsymbol{\nu}) - \boldsymbol{d}_{rb}(\boldsymbol{\nu}) + \boldsymbol{g}(\boldsymbol{\eta}) + \boldsymbol{\tau},$$

This leads to

$$\dot{\boldsymbol{\nu}} = [\boldsymbol{M}_{rb} - \boldsymbol{M}_A]^{-1}\,[\boldsymbol{d}(\boldsymbol{\nu}) - \boldsymbol{d}_{rb}(\boldsymbol{\nu}) + \boldsymbol{g}(\boldsymbol{\eta}) + \boldsymbol{\tau}]\,.$$

Thus, the function f_2 is determined by,

$$f_2(\boldsymbol{s}_{\mathbf{v}}, \boldsymbol{c}) = [\boldsymbol{M}_{rb} - \boldsymbol{M}_A]^{-1}\,[\boldsymbol{d}(\boldsymbol{\nu}) - \boldsymbol{d}_{rb}(\boldsymbol{\nu}) + \boldsymbol{g}(\boldsymbol{\eta}) + \boldsymbol{\tau}]\,.$$

5.4.2 Calculating $\dot{s}_{\mathbf{v}}$

Combining the equations above lead to

$$\dot{s}_{\mathbf{v}} = \begin{bmatrix} \dot{\eta} \\ \dot{\nu} \end{bmatrix} = \begin{bmatrix} J(\eta_2)\nu \\ [M_{rb} - M_A]^{-1} [d(\nu) - d_{rb}(\nu) + g(\eta) + \tau] \end{bmatrix}.$$

This formulation of the equations of motion is ideally suited to integration as at each time step the first derivative of the state vector can be found and integrated.

5.5 Selection of Integration Routines

The submarine state vector equations described form a set of coupled non-linear differential equations. They are from a class of initial value problems which can be represented in the general form by,

$$\frac{dy}{dt} = f(y, t), \qquad y(t_0) = y_0.$$

As analytical solutions to these equations are notoriously difficult to find the usual solution method is to use numerical techniques to obtain an approximate solution. Numerous routines are available to perform this time domain integration. This section considers some of the properties of integration routines and describes the chosen routine in detail.

5.5.1 Accuracy, Efficiency and Stability of Integration Routines

The three key features of interest in selecting an integration routine are its accuracy, efficiency and stability. Usually the accuracy of a routine can be increased by using a smaller step size, however, this increases the time taken to solve the initial value problem and hence increase the CPU demands of the integration routine. Thus, the accuracy and execution times are closely coupled.

The stability of an integration routine depends principally on the function f and the step-size adopted. When instability occurs the predicted value of $\boldsymbol{y}$ rapidly diverges from the true value of $\boldsymbol{y}$. This is usually preceded by oscillations in the solution, when the system becomes unstable it is said to 'blow-up'. If a system is unstable it is possible to remove the instability by changing the integration routine used or by decreasing the step-size.

5.5.2 Errors in Numerical Integration Routines

There are two types of error associated with stable solutions produced by numerical integration routines, these are *truncation* and *rounding* errors. The truncation error is caused by the mathematical discretization of the problem and arises from how the integration routine approximates the function to be integrated. There are two measures of truncation error, namely *local* and *global*. The local truncation error represents the error in one time step, whereas the global error represents the total error produced from all time steps.

Where the truncation error comes from the mathematical approximation used the rounding error comes from the implementation of the mathematics within the computer. The errors arise from the way that computers store numbers. As only a finite number of bytes is used to represent a number only a limited set of numbers can be described. Hence when numerical operations produce a number which cannot be represented it is 'rounded' to a number which can. Hence rounding errors are produced.

These two error types are discussed in detail next.

Truncation Errors

All numerical integration routines considered calculate the value $\boldsymbol{y}_{n+1}$ at t_{n+1} from an initial value of $\boldsymbol{y}_n$ at t_n. Thus, each step can be considered in isolation as a separate initial value problem. The different methods considered use a truncated Taylor series expansion to approximate the function and hence produce the estimate $\boldsymbol{y}_{n+1}$. As the

Taylor series is truncated the discarded terms produce the *truncation error* in $\boldsymbol{y}_{n+1}$.

It is known from Taylor's Theorem that a truncated Taylor series of a function $f(x)$ taken about a point a and consisting of the first n terms has an error (or remainder) at some point x given by,

$$\varepsilon(x) = \frac{1}{(n+1)!} h^{n+1} f^{n+1}(c_x) \qquad \text{where,} \quad a \leq c_x \leq x.$$

The value c_x is not known. However, the error is bounded as the size of $\frac{1}{(n+1)!} f^{n+1}(c_x)$ is finite. Thus, the error cannot become greater than some multiple of h^{n+1}. This concept is represented by the 'big O' notation $O(\cdot)$. This is written as,

$$\varepsilon(x) = O(h^{n+1}) \quad \text{as } h \to 0$$

which means that

$$|\varepsilon(x)| \leq |Ah^{n+1}| \quad \text{for some constant } A.$$

This $O(\cdot)$ notation describes how the error will decrease as the step size h is made smaller. However, the error at each step produces a *local* truncation error. The real question is to understand the *global* truncation error. If the local truncation error is $O(h_{n+1})$ the global truncation error is $O(h_n)$. Thus, the global truncation error is said to be of order n, which is one less than the order of the local truncation error.

In general higher order methods are more accurate than lower order methods, Press et al. (1992). Unfortunately, the mathematics does not prove that higher order methods are always better as the value of A is not known.

Rounding Errors

As was implied above decreasing the step size improves the accuracy of the integration routine. However, this assumes perfect calculations which computers cannot reproduce. If the step size is small the approximations introduced by the method the computer uses to store and process numbers can generate large rounding errors. If the step size becomes too small the errors from rounding become larger than the

improved accuracy generated by the smaller step size. Thus, the step size should be sufficiently large to minimize the rounding errors.

5.5.3 The Chosen Approach: The 4^{th}-order Runge-Kutta Method

As was discussed in Section 5.2 both the input to the simulation $\boldsymbol{T_c}$ and the output $\boldsymbol{N}$ had to be calculated at fixed time steps, thus a fixed step-sized integration routine would be appropriate. Although it would be possible to use variable time-step routines it would complicate the implementation.

The chosen routine was a standard 4^{th} order Runge-Kutta method described in Press et al. (1992). This has a global truncation error of $O(h^4)$. It is a 'workhorse' routine that is commonly used because of its simple implementation, robustness and accuracy. The method calculates the function values at the next time step using the following procedure:

$$
\begin{aligned}
\boldsymbol{k}_1 &= \Delta t f(\boldsymbol{y}_n, t_n) \\
\boldsymbol{k}_2 &= \Delta t f\left(\boldsymbol{y}_n + \frac{\boldsymbol{k}_1}{2}, t_n + \frac{\Delta t}{2}\right) \\
\boldsymbol{k}_3 &= \Delta t f\left(\boldsymbol{y}_n + \frac{\boldsymbol{k}_2}{2}, t_n + \frac{\Delta t}{2}\right) \\
\boldsymbol{k}_4 &= \Delta t f\left(\boldsymbol{y}_n + \boldsymbol{k}_3, t_n + \Delta t\right)
\end{aligned}
$$

$$
\hat{\boldsymbol{y}}_{n+1} = \boldsymbol{y}_n + \frac{\boldsymbol{k}_1}{6} + \frac{\boldsymbol{k}_2}{3} + \frac{\boldsymbol{k}_3}{3} + \frac{\boldsymbol{k}_4}{6}
$$

$$
\boldsymbol{y}_{n+1} - \hat{\boldsymbol{y}}_{n+1} = O(h^5),
$$

where,

$O(h^5)$ represents the local truncation error.

This method can then be used to integrate the submarine state vector differential

Equation (7), by notating in,

$$\dot{\boldsymbol{s}}_{\mathbf{v}} = f_1(\boldsymbol{s}_{\mathbf{v}}, \boldsymbol{c}),$$

that

$$\boldsymbol{c} = f_2(t)$$

then the equation can be written the initial value problem form as

$$\dot{\boldsymbol{s}}_{\mathbf{v}} = f_3(\boldsymbol{s}_{\mathbf{v}}, t).$$

The Runge-Kutta method outline above can then be used to integrate the equation.

5.6 Creating the UV Simulation Code

The submarine equations were implemented in the Matlab computing environment to create the Matlab UV simulation. The associated inputs and outputs of the simulation are shown in Figure 21. By changing the UV hydrodynamics ($\boldsymbol{\xi}$), mechanical ($\boldsymbol{m}$) and propulsion coefficients $\boldsymbol{n}$ a different UV could be modelled.

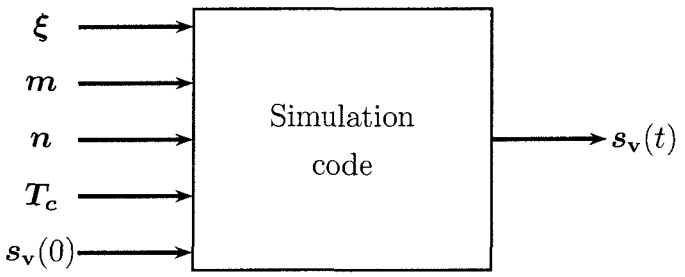

Figure 21: Inputs to the generic simulation code

The inputs to the simulation are:

$\boldsymbol{\xi} \in \mathbb{R}^{101}$	The UV hydrodynamic coefficients vector.
$\boldsymbol{m} \in \mathbb{R}^{15}$	The UV mechanical coefficients vector.
$\boldsymbol{n} \in \mathbb{R}^{9}$	The UV propulsion coefficient vector.
$\boldsymbol{T_c} \in \mathbb{R}^{4,n}$	The manoeuvre control input matrix.
$\boldsymbol{s}_{\mathbf{v}}^{(0)} \in \mathbb{R}^{12}$	The initial UV conditions.

And the corresponding output is:

$\boldsymbol{s}_{\mathbf{v}}(t) \in \mathbb{R}^{12}$ The UV state vector at time t.

The full definition of vectors $\boldsymbol{\xi}$, $\boldsymbol{m}$ and $\boldsymbol{n}$ is given in Appendix E.

5.6.1 Three Versions of the Generic Submarine Simulation

The Matlab simulation was implemented in three different ways within the Matlab environment. All three versions produced the same output but the execution time of the code was improved in each subsequent version.

The first version of the code was implemented as a series of m-file functions within Matlab. The code was written to be easy to understand and debug. However, the code took a long time (three minutes) to execute the standard horizontal manoeuvre. As the simulation had to be run many thousands of times before the optimization routine converged this initial code needed to be speeded up.

In the second version of the simulation the previous m-files were optimized to reduce the execution time. This was achieved by removing some inefficient code sections and re-coding the files in a Matlab 'friendly' style. This greatly reduced the readability of the code. The optimized code was then compiled using the Matlab compiler. The final compiled code executed the standard horizontal manoeuvre considerably faster than the first version. However, the code still took 18.5 seconds to execute. Consequently the non-linear parameter identification procedure still took a long time to run. This became a problem when the full identification procedure was being tested as the code was taking approximately 2–3 days to converge. As the simulation task was taking 99.8% of total execution time it became clear that a significant increase in the speed of simulation was necessary reduce the identification procedure run time.

The final version of code was written in C within a Matlab '.mex' wrapper. This 'wrapper' allowed the code to be called as a Matlab function. This meant that the simulation could be called in the same fashion as the previous versions of the code. The simulation written in C took 0.04 seconds to execute the standard horizontal manoeuvre. This speeded up the code by a factor of 450 approximately compared

to the optimized m-file version. This made the non-linear parameter identification routine far easier to test.

The execution times for all three simulation versions are shown in Table 1.

Simulation version	Execution time (s)
Matlab m-file	180
Optimized and compiled m-file	18.5
C coded .mex file	0.04

Table 1: Comparison of simulation time for the standard horizontal manoeuvre.

5.7 Testing and Validating the Simulation Code

Once the simulation was created it needed to be tested and validated to make sure it would produce the same output as the QinetiQ SubHov simulation. For the purpose of the testing it was assumed that the SubHov simulation was an accurate, error free implementation of the Booth et al equations. Thus provided the Matlab simulation produced the same output at SubHov for all manoeuvres the Matlab code could be assumed to be correct.

The Matlab simulation versions were tested in three broad stages, these were:

1. Initially test the simulation to see if a 'reasonable' output was produced.
2. Compare the Matlab simulation output for a defined test manoeuvre(described in Section 5.8.1) to that produced by SubHov.
3. Finally perform a line by line check of the code to attempt to find any errors that had been missed during stages 1 and 2. This was necessary as only one manoeuvre was tested during stage 2.

As the first simulation version was clearly going to be too slow and was 'development' code it was not as thoroughly tested. The second version of the code was used with the non-linear identification procedure, and was tested far more thoroughly.

The third Matlab simulation version was first compared to the second code version and then subsequently to the SubHov output. All three Matlab versions produced effectively identical outputs. There were very slight numeric differences but these were discounted as being due to the different coding used. The comparisons show that all three versions implemented the equations in the same fashion. However, when the Matlab simulations were compared to the SubHov output there was a small but consistent difference between the results. This is discussed in the following section.

5.8 Comparing the Matlab and QinetiQ's SubHov Simulations

As mentioned in Section 5.2 neither implementation details nor source code were available for SubHov. Therefore it was not possible to reproduce SubHov directly within Matlab. But as SubHov uses the Booth et al. (1980) equations a simulation based on these equations should produce approximately the same output. However, as SubHov has many other functions along side the basic Booth et al. (1980) equations it is quite likely that there are difference in how the Booth et al. (1980) equations are implemented in SubHov compared to the Matlab simulation. Thus, it was expected that there would be slight differences between the outputs of the simulations even when both simulations were 'correct'. Thus, the validation phase of the testing would give a guide to this error as well as validating the Matlab simulation.

The simulations were compared by running a manoeuvre in SubHov and then running the same manoeuvre in the Matlab simulation. The resultant paths of the manoeuvres could then be compared. This comparison was performed with all three test submarines.

5.8.1 Specification of Manoeuvre Used in Comparative Studies

The manoeuvre used for the comparison was a depth controlled spiral manoeuvre. This manoeuvre was chosen so that along side the specified rudder angle SubHov would control the depth by adjusting the bow and stern dive planes, hence all control planes would be active during the manoeuvre. This allowed all the control plane code to be tested along with the general UV dynamics code.

The starting conditions for the manoeuvre were:

$z = 300\text{m}$ Submarine depth,

$u = 7.5\text{ms}^{-1}$ Submarine forward speed.

In the SubHov manoeuvre at $t = 10\text{s}$ the control depth was set to 125m and a spiral turn was started by ramping up the rudder control angle in 5° increments to 30° and then reducing rudder control angles in 5° increments to 0°. The control plane angles are shown for submarine 1 in Figure 22. In Figure 22 the dynamic step response of the rudder, although plotted, is not obvious as the time constant of the rudder is very small.

During the manoeuvre each rudder angle step was supposed to be held for 60s unfortunately due to an oversight the 10°–15° & 15°–20° steps were only 50s long while the 20–25° step was 70s long. Once the rudder angle had returned to 0° at 660s it was held constant until the manoeuvre terminated at 750s.

There was no change in the submarine's required speed during the manoeuvre.

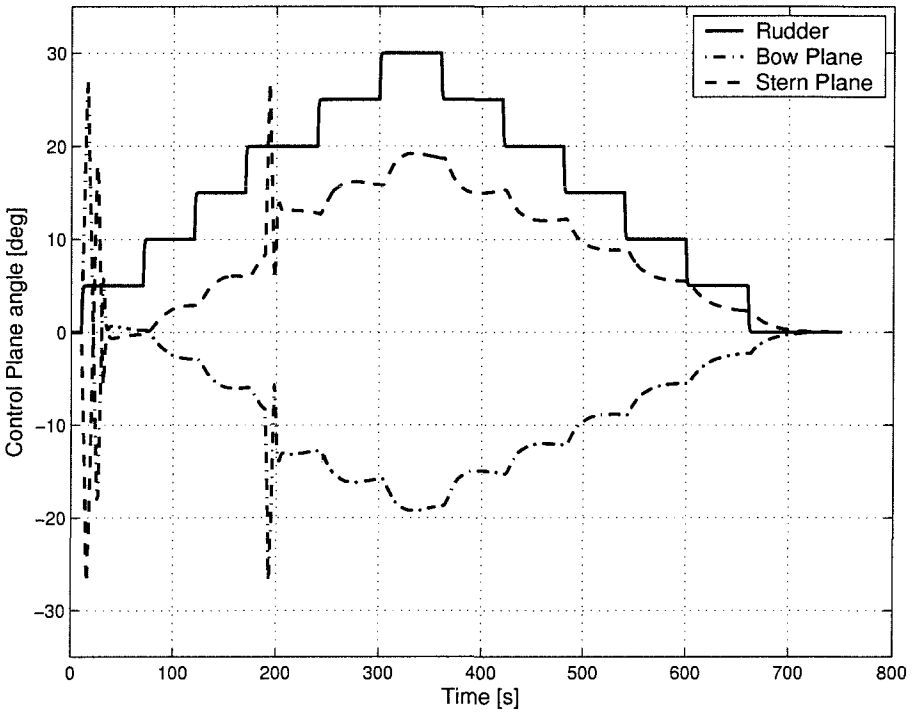

Figure 22: The control plane angle time history for submarine 1 performing the SubHov comparison manoeuvre.

5.8.2 Comparison of the Predictions

The positional time history of Submarine 1 generated by SubHov and the Matlab (version 3) simulations are shown in Figure 23. The submarine 1 path for each simulation appear identical. However, on closer inspection small differences can be seen. Figures 24 and 25 present differences along with the actual outputs for the x and u values. Similar plots for other observed differences are provided in Appendix E.

The x and u values are highlighted as they show a feature common to each of the three test submarines performing the defined comparison manoeuvre, that is, the Matlab simulation consistently generates slightly larger forward speeds than that of SubHov. The reason for this is not clear, the Matlab simulation has been checked repeatedly for errors and nothing has been found. As the effect is quite small it is assumed to be due to a difference in implementation between SubHov and the Matlab simulation.

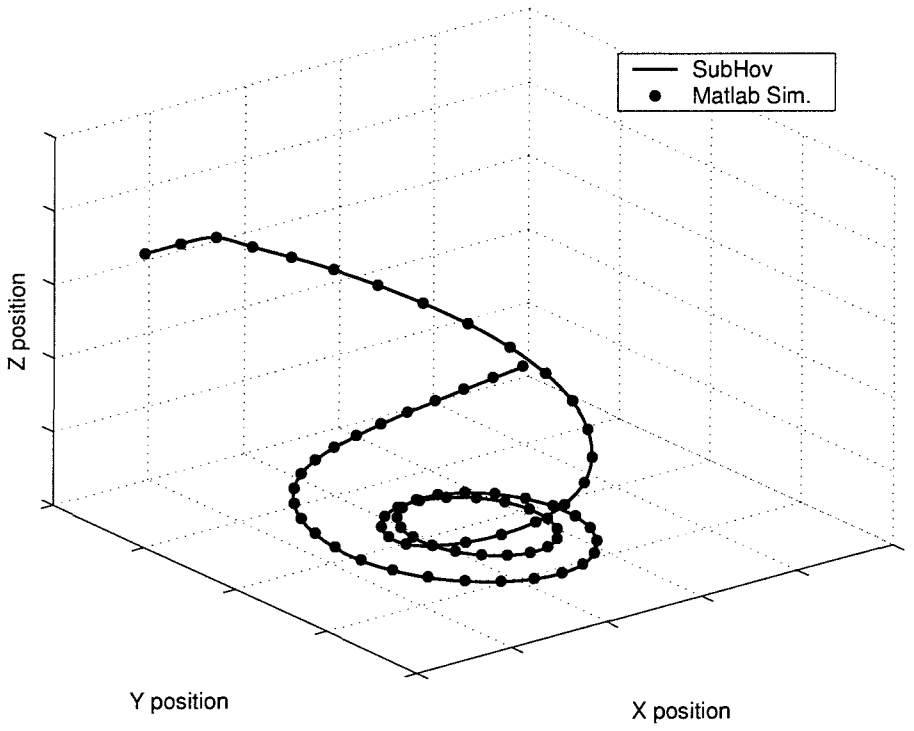

Figure 23: Comparison of the SubHov and Matlab simulation positional time history.

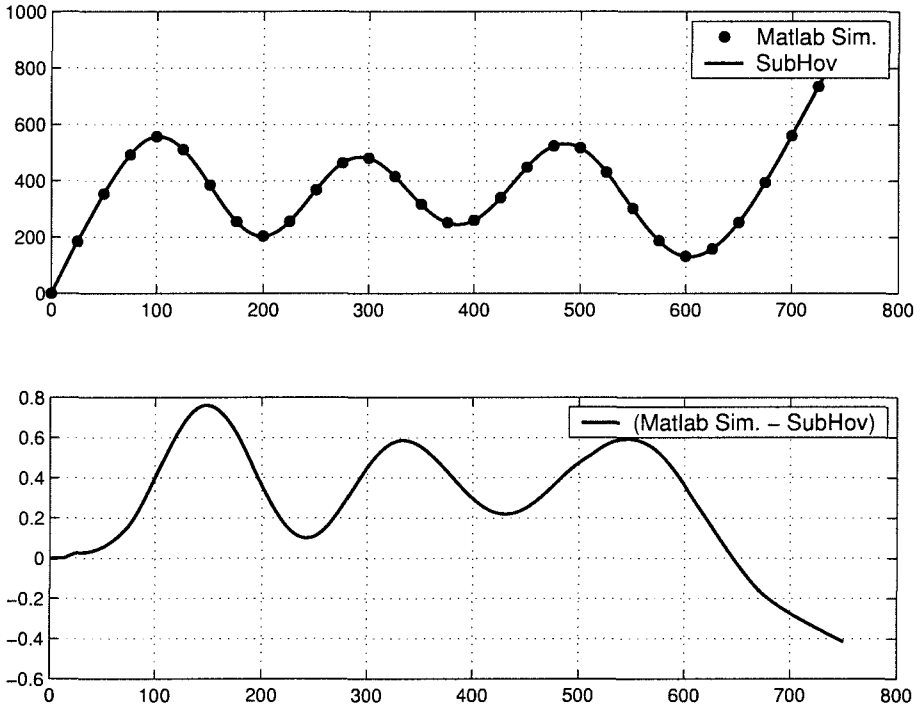

Figure 24: Plot of x and x error.

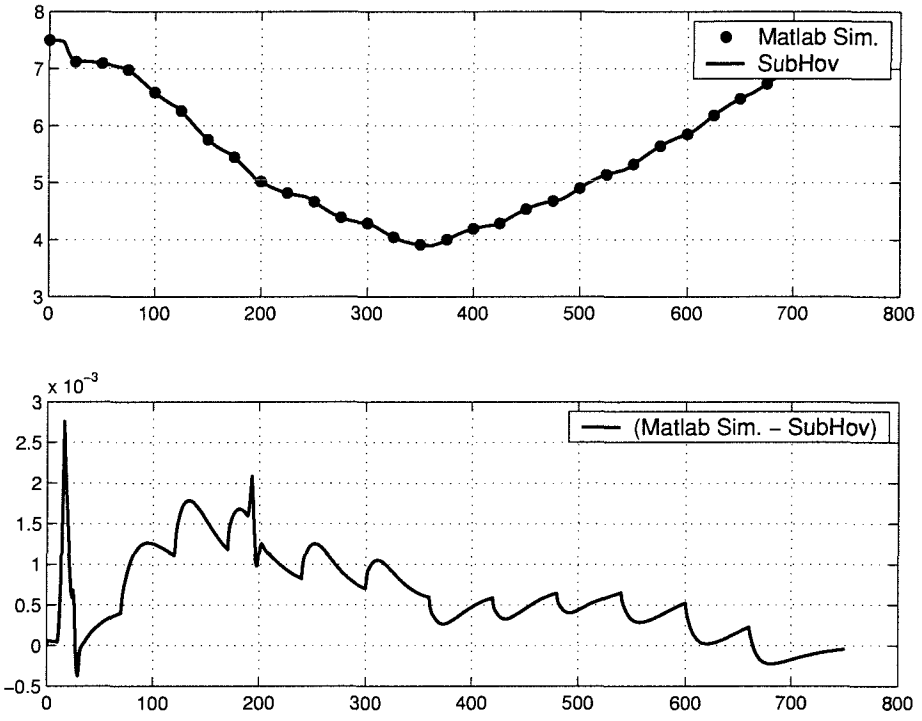

Figure 25: Plot of u and u error.

As it is not practical to describe the difference in the simulations by plotting the graphs of each state vector variable the maximum absolute error for each has been calculated along with the associated cost function value (using the cost function described in Section 4.4.2). This data is presented in Table 2.

	submarine 1	submarine 2	submarine 3	units
x	0.761	0.772	0.659	m
y	0.397	0.415	0.300	m
z	0.570	0.179	0.108	m
ϕ	0.244×10^{-3}	0.332×10^{-3}	0.122×10^{-3}	rad
θ	1.623×10^{-3}	1.379×10^{-3}	1.187×10^{-3}	rad
ψ	2.391×10^{-3}	2.531×10^{-3}	1.187×10^{-3}	rad
u	2.868×10^{-3}	2.502×10^{-3}	3.585×10^{-3}	$\text{m}\cdot\text{s}^{-1}$
v	0.960×10^{-3}	1.443×10^{-3}	0.912×10^{-3}	$\text{m}\cdot\text{s}^{-1}$
w	4.693×10^{-3}	4.378×10^{-3}	3.184×10^{-3}	$\text{m}\cdot\text{s}^{-1}$
p	0.070×10^{-3}	0.203×10^{-3}	0.066×10^{-3}	$\text{rad}\cdot\text{s}^{-1}$
q	0.375×10^{-3}	0.319×10^{-3}	0.215×10^{-3}	$\text{rad}\cdot\text{s}^{-1}$
r	0.071×10^{-3}	0.111×10^{-3}	0.045×10^{-3}	$\text{rad}\cdot\text{s}^{-1}$
cost function	2434.4	2215.9	1648.1	

Table 2: Maximum differences between SubHov and the Matlab simulation for three submarines performing the comparison manoeuvre.

The table shows that the errors associated with the different submarines are not that large and would be perfectly acceptable in predicting the motion of a submarine from an engineering standpoint. However, they are not the same.

To better appreciate this error a comparison of the relative difference between SubHov outputs using different integration time step sizes was undertaken. The SubHov simulation was tested performing the comparison manoeuvre with time step of 1s, 0.1s and 0.01s. The 0.01s time step was assumed to be correct and all the errors are related to this. The results for the difference produced by time steps of 1s and 0.1s are shown in Table 3.

	$\Delta t = 1$s	$\Delta t = 0.1$s	units
x	4.536	1.635	m
y	6.549	2.284	m
z	1.242	0.114	m
ϕ	5.11×10^{-3}	0.32×10^{-3}	rad
θ	38.62×10^{-3}	3.30×10^{-3}	rad
ψ	29.86×10^{-3}	10.26×10^{-3}	rad
u	0.101	7.693×10^{-3}	$\text{m}\cdot\text{s}^{-1}$
v	0.010	0.482×10^{-3}	$\text{m}\cdot\text{s}^{-1}$
w	0.122	7.935×10^{-3}	$\text{m}\cdot\text{s}^{-1}$
p	2.67×10^{-3}	0.120×10^{-3}	$\text{rad}\cdot\text{s}^{-1}$
q	12.47×10^{-3}	1.205×10^{-3}	$\text{rad}\cdot\text{s}^{-1}$
r	0.86×10^{-3}	0.029×10^{-3}	$\text{rad}\cdot\text{s}^{-1}$
cost function	102150	4325.0	

Table 3: Maximum differences between SubHov simulating the comparison manoeuvre with a 0.01s time step and SubHov simulating the same manoeuvre with 1.0s and 0.1s time steps.

It is not possible to say which time step is more accurate but reducing the time step to 0.01s increases the simulation time ten fold from that of the 0.1s time step. As the difference between the 0.1s and 0.01s time steps is small the extra effort in computing the vehicle track using the 0.01s time step was not justified. Also considerable degradation in performance was shown when the 1s time step was used. This large error occurred because the simulation was becoming unstable. The instability manifested itself as oscillatory behaviour in certain state vector variables. Hence, the time savings associated with the 1s time interval are outweighed by the increase in accuracy associated with the 0.1s time step.

Also Table 3 shows that the errors associated with different step sizes are larger than those between the SubHov and Matlab simulation with a 0.1s time step. It was therefore felt that the Matlab simulation produce an acceptable level of accuracy and

could be used in the parameter identification task.

5.9 The Accuracy of the Matlab Simulation

The previous section showed that the SubHov simulation output was sensitive to the time step used. It was considered necessary to repeat the indicated testing using the Matlab simulation to establish the accuracy of the Matlab simulation. However, instead of using the comparison manoeuvre previously described for the SubHov comparison the three parameter identification manoeuvres described in Section 4.6 were selected. The accuracy of the simulation in predicting these manoeuvres would be useful in assessing how well $\hat{\boldsymbol{N}}$ converged to $\boldsymbol{N}$ in the non-linear identification manoeuvre.

It was assumed that as the time step was decreased the simulation would become more accurate, as the truncation error is reduced and the rounding error was assumed to be small. Thus, by reducing the step size it is possible to assess the 'accuracy' of the simulation using a specified time step. In this case 'accuracy' does not describe how well the simulation predicts UV motion, but how well the simulation approximates the Booth et al. (1980) equations.

The proposed simulation time step size was 0.1s to allow the simulation to identify the coefficients used to produce the QinetiQ test manoeuvres. However, the accuracy of the manoeuvres was investigated using a range of time steps.

The accuracy was assessed by simulating the horizontal plane, vertical plane and coupled standard manoeuvres described in Section 4.6 with time steps of 0.001, 0.01, 0.1 and 1 second. This examination was repeated fore each of the three submarines. This was done to assess whether the accuracy was dependent on the UV simulated.

The 0.01s, 0.1s and 1s predictions are compared with the 0.001s simulation results. The associated cost function variations are shown in Table 4 and the maximum positional error results are shown in Table 5. Both tables shows how the 'error' reduces as the time step is reduced.

Manoeuvre	Δt	Submarine 1	Submarine 2	Submarine 3
Horizontal	0.01	1.116×10^{1}	9.850×10^{0}	1.016×10^{1}
	0.1	1.349×10^{3}	1.191×10^{3}	1.229×10^{3}
	1.0	1.911×10^{5}	1.693×10^{5}	1.744×10^{5}
Vertical	0.01	1.269×10^{-2}	1.140×10^{-2}	1.269×10^{-2}
	0.1	2.416×10^{0}	1.424×10^{0}	1.628×10^{0}
	1.0	1.427×10^{4}	6.251×10^{3}	2.617×10^{4}
Coupled	0.01	1.096×10^{1}	1.006×10^{1}	1.016×10^{1}
	0.1	1.326×10^{3}	1.216×10^{3}	1.231×10^{3}
	1.0	1.874×10^{5}	1.726×10^{5}	1.795×10^{5}

Table 4: Variation of cost function for each submarine undertaking the three standard manoeuvres using different times steps.

To make the cost function comparison meaningful the 0.01s and 0.1s time step cost functions were calculated using data selected at a 0.1s interval. Thus comparable results were produced as the number of data entries in each case was the same. However, it was not possible to use a 0.1s interval for the 1.0s time step without interpolating the values. To overcome this problem the 1.0s time step cost function was calculated at 1.0s intervals and then multiplied by 10 to produce an estimate of the cost function value based on data sampled at a 0.1s interval.

Manoeuvre	Δt	Submarine 1	Submarine 2	Submarine3
Horizontal	0.01	0.062	0.063	0.063
	0.1	0.682	0.688	0.695
	1.0	8.128	8.197	8.296
Vertical	0.01	0.004	0.003	0.003
	0.1	0.041	0.028	0.033
	1.0	3.753	2.423	4.653
Coupled	0.01	0.063	0.062	0.064
	0.1	0.694	0.686	0.706
	1.0	8.160	8.146	8.330

Table 5: Maximum positional difference for each submarine undertaking the three standard manoeuvres using different times steps.

The data shows that the submarine used has little effect upon the manoeuvre error. However, the particular manoeuvre performed has a significant effect. The results show that the truncation error at a time step of 0.1s produces a cost function of approximately 1300 and a positional error of approximately 0.7 metres for both the horizontal and coupled cases. The error is substantially less for the vertical with a maximum cost function of approximately 2.5 and a positional error of approximately 0.04 metres. This difference is explained by the vertical manoeuvre being less severe, with a maximum control plane deflection of $\pm 5^\circ$ compared to 30° for the horizontal and coupled manoeuvres. Also, the manoeuvre is also shorter in duration and so errors do not have as much time to build up.

To conclude the results show that, like SubHov, the choice of a 0.1s time step is a reasonable trade off between speed and accuracy.

5.10 Conclusions

This chapter has described how the Booth et al. (1980) submarine equations have been turned into a simulation that can be used with the linear and non-linear parameter identification procedures.

The chapter started by describing the requirements for the simulation and discussed some of the issues of matching the output of the Matlab simulation to that of QinetiQ simulation SubHov. Next, the equations were described using notation similar to that of Fossen and thereafter rearranged into a form suitable for computer simulation. Following this the numerical integration of the equations was considered and the chosen integration routine was described.

Having described the simulation in theory the implementation within the Matlab environment was discussed. This described the three simulation versions implemented and their respective simulation speed. Following this the testing and validation of the simulation was described. Here it was shown that although the various simulation versions agreed almost exactly with each other there was a distinct difference in output compared to the SubHov simulation. This difference was assumed to be due to a slightly different implementation of the equations. However, as the difference between the Matlab simulation and SubHov was less than that produced by reducing the SubHov integration time step the accuracy of the Matlab simulation was considered to be acceptable.

The chapter concluded with an analysis of the accuracy of producing the three test manoeuvres using the Matlab simulation. This accuracy was calculated by reducing the time step of the Matlab simulation and was based on the assumption that reducing the time step improved the accuracy of the simulation.

Chapter 6

Assessment of the Uniqueness of the Hydrodynamic Coefficients

6.1 Introduction

Having created the simulation and linked it with the associated optimization routine, as will be discussed in Chapter 7, initial testing showed that although the simulated track converged to the target manoeuvre, the identified hydrodynamic coefficients were substantially different to those used to produce the target track. It was not immediately clear whether this situation was due to the hydrodynamic coefficients being *non-unique*, and hence other sets of coefficients could produce the same manoeuvre, or whether the equations were *ill-conditioned* and so very similar manoeuvres could be produced by grossly different sets of hydrodynamic coefficients. These issues were previously discussed in Section 4.5.1. This chapter answers the question of whether the hydrodynamic coefficients are non-unique.

For the coefficients to be non-unique, a different set of coefficients has to be capable of producing the same acceleration in any manoeuvre. The question of non-uniqueness can be addressed by using ideas developed in the linear identification procedure outlined in Section 4.4.1.

Taking the X force equation as an example. The equation describing the forces,

moments and accelerations in the x direction can be written as the linear equation,

$$\boldsymbol{A}_X \boldsymbol{\xi}_X = \boldsymbol{b}_X. \tag{8}$$

Where $\boldsymbol{A}_X$ is a matrix of the X hydrodynamic coefficient multipliers, $\boldsymbol{\xi}_X$ is a vector of the X hydrodynamic coefficients and $\boldsymbol{b}_X$ is a vector of the resultant forces. The values $\boldsymbol{A}_X$ and $\boldsymbol{b}_X$ are specific to a given submarine performing a given manoeuvre.

For there to be a unique set of coefficient for this manoeuvre there has to be a unique solution to Equation (8). This will not happen if there is a solution for

$$\boldsymbol{A}_X \boldsymbol{\xi}_X^\sharp = 0 \tag{9}$$

as then

$$\boldsymbol{A}_X \boldsymbol{\xi}_X = \boldsymbol{A}_X \boldsymbol{\xi}_X + k\boldsymbol{A}_X \boldsymbol{\xi}_X^\sharp = \boldsymbol{A}_X(\boldsymbol{\xi}_X + k\boldsymbol{\xi}_X^\sharp) = \boldsymbol{b}$$

for any scalar k. Therefore any vector defined by $(\boldsymbol{\xi}_x + k\boldsymbol{\xi}_x^\sharp)$ will be a solution to Equation (8) and if follows that there will be an infinite number of sets of hydrodynamic coefficients which will produce the same manoeuvre.

Equation (9) defines the null space of $\boldsymbol{A}_X$, see Strang (1988), and is written as $\mathcal{N}(\boldsymbol{A}_X)$ in this thesis. If the null space is zero dimensional (i.e only containing the zero vector) then the solution is unique and the X force hydrodynamic coefficients would be unique. If on the other hand $\mathcal{N}(\boldsymbol{A}_X)$ is not zero dimensional then there would be an infinite number of solutions which satisfy the equation and there would be an infinite number of sets of hydrodynamic coefficients which would produce the same X force during the performed manoeuvre.

The dimensions of the null space can be determined from a fundamental theorem of linear algebra that states,

$$\text{dimension of } \mathcal{N}(\boldsymbol{A}) = n - r$$

where,

$$n = \text{number of columns in A,}$$
$$r = \text{the rank of A.}$$

So to assess whether there is a unique set of X force hydrodynamic coefficients for a given manoeuvre it is only necessary to determine the rank of the $\boldsymbol{A}_X$ matrix and to compare this to the number of hydrodynamic coefficients in the associated $\boldsymbol{\xi}_X$ vector. However, this approach does not prove that the coefficients will be non-unique for every manoeuvre, but, as will be seen, the approach does provide insight into how to show that the coefficients are non-unique.

If the coefficients are non-unique all is not totally lost. As by specifying the value of a coefficient in $\boldsymbol{\xi}_X$ the dimension of $\mathcal{N}(\boldsymbol{A}_X)$ will be reduced by one (provided the $\mathcal{N}(\boldsymbol{A}_X)$ includes that coefficient). Thus, by specifying enough coefficient the $\mathcal{N}(\boldsymbol{A}_X)$ will become zero dimensional and the remaining coefficient values can be determined. However, the values of the specified coefficients need to be accurately determined as errors in their values will lead to errors in the identified coefficients. For this reason is is preferable to specify the added-mass coefficients as they are relatively simple to determine accurately as described in Section ??.

The forgoing discussion is directly applicable to the Y & Z force and K, M & N moment hydrodynamic coefficient.

To calculate all the associated matrices $\boldsymbol{A}$ it was necessary to know the accelerations at every time step of the simulations as well as the velocities and attitude. To achieve this the simulation was modified to output the accelerations of the vehicle $\dot{\boldsymbol{\nu}}$ as well as the vehicle state vector $\boldsymbol{s}_{\mathbf{v}}$.

The remainder of this chapter describes the identification of the rank of the different force and moment $\boldsymbol{A}$ matrices associated with the three test manoeuvres performed by each of the three submarines. The $\boldsymbol{A}$ matrices associated with a given coefficient set are identified by a subscript, for example $\boldsymbol{A}_X$ is the $\boldsymbol{A}$ matrix associated with the unknown X coefficients.

6.2 The Horizontal Manoeuvre Rank Analysis

The horizontal manoeuvre was run using the modified simulation and the $\boldsymbol{A}$ matrices were calculated for the three submarines, the results of the rank analysis are presented

in Table 6. They show that the $\boldsymbol{A}$ matrices are under-determined for the Y and N coefficients. This was a surprise as it was assumed that the matrices would be of full rank.

Matrix	Rank for the submarine 1	Rank for the submarine 2	Rank for the submarine 3	Columns of $\boldsymbol{A}$
$\boldsymbol{A}_X$	6	6	6	6
$\boldsymbol{A}_Y$	8	8	8	9
$\boldsymbol{A}_N$	8	8	8	10

Matrix	Dimension of $\mathcal{N}(\boldsymbol{A})$ sub. 1	Dimension of $\mathcal{N}(\boldsymbol{A})$ sub. 2	Dimension of $\mathcal{N}(\boldsymbol{A})$ sub. 3	Associated added-mass
$\boldsymbol{A}_X$	0	0	0	–
$\boldsymbol{A}_Y$	1	1	1	$Y'_{\dot{v}}$
$\boldsymbol{A}_N$	2	2	2	$N'_{\dot{v}}$ & $N'_{\dot{r}}$

Table 6: Horizontal manoeuvre rank analysis.

The table also shows the added-mass that is associated with the rank reduction and hence by specifying this added-mass the remaining coefficients would be identifiable.

The causes of the rank reduction in the horizontal manoeuvre are outlined in the following sections.

6.2.1 The Causes of the Reduced Rank of the $\boldsymbol{A}_Y$ Matrix

To explain this phenomenon it is necessary to consider the simplified horizontal equation of motion used to calculate the acceleration in the Y direction. The horizontal sway equation given in Appendix D.2 can be expressed as,

$$m[\dot{v} + ur - y_G r^2 + x_G \dot{r}] = Y_{rhs} + \frac{1}{2}\rho l^3 (Y'_{\dot{v}}\dot{v} + Y'_{ur}ur + lY'_{\dot{r}}\dot{r}),$$

where,

$$\begin{aligned} Y_{rhs} &= \frac{1}{2}\rho l^2(Y'_{uu}u^2 + Y'_{uv}uv + Y'_{v\nu}v\nu + Y'_{uu\delta R}u^2\delta R) \\ &+ \frac{1}{2}\rho l^3(Y'_{v\nu|\frac{r}{v}|}v|r| + Y'_{u|r|\delta R}u|r|\delta R)). \end{aligned} \tag{10}$$

The Y-direction motion equation can be rearranged to give $\dot{v}$ as a function of the hydrodynamic coefficients ($\boldsymbol{\xi}_Y$), namely,

$$\dot{v}(\boldsymbol{\xi}_Y) = \left[\frac{Y_{rhs} + (\frac{1}{2}\rho l^3 Y'_{ur} - m)ur + (\frac{1}{2}\rho l^4 Y'_{\dot{r}} - mx_G)\dot{r}}{m - \frac{1}{2}\rho l^3 Y'_{\dot{v}}}\right] + \left[\frac{my_G r^2}{m - \frac{1}{2}\rho l^3 Y'_{\dot{v}}}\right]. \tag{11}$$

For the hydrodynamic coefficients to be non-unique at least two sets of coefficients have to produce the same sway acceleration ($\dot{v}$) for every manoeuvre. Thus,

$$\dot{v}(\boldsymbol{\xi}_Y) = \dot{v}(\hat{\boldsymbol{\xi}}_Y) \qquad \text{and} \qquad \boldsymbol{\xi}_Y \neq \hat{\boldsymbol{\xi}}_Y \,.$$

This can only occur if the hydrodynamic coefficients can be modified to scale the numerator and denominator of Equation (11) by the same amount (i.e. effectively multiply by $\frac{k}{k}$). This would mean,

$$\begin{aligned} \dot{v}(\hat{\boldsymbol{\xi}}_Y) &= \dot{v}(\boldsymbol{\xi}_Y) \cdot \left[\frac{k}{k}\right] \\ &= \left[\frac{Y_{rhs} + (\frac{1}{2}\rho l^3 Y'_{ur} - m)ur + (\frac{1}{2}\rho l^4 Y'_{\dot{r}} - mx_G)\dot{r}}{m - \frac{1}{2}\rho l^3 Y'_{\dot{v}}}\right] \cdot \left[\frac{k}{k}\right] + \left[\frac{my_G r^2}{m - \frac{1}{2}\rho l^3 Y'_{\dot{v}}}\right] \cdot \left[\frac{k}{k}\right]. \end{aligned} \tag{12}$$

It is assumed, unless otherwise stated, that the UV motions are independent and so by inspecting Equation (12) it can be seen that the $my_G r^2$ term can make it impossible to modify $\boldsymbol{\xi}_Y$ and still have the same $\dot{v}$, as there is no hydrodynamic coefficient in the numerator. However, the three submarines used with the horizontal manoeuvre have $y_G = 0$. Thus, the Equation (12) reduces to,

$$\begin{aligned} \dot{v}(\hat{\boldsymbol{\xi}}_Y) &= \left[\frac{Y_{rhs} + (\frac{1}{2}\rho l^3 Y'_{ur} - m)ur + (\frac{1}{2}\rho l^4 Y'_{\dot{r}} - mx_G)\dot{r}}{m - \frac{1}{2}\rho l^3 Y'_{\dot{v}}}\right] \cdot \left[\frac{k}{k}\right] \\ &= \frac{kY_{rhs} + k(\frac{1}{2}\rho l^3 Y'_{ur} - m)ur + k(\frac{1}{2}\rho l^4 Y'_{\dot{r}} - mx_G)\dot{r}}{k(m - \frac{1}{2}\rho l^3 Y'_{\dot{v}})}. \end{aligned} \tag{13}$$

Multiplying all the hydrodynamic coefficient of Equation (10) by a scalar k results in kY_{rhs}. From Equation (13) it is possible to identify how to modify coefficients $Y'_{\dot{v}}$ and Y'_{ur} & $Y'_{\dot{r}}$ to make $\dot{v}(\hat{\boldsymbol{\xi}}_Y) = \dot{v}(\boldsymbol{\xi}_Y)$. Thus, provided y_G is zero the horizontal yaw equations have a non-unique set of hydrodynamic coefficients, thereby explaining the rank deficiency of $\boldsymbol{A}_Y$ for this manoeuvre. Also as no assumptions about $\boldsymbol{A}_Y$ have been made it follows that the coefficients will be non-unique for all manoeuvres.

As UVs tend to have their centre of gravity on the $x-y$ plane the value of y_G tends to be zero, thus for a horizontal manoeuvre the $\boldsymbol{A}_Y$ matrix will tend to be rank deficient. As the $Y'_{\dot{v}}$ term forms the denominator of Equation (13) it is chosen to be specified.

6.2.2 The Causes of the Reduced Rank of the $\boldsymbol{A}_N$ Matrix

The rank of $\boldsymbol{A}_N$ for the spiral manoeuvre corresponds to a $\mathcal{N}(\boldsymbol{A}_N)$ having a dimension of 2. Hence the solution is non-unique and two separate coefficient relationships are required to span $\mathcal{N}(\boldsymbol{A}_N)$. Following the same basic approach to that described above, two added mass coefficients were identified as being associated with the reduction in rank; these $N'_{\dot{r}}$ and $N'_{\dot{v}}$. The reasons for the rank reduction are discussed next.

Rank reduction of $\boldsymbol{A}_N$ associated with $N'_{\dot{r}}$

The equation describing the yaw acceleration for the horizontal manoeuvre (described in Appendix D.2) can be written as,

$$I_{ZZ}\dot{r} + m\left[x_G\left(\dot{v} + ur\right) - y_G\left(\dot{u} - vr\right)\right] = N_{rhs} + \frac{1}{2}\rho l^4\left(N'_{\dot{v}}\dot{v} + N'_{ur}ur\right) + \frac{1}{2}\rho l^5 N'_{\dot{r}}\dot{r}, \quad (14)$$

with,

$$\begin{aligned} N_{rhs} = &\frac{1}{2}\rho l^3\left(N'_{uu}u^2 + N'_{uv}uv + N'_{uu\delta R}u^2\delta R\right) \\ &+ \frac{1}{2}\rho l^3\left(N'_{v\nu}v|v|\right) \\ &+ \frac{1}{2}\rho l^4\left(N'_{r\nu}r|v| + N'_{u|r|\delta R}u|r|\delta R\right) \\ &+ \frac{1}{2}\rho l^5\left(N'_{r|r|}r|r|\right). \end{aligned}$$

Equation 14 can be rearranged to give,

$$\dot{r} = \left[\frac{N_{rhs} + \left(\frac{1}{2}\rho l^4 N'_{\dot{v}} - m x_G\right)\dot{v} + \left(\frac{1}{2}\rho l^4 N'_{ur} - m x_G\right) ur}{I_{ZZ} - \frac{1}{2}\rho l^5 N'_{\dot{r}}}\right] + \left[\frac{m y_G\left(\dot{u} - vr\right)}{I_{ZZ} - \frac{1}{2}\rho l^5 N'_{\dot{r}}}\right]. \quad (15)$$

For the same manner described for Equations (13), provide $y_G = 0$ the hydrodynamic coefficients can be changed without affecting $\dot{r}$. This explains the reduction in the rank of $\mathcal{N}(\boldsymbol{A}_N)$ by one, the second cause of rank reduction is due to $N'_{\dot{v}}$ and is explained next.

Rank reduction of $\boldsymbol{A}_N$ associated with $N'_{\dot{v}}$

The $N'_{\dot{v}}$ term reduces the rank of $\boldsymbol{A}_N$ as shown by first writing Equation (15) in the form,

$$\begin{aligned}\dot{v} = {} & C_{hv1}u^2 + C_{hv2}uv + C_{hv3}u^2\delta R \\ & + C_{hv4}v|r| + C_{hv5}u|r|\delta R \\ & + C_{hv6}ur + C_{hv7}\dot{r} + C_{hv8}y_G r^2\end{aligned} \quad (16)$$

Here, the constants represent the the velocity multipliers, for example C_{hv1} represents,

$$C_{hv1} = \frac{\frac{1}{2}\rho l^2 Y'_{uu}}{m - \frac{1}{2}\rho l^3 Y'_{\dot{v}}}.$$

These constants can be changed by changing the hydrodynamic coefficients. Equation (15) can also be written in the same fashion and becomes,

$$\begin{aligned}\dot{r} = {} & C_{hr1}u^2 + C_{hr2}uv + C_{hr3}u^2\delta R \\ & + C_{hr4}r|v| + C_{hr5}u|r|\delta R \\ & + C_{hr6}ur + C_{hr7}\dot{v} \\ & + C_{hr9}v|v| + C_{hr8}r|r| + C_{hr10}y_G\left(\dot{u} - vr\right).\end{aligned} \quad (17)$$

Comparing Equations (16) and (17) we see that if Equation (16) was substituted into Equation (17) the $\dot{v}$ dependence would disappear and that the two 'new' terms

$C_{hv8}y_G r^2$ and $C_{hv4}v|r|$ would be added to Equation (17). But as was noted earlier $y_G = 0$ for the test submarines so the 'new' $C_{hv8}y_G r^2$ term can be ignored. The remaining 'new' term $C_{hv4}v|r|$ is very similar to $C_{hr4}r|v|$ with the only difference being the location of the modulus sign ie $v|r|$ and $r|v|$. So if either $v|r| = r|v|$ or $v|r| = -r|v|$ is also always true then Equation (16) can be substituted into Equation (17) without adding any new terms. This would occur because $\dot{v}$ would be a linear combination of the remaining motions.

From a consideration of the physics of UV motions it was assumed that it was not possible to induce a yaw rate without a corresponding sway velocity. Combining this assumption with the axis system used to describe the UV motion, it is shown that during normal turning manoeuvre the sign of v is always opposite to that of r as is illustrated in Figure 26.

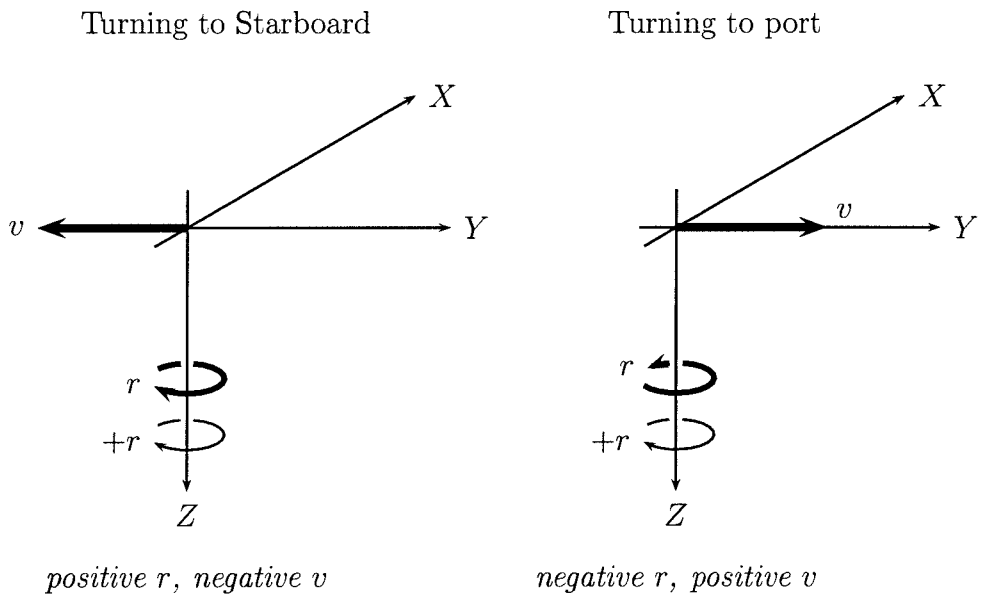

Figure 26: Horizontal Manoeuvre showing the relationship between v & r

Hence, during normal turning manoeuvres $v|r|$ is of opposite sign to $r|v|$ as,

$$+ve|-ve| = -(-ve|+ve|).$$

Therefore,

$$v|r| = -r|v|.$$

This assumption was tested for the horizontal manoeuvre by plotting $\frac{\text{sign}(v)}{\text{sign}(r)}$ against time. This plot showed the assumption to be true for the tested manoeuvre.

Thus, as $y_G = 0$ for the three submarines and $\dot{v}$ is a linear combination of the terms of $\dot{r}$ Equation (17) it follows that $N'_{\dot{v}}$ can be written as a linear combination of the other N moment terms. Thus, the rank of $\mathcal{N}(\boldsymbol{A}_N)$ is reduced by 1.

The proceeding analysis outlines the causes of the the rank reduction of $\boldsymbol{A}_N$ which occur when the y_G term is zero.

6.3 The Vertical Manoeuvre Rank Analysis

The vertical simulation was run with the three submarines and the associated $\boldsymbol{A}$ matrices were produced. As the bow planes were not used during the vertical manoeuvre, all the coefficients associated with δB could not be identified. Hence the columns in the $\boldsymbol{A}$ matrices associated with the δB coefficients have no effect on the manoeuvre, and so were removed for the rank calculations. The rank of $\boldsymbol{A}$, the number of columns of $\boldsymbol{A}$ and the dimension of $\mathcal{N}(\boldsymbol{A})$ are shown in Table 7.

Matrix	Rank for the submarine 1	Rank for the submarine 2	Rank for the submarine 3	Columns of $\boldsymbol{A}$
$\boldsymbol{A}_X$	6	6	6	6
$\boldsymbol{A}_Z$	10	11	11	11
$\boldsymbol{A}_M$	11	12	12	12

Matrix	Dimension of $\mathcal{N}(\boldsymbol{A})$ sub. 1	Dimension of $\mathcal{N}(\boldsymbol{A})$ sub. 2	Dimension of $\mathcal{N}(\boldsymbol{A})$ sub. 3	Associated added-mass
$\boldsymbol{A}_X$	0	0	0	–
$\boldsymbol{A}_Z$	1	0	0	$Z'_{\dot{w}}$
$\boldsymbol{A}_M$	1	0	0	$M'_{\dot{w}}$

Table 7: Vertical manoeuvre rank analysis.

These results show that submarine 1 has a non-unique set of hydrodynamic coefficients, whereas submarines 2 & 3 have unique sets of hydrodynamic coefficients. This difference was a surprise, but it justified the decision to test three different submarines so as not to 'tune' the procedure to any one submarine.

6.3.1 The Causes of the Reduced Rank of the $\boldsymbol{A}_Z$ Matrix

Using the vertical submarine equations of motion described in Appendix D.3 and combining them in the way outlined for the horizontal manoeuvre, the vertical acceleration $\dot{w}$ can be written as,

$$\dot{w} = \left[\frac{Z_{rhs} + \left(\frac{1}{2}\rho l^3 Z'_{uq} + m\right) + \left(\frac{1}{2}\rho l^4 Z'_{\dot{q}} - m x_G\right)}{m - \frac{1}{2}\rho l^3 Z'_{\dot{w}}}\right] + \left[\frac{m z_G q^2 - \Delta B \cos\theta}{m - \frac{1}{2}\rho l^3 Z'_{\dot{w}}}\right]. \quad (18)$$

Where, $\Delta B = B - mg.$

Equation (18) shows that provided $m z_G q^2$ and $\Delta B \cos\theta$ are zero then the hydrodynamic coefficients can be adjusted while maintaining $\dot{w}$, and hence the coefficients are non-unique. Submarines 2 & 3 have non-zero values of z_G, explains why their associated $\boldsymbol{A}_Z$ matrices are of full rank, but for submarine 1 $z_G = 0$, explaining why its coefficients are non-unique.

6.3.2 The Causes of the Reduced Rank of the A_M Matrix

The pitch rate acceleration $\dot{q}$ for the vertical sub-problem can be written as:

$$\dot{q} = \left[\frac{M_{rhs} + \left(\frac{1}{2}\rho l^4 M'_{uq} - mx_G\right) uq + \left(\frac{1}{2}\rho l^4 M'_{\dot{w}} + mx_G\right) \dot{w}}{I_{YY} - \frac{1}{2}\rho l^5 M'_{\dot{q}}}\right] + \left[\frac{-mz_G\left(\dot{u} + wq\right) - \left(mgx_G - Bx_B\right)\cos\theta - \left(mgz_G - Bz_B\right)\sin\theta}{I_{YY} - \frac{1}{2}\rho l^5 M'_{\dot{q}}}\right]. \quad (19)$$

From Equation (19) it can be seen that for $\dot{q}$ to remain unchanged for different sets of hydrodynamic coefficients then the terms z_G, z_B and $(mgx_G - Bx_B)$ must equal zero. However, this is not so for any of the submarines. Thus, an alternative mechanism is required to explain the rank reduction in the $\boldsymbol{A}_M$ matrix.

Rank reduction of $\boldsymbol{A}_M$ associated with $M'_{\dot{w}}$

The $\dot{w}$ equation can be written as

$$\begin{aligned}\dot{w} = {} & C_{v1}u^2 + C_{v2}uw + C_{v3}u^2\delta B + C_{v4}u^2\delta S \\ & + C_{v5}w|w| + C_{v6}u|w| + C_{v7}w^2 \\ & + C_{v8}uq \\ & + C_{v9}u|q|\delta S + C_{v10}w|q| \\ & + C_{v11}\dot{q} \\ & + \Delta B\cos\theta + mz_G q^2\end{aligned} \quad (20)$$

and the $\dot{q}$ can be written as

$$\begin{aligned}\dot{q} = {} & C_{m1}u^2 + C_{m2}uw + C_{m3}u^2\delta B + C_{m4}u^2\delta S \\ & + C_{m5}w|w| + C_{m6}u|w| + C_{m7}w^2 \\ & + C_{m8}uq \\ & + C_{m9}u|q|\delta S + C_{m10}q|w| \\ & + C_{m11}q|q| \\ & + C_{m12}uq + C_{m13}\dot{w} \\ & - mz_G\left(\dot{u} + wq\right) - \left(mgx_G - Bx_B\right)\cos\theta \\ & - \left(mgz_G - Bz_B\right)\sin\theta.\end{aligned} \quad (21)$$

In the same manner as the horizontal manoeuvre, in the vertical manoeuvre Equation (20) can be substituted into the Equation (21). This introduces the 'new' terms $(C_{v10}w|q|)$, $(\Delta B\cos\theta)$ and (mz_Gq^2) into the $\dot{q}$ equation while removing the $\dot{w}$ term. As mentioned earlier, ΔB is zero for all submarines, and z_G is zero for submarine 1 but not submarines 2 & 3. Hence, the rank of $\boldsymbol{A}_M$ for submarines 2 & 3 cannot be reduced using this technique.

The remaining 'new' term is multiplied by $w|q|$, which is very similar to the C_{m10} multiplier $q|w|$. Considering the physics of UV motions and noting $\Delta B = 0$, it is reasonable to assume that no heave velocity can be induced without a corresponding pitch rate. Thus, one can assume that

$$q|w| = w|q|.$$

This was the assumption that was tested for the vertical manoeuvres and was shown to be correct.

From this assumption, it becomes clear that Equation (20) can be substituted into Equation (21), thereby removing the $\dot{w}$ dependence, without adding any new terms. Hence, the $M'_{\dot{w}}$ coefficient can be written as a linear combination of the other M moment coefficients.

6.4 The Coupled Manoeuvre Rank Analysis

The coupled simulation was run with the three submarines, and the associated $\boldsymbol{A}$ matrices were produced. However, as with the vertical manoeuvre, the coupled manoeuvre does not use the bow plane, hence the columns associated with the δB were removed from the $\boldsymbol{A}$ matrix for the rank calculations. The rank of the matrix $\boldsymbol{A}$ and the number of columns of $\boldsymbol{A}$ are shown in Table 8. The dimension of $\mathcal{N}(\boldsymbol{A})$ along with the coefficients associated with the non-uniqueness are shown in Table 9.

Matrix	Rank for the submarine 1	Rank for the submarine 2	Rank for the submarine 3	Columns of $\boldsymbol{A}$
$\boldsymbol{A}_X$	11	11	11	11
$\boldsymbol{A}_Y$	17	17	17	18
$\boldsymbol{A}_Z$	16	17	17	17
$\boldsymbol{A}_K$	16	16	16	16
$\boldsymbol{A}_M$	17	18	18	18
$\boldsymbol{A}_N$	16	17	17	18

Table 8: Fully coupled case rank analysis.

Matrix	Dimension of $\mathcal{N}(\boldsymbol{A})$ sub. 1	Dimension of $\mathcal{N}(\boldsymbol{A})$ sub. 2	Dimension of $\mathcal{N}(\boldsymbol{A})$ sub. 3	Associated added-mass
$\boldsymbol{A}_X$	0	0	0	–
$\boldsymbol{A}_Y$	1	1	1	$Y'_{\dot{v}}$
$\boldsymbol{A}_Z$	1	0	0	$Z'_{\dot{w}}$
$\boldsymbol{A}_K$	0	0	0	–
$\boldsymbol{A}_M$	1	0	0	$M'_{\dot{w}}$
$\boldsymbol{A}_N$	2	1	1	$N'_{\dot{v}}$ & $N'_{\dot{r}}$

Table 9: The dimensions of the null spaces, $\mathcal{N}(\boldsymbol{A})$'s, for the coupled manoeuvre, and the causes of the rank reductions.

6.4.1 The Causes of the Reduced Rank of the $\boldsymbol{A}_Y$ Matrix

The acceleration $\dot{v}$ for the fully coupled submarine equation can be written as,

$$\dot{v} = \frac{\begin{pmatrix} Y_{rhs} - \left(Y'_{wp} + m\right) wp + \left(Y'_{ur} - m\right) ur + \left(Y'_{qr} - mz_G\right) qr \\ + \left(Y'_{\dot{p}} + mz_G\right) \dot{p} + \left(Y'_{pq} - mx_G\right) pq + \left(Y'_{\dot{r}} - mx_G\right) \dot{r} \end{pmatrix}}{m - \frac{1}{2}\rho l^3 Y'_{\dot{v}}}$$

$$+ \left[\frac{y_G\left(r^2 + p^2\right) - (\Delta B)\sin\phi\cos\theta}{m - \frac{1}{2}\rho l^3 Y'_{\dot{v}}}\right]. \quad (22)$$

The conditions under which the hydrodynamic coefficients can be changed but $\dot{v}$ kept constant are

$$y_G = 0 \quad \text{and} \quad \Delta B = 0.$$

The submarines examined were neutrally buoyant so $\Delta B = 0$, and as previously stated y_G was zero for all the submarines. Thus, non-unique assignment of the coefficients is possible, and the $Y'_{\dot{v}}$ term is considered responsible for the rank reduction in the $\boldsymbol{A}_Y$ matrix.

6.4.2 The Causes of the Reduced Rank of the $\boldsymbol{A}_Z$ Matrix

The acceleration $\dot{w}$ for the fully coupled submarine equation can be written as,

$$\dot{w} = \frac{\begin{pmatrix} Y_{rhs} + \left(\frac{1}{2}\rho l^3 Z'_{uq} + m\right) uq + \left(\frac{1}{2}\rho l^3 Z'_{vp} - m\right) vp + \left(\frac{1}{2}\rho l^4 Z'_{pp} + mz_G\right) p^2 \\ + \left(\frac{1}{2}\rho l^4 Z'_{rp} - mx_G\right) rp + \left(\frac{1}{2}\rho l^4 Z'_{\dot{q}} + mx_G\right) \dot{q} \end{pmatrix}}{m - \frac{1}{2}\rho l^3 Z'_{\dot{w}}}$$

$$+ \left[\frac{mz_G q^2 - my_G(rp + \dot{p}) - (\Delta B)\cos\phi\cos\theta}{m - \frac{1}{2}\rho l^3 Z'_{\dot{w}}}\right]. \quad (23)$$

Here, the conditions under which the hydrodynamic coefficients can be changed while maintaining $\dot{w}$ are,

$$z_G = 0, \quad y_G = 0 \quad \text{and} \quad \Delta B = 0.$$

As already noted both ΔB and y_G are zero for all three submarines. However, z_G is not zero for submarines 2 & 3, and so the rank of $\boldsymbol{A}_Z$ is not reduced for these two submarines.

6.4.3 The Causes of the Reduced Rank of the $\boldsymbol{A}_M$ Matrix

The acceleration $\dot{q}$ can be written as

$$\dot{q} = \frac{\begin{bmatrix} M_{rhs} + \left(\frac{1}{2}\rho l^5 M'_{pr} - I_{XX} + I_{YY}\right) pr + \left(\frac{1}{2}\rho l^5 M'_{pp} - I_{ZX}\right) p^2 \\ + \left(\frac{1}{2}\rho l^5 M'_{rr} + I_{ZX}\right) r^2 + \left(\frac{1}{2}\rho l^4 M'_{vr} + m z_G\right) vr \\ + \left(\frac{1}{2}\rho l^4 M'_{\dot{w}} + m x_G\right) \dot{w} + \left(\frac{1}{2}\rho l^4 M'_{uq} - m x_G\right) uq \\ + \left(\frac{1}{2}\rho l^4 M'_{vp} + m x_G\right) vp \end{bmatrix}}{I_{YY} - \frac{1}{2}\rho l^5 M'_{\dot{q}}}$$

$$+ \frac{\begin{bmatrix} (\dot{p} + qr) I_{XY} - (qr - \dot{r}) I_{YZ} - m z_G (\dot{u} + wq) \\ (m g x_G - B x_B) \cos\phi \cos\theta - (m g z_G - B z_B) \sin\theta \end{bmatrix}}{I_{YY} - \frac{1}{2}\rho l^5 M'_{\dot{q}}} \quad (24)$$

in the fully coupled submarine equations. The conditions under which the hydrodynamic coefficients can be changed while maintaining $\dot{q}$ are therefore

$$I_{XY} = 0, \quad I_{YZ} = 0, \quad z_G = 0, \quad z_B = 0,$$
$$\text{and} \quad m g x_G - B x_B = 0.$$

For the three submarines tested, I_{XY}, I_{YZ}, x_G and x_B are zero. However, for all three submarines $z_B \neq 0$. Thus, the $M'_{\dot{q}}$ coefficient does not explain the reduction in rank of the $\boldsymbol{A}_M$ matrix.

Rank reduction of $\boldsymbol{A}_M$ associated with $M'_{\dot{w}}$

An alternative cause of the linear combination is through the $\dot{w}$ equation. This equation can be written as,

$$\begin{aligned}\dot{w} &= C_{cw1}u^2 + C_{cw2}uw + C_{cw3}v^2 + C_{cw4}u^2\delta B + C_{cw5}u^2\delta S \\ &+ C_{cw6}w\nu + C_{cw7}u|w| + C_{cw8}|w\nu| \\ &+ C_{cw9}uq + C_{cw10}vp + C_{cw11}vr \\ &+ C_{cw12}u|q|\delta S + C_{cw13}w\nu\left|\frac{q}{w}\right| \\ &+ C_{cw14}p^2 + C_{cw15}r^2 + C_{cw16}rp + C_{cw17}\dot{q} \\ &+ \frac{mz_Gq^2 - my_G(rp+\dot{p}) + \Delta B\cos\phi\cos\theta}{m - \frac{1}{2}\rho l^3 Z'_{\dot{w}}}.\end{aligned} \tag{25}$$

Noting that the sign of q is the same as the sign of w, then it follow that

$$w\nu\left|\frac{q}{w}\right| = \text{sign}(w)|q|\nu = q\nu.$$

Combining this information with the fact that for submarine 1 z_G, y_G and ΔB are zero, then for submarine 1 Equation (25) becomes

$$\begin{aligned}\dot{w} &= C_{cw1}u^2 + C_{cw2}uw + C_{cw3}v^2 + C_{cw4}u^2\delta B + C_{cw5}u^2\delta S \\ &+ C_{cw6}w\nu + C_{cw7}u|w| + C_{cw8}|w\nu| \\ &+ C_{cw9}uq + C_{cw10}vp + C_{cw11}vr \\ &+ C_{cw12}u|q|\delta S + C_{cw13}q\nu \\ &+ C_{cw14}p^2 + C_{cw15}r^2 + C_{cw16}rp + C_{cw17}\dot{q}.\end{aligned} \tag{26}$$

Also, Equation (24) can be written as

$$\begin{aligned}\dot{q} &= C_{cq1}u^2 + C_{cq2}uw + C_{cq3}v^2 + C_{cq4}u^2\delta B + C_{cq5}u^2\delta S \\ &+ C_{cq6}w\nu + C_{cq7}u|w| + C_{cq8}|w\nu| \\ &+ C_{cq9}uq + C_{cq10}vp + C_{cq11}vr \\ &+ C_{cq12}u|q|\delta S + C_{cq13}q\nu \\ &+ C_{cq14}p^2 + C_{cq15}r^2 + C_{cq16}rp \\ &+ C_{cq17}\dot{w} + C_{cq18}p|p| + C_{q_{remainder}}.\end{aligned} \tag{27}$$

Comparing Equations (26) and (27), it can be seen that Equations (26) can be described by a linear combination of the first 16 terms of Equation (27). The rank of $\boldsymbol{A}_M$ was not reduced for submarine 2 & 3 as z_G was not equal to zero in their case.

6.4.4 The Causes of the Reduced Rank of the $\boldsymbol{A}_N$ Matrix

The $\dot{r}$ equation can be written as,

$$\dot{r} = \frac{\begin{bmatrix} N_{rhs} + (\frac{1}{2}\rho l^5 N'_{pq} - I_{YY} + I_{XX})pq + (\frac{1}{2}\rho l^5 N'_{qr} - I_{ZX})qr \\ +(\frac{1}{2}\rho l^5 N'_{\dot{p}} + I_{ZX})\dot{p} + (\frac{1}{2}\rho l^4 N'_{\dot{v}} - mx_G)\dot{v} \\ +(N'_{wp} + mx_G)wp + (\frac{1}{2}\rho l^4 N'_{ur} - mx_G)ur \end{bmatrix}}{I_{ZZ} + \frac{1}{2}\rho l^5 N'_{\dot{r}}}$$

$$+ \frac{\begin{bmatrix} (q + rp)I_{YZ} - (q^2 - p^2)I_{XY} + my_G(\dot{u} - vr + wq) \\ (mgx_G - Bx_B)\sin\phi\cos\theta + (mgy_G - By_B)\sin\theta \end{bmatrix}}{I_{ZZ} + \frac{1}{2}\rho l^5 N'_{\dot{r}}}. \quad (28)$$

The conditions under which the hydrodynamic coefficients can be changed while maintaining $\dot{r}$ are therefore,

$$I_{YZ} = 0, \quad I_{XY} = 0, \quad x_G = 0, \quad x_B = 0, \quad y_G = 0 \quad \text{and} \quad y_B = 0.$$

All these conditions are met by submarines 1, 2 & 3, this completely explains the reduction in rank of $\boldsymbol{A}_N$ submarines 2 & 3 but not for submarine 1. As the rank of the $\boldsymbol{A}_N$ matrix of submarine 1 is reduced by two then another coefficient can be written as a linear combination of the other coefficients.

Rank reduction of $\boldsymbol{A}_N$ associated with $N'_{\dot{v}}$

There are two possible added-mass coefficients that could be instrumental in reducing the rank of the $\boldsymbol{A}_N$ matrix, these are $N'_{\dot{v}}$ and $N'_{\dot{p}}$. The $\dot{p}$ equation contains the term,

$$(mgz_G - Bz_B)\sin\phi\cos\theta.$$

This term is not zero for all of the submarines; thus the $\dot{p}$ equation cannot be substituted into the $\dot{r}$ equation without adding this 'new' term. Hence, $N'_{\dot{p}}$ cannot be written as a linear combination of the N coefficients, so the rank of $\boldsymbol{A}_N$ would not be reduced.

On the other hand the $N'_{\dot{v}}$ term looks more promising. The $\dot{v}$ equation can be written as

$$\begin{aligned}\dot{v} &= C_{cv1}u^2 + C_{cv2}uv + C_{cv3}vw + C_{cv4}v\nu + C_{cv5}u^2\delta R \\ &+ C_{cv6}up + C_{cv7}ur + C_{cv8}vq + C_{cv9}wp + C_{cv10}wr \\ &+ C_{cv11}v\nu\left|\frac{r}{v}\right| + C_{cv12}u|r|\delta R \\ &+ C_{cv13}\dot{p} + C_{cv14}\dot{r} + C_{cv15}pq + C_{cv16}qr + C_{cv17}p|p| \\ &+ C_{cv18}\Delta B\sin\phi\cos\theta + C_{cv19}y_G(r^2+p^2),\end{aligned} \tag{29}$$

and as both ΔB and y_G equal zero the last two terms can be ignored.

The $\dot{r}$ equation can be written as,

$$\begin{aligned}\dot{r} &= C_{cr1}u^2 + C_{cr2}uv + C_{cr3}vw + C_{cr4}v\nu + C_{cr5}u^2\delta R \\ &+ C_{cr6}up + C_{cr7}ur + C_{cr8}vq + C_{cr9}wp + C_{cr10}wr \\ &+ C_{cr11}r\nu + C_{cr12}u|r|\delta R \\ &+ C_{cr13}\dot{p} + C_{cr14}\dot{r} + C_{cr15}pq + C_{cr16}qr + C_{cr17}r|r| \\ &+ C_{cr18}\dot{v} + C_{cr19}(mgx_G - Bx_B)\sin\phi\cos\theta \\ &+ C_{cr20}(mgy_G - by_B)\sin\theta \\ &+ C_{cr21}(\dot{q}+rp)I_{YZ} + C_{cr22}(q^2-p^2)I_{XY} \\ &+ C_{cr23}y_G(\dot{u} - vr + wq).\end{aligned} \tag{30}$$

By inspecting Equations (29) and (30) it can be seen that Equation (29) can be substituted directly into Equation (30) to reduce the coefficient count provided that,

$$\Delta B = 0, \quad y_G = 0, \quad Y'_{p|p|} = 0 \quad \text{and} \quad v\nu\left|\frac{r}{v}\right| = r\nu \quad \text{or} \quad v\nu\left|\frac{r}{v}\right| = -r\nu.$$

For the three test submarines the first three conditions are met. Also, as was discussed earlier one would expect from the physics that r and v would have the opposite sign. Thus,

$$v\nu\left|\frac{r}{v}\right| = \nu\,\text{sign}(v)|r| = -r\nu.$$

However, this posses a problem because this would imply that submarines 2 & 3 should also have a reduced rank due to this coupling, but they do not. The assumption that

the sign of r and v were of opposite sign was tested and the results of sign(v)/sign(r)) for every time step are shown in Figure 27.

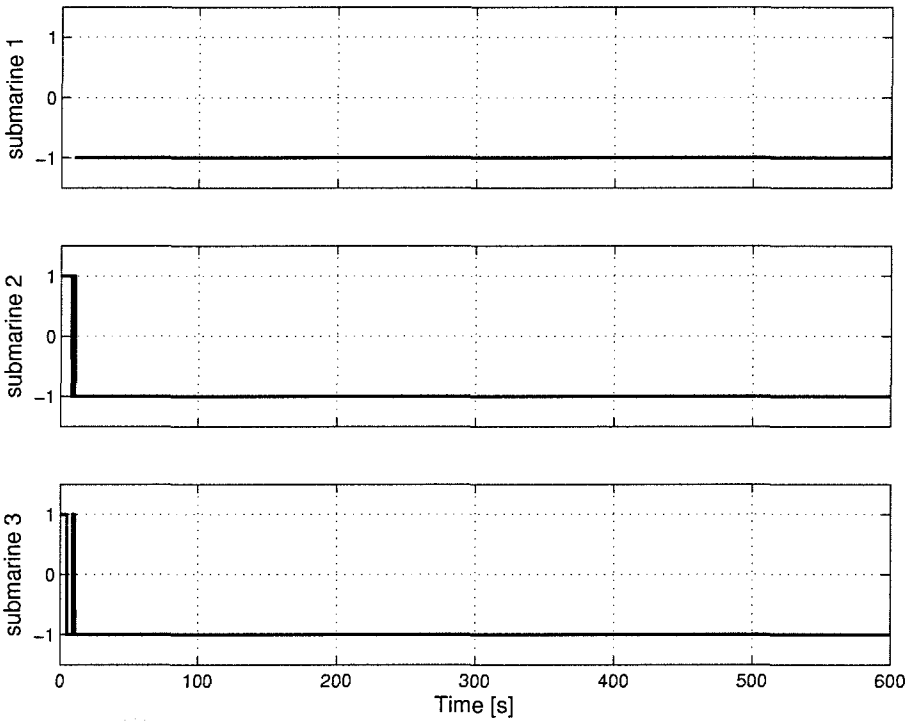

Figure 27: Results of the sign(v)/sign(r)) analysis for the three test submarines

The figure shows that the assumption is not true for submarine 2 & 3 but is true for submarine 1. The assumption is violated at the start of the manoeuvre prior to the rudder or dive planes being moved. For submarine 1 both v and r are zero and this is why the sign of v/r is not given in the plot. However, for submarines 2 & 3 there are small values of v and r, the exact cause of this is not understood, but since the effect was small it was not investigated.

The fact that the sign of v is not always opposite to the sign of r for submarines 2 & 3 explains why their associated $\mathcal{N}(\boldsymbol{A}_N)$ are only one dimensional. However, it is only not opposite during the initial stage of the manoeuvre. During this part of the manoeuvre no control inputs are made and no control inputs are given while during the rest of the manoeuvre v is of opposite sign to r. As not much of interest happens in this phase and one would only expect X'_{uu} to be relevant, it is likely that the N'_v relationship will be relevant for the majority of the manoeuvre. Therefore it is

expected that the N'_v relationship, although not making the coefficients non-unique, will make the coefficients ill-conditioned.

6.5 Conclusions

This chapter has shown that the hydrodynamic coefficients of the test submarines are non-unique. The mechanisms within the equations of motion which cause the non-uniqueness have been outlined, and the added-mass coefficients associated with the non-uniqueness have been identified. As the coefficients are non-unique it follows that it is not possible to identify all of the hydrodynamic coefficient values. However, by specifying the values of the associated added-mass coefficients the values of the remaining coefficients can be determined.

Chapter 7

Building and Testing the Non-linear Parameter Identification Procedure

7.1 Introduction

This chapter describes the creation and testing of the non-linear parameter identification procedure.

The chapter starts by describing how the basic outline of the non-linear parameter identification procedure described in Section 4.4.2 was turned into a working system. It considers how the simulation was integrated within the system identification procedure, it also outlines the working of the optimization routine used and discusses some of the problems with the process. The section concludes with a discussion on when the simulation is called as it represents the majority of the computing effort in the search procedure.

Following the outline of the building of the procedure the parameter identification testing is described. This testing made unrealistic assumptions about the problem and assumed knowledge that would not be available during the identification of a real UV. This was done to simplify the identification problem and thus allowed rapid

testing of the procedure. If the procedure failed to determine the coefficients under these idealized conditions then it would fail when used with the more demanding case of identifying real UV coefficients. Thus, the unrealistic identification problem testing allowed a rapid analysis of the approach without the extra effort required to test the real problem.

The first section on testing describes the simplifying assumptions made and explains why they were important. This is followed by describing the testing procedure. Thereafter the results of the testing are presented and are discussed in terms of track convergence, coefficient convergence and non-linear procedure performance. The result presented show that the system is ill-conditioned and the chapter concludes with a discussion on the causes of this ill-conditioning.

7.2 Implementing the Non-Linear Parameter Identification Procedure in Matlab

Before it was possible to test the non-linear parameter identification procedure outlined in Section 4.4.2 it was necessary to code the system into Matlab. The identification procedure consists of three parts that needed to be integrated into one system, these parts were: the optimization routine; the submarine simulation; and the cost function.

Before it is possible to integrate the parts together it was necessary to understand how the optimization routine works. Most optimization routine works by adjusting a function's input, in this case the hydrodynamic coefficient vector ($\boldsymbol{\xi}$), to minimize a scalar output, here the cost function ε. As the optimization routine progresses it produces a sequence of estimates of the hydrodynamic coefficient ($\hat{\boldsymbol{\xi}}^{(1)}$, $\hat{\boldsymbol{\xi}}^{(2)}$, ... ,$\hat{\boldsymbol{\xi}}^{(k)}$) which in turn produce a sequence of cost functions ($\varepsilon^{(1)}$, $\varepsilon^{(2)}$, ...,$\varepsilon^{(k)}$) with $\varepsilon^{(k)} < \varepsilon^{(k-1)}$. Once certain convergence criteria are met the sequence is terminated. The last $\hat{\boldsymbol{\xi}}$ in the sequence will be denoted by $\hat{\boldsymbol{\xi}}^{*}$. Ideally, during the identification procedure $\hat{\boldsymbol{\xi}}^{(k)} \rightarrow \boldsymbol{\xi}$ as $\varepsilon^{(k)} \rightarrow 0$.

As the shape of the cost function surface was not known and was potentially full of

local minima it was decided to constrain the possible values of $\hat{\boldsymbol{\xi}}$ to a region close to $\boldsymbol{\xi}$. This was done because non-linear functions tend to be better behaved when close to minima and as our target minimum was $\boldsymbol{\xi}$ it was sensible to constrain $\hat{\boldsymbol{\xi}}$ to be close to $\boldsymbol{\xi}$. Following from this the optimization routine had to be capable of minimizing a non-linear function with constraints. The routine used was an implementation of the Sequential Quadratic Programming (SQP) approach. The optimization code was written by Professor Veres of the University of Southampton, see Veres (2003). In general SQP is used to solve problems of the form,

$$\begin{aligned} \text{Minimize} \quad & f(\boldsymbol{x}) && \boldsymbol{x} \in \mathbb{R}^n \\ \text{subject to} \quad & c_i(\boldsymbol{x}) = 0, && i \in \boldsymbol{E} \\ & c_i(\boldsymbol{c}) \geq 0, && i \in \boldsymbol{I} \end{aligned}$$

where, E and I are the indexes to the equality and inequality constraints.

However, for the parameter identification procedure the problem is slightly simpler as the constraints are linear bounds on the coefficients. Thus, the problem can be written as,

$$\begin{aligned} \text{Minimize} \quad & f(\boldsymbol{x}) && \boldsymbol{x} \in \mathbb{R}^n \\ \text{subject to} \quad & \boldsymbol{\xi}_i \geq C_L \boldsymbol{\xi} \\ & -\boldsymbol{\xi}_i \geq -C_U \boldsymbol{\xi}, && i \in \boldsymbol{I} \end{aligned}$$

where, C_U and C_L are the upper and lower bounds on the coefficients.

For the optimization routine to be able to minimize ε it must be able to calculate ε for a given $\hat{\boldsymbol{\xi}}$. This was accomplished by writing a *cost function* routine which took $\boldsymbol{x}$ as an input and returned ε. The reason the cost function routine took $\boldsymbol{x}$ instead of $\hat{\boldsymbol{\xi}}$ as an input is explained next.

7.2.1 The Cost Function Routine

The cost function routine is represented pictorially in Figure 28.

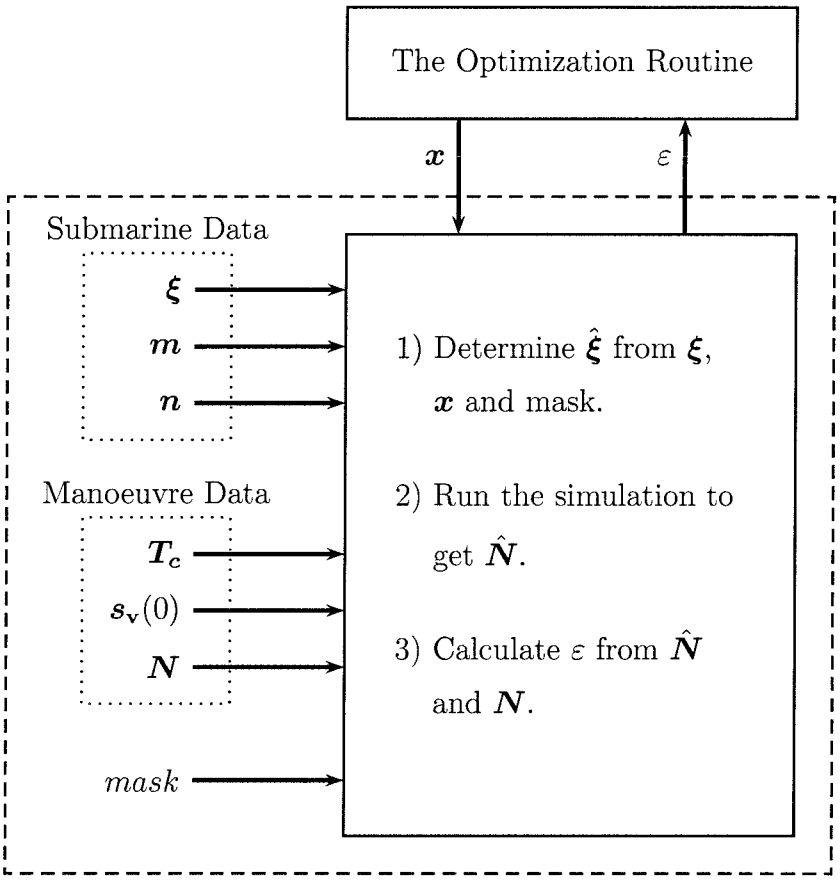

Figure 28: Overview of the cost function and optimization routine.

Figure 28 shows that the optimization routine does not pass $\hat{\xi}$ directly to the cost function routine. This was done because after some initial trials it was found that using the normalized coefficient value $x_i = \hat{\xi}_i/\xi_i$ simplified the specification of the coefficient constraints and also simplified the post processing of the results. The post processing was simplified because the results were to be presented as ratios of $\hat{\xi}_i/\xi_i$.

Figure 28 also shows a considerable amount of setup data was required by the cost function routine. This comprised broadly of the actual submarine data used to generate the manoeuvre, the manoeuvre details and a 'mask'. The 'mask' was used to set which coefficient of ξ would be identified. This allowed the identification of each individual coefficient to be turned on or off at will.

Within the routine there are three basic stages. The first stage is to determine $\hat{\boldsymbol{\xi}}$, this is done using $\boldsymbol{\xi}$, $\boldsymbol{x}$ and the mask. The pseudo code to determined $\hat{\boldsymbol{\xi}}$ is as follows,

$$\begin{aligned} \text{set} \quad & \hat{\boldsymbol{\xi}} = \boldsymbol{\xi} \\ \text{set} \quad & \hat{\boldsymbol{\xi}}(mask)_i = \boldsymbol{\xi}(mask)_i \cdot \boldsymbol{x}_i \end{aligned}$$

Once $\hat{\boldsymbol{\xi}}$ had been determined the second stage of the cost function routine is to run the simulation using the appropriate submarine and manoeuvre data to produce $\hat{\boldsymbol{N}}$. Finally the third stage calculates ε from $\hat{\boldsymbol{N}}$ and $\boldsymbol{N}$ using the cost function described in Section 4.4.2. Once calculated, ε is returned to the optimization routine.

The process of evaluating the cost function is computationally expensive. As described in Section 5.6.1 running the simulation of itself is time consuming and the extra effort involved in calculating the cost function has to be added to this. As the cost function evaluation is the prime computational expense in the parameter identification process it is worth considering how the optimization procedure calls the cost function routine. It is also important to highlight how the optimization routine measures convergence and what conditions cause it to terminate. These features of the optimization routine are discussed next.

7.2.2 Overview of the Optimization Routine

The SQP optimization approach is described in detail in Fletcher (1987) and the implementation of SQP used here is given in Veres (2003).

The SQP implementation used in the thesis consists of three distinct stages, these are:

1. The function $f(\boldsymbol{x})$ is approximated at point $\boldsymbol{x}$ by a quadratic model and the constraints $\boldsymbol{c}_i$ are linearized. The quadratic model and linearized constraints are then solved using quadratic programming techniques. The solution to the problem gives a search direction $\boldsymbol{s}$.

2. A search is conducted along the line $\boldsymbol{x} + \alpha \boldsymbol{s}$ to find a minimum value of ε which does not violate any of the constraints. The line search routine does not try and

find the actual minimum along the line, as performing an exact line searches is less efficient. Hence, the line search terminates when a 'better' $\boldsymbol{x}$ value has been found.

3. The convergence criteria are checked to determine whether to stop the optimization routine.

These three stages are outline in more detail in the following sections with an emphasis on describing when the cost function is evaluated.

The Quadratic Programming Sub-Problem

To solve the quadratic programming sub-problem it is necessary to know the gradient of the cost function ($\nabla f(\boldsymbol{x})$). The gradient is calculated numerically using the forward difference method that is,

$$\nabla f(\boldsymbol{x})_i = \frac{f(\boldsymbol{x} + h\boldsymbol{e}_i) - f(\boldsymbol{x})}{h}$$

where e_i is a vector whose i'th element is 1 and whose remaining element are zero.

Hence during the quadratic programming stage it is necessary to evaluate the cost function once per coefficient to identify to calculate $\nabla f(\boldsymbol{x})$.

The Line Search

Once the search direction ($\boldsymbol{s}$) has been determined from the quadratic programming sub-problem the line-search routine is run. In pseudo code the line-search algorithm is:

$\alpha = 2$, $\varepsilon^{(\alpha)} = 2\varepsilon^{(k)}$
while $\varepsilon^{(\alpha)} > \varepsilon^{(k)}$
    $\alpha = \alpha/2$
    if $\alpha < 1 \times 10^{-4}$ then $\alpha = -\alpha$
    $\varepsilon^{(\alpha)} = f(\boldsymbol{x} + \alpha\boldsymbol{s})$
end while

Here, $\varepsilon^{(k)}$ is the current cost function value at step k and $\varepsilon^{(\alpha)}$ is the line search cost function value.

The line-search routine starts by testing the quadratic subproblem solution ($\alpha = 1$). If this fails to produce the same or a smaller cost function value compared to the current value then the distance along the line is halved. This continues until either $\varepsilon^{(\alpha)} \leq \varepsilon^{(k)}$ or $\alpha < 1 \times 10^{-4}$ at which point the search direction is reversed. During the line search there is no attempt to find the minimum cost function value along $\boldsymbol{x} + \alpha \boldsymbol{s}$, but merely to find a similar or lower value of ε.

One problem encountered in the line-search was when the value of $f(\boldsymbol{x} + \alpha \boldsymbol{s})$ was undetermined. This occurred when the values of the hydrodynamic coefficients caused the simulation to crash. When this occurred the line-search would terminate at $\boldsymbol{x}+\alpha \boldsymbol{s}$, an unsatisfactory situation. To overcome this problem ε was set to 1×10^9 when the cost function was undetermined. This still had the potential to cause the system to crash if the value of $\varepsilon^{(k)}$ was greater than 1×10^9 and the first step produced an undetermined coefficient. However, this did not occur during the tests performed and the 'hack' removed the problem for this case.

As the line-search was inexact the number of cost function evaluations performed per search was relatively small, typically comprising 4 or 5 evaluation. A plot of the cost function evaluations performed during a parameter identification test is shown in Figure 29. The plot shows the cost function reduction for submarine 1 performing the first test of the horizontal sub-problem. The results of this test are given in Section 7.5. In the test 19 coefficients were being identified. The plot shows the QP sub-problem evaluation stage to determine the gradient vector $\nabla f(\boldsymbol{x})$ as the level section in ε. This is due to h being small when calculating $\nabla f(\boldsymbol{x})$ numerically and hence $\varepsilon^{(k+1)} \approx \varepsilon^{(k)}$. The line-search stage is shown by the large spikes in the values of ε.

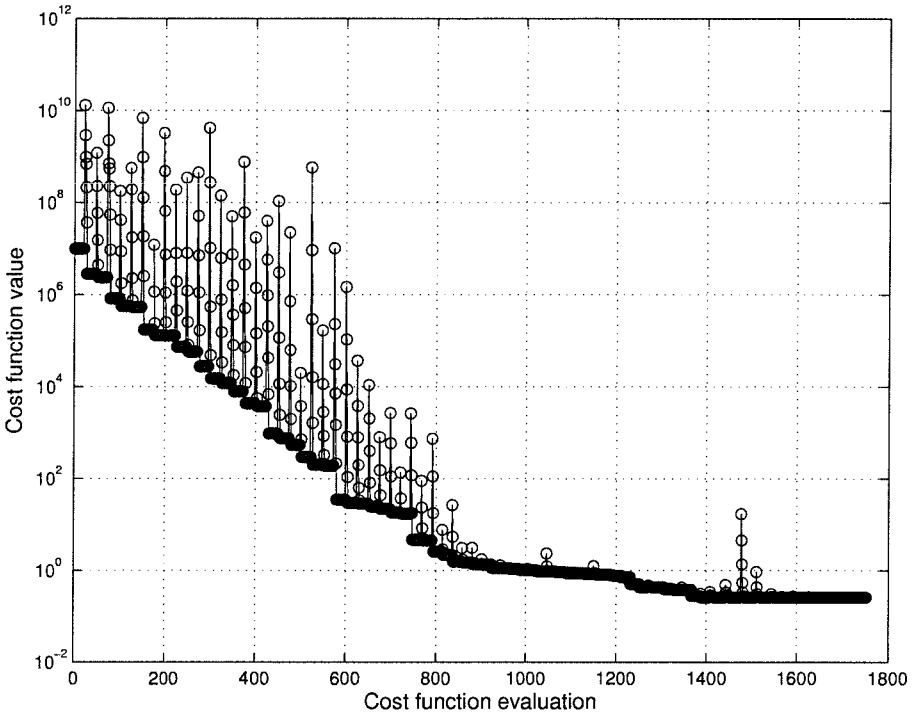

Figure 29: Example of the cost function reduction during a parameter identification test.

The Convergence Criteria

The convergence criteria for the optimization routine is composed of two parts. The first considers the size of the solution vector $\boldsymbol{s}$ and the second how much the cost function is reduced by moving to $\boldsymbol{x} + \boldsymbol{s}$. The optimization routine stops when the following conditions are satisfied.

$$||\boldsymbol{s}||_\infty < \text{parTol} \quad \text{and} \quad |\nabla f(\boldsymbol{x})^T \boldsymbol{s}| < \text{funcTol}.$$

Where $||\boldsymbol{s}||_\infty$ is the *L-infinity norm* of $\boldsymbol{s}$ and is defined by,

$$||\boldsymbol{x}||_\infty = \max_i |x_i|,$$

and 'parTol' and 'funcTol' are user defined inputs. For the testing performed these initially were set to,

$$\text{parTol} = 0.1$$

$$\text{funcTol} = 0.01$$

However, they were modified for some of the coupled manoeuvre testing to aid the convergence of the non-linear identification procedure.

Having discussed how the non-linear identification routine was constructed we now look at the assumptions made during the testing of the procedure.

7.3 Assumptions Made During the Non-Linear Identification Procedure Testing

To simplify the testing of the non-linear identification procedure several assumptions were made. These assumptions were:

The UV measurements were accurate and precise.

The first simplifying assumption was that all of the measurements of position, attitude and time were accurate and precise. Thus, the measurements are not subject to noise and hence $\boldsymbol{\varepsilon}_N = 0$. This reduced the complexity of the problem as no assessment of the sensor accuracy and the noise on the measurement was required. However, this is unrealistic as there will always be some measurement error and the sensors are always subject to a certain level of noise.

The UV was not subject to disturbances.

The second assumption was that the UV was not subject to disturbances, for example from currents, and hence $\boldsymbol{\tau}_d = 0$. This simplified the problem as no model of potential disturbances needed to be created and tested. However, it is unrealistic as the UV will always be subject to disturbances, principally from the un-modelled motion of the water, but also from other unknown sources.

The initial estimate of the hydrodynamic coefficients was accurate.

The third assumption was that the initial estimated submarine hydrodynamic vector $\hat{\boldsymbol{\xi}}$ was within $\pm 10\%$ of the actual hydrodynamic coefficient vector $\boldsymbol{\xi}$. This equates to a very accurate 'guess' of the correct coefficient values. This range was chosen as a starting point as it was assumed that a close initial guess would

simplify the identification problem and hence make a sensible starting point for the testing.

The zero valued coefficients were known.

One difficulty with specifying the coefficients with $\pm 10\%$ of the correct value was what to do when the correct coefficient value was zero. In this case it was decided to assume that the coefficient value was known to be zero for the testing as no 'sensible' range for the coefficient was known. Hence, the zero valued coefficients were not identified in the testing. It is unrealistic to assume these coefficient values would be known but the assumption removed the problem of identifying suitable ranges for the coefficients.

The values of $\hat{\xi}$ was restricted to $\pm 75\%$ of ξ.

The fifth assumption was that there was a range of the possible coefficient values and range was $\pm 75\%$ of the correct hydrodynamic coefficient value. This assumption was made to restrict the possible coefficient values to simplify the problem and increased the robustness of the procedure. The range was chosen after some preliminary testing, when it was found that the identification procedure became numerically less stable when the range was extended. Although in practise it would not be possible to impose this range during the identification of a real UV it was hoped that a 'reasonable' range could be determined for each coefficient when identifying the coefficients of real UVs. Also, the numerical problems found in the optimization routine when the range was extended could be addressed at this point.

The added-mass rank-reduction coefficients values were known.

The sixth assumption was that the values of the added-mass coefficients associated with the rank-reduction, described in Chapter 6, were known. This assumption meant that the system of equations was not rank-deficient and hence there was a unique set of coefficients which could be identified.

These added-mass coefficient values would not be known accurately priori. However, if the procedure identified the remaining coefficient values correctly it would suggest that by setting the added-mass coefficient to a value calculated

from potential theory or to zero the procedure would converge to another coefficient set that was also in the null space of $\boldsymbol{A}$.

The propulsion coefficients for the UV were known.

The seventh assumption was that the propulsion coefficients were known for the UV to be identified. This simplified the testing as the thorny issue of identifying the propulsion coefficients with the hydrodynamic coefficients could be ignored. For real submarines these coefficients are determined from acceleration and deceleration trials of the full size submarine. When identifying a real UV it would be necessary to find an alternative method of determining the propulsion coefficients.

When the propulsion coefficients are known it is possible to calculate the drag coefficient directly. This is possible as in the steady state when the UV is travelling straight and level the drag becomes,

$$\frac{1}{2}\rho l^2 X'_{uu} u^2 = X_n = \frac{1}{2}\rho l^2 u|u|(b'_1 + b'_2 n' + b'_3 (n')^2).$$

As, $n' = 1$ and b'_1– b'_3 are known X'_{uu} can be determined directly.

Although X'_{uu} could be determined in this way it was decided to attempt to identify X'_{uu} along with the remaining coefficients using the non-linear identification procedure.

All the mechanical coefficients of the UV were known precisely.

The final assumption was that all the mechanical coefficient (such as mass, length, moments of inertia etc.) were known precisely and were constant throughout the manoeuvre. Although these coefficients can be relatively simply determined to quite a high accuracy there will be always be some uncertainty in the values used. The effect of this uncertainty was not considered in this testing.

The UV was neutrally buoyant.

The final assumption was that the UV was neutrally buoyant and remained so throughout the manoeuvre. This was assumed as UVs tend to be neutrally buoyant. However, the buoyancy of UVs is slightly dependent on depth so this assumption is not strictly accurate.

The assumptions described greatly simplify the real UV identification problem. But they do allow the basic procedure to be tested and give an assessment of the suitability of the test procedure for the real UV identification task.

7.4 The Tests Performed

The non-linear system identification procedure was tested using the three different submarines in each of the three different test manoeuvres. This led to nine sets of identification tests. As the initial estimate of the submarine's coefficients had a significant impact on the convergence of the identification procedure each submarine and manoeuvre combination was tested using 50 different starting estimates of the hydrodynamic coefficient vector ($\boldsymbol{\xi}$). It was hoped that these 50 tests would produce a spread of the possible result and would reduce the chance of converging to false minima and hence would give a better estimate of the reliability of the procedure.

The initial submarine hydrodynamic coefficient estimate $\hat{\boldsymbol{\xi}}$ was determined by randomly perturbing the correct coefficient vector $\boldsymbol{\xi}$ by up to $\pm 10\%$. This random perturbation was uniformly distributed throughout the $\pm 10\%$ range.

Three representative data sets were used during the initial identification testing phase of the process. When the results are displayed in a non-dimensional form the performance of the identification procedure can assessed. As the identification procedure results were for 'standard' submarines it was thought that the presented results, although not containing the coefficient data, would still be of use to the research community.

7.5 Horizontal Manoeuvre Results

The results of the numerical experiments are broken down into the following categories:

- Track convergence (cost function minimization).

- Coefficient convergence.
- Optimization routine efficiency.

The track convergence represents how well the optimization routine minimizes the cost function and hence how well the estimated track ($\hat{\boldsymbol{N}}$) compares with the target track ($\boldsymbol{N}$). The coefficient convergence shows how close the converged coefficients ($\hat{\boldsymbol{\xi}}$) are to the correct coefficients ($\boldsymbol{\xi}$). Finally the efficiency of the optimization routine is analysed by considering the time taken and the number of cost function evaluations performed before the system converged.

7.5.1 Horizontal Manoeuvre Track Convergence

The results of the fifty trials of this minimization process for the three test submarines are shown in Figures 30–32. These figures comprise two histograms. The first histogram shows the initial and converged cost function. This is represented on a logarithmic scale due to the large decrease in the cost functions. The second histogram shows the maximum positional error between $\hat{\boldsymbol{N}}$ and $\boldsymbol{N}$ produced by the converged coefficients. This is also plotted on a logarithmic scale. The mean results of the track convergence (or reduction in ε) are summarized in Tables 10–12.

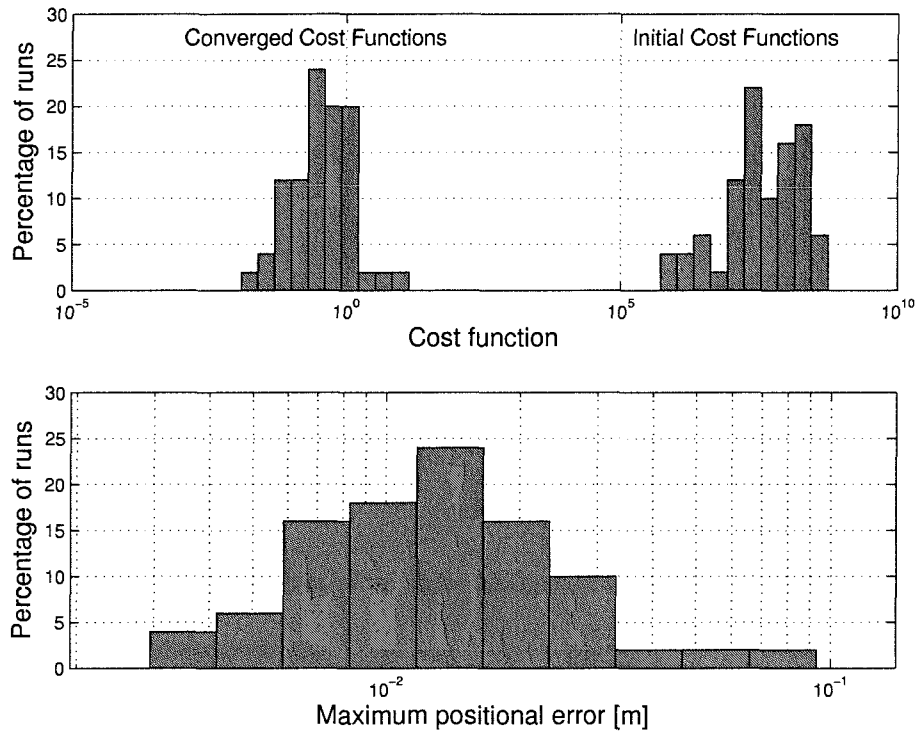

Figure 30: Track convergence results for the horizontal manoeuvre — submarine 1.

Mean initial cost function value	$= 8.66 \times 10^{7}$
Mean converged cost function	$= 7.85 \times 10^{-1}$
Reduction in mean value	≈ 8 orders of magnitude
Mean maximum positional error	$= 16$ mm

Table 10: Summary of the horizontal manoeuvre convergence results — submarine 1.

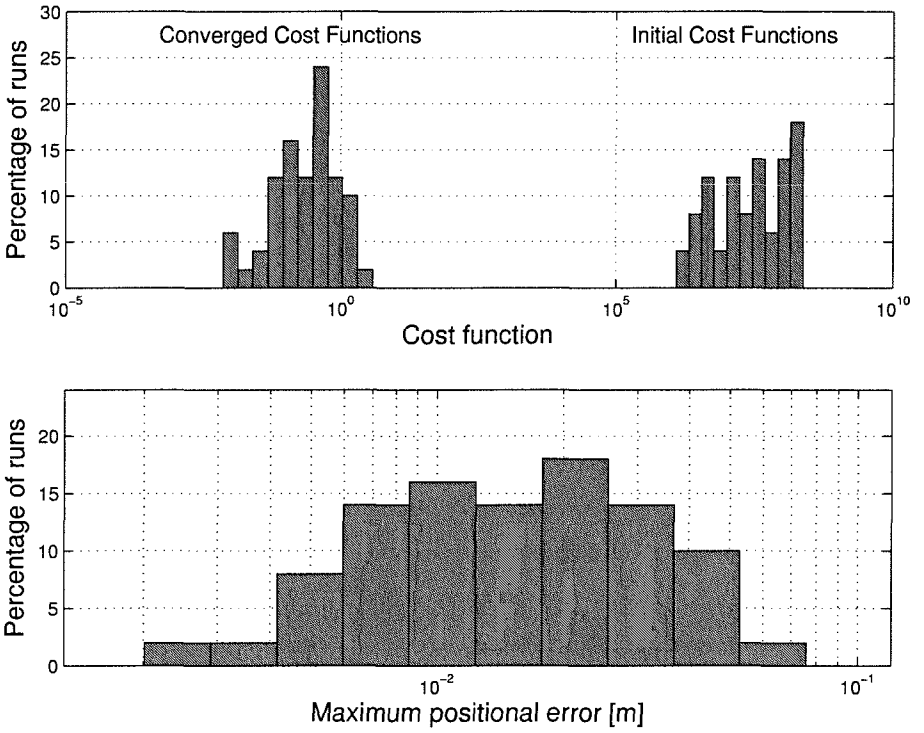

Figure 31: Track convergence results for the horizontal manoeuvre — submarine 2.

Mean initial cost function value	$= 6.23 \times 10^{7}$
Mean converged cost function	$= 4.78 \times 10^{-1}$
Reduction in mean value	≈ 8 orders of magnitude
Mean maximum positional error	$= 19$ mm

Table 11: Summary of the horizontal manoeuvre convergence results — submarine 2.

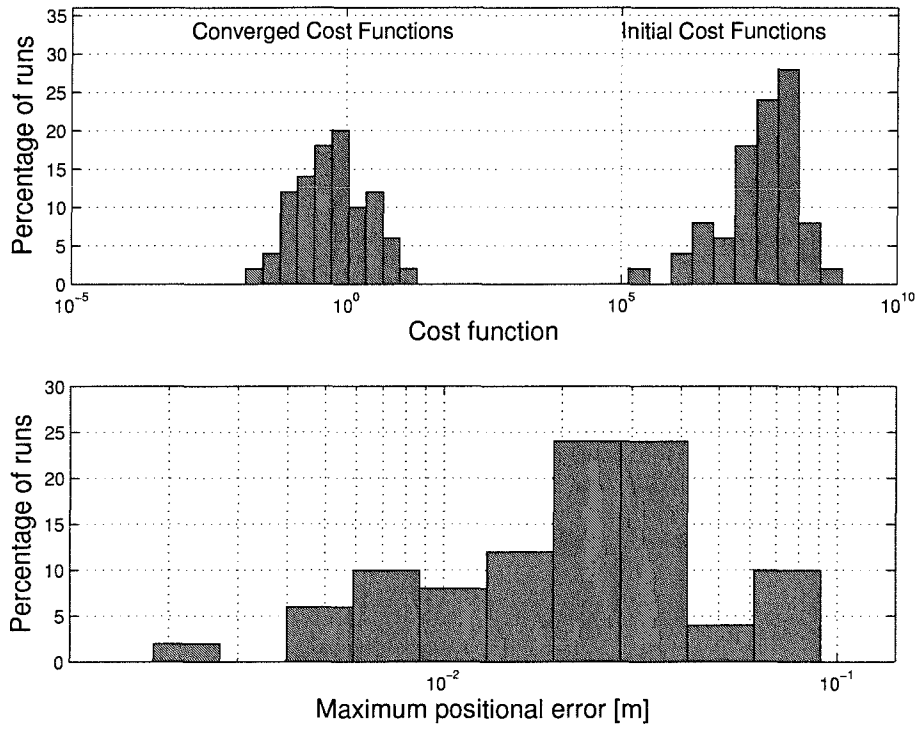

Figure 32: Track convergence results for the horizontal manoeuvre — submarine 3.

Mean initial cost function value	$= 7.90 \times 10^7$
Mean converged cost function	$= 1.42$
Reduction in mean value	≈ 7 orders of magnitude
Mean maximum positional error	$= 27$ mm

Table 12: Summary of the horizontal manoeuvre convergence results — submarine 3.

The results for the three submarine show excellent track convergence. The mean values of ε are reduced by between seven and eight orders of magnitude and when converged are less than one. Although ε for different manoeuvres and submarines cannot be directly compared due to the method of calculation, it worth noting that the ε value produced when comparing the output of SubHov and the Matlab simulation for the comparison manoeuvre was approximately 2000 (Section 5.8). This is three orders of magnitude larger than that produced by the converged coefficients. Also, the accuracy at which the estimated track converges to the target track is far greater

than the accuracy of the simulation when using the 0.1s integration time-step. As the simulation with a time step of 0.1s produces a ε value of between 1100–1350 and a maximum positional error of between 0.68–0.695 metres when compared to the simulation with a time step of 0.001s (Section 5.9). Thus, the converged tracks are effectively identical to the target track.

7.5.2 Horizontal Manoeuvre Coefficient Convergence

Although the estimated track converged exceedingly well to the target track, the estimated coefficients do not converge to the correct values. Illustrations of coefficient convergence are shown in Figures 33–35. In these plots each vertical line represents an identified hydrodynamic coefficient. The coefficient convergence ratio is shown on the y-axis. The convergence ratio is the ratio of $\hat{\boldsymbol{\xi}}_i^*$ to $\boldsymbol{\xi}_i$. Each filled circle represents the converged coefficient value for one of the 50 tests performed. Using this approach the converged coefficients for the 50 tests can be plotted on the same figure.

The $\times$'s in each figure represent the zero valued submarine coefficients and thus were assumed to be known. The $\triangle$'s represent the added-mass rank-reduction coefficient whose value was also assumed to be known. The upper and lower limit of the possible coefficient values are also plotted on the graph along with the band in which the initial estimate for the hydrodynamic coefficient vector fall.

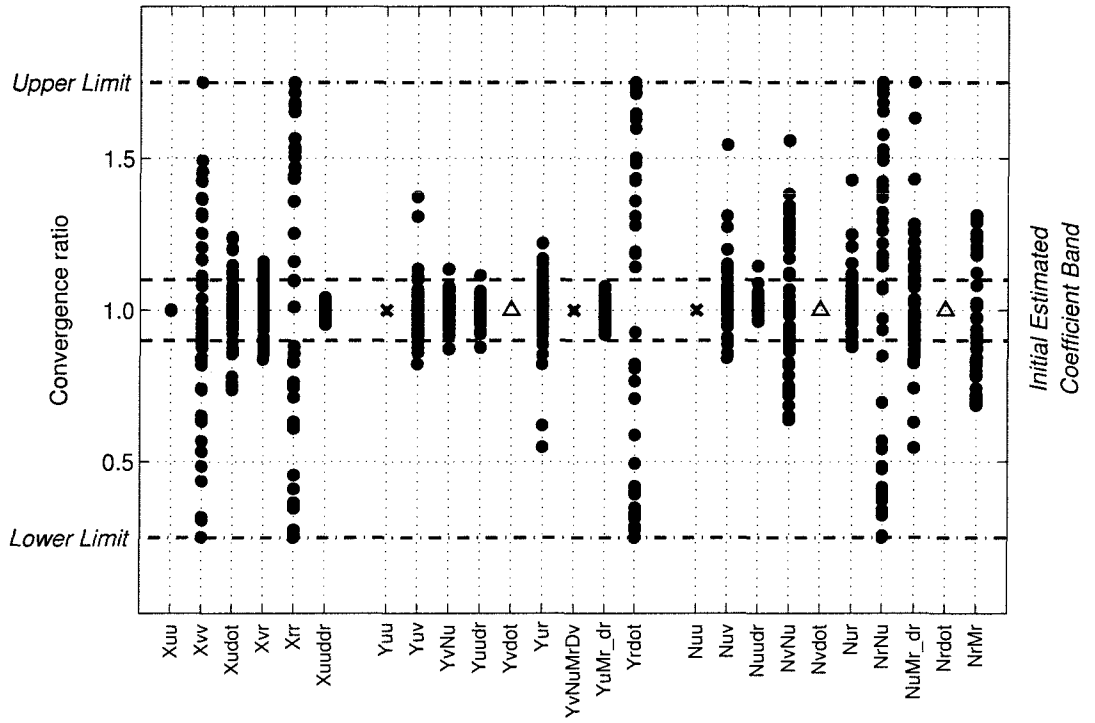

Figure 33: Coefficient convergence for the horizontal manoeuvre — submarine 1.

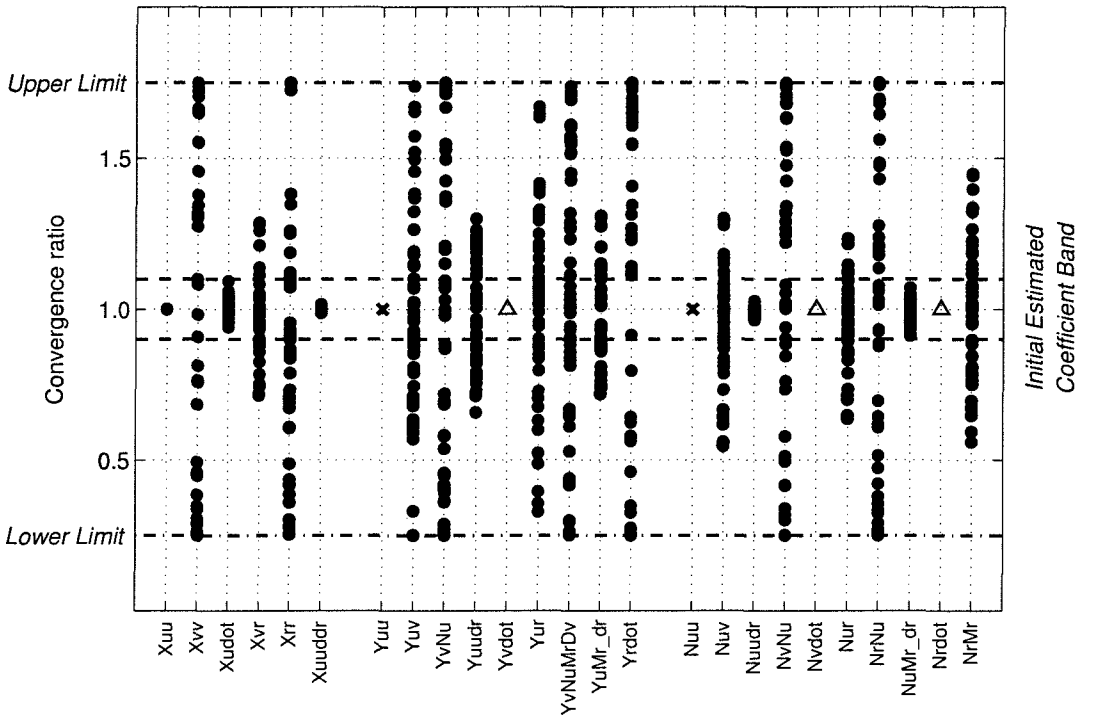

Figure 34: Coefficient convergence for the horizontal manoeuvre — submarine 2.

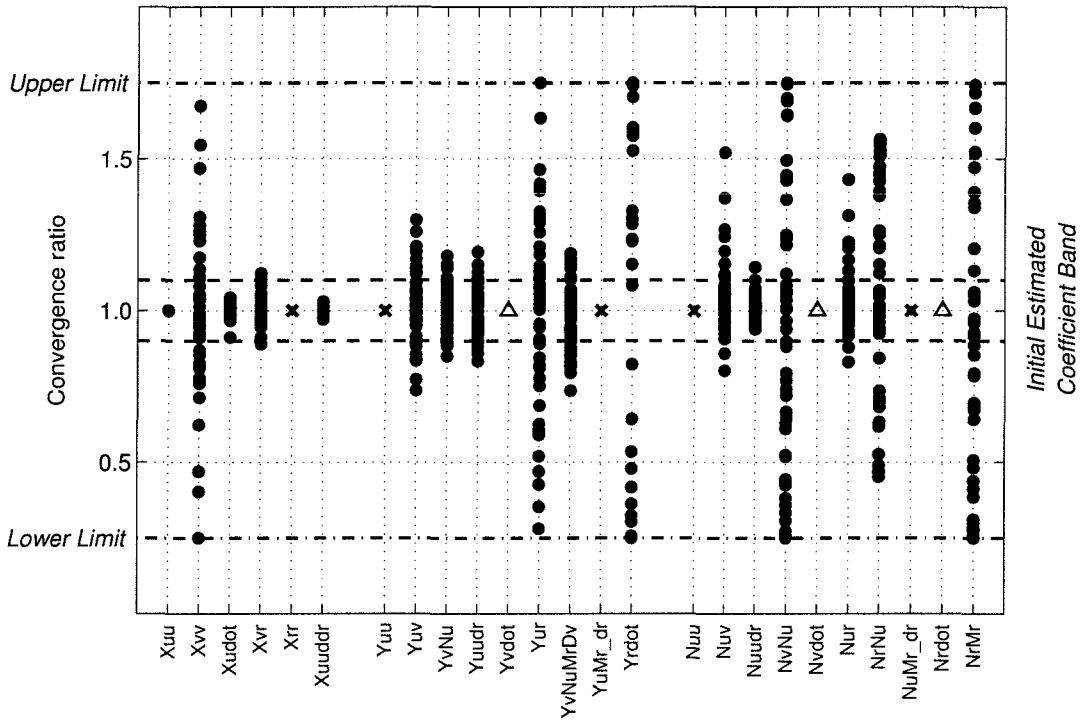

Figure 35: Coefficient convergence for the horizontal manoeuvre — submarine 3.

The three coefficient convergence plots show that only X'_{uu} is consistently well identified. The other coefficients are usually identified less well than they were in the initial coefficient estimate. However, as was shown in Section 7.5.1 the tracks converged exceptionally well. Thus, it can be concluded that for *this* manoeuvre the Booth et al. (1980) equations produce an ill-conditioned system, that is practically identical manoeuvres are produced by substantially different sets of coefficient values.

7.5.3 Optimization Routine Performance — Horizontal Manoeuvre

The efficiency of the optimization routine is a measure of how quickly it converges. The more efficient the routine the fewer steps required before convergence. It is necessary to have an efficient routine as the time to converge to a solution has a direct effect on the usefulness of the technique. Another factor affecting the performance of the routine is its robustness, that is whether it fails to converge to a solution. This section considers the robustness and efficiency of the optimization routine.

During the 150 horizontal sub-problem identification tests performed the optimization routine converged without incident. Histograms of the time to converge and the number of cost function evaluations for the three submarines are shown in Figures 36–38. Also, Tables 13–15 summarize the number of coefficient to identify, the mean number of function calls, the ratio of function calls to coefficients to identify and the mean time to converge for the different submarine sets.

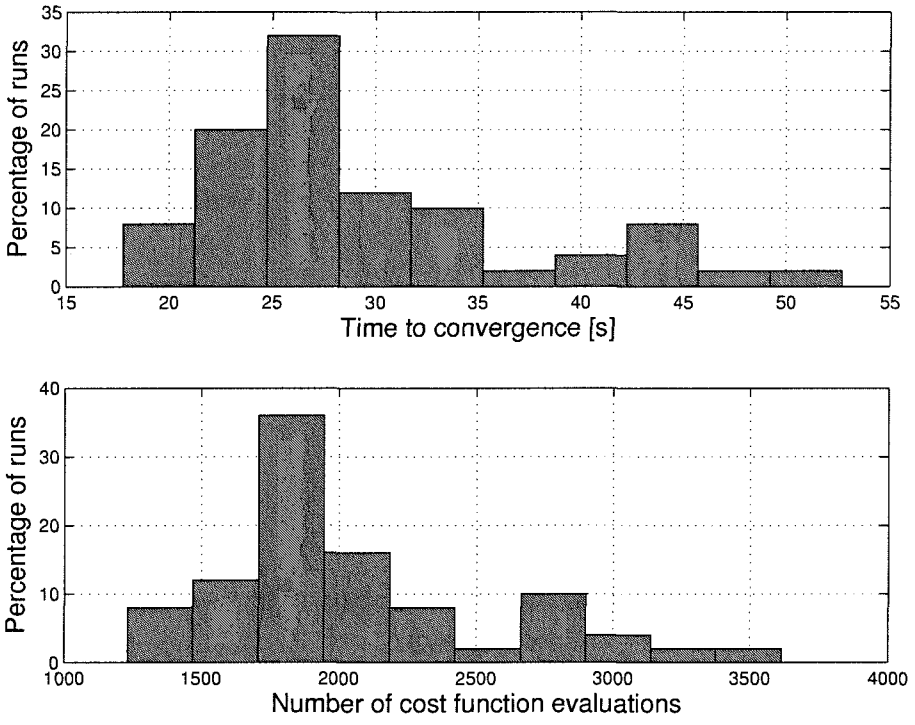

Figure 36: Optimization routine efficiency results for the horizontal manoeuvre — submarine 1.

Number of coefficients to identify (m)	$= 19$
Mean cost function evaluations (ε_N)	$= 2054$
ε_N/m	$= 108.1$
Mean time to converge	$= 52$s

Table 13: Summary of the optimization routine efficiency — horizontal manoeuvre, submarine 1.

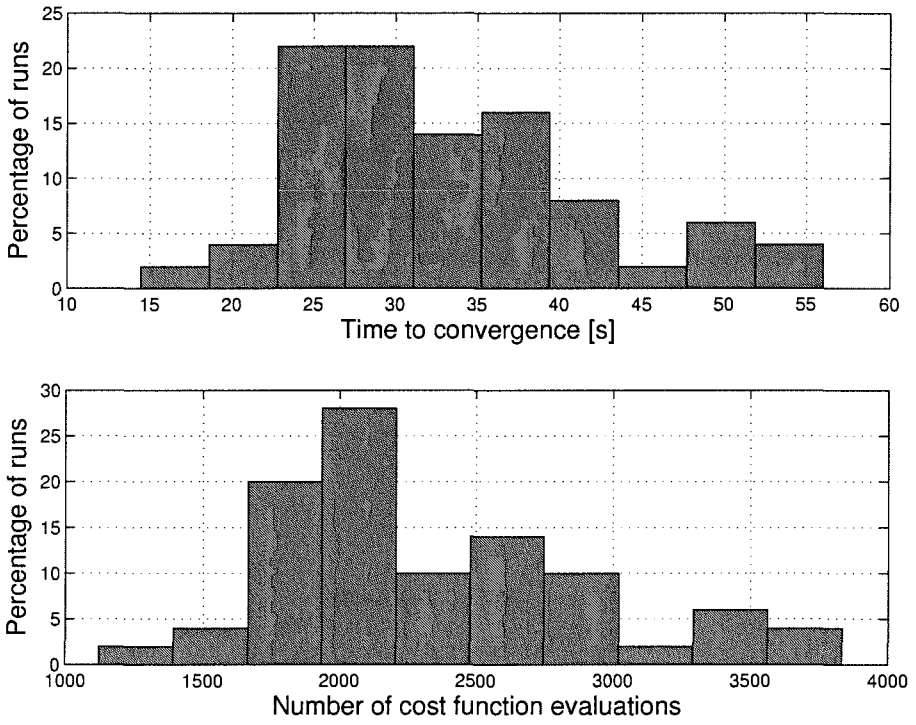

Figure 37: Optimization routine efficiency results for the horizontal manoeuvre — submarine 2.

Number of coefficients to identify (m)	$= 20$
Mean cost function evaluations (ε_N)	$= 2323$
ε_N/m	$= 116.2$
Mean time to converge	$= 58$s

Table 14: Summary of the optimization routine efficiency — horizontal manoeuvre, submarine 2.

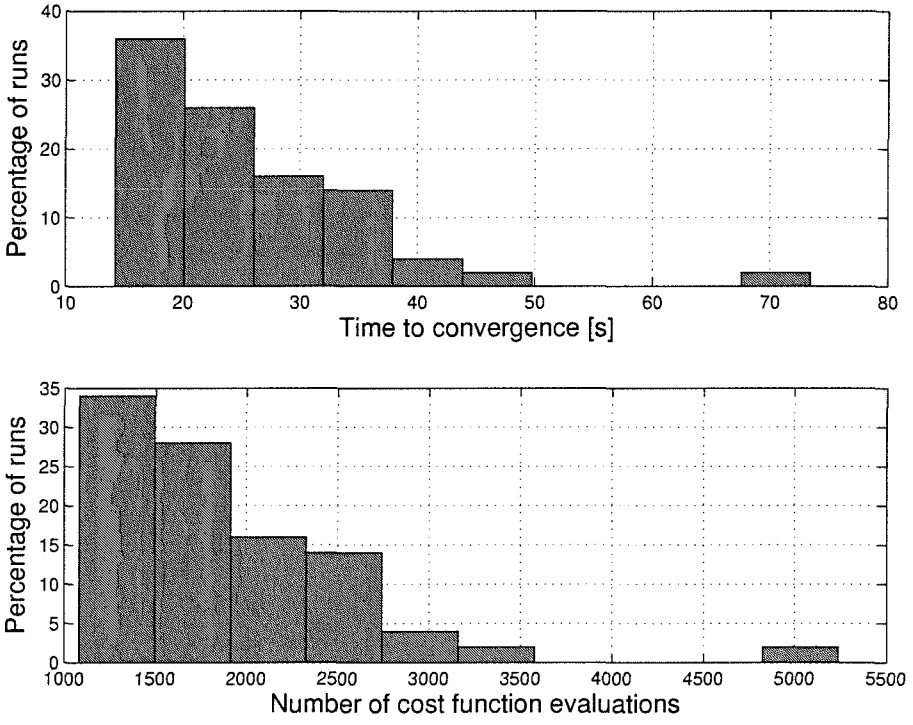

Figure 38: Optimization routine efficiency results for the horizontal manoeuvre — submarine 3.

Number of coefficients to identify (m)	$= 17$
Mean cost function evaluations (ε_N)	$= 1894$
ε_N/m	$= 111.4$
Mean time to converge	$= 45$s

Table 15: Summary of the optimization routine efficiency — horizontal manoeuvre, submarine 3.

The results show a strong correlation between the time to convergence and the number of cost function evaluations. After some examination it was found that the cost function evaluations took between 90-95% of the total simulation time. Hence the biggest improvement in performance could be gained from speeding up the cost function evaluation.

The results also show that there was a large spread of times to converge with the testing of submarines 1 & 2 showing a central peak. Whereas the peak for Submarine 3

was at the minimum convergence time. The cause of this difference is unknown, it could be due to some feature of the hydrodynamic coefficients of submarine 3 or could be due purely to chance.

Also, examining the tabulated data the number of cost function evaluations until convergence is strongly related to the number of coefficient to identify, as expressed by the ε_N/m ratio. This relationship was expected as calculating $\nabla f(\boldsymbol{x})$ during each optimization step required the cost function to be evaluated once for every coefficient to identify. Also, one would expect a high dimensional problem to be more complex and require a larger number of steps before convergence.

In general the simulation was converging in less than 2500 cost function evaluations for all cases. If one assumes that the line-search stage of the optimization routine takes 4 cost function evaluations, as suggested by Figure 29, then each optimization routine step should take $m+4$ cost function evaluations. Calculating the ratio $\varepsilon_N/(m+4)$ for each submarines produces a ratio between 90–97. Hence, it is can be assumed that the optimization routine converges in under 100 steps, this is a small number when considering that there were between 17 and 20 coefficients to identify. Thus, one can conclude that the optimization routine rapidly converges to a minimum.

7.5.4 Horizontal Manoeuvre Testing Conclusions

The testing of the standard manoeuvre of the horizontal sub-problem has shown that the $\hat{\boldsymbol{N}}$ converged accurately to $\boldsymbol{N}$ with an ε value being insignificant compared to the simulation error. However, $\hat{\boldsymbol{\xi}}$ does not converge to $\boldsymbol{\xi}$ and appear to be worse that the initially estimated value $\hat{\boldsymbol{\xi}}^{(1)}$ with the one exception of X'_{uu}. Thus, it can be concluded that *the standard horizontal manoeuvre* produces an ill-conditioned system.

The results also show that the optimization routine rapidly converges to the solution and always took less than 2 minutes to converge. This is using the third version of the Matlab simulation, the second version would take approximately 450 times longer to complete the identification (Section 5.6.1). Even so, the bulk of the computing effort for the identification procedure was still spent evaluating the cost function value with the simulation taking a large portion of this process.

When the different submarines are compared they do not appear to produce any significant differences in the optimization routine performance. The main difference stems from the different number of coefficients that needed to be identified.

7.6 Vertical Manoeuvre Results

The examination of the identification procedure outlined for the horizontal manoeuvre was repeated for the vertical sub-problem. As with the horizontal testing the track convergence, the coefficient convergence and the optimization routine efficiency are analysed.

7.6.1 Vertical Manoeuvre Track Convergence

The results of the track convergence for submarines 1–3 are shown in Figures 39–41 and Tables 16–18.

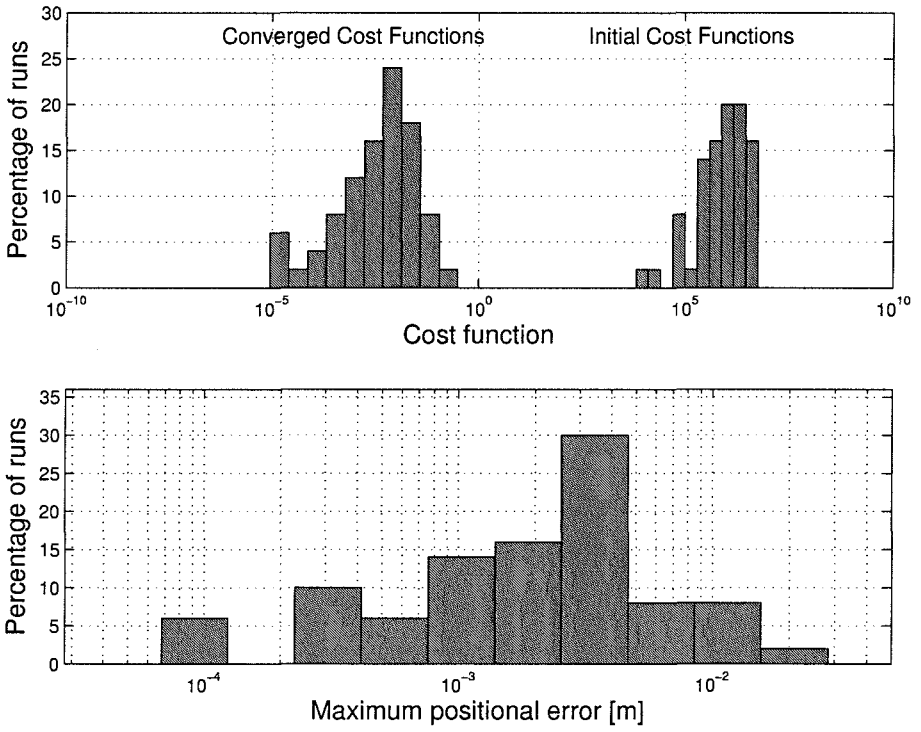

Figure 39: Track convergence results for the vertical manoeuvre — submarine 1.

Mean initial cost function value	$= 1.33 \times 10^{6}$
Mean converged cost function	$= 1.65 \times 10^{-2}$
Reduction in mean value	≈ 7 orders of magnitude
Mean maximum positional error	$= 3.3$ mm

Table 16: Summary of the vertical manoeuvre convergence results — submarine 1.

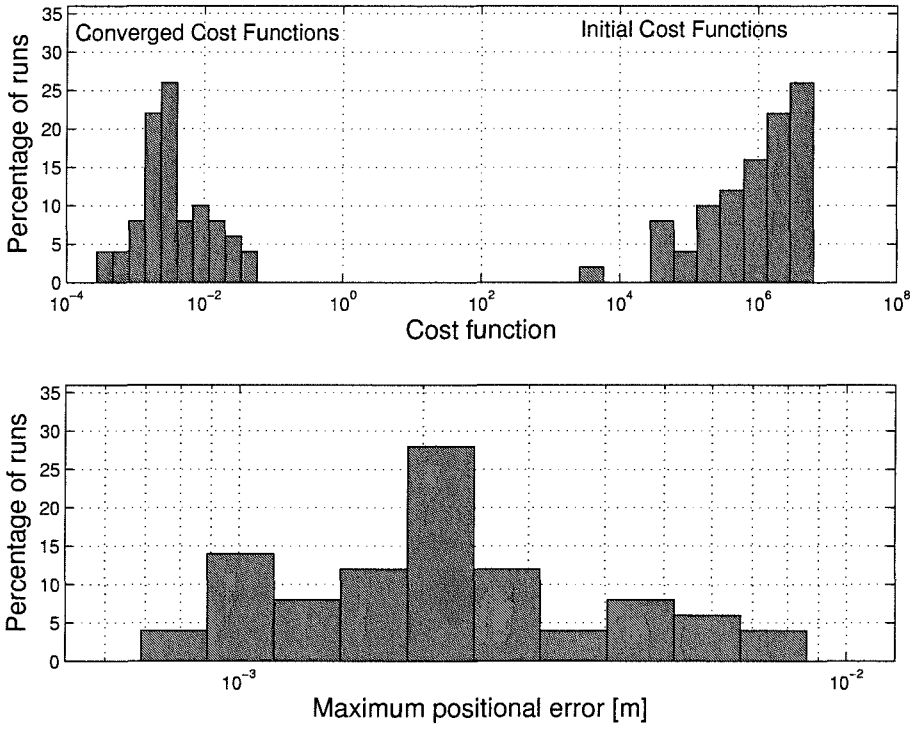

Figure 40: Track convergence results for the vertical manoeuvre — submarine 2.

Mean initial cost function value	$= 1.65 \times 10^{6}$
Mean converged cost function	$= 7.15 \times 10^{-3}$
Reduction in mean value	≈ 8 orders of magnitude
Mean maximum positional error	$= 2.5$ mm

Table 17: Summary of the vertical manoeuvre convergence results — submarine 2.

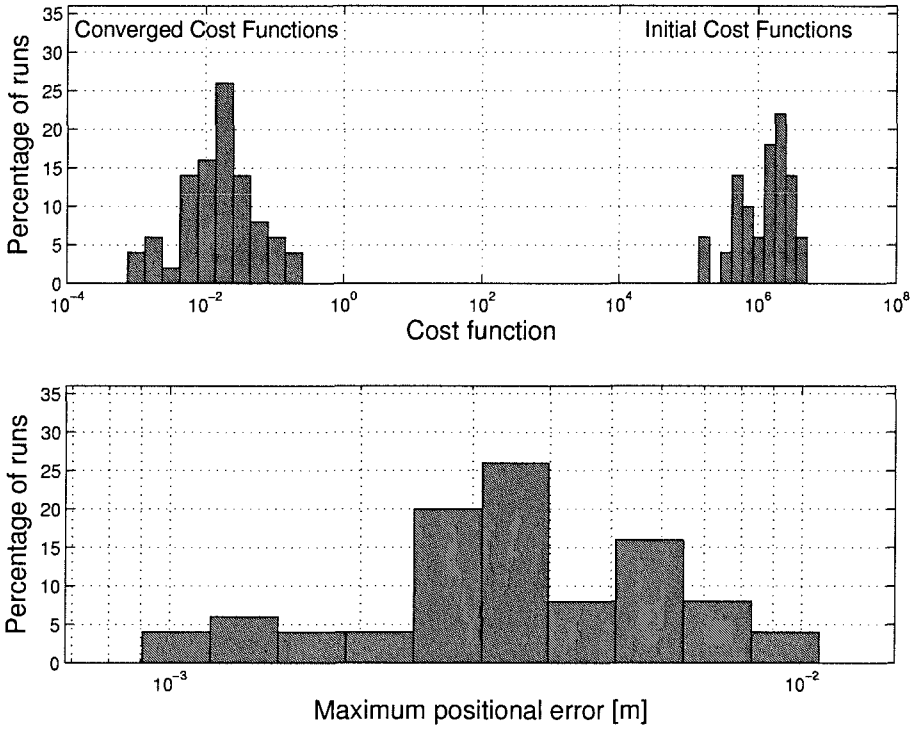

Figure 41: Track convergence results for the vertical manoeuvre — submarine 3.

Mean initial cost function value	$= 1.66 \times 10^{6}$
Mean converged cost function	$= 2.93 \times 10^{-2}$
Reduction in mean value	≈ 7 orders of magnitude
Mean maximum positional error	$= 3.9$ mm

Table 18: Summary of the vertical manoeuvre convergence results — submarine 3.

The results presented again show that $\hat{\boldsymbol{N}}$ converges exceptionally accurately to $\boldsymbol{N}$ for all three submarines, with a similar level of convergence. The actual maximum positional error in the track is substantially better than that shown in the horizontal manoeuvre. However, when this is compared to the accuracy of the standard vertical manoeuvre performed by the Matlab simulation (Section 5.9) the results are less impressive. The 0.1s simulation has ε value of between 1.5–2.5 and a maximum positional error of between 28–41mm. This is only approximately 100 times and 10 times larger respectively than the mean converged results. Compared to the horizontal

case ε for the vertical manoeuvre simulation accuracy is 1000 times larger than the horizontal manoeuvre converged ε and the maximum positional error is over 25 times bigger. So although the convergence is still better than the accuracy of the simulation, the difference is proportionally less than that seen in the horizontal manoeuvre.

The reason that the vertical manoeuvre is more accurately predicted by the Matlab simulation than the horizontal manoeuvre is because it is both less extreme and shorter in duration. The manoeuvre is less extreme as the maximum dive plane angle is only $\pm 5^\circ$ compared to the 30° used in the horizontal test manoeuvre. Also the shorter duration does not allow the errors as much time to build up.

The reason for the proportionally less accurate convergence of the optimization routine in the vertical case is thought to be due to the convergence criteria used. Since the same convergence criteria ($funcTol$ & $parTol$) were used in both the horizontal and vertical manoeuvres, and these are absolute values, the less extreme vertical manoeuvre converge more quickly than the horizontal manoeuvre. This is illustrated in the optimization routine efficiency text (Section 7.6.3). The ratio of ε_N/m is less for the vertical manoeuvre than the horizontal manoeuvre. This faster convergence led to a relatively less accurate prediction of the vertical manoeuvre.

7.6.2 Vertical Manoeuvre Coefficient Convergence

The coefficient convergence results for submarines 1–3 are shown in Figures 42–44.

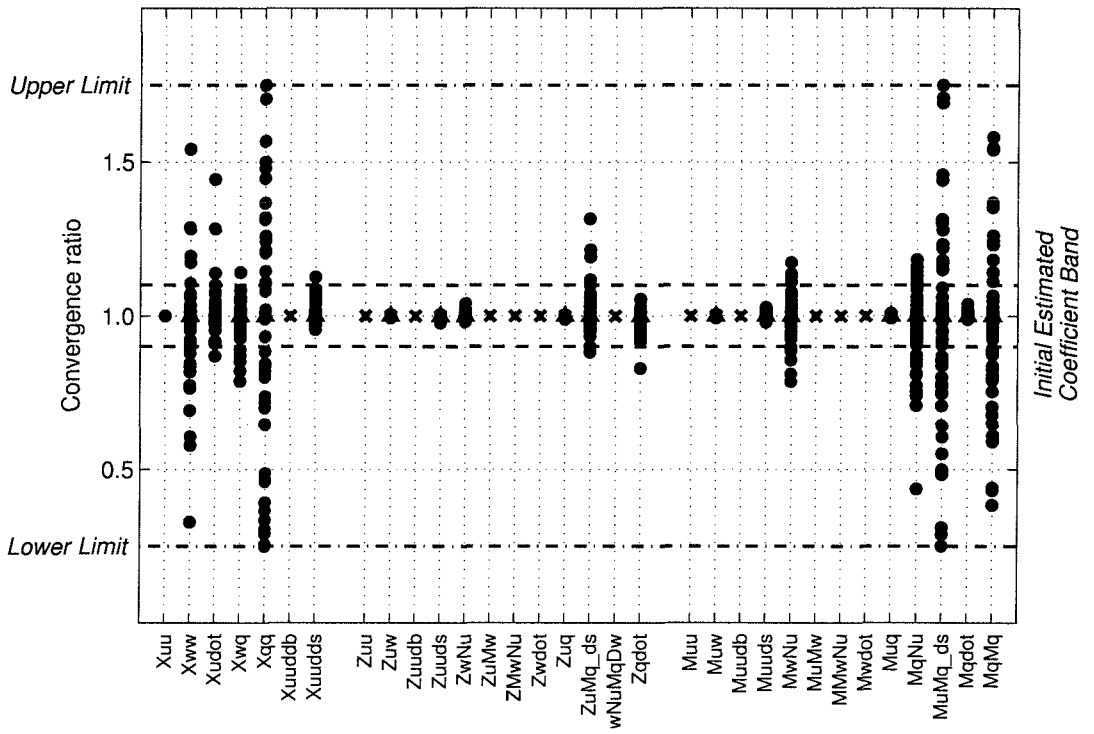

Figure 42: Coefficient convergence for the vertical manoeuvre — submarine 1.

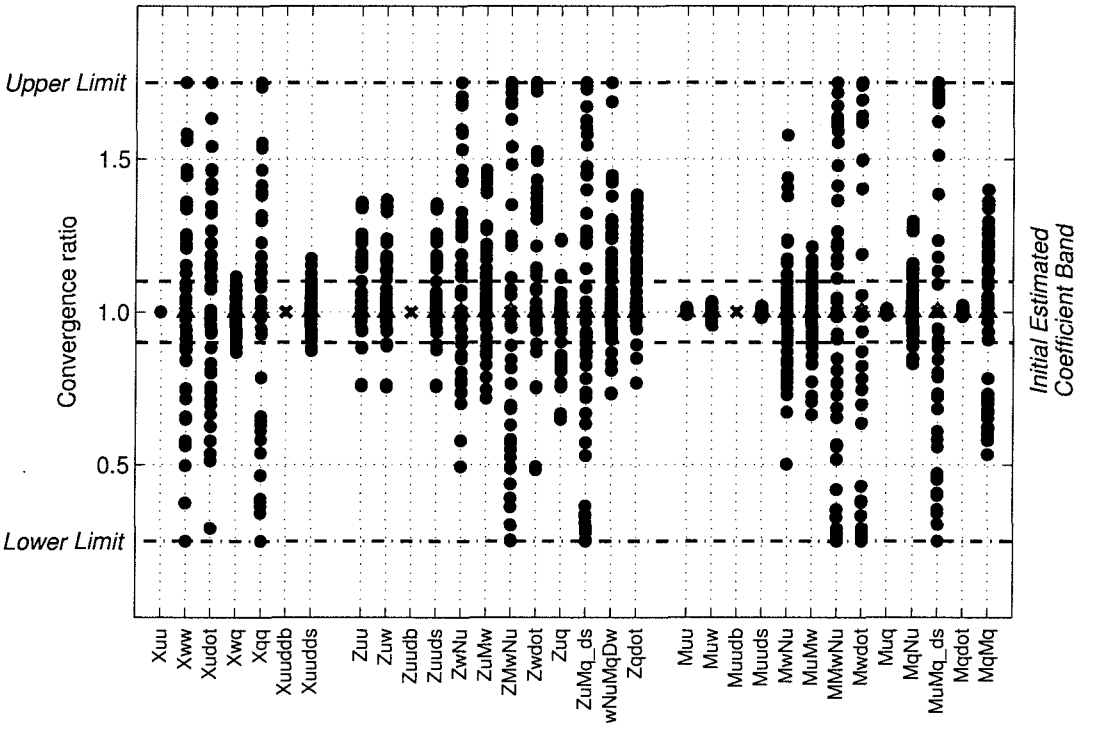

Figure 43: Coefficient convergence for the vertical manoeuvre — submarine 2.

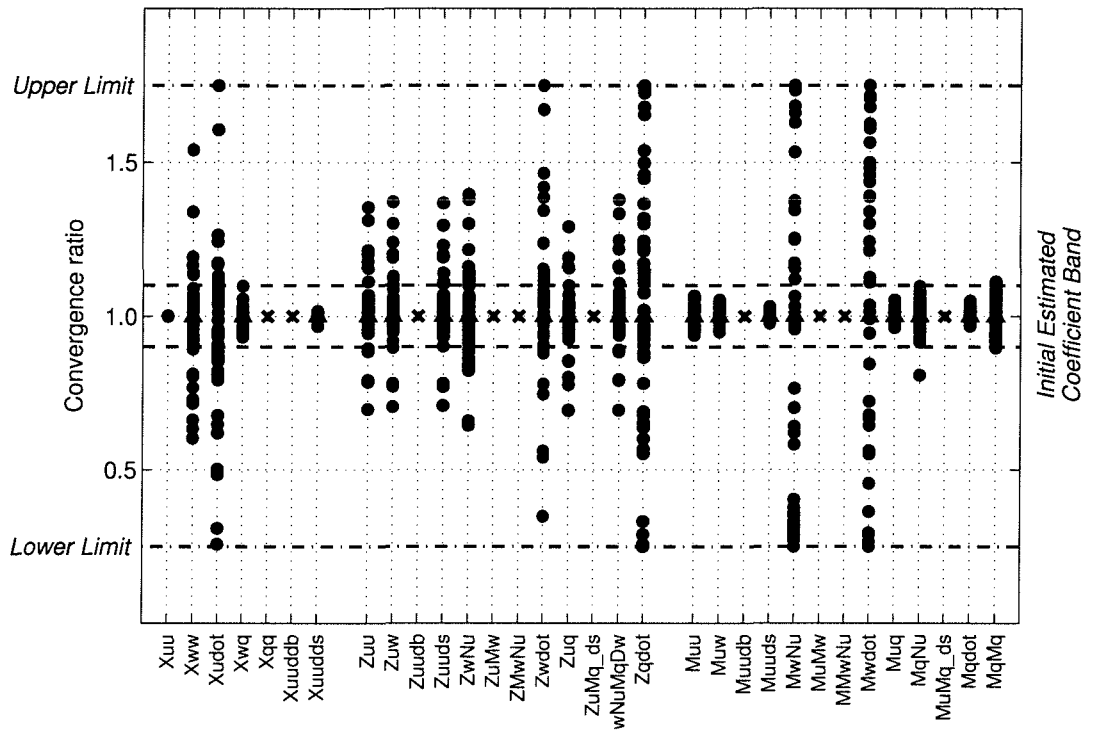

Figure 44: Coefficient convergence for the vertical manoeuvre — submarine 3.

The coefficients divide into three sets the X, Z and M coefficients. The X coefficient results show that only X'_{uu} is well identified for all three submarines. All the remaining X coefficients are poorly identified.

For the Z coefficients several coefficients are well identified for Submarine 1 with Z'_{uw} and Z'_{uq} being notable examples. However, this quality is not matched by submarines 2 & 3. These submarines consistently exhibit poorly identified coefficients. However, looking at Figure 43, submarine 2's results, the distribution for Z'_{uu}, Z'_{uw}, and $Z'_{uu\delta S}$ coefficients appear similar. Also, examining Figure 44, submarine 3's results, the distribution for Z'_{uu}, Z'_{uw}, $Z'_{uu\delta S}$ and $Z'_{wv|\frac{q}{w}|}$ coefficients also resemble each other. On further analysis it was found that for submarine 3 the four coefficients mentioned all had similar errors in each converged test. For submarine 2 the same results were seen except that unlike submarine 3 $Z'_{wv|\frac{q}{w}|}$ did not have a similar error. Assuming that this link between Z'_{uu}, Z'_{uw} and $Z'_{uu\delta S}$ exist in submarine 1 then this explains why Z'_{uw} and $Z'_{uu\delta S}$ are well determined as Z'_{uu} is fixed at zero. Hence, it would appear that the Z coefficients of submarine 1 only converge well because Z'_{uu}

is known to be zero.

Examining the M coefficients some coefficients converge relatively well such as $M'_{uu\delta S}$ whereas others converge very badly such as $M'_{u|q|\delta S}$. The pattern is similar for all three submarines.

7.6.3 Optimization Routine Performance — Vertical Manoeuvre

During all the testing the optimization routine converged without incident and as such the vertical manoeuvre did not appear to affect the procedure's robustness.

The histograms of the time and cost function evaluations to convergence for the three submarines are shown in Figures 45–47 with the mean data presented in Tables 19–21.

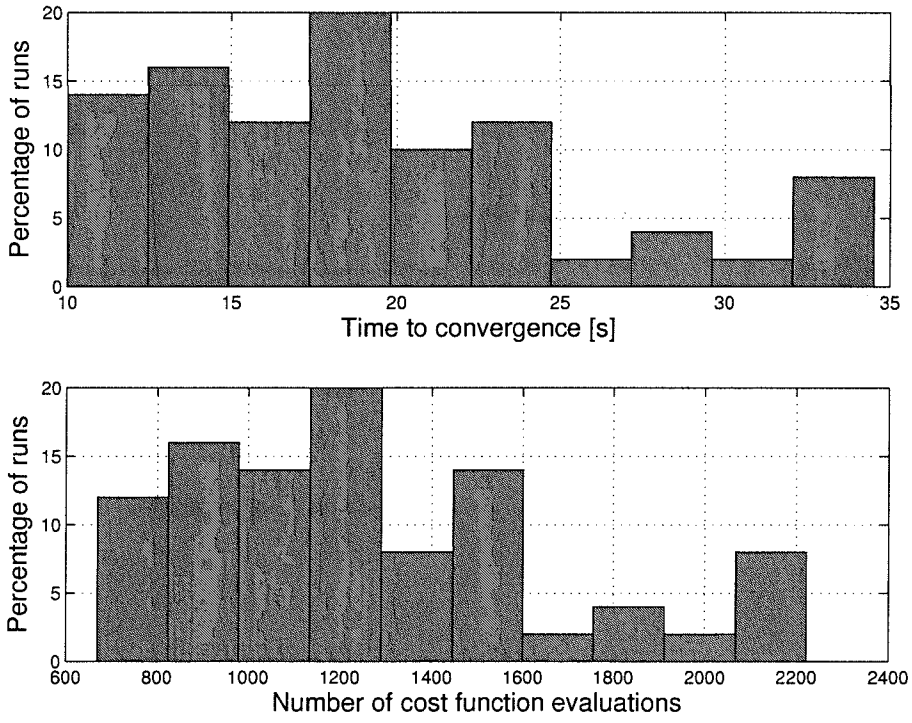

Figure 45: System performance results for the vertical manoeuvre — submarine 1.

Number of coefficients to identify (m)	$= 20$
Mean cost function evaluations (ε_N)	$= 1258$
ε_N/m	$= 62.9$
Mean time to converge	$= 34$s

Table 19: Summary of the optimization routine efficiency — vertical manoeuvre, submarine 1.

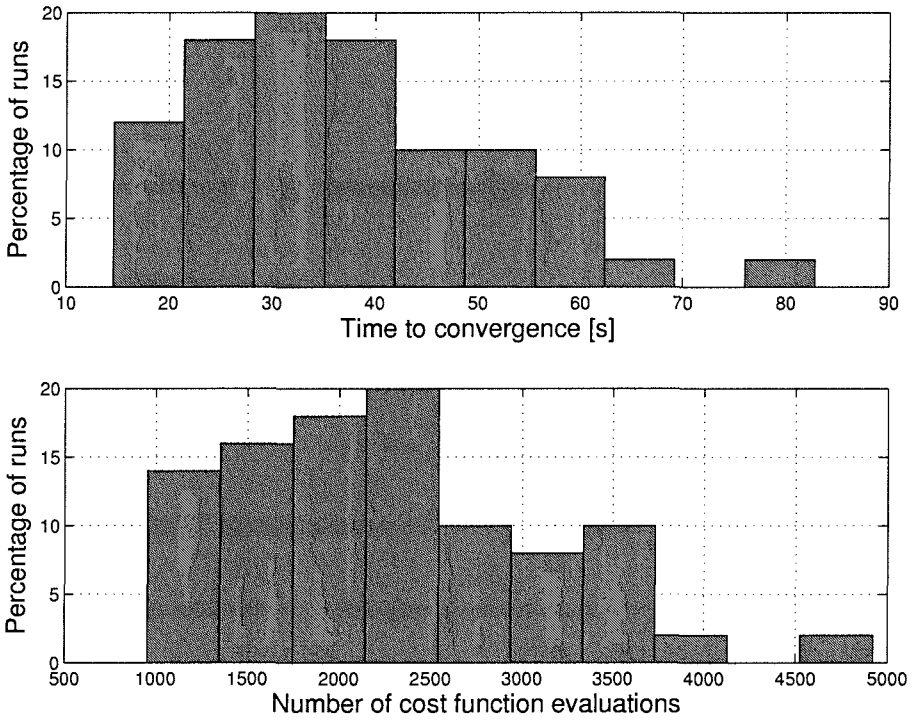

Figure 46: System performance results for the vertical manoeuvre — submarine 2.

Number of coefficients to identify (m)	$= 29$
Mean cost function evaluations (ε_N)	$= 2261$
ε_N/m	$= 78.0$
Mean time to converge	$= 66$s

Table 20: Summary of the optimization routine efficiency — vertical manoeuvre, submarine 2.

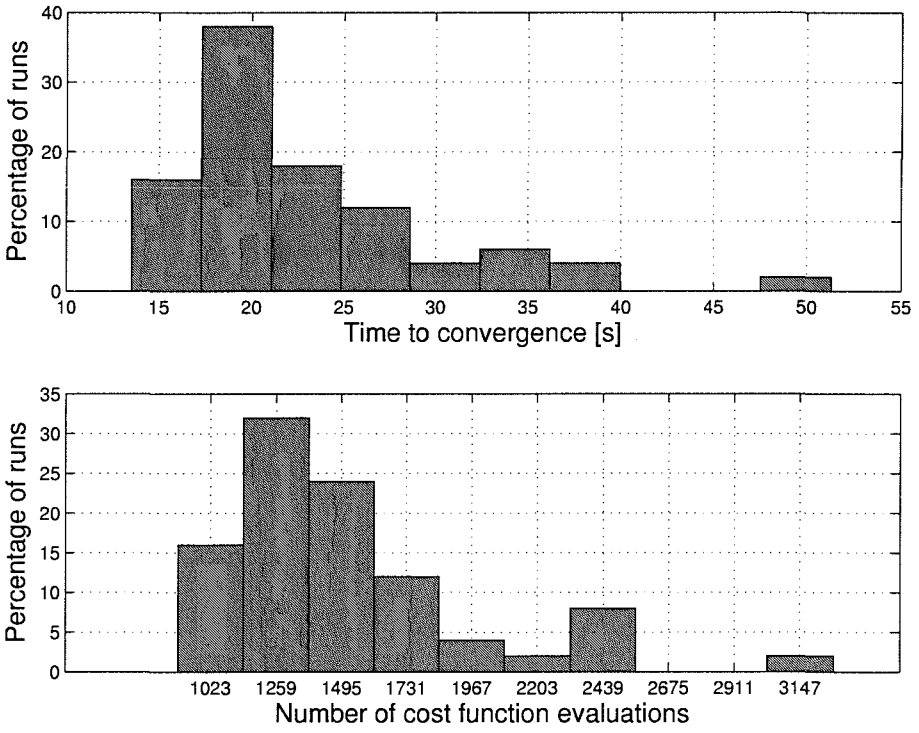

Figure 47: System performance results for the vertical manoeuvre — submarine 3.

Number of coefficients to identify (m)	$= 22$
Mean cost function evaluations (ε_N)	$= 1514$
ε_N/m	$= 68.8$
Mean time to converge	$= 41$s

Table 21: Summary of the optimization routine efficiency — vertical manoeuvre, submarine 3.

The results show that the optimization routine converges in less cost function evaluations per coefficient for the vertical case than in the horizontal case. This is demonstrated by the ratio ε_N/m being between 60–80 for the vertical manoeuvre compared to the 105-110 level for the horizontal case. As mentioned previously, the cause of this is thought to be due to the absolute convergence criteria used in the optimization routine.

Also whereas in the horizontal manoeuvre the ε_N/m ratio decreases, with increased coefficients in the vertical manoeuvre this pattern is reversed. The cause of this is

not clear, although one would expect problems with high dimensionality (i.e. more coefficients to identify) would require proportionally longer to solve. One possible explanation is that the difference in function calls is due to the difference in identifying the Z coefficients.

7.6.4 Vertical Manoeuvre Testing Conclusions

The main results of the vertical manoeuvre are very similar to those of the horizontal manoeuvre. Firstly, $\hat{\boldsymbol{N}}$ converges to $\boldsymbol{N}$ with an ε value approximately 100 times less than the ε value associated with the accuracy of the simulation. Second, $\hat{\boldsymbol{\xi}}$ converges very poorly to $\boldsymbol{\xi}$ and in most cases the coefficients have a larger spread of errors than in the initially estimated $\hat{\boldsymbol{\xi}}^{(1)}$ vector. Thus, the system produce by *the standard vertical manoeuvre* is ill-conditioned.

The results also show some more subtle features of the identification procedure. The first feature being the relationship between the errors in Z'_{uu}, Z'_{uw} and $Z'_{uu\delta S}$ and the second being the effect of the convergence criteria on the total number of cost function evaluations.

7.7 Coupled Test Results

The fully coupled manoeuvre tests were substantially more challenging than the vertical and horizontal manoeuvres because the number of coefficient to identify increased substantially. The number of coefficients to identify went from less than 30 in the horizontal and vertical manoeuvre to between 56 and 73 in the coupled case.

As per the horizontal and vertical manoeuvres the results are presented in three sections, the estimated track convergence the coefficient convergence and the optimization routine performance.

7.7.1 Coupled Manoeuvre Track Convergence

The histogram of the cost function reduction and the maximum positional error for the three submarines are shown in Figures 48–50. Tables 22–24 show the mean convergence data.

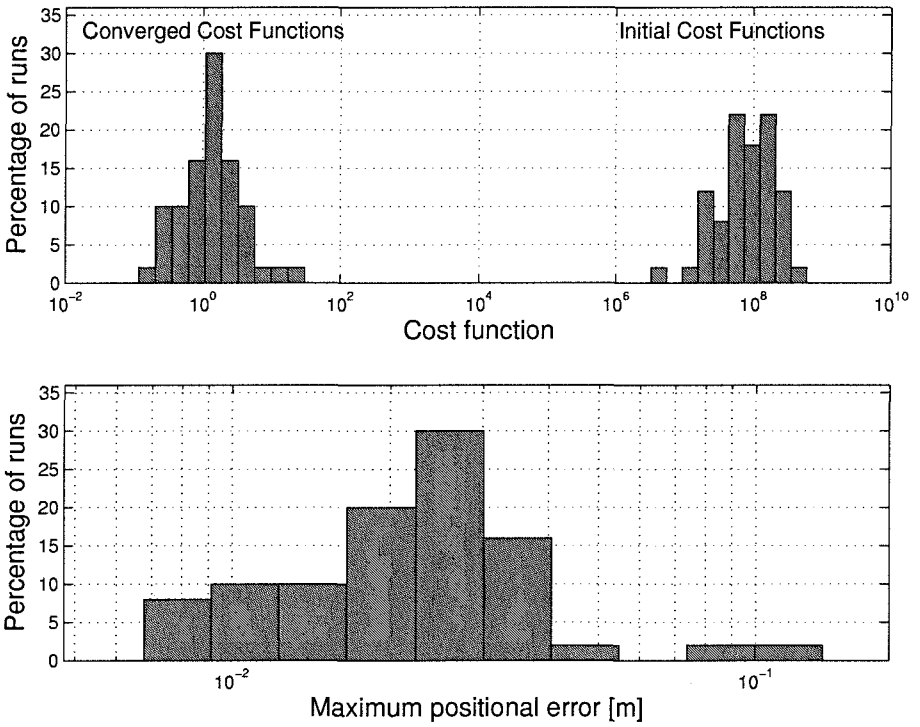

Figure 48: Track convergence results for the coupled manoeuvre — submarine 1.

Mean initial cost function value	$= 1.14 \times 10^8$
Mean converged cost function	$= 2.34$
Reduction in mean value	≈ 7 orders of magnitude
Mean maximum positional error	$= 25.4$ mm

Table 22: Summary of the coupled manoeuvre convergence results — submarine 1.

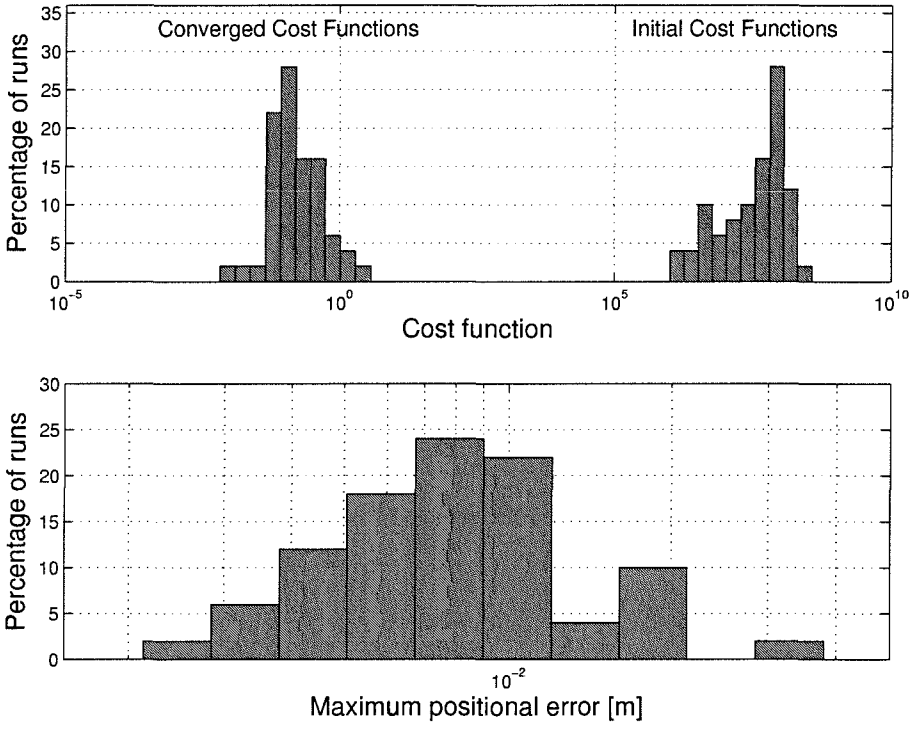

Figure 49: Track convergence results for the coupled manoeuvre — submarine 2.

Mean initial cost function value	$= 6.21 \times 10^{7}$
Mean converged cost function	$= 2.80 \times 10^{-1}$
Reduction in mean value	≈ 8 orders of magnitude
Mean maximum positional error	$= 9.0$ mm

Table 23: Summary of the coupled manoeuvre convergence results — submarine 2.

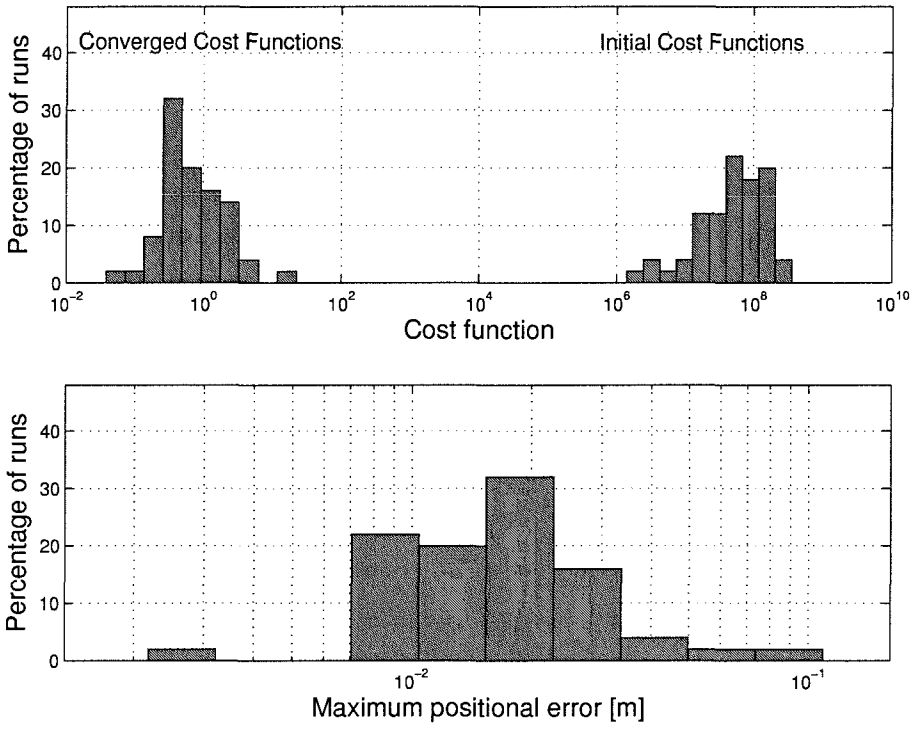

Figure 50: Track convergence results for the coupled manoeuvre — submarine 3.

Mean initial cost function value	$= 7.51 \times 10^7$
Mean converged cost function	$= 1.20$
Reduction in mean value	$\approx$ 7 orders of magnitude
Mean maximum positional error	$= 19.3$ mm

Table 24: Summary of the coupled manoeuvre convergence results — submarine 3.

The results for the three submarines are very close to those of the horizontal manoeuvre with the initial cost functions, converged cost functions and the maximum positional error being of the same order of magnitude. This is not too much of a surprise. The coupled manoeuvre uses the same rudder control plane input time history, but also has a stern dive plane time history to change the depth of the submarine.

Again the converged $\hat{\boldsymbol{N}}$ is closer to $\boldsymbol{N}$ than the accuracy of the simulation (Section 5.9).

7.7.2 Coupled Manoeuvre Coefficient Convergence

The converged coefficients for the three test submarines are shown in Figures 51–56. Due to the number of coefficient involved in the fully coupled equations of motions the converged data is split into two plots. The first figure shows the force coefficients (X, Y & Z) and the second shows the moment coefficients (K, M & N).

The results show that in general, as with the horizontal and vertical manoeuvre, the coefficients converge badly and the converged coefficients are generally further from the true coefficient value than that of the initial coefficient estimate. The only exception to this rule is X'_{uu} which had been universally well identified in all manoeuvres for all submarines.

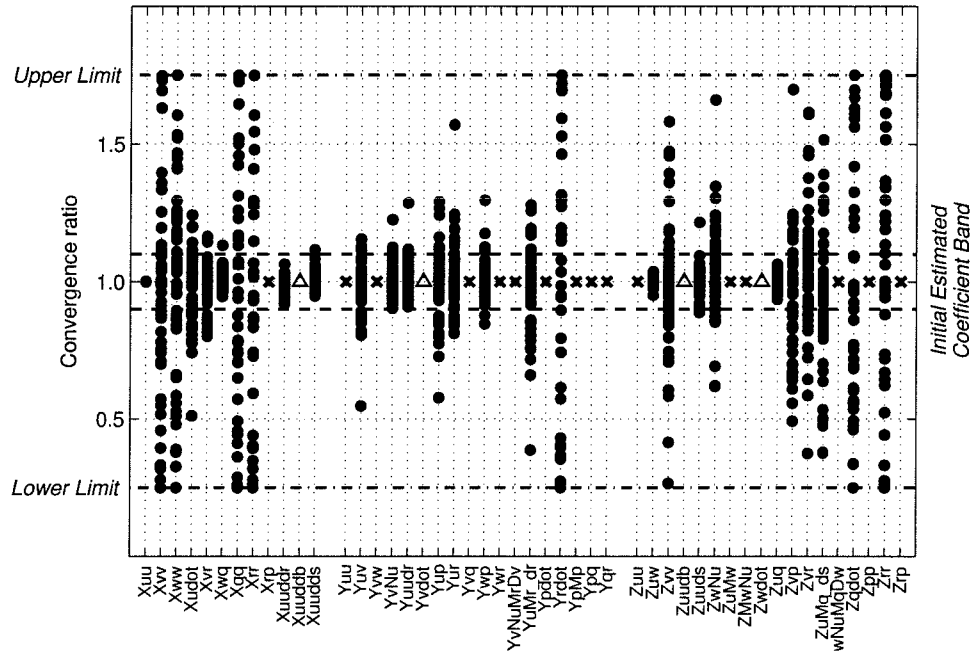

Figure 51: Converged force coefficient for the coupled manoeuvre — submarine 1.

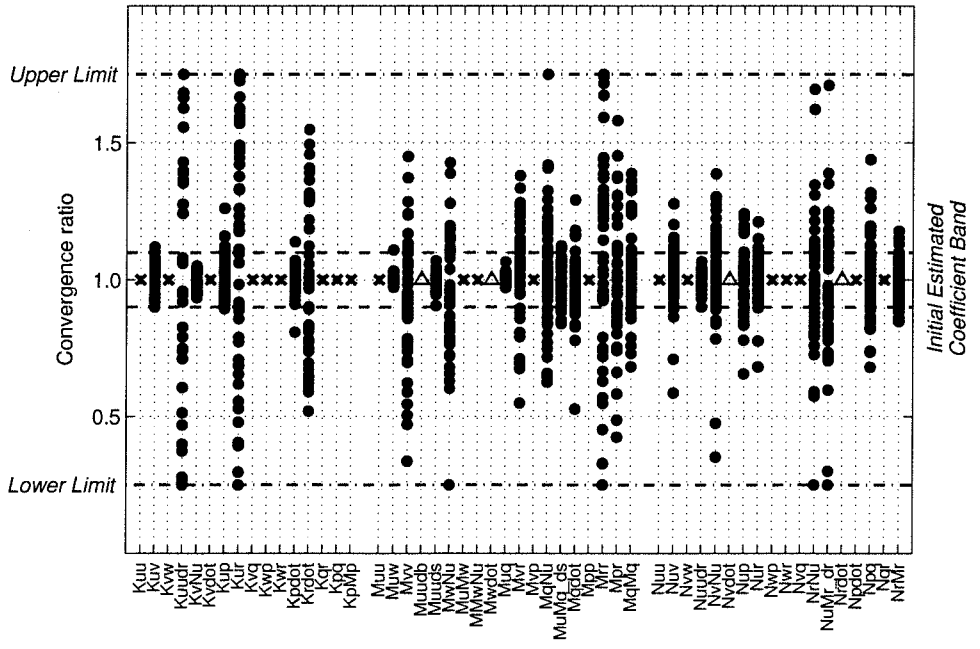

Figure 52: Converged moment coefficient for the coupled manoeuvre — submarine 1.

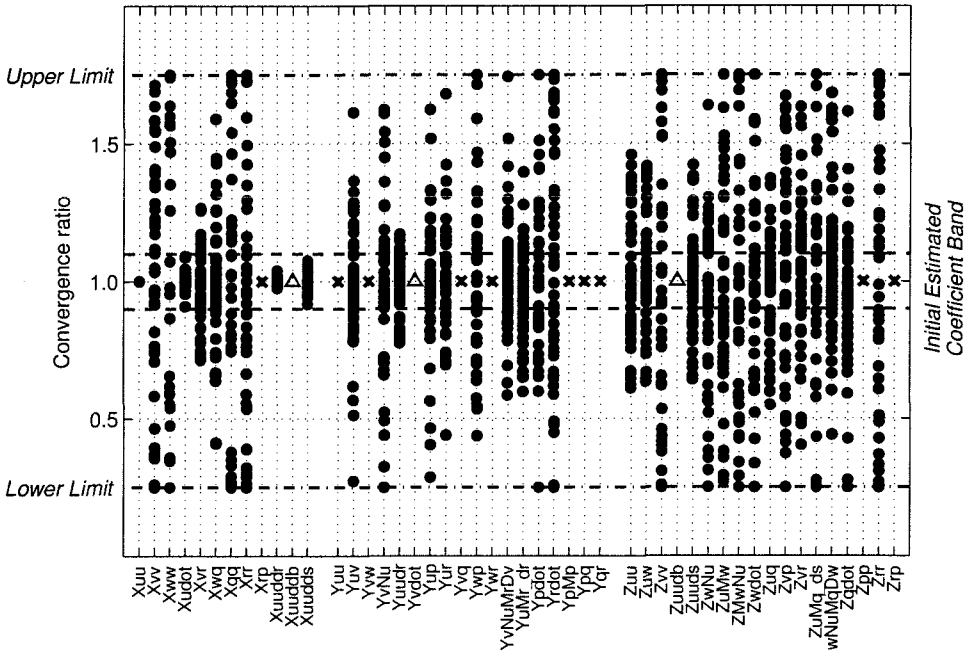

Figure 53: Converged force coefficient for the coupled manoeuvre — submarine 2.

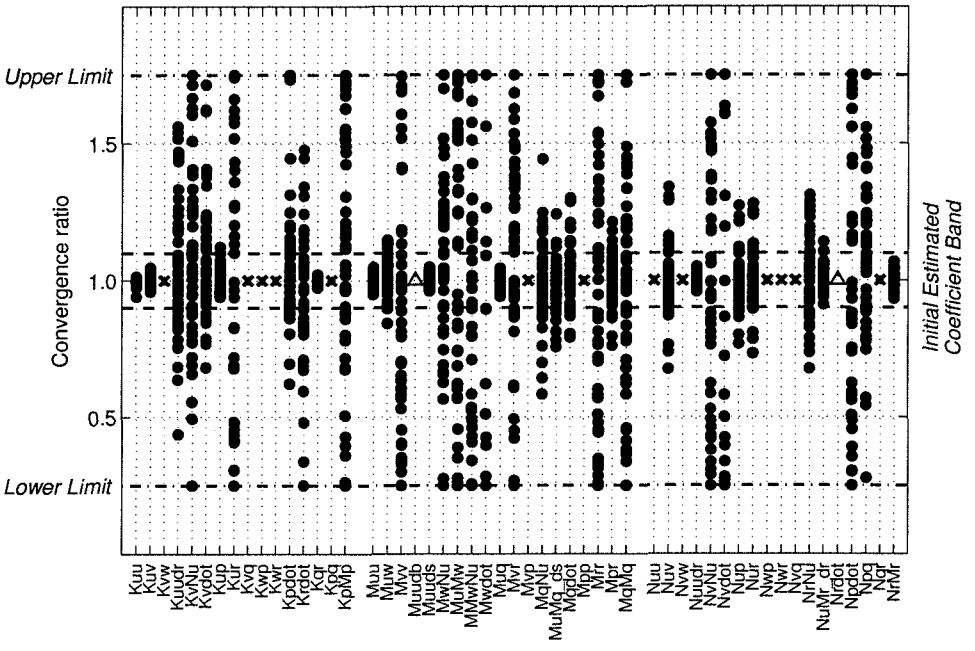

Figure 54: Converged moment coefficient for the coupled manoeuvre — submarine 2.

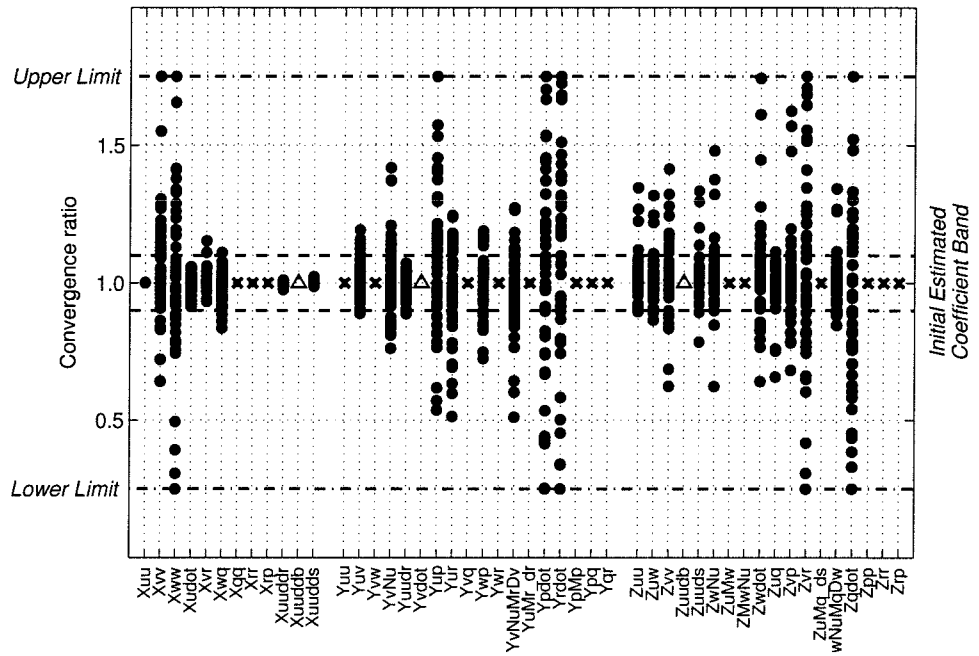

Figure 55: Converged force coefficient for the coupled manoeuvre — submarine 3.

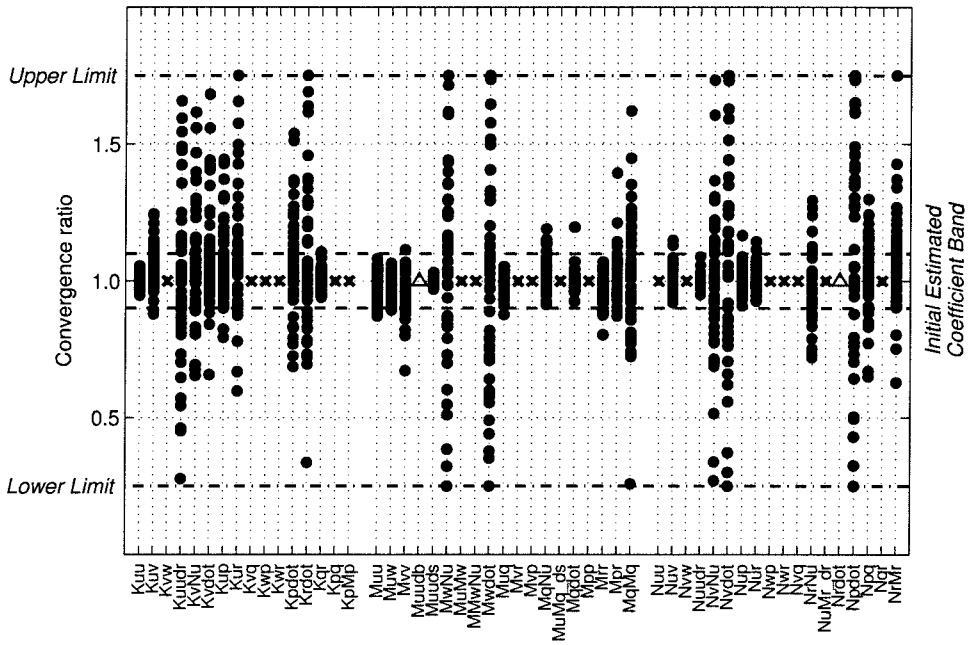

Figure 56: Converged moment coefficient for the coupled manoeuvre — submarine 3.

7.7.3 Optimization Routine Performance — Coupled Manoeuvre

The optimization routine proved to be less robust when trying to identify all the coefficient values as it failed in a large number of cases. The routine managed to converge for every test of submarine 1. However, the routine failed during three tests applied to submarine 2. The failure was expressed by the optimization routine appearing to be stuck in an infinite loop within the code. When this occurred the system would fail to regularly evaluate the cost function. The convergence criteria for the three failed tests were relaxed and the system then converged successfully. The relaxed values were

$$parTol = 1.0 \quad \text{and} \quad funcTol = 0.1.$$

The convergence for submarine 3 was particularly poor. Many of the tests failed with the starting convergence criteria. These criteria had to be relaxed greatly to allow all the tests to converge. The final values that allowed all the coefficients to converge were

$$parTol = 10 \quad \text{and} \quad funcTol = 10.$$

Surprisingly the converged cost function values do not appear to be substantially worse for submarine 3 than submarine 1 or 2 and so one must assume that the relaxed convergence criteria did not greatly affect the cost function minimization.

As seen from the ε_N/m ratio the convergence of the routine takes proportionally longer per coefficient than that of the horizontal or vertical cases. And in general the fully coupled case takes between 7–10 minutes to converge for the 10 minute coupled manoeuvre. Interesting the reduction in the convergence criteria for submarine 3 has affected the number of cost function evaluations before convergence, as seen in the difference between the ε_N/m ratios of submarine 1 and submarine 3.

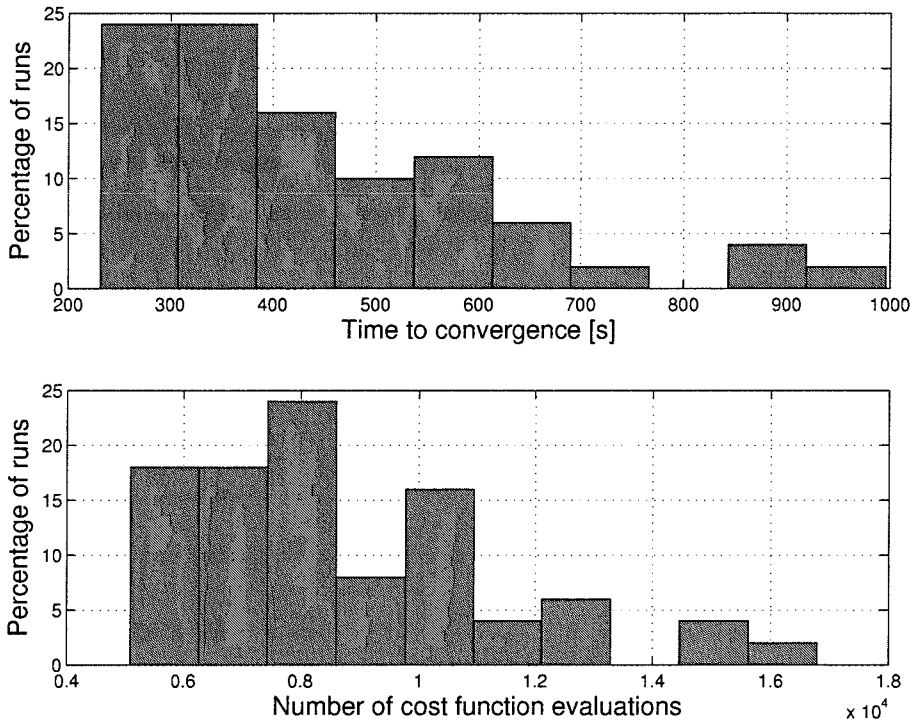

Figure 57: System performance results for the coupled manoeuvre — submarine 1.

Number of coefficients to identify (m)	$= 56$
Mean cost function evaluations (ε_N)	$= 8715$
ε_N/m	$= 155.6$
Mean time to converge	$=$ 7min 22s

Table 25: Summary of the optimization routine performance — coupled manoeuvre, submarine 1.

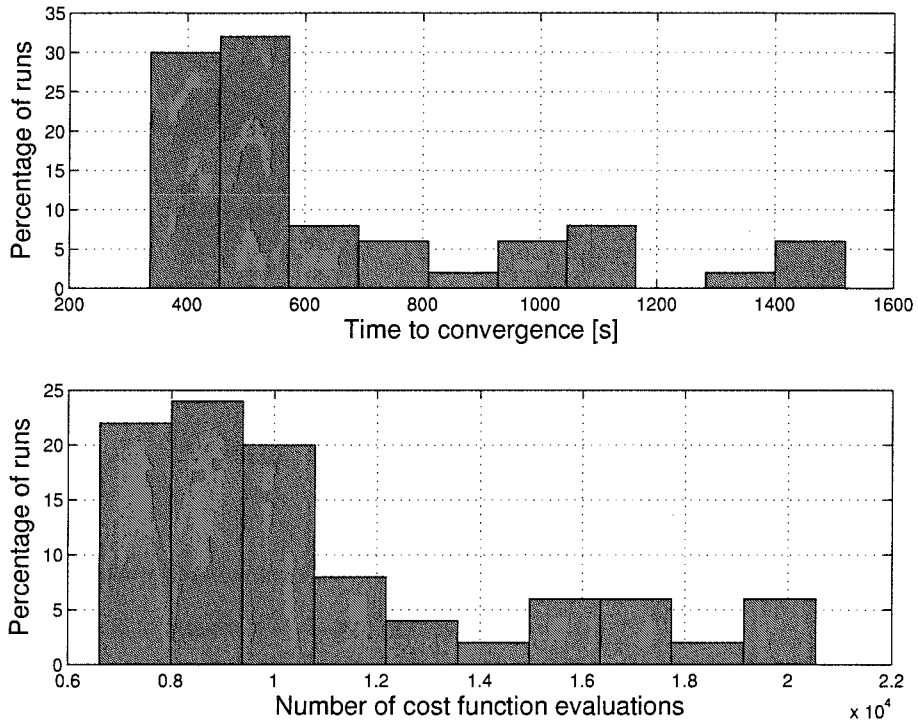

Figure 58: System performance results for the coupled manoeuvre — submarine 2.

Number of coefficients to identify (m)	$= 73$
Mean cost function evaluations (ε_N)	$= 10928$
ε_N/m	$= 149.7$
Mean time to converge	$=$ 10min 52s

Table 26: Summary of the optimization routine performance — coupled manoeuvre, submarine 2.

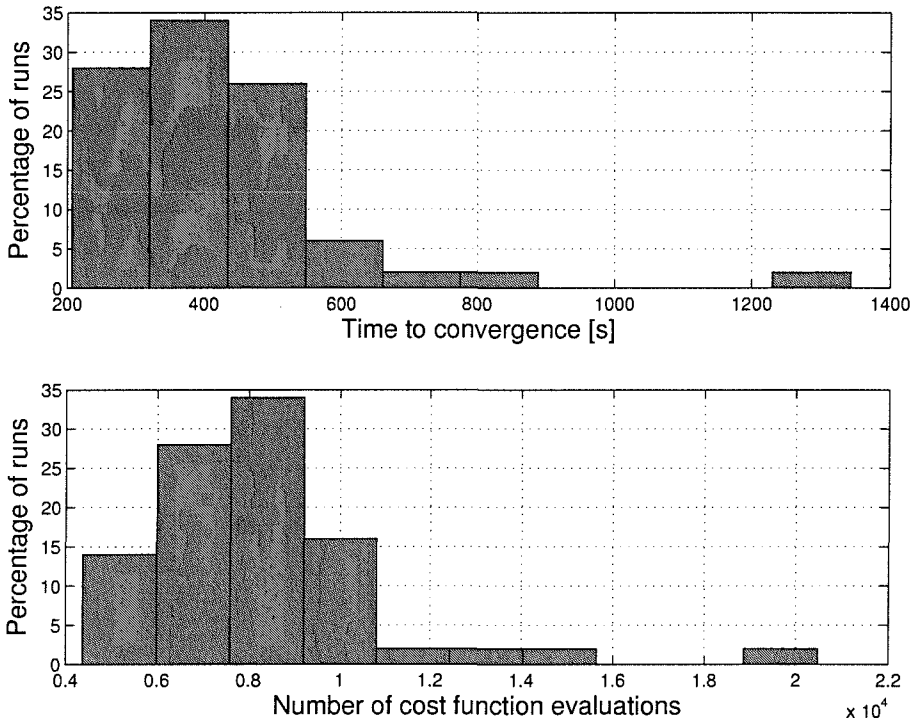

Figure 59: System performance results for the coupled manoeuvre — submarine 3.

Number of coefficients to identify (m)	$= 60$
Mean cost function evaluations (ε_N)	$= 8231$
ε_N/m	$= 137.2$
Mean time to converge	$=$ 7min 4s

Table 27: Summary of the optimization routine efficiency — coupled manoeuvre, submarine 3.

7.7.4 Coupled Manoeuvre Testing Conclusions

Again as with the horizonal and vertical manoeuvres $\hat{\boldsymbol{N}}$ convergence exceptionally accurately to $\boldsymbol{N}$ and the associated ε value was substantially less than that produced by the accuracy of the simulation. However, again $\hat{\boldsymbol{\xi}}$ does not converge well to $\boldsymbol{\xi}$ and in most cases the errors on the coefficients are larger than those of the initial estimate $\hat{\boldsymbol{\xi}}^{(1)}$. Hence *the coupled manoeuvre* is also ill-conditioned.

Also, the coupled manoeuvre takes longer to converge than the horizontal and vertical manoeuvres. This is, in part, due to the increased number of coefficients to identify but also due to the increased number of cost function evaluations required per coefficient. The optimization routine also showed some numerical instability in that it failed to converge for a large portion of the submarine 3 tests and some of the submarine 2 tests. This was solved by reducing the convergence criteria. It is possible that by suitably tuning the convergence criteria the ε_N/m ratio can be reduced and the numerical stability increased without the optimization routine terminating before getting close to a true minima.

7.8 Analysis of the Ill-Conditioning Phenomenon

The results presented for the horizontal, vertical and coupled coefficient convergence tests show all the manoeuvres form ill-conditioned systems. That is, very small changes in manoeuvres are generated by significant differences in the hydrodynamic coefficient sets. Thus, it is extremely difficult to identify the correct hydrodynamic coefficients using the manoeuvre time history ($\boldsymbol{T_c}$) and the target path ($\boldsymbol{N}$). The cause of this ill-conditioning is analysed next.

As $\hat{\boldsymbol{N}}$ is almost identical to $\boldsymbol{N}$ it follows that the velocities, accelerations and forces & moments must also be very similar. As shown in Chapter 6 the coefficient sets are unique, but the ill-conditioning means that large differences in the coefficient values can produce very small differences in the test manoeuvres. Even for the ill-conditioned situation the forces have to be almost identical. This can occur in the following two possible ways:

- The coefficient provides only a small contribution to the total force or moment.
- Two or more coefficients produce large errors that cancel out. This error cancellation can only occurs if the multipliers of the coefficients are strongly related.

These two possible causes are now examined in detail. The first cause can be considered by assessing the contribution made to the cost function by individual coefficients.

A small cost function contribution will be produced by a small difference in total force or moment.

7.8.1 Coefficient Cost Function Contribution

A coefficient will be difficult to identify if it does not affect the cost function of the manoeuvre in any significant way. In practise this will mean any coefficient associated with very small force or moment contributions. The significance of each coefficient was determined by calculating the resulting cost function value when that coefficient had been moved to the lower tolerance band threshold (i.e. 25% of its original value). This produced the maximum cost function that could be produced by the single coefficient.

Figure 60 presents the results for three test submarines performing the horizontal manoeuvre. The plot shows the cost function produced by perturbing each coefficient to be identified in turn for each submarine. The horizontal coefficients not identified have no associated cost function, and so there is no marker for these coefficients. The plot also shows the maximum mean converged cost function (1.42) for the least well converged submarine (submarine 3) and the simulation accuracy calculated cost function of Section 5.9.

The results show that all the coefficients identified in the horizontal manoeuvre are all capable of producing a larger cost function change than that produced by the converged coefficients. However, the relationship between the cost function and the coefficient perturbation is non-linear and so it could be that close to the real coefficient value the cost function contribution is very small. This possibility was investigated by repeating the above analysis with a perturbation level for coefficients of 99% of their correct value. The results of this analysis are shown in Figure 61. This figure shows that most of the coefficients when perturbed by -1% of their correct value produce a cost function that is still greater than the maximum mean converged cost function. From this plot one could draw the conclusion that insignificant coefficients such as $Y'_{\dot{r}}$ would be badly converged. However, $X'_{\dot{u}}$ which also produces a small contribution to the cost function is generally better identified than many of the other coefficients.

Thus, it would appear that the size of the contribution from the coefficients in the horizontal manoeuvre have at best a limited impact on their identification performance.

The analysis was repeated for the vertical and coupled manoeuvres. The vertical results are shown in Figures 62 & 63 and the coupled results are shown in Figures 64 & 67. Due to the number of coefficients involved in the coupled case the plots are split into the force coefficients and the moment coefficients.

The results for the vertical and coupled manoeuvre show that all the coefficients, with the exception of X'_{qq} and $K'_{\dot{p}}$ for submarine 1 performing the coupled manoeuvre, are capable of producing a cost function greater than that of the mean converged coefficient value. But when considering the 99% trial there are a large number of coefficients which produce a cost function contribution lower than the maximum mean converged cost function value. Thus, all these coefficients could individually be determined between 99% and 25% of their correct value and produce the observed cost function. If cost function contributions from these coefficients was linearly addable (which is highly unlikely) then a set of poorly converged coefficients could be responsible for the observed cost functions. However, this does not explain the poor convergence of coefficients such as X'_{vv} which is poorly identified in the coupled manoeuvre for all three submarines, but still has a cost function contribution of over 1000 times greater than the converged value at the 99% level. Thus, although the relative size of the contributions may be responsible for the poor convergence of some coefficients it only explains in part the ill-conditioning.

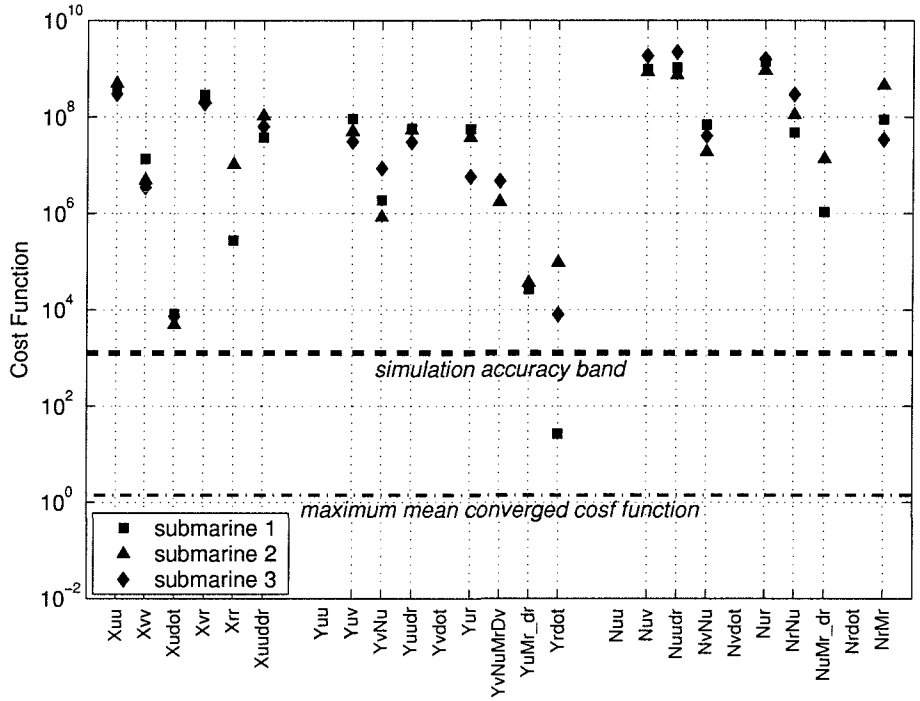

Figure 60: Cost functions for assigned coefficients corresponding to 25% of true value — horizontal manoeuvre.

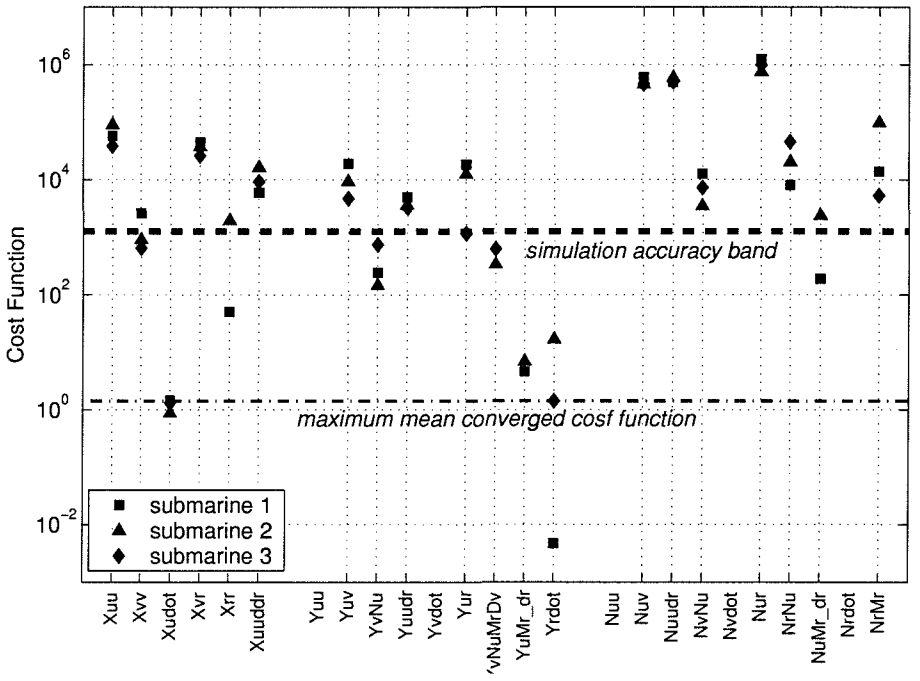

Figure 61: Cost functions for assigned coefficients corresponding to 99% of true value — horizontal manoeuvre.

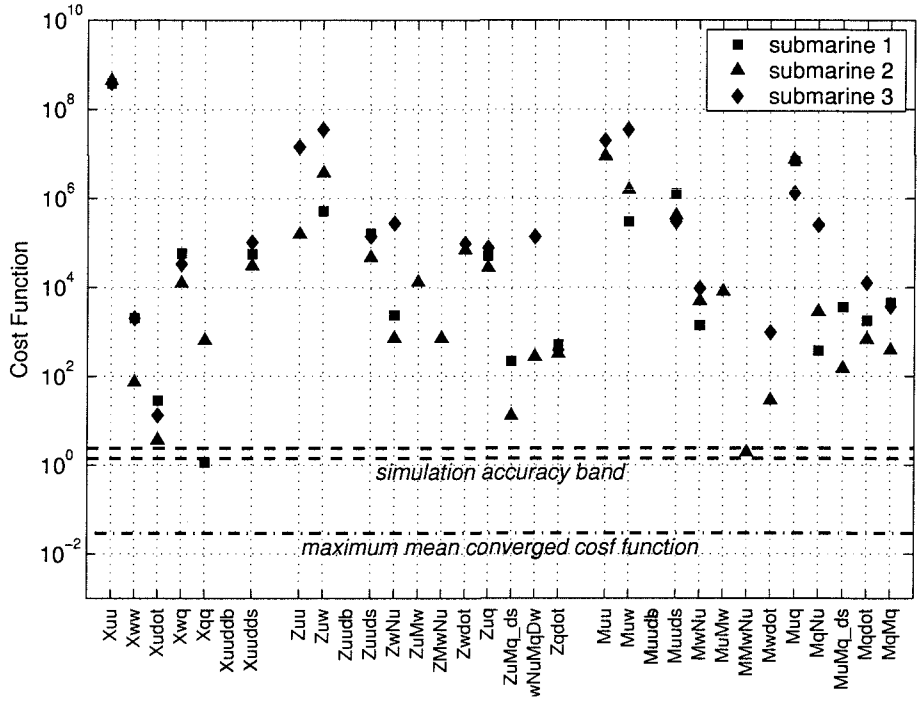

Figure 62: Cost functions for assigned coefficients corresponding to 25% of true value — vertical manoeuvre.

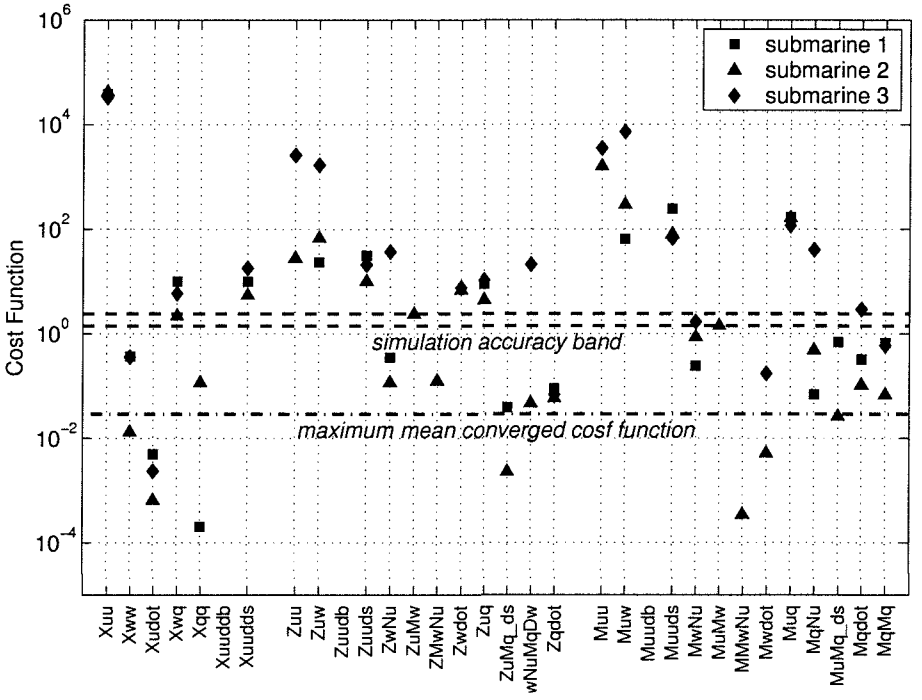

Figure 63: Cost functions for assigned coefficients corresponding to 99% of true value — vertical manoeuvre.

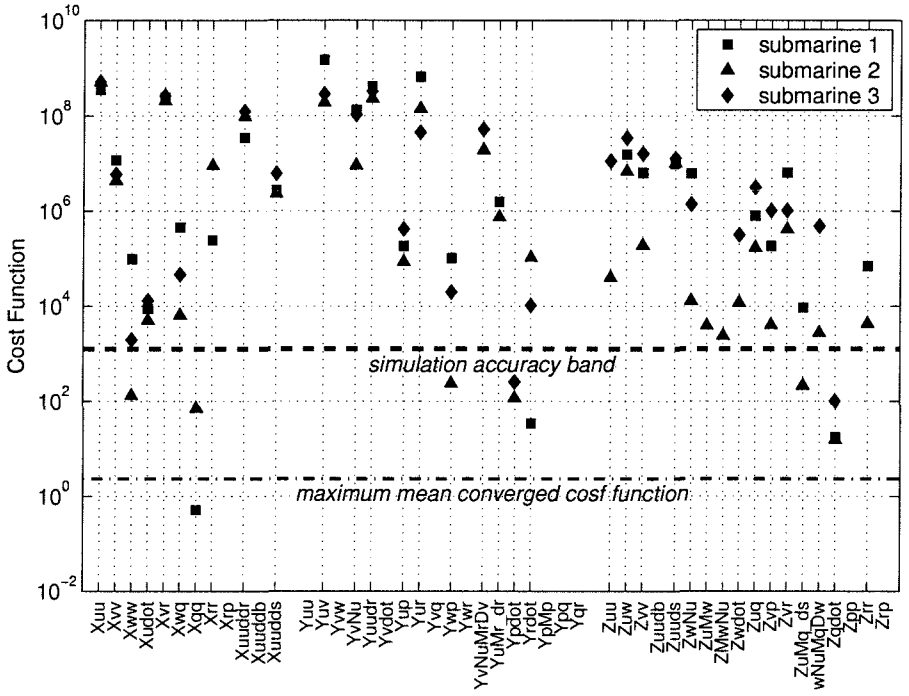

Figure 64: Cost functions for assigned force coefficients corresponding to 25% of true value — coupled manoeuvre.

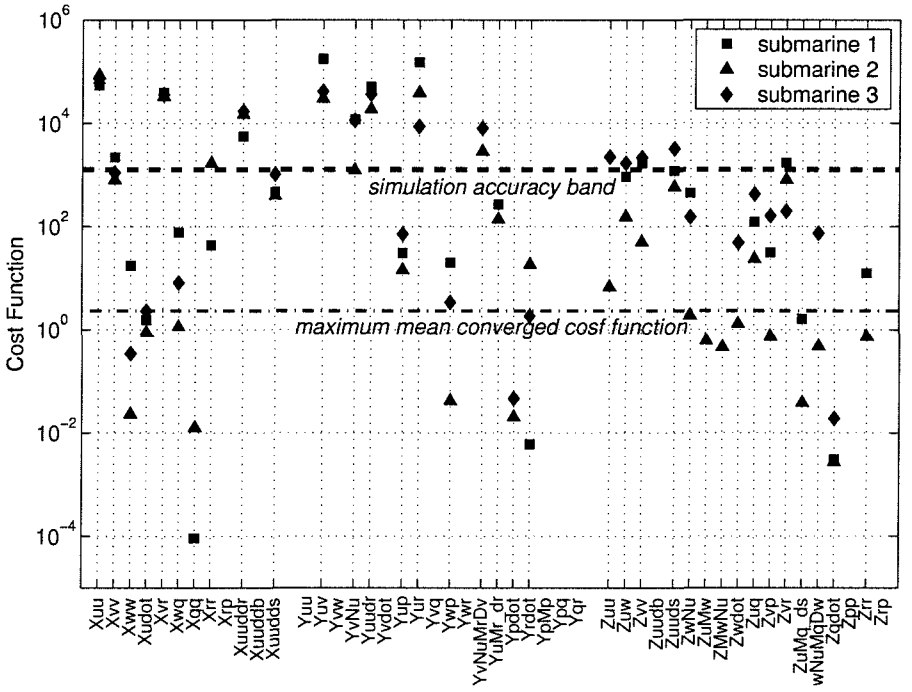

Figure 65: Cost functions for assigned force coefficients corresponding to 99% of true value — coupled manoeuvre.

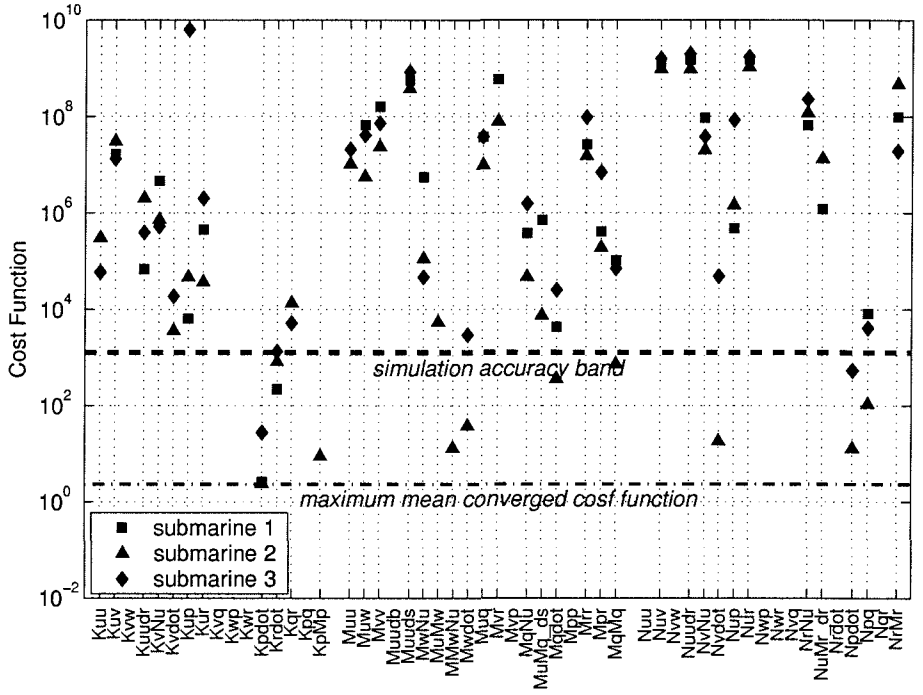

Figure 66: Cost functions for assigned moment coefficients corresponding to 25% of true value — coupled manoeuvre.

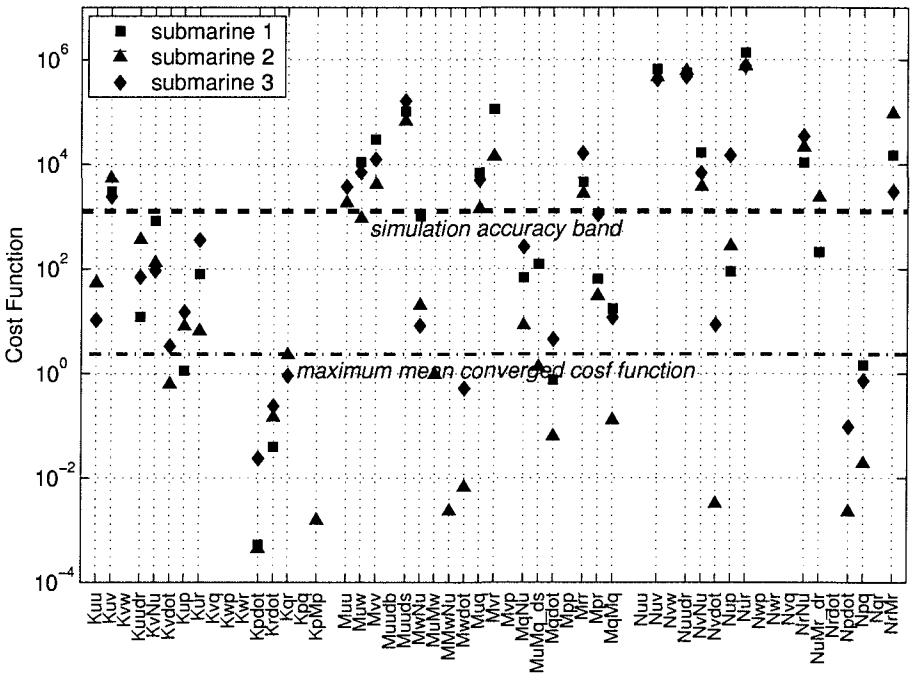

Figure 67: Cost functions for assigned moment coefficients corresponding to 99% of true value — coupled manoeuvre.

7.8.2 Coefficient Error Cancellation

Having examined and discounted the possibility that the poorly identified coefficients produce only a small contribution to the cost function as the cause of the ill-conditioning, the other alternative is that the errors in the coefficients cancel.

This is based on the idea that approximately the correct force or moment is produced by the wrong coefficients. For this to occur it is necessary for the values that the coefficients are multiplied by to be strongly related. To take a simple example of complete error cancellation if $X = (a + b)u$ then given X and u it is not possible to find a or b.

To investigate this phenomena the horizontal manoeuvre case was examined for the X force. This case was considered as it greatly simplified the analysis over the general case. The equations of motion for the X coefficient, in the horizontal case, are:

$$\begin{aligned} m\left[\dot{u} - vr - x_G r^2 + y_G \dot{r}\right] = & \frac{1}{2}\rho l^2 \left(X'_{uu}u^2 + X'_{vv}v^2\right) \\ & + \frac{1}{2}\rho l^3 \left(X'_{\dot{u}}\dot{u} + X'_{vr}vr\right) \\ & + \frac{1}{2}\rho l^4 \left(X'_{rr}r^2\right) \\ & + \frac{1}{2}\rho l^2 u^2 \left(X'_{uu\delta\delta R}\delta R^2\right) \\ & + X_n \end{aligned}$$

Check whether the y_G and x_G need to be zero

Considering the physics that the equation represents, it seemed likely that the yaw rate (r) and the sway velocity (v) would be related in any turning manoeuvre. The correlation between these coefficients was analysed by plotting the coefficient multipliers v^2 and r^2 against each other as shown in Figure 68.

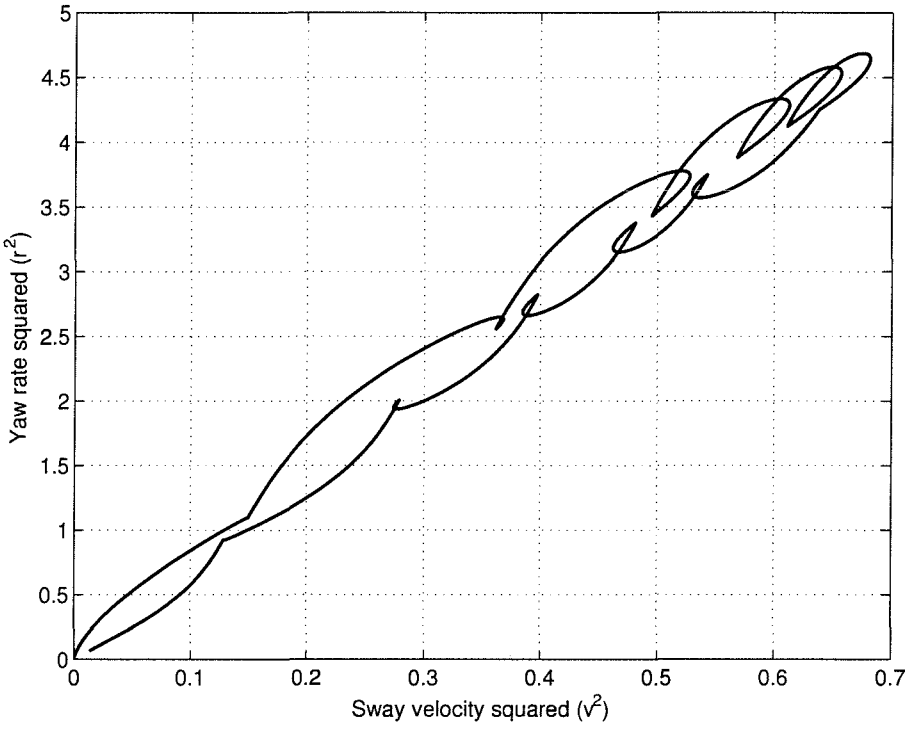

Figure 68: The relationship between v^2 and r^2 for the horizontal test manoeuvre performed by submarine 1.

The figure shows the strong coupling between the yaw rate and the sway velocity in the manoeuvre. Ideally to identify the coefficients there should be no coupling between the coefficient multipliers and no discernable pattern should be apparent in Figure 68. Unfortunately this is not the case and the coefficients are heavily coupled. Thus from this simple analysis one can conclude that total error produce by the sum of coefficients X'_{vr}, X'_{vv} and X'_{rr} can be substantially smaller than that associated with each individual coefficient due to error cancellation from the other coefficients. This is illustrated in Figure 69. This figure shows the error produced in the X'_{vv}, X'_{vr} and X'_{rr} force components when using the first set of converged coefficients produced by submarine 1 performing the horizontal manoeuvre. The plot shows the difference in force contribution from the correct and converged coefficient. The sum of the three coefficients is also shown. As can be seen from the plot the force error on each coefficient is substantially larger than the sum of the errors. Table 28 shows the maximum absolute error in the force for each coefficient and the sum of the coefficients.

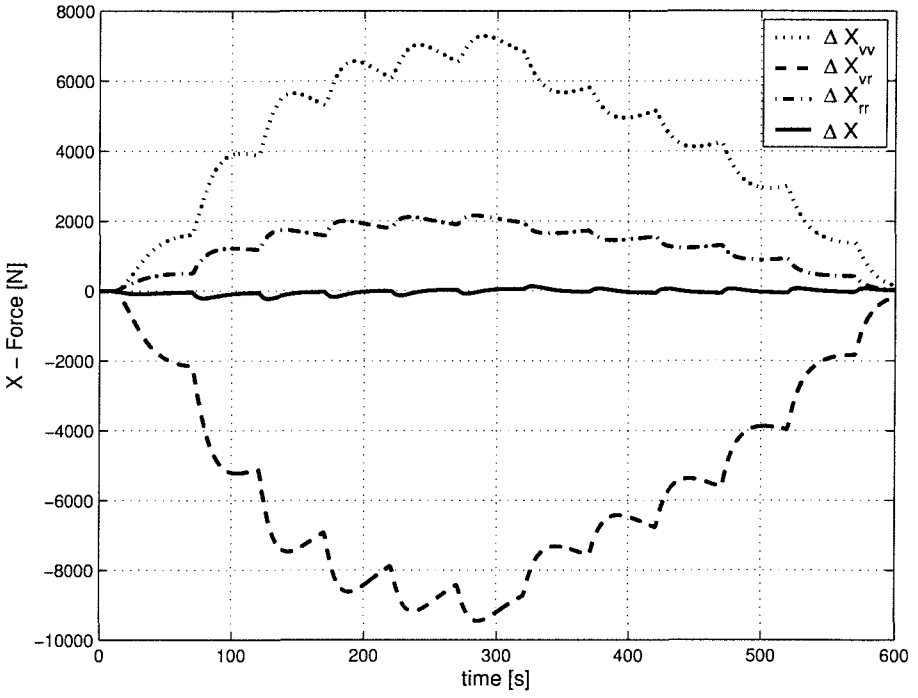

Figure 69: The relationship between v^2 and r^2 for the horizontal test manoeuvre performed by submarine 1.

Coefficient	Maximum absolute error [N]
$\Delta\ X'_{vv}$	7292.4
$\Delta\ X'_{vr}$	9454.4
$\Delta\ X'_{rr}$	2159.4
ΔX	223.3

Table 28: Maximum absolute error associated with the differences produced by the X'_{vv}, X'_{vr} & X'_{rr} hydrodynamic coefficients.

This type of analysis could be performed for all the manoeuvres and all the coefficients to see how the cancellation can occur. However, this process would be of little merit as it does not indicate how the ill-conditioning can be removed.

7.8.3 Ill-conditioning Conclusions

The foregoing analysis has shown how the ill-conditioning can occur in the three submarine manoeuvres. However, there is no clear way forward to improve the situation. The primary problem is that the results are only valid for the manoeuvres tested and it is not clear if there is a manoeuvre that produces a well conditioned system that allows for accurate identification of the correct coefficients.

It would be possible to test many different manoeuvres but this is impractical because it is not possible to test every manoeuvre and the time to perform each test is such that for the fully coupled manoeuvres the computing effort required is too large.

The second problem is that it is not known whether the identified coefficient accurately reproduce other manoeuvre or whether they only reproduce the target manoeuvre. If they do not reproduce the other manoeuvre it would be possible to add manoeuvres together to see if the new manoeuvre produced a better set of coefficients. However all the approaches require many more identification runs, for each manoeuvre.

7.9 Conclusions

This chapter has discussed how the non-linear identification procedure was tested. The results for the three different submarines performing the three different test manoeuvres (horizontal, vertical and fully-coupled) have been presented and some surprising conclusions drawn.

The results presented showed that the optimization routine converged to a set of coefficients which produce a track almost identical to the target track. However, the converged coefficients are very different from those used to generate the target track. From these results the conclusion was drawn that the manoeuvres used to test the submarines produced an ill-conditioned set of equations. This ill-conditioning is expressed by the very different coefficients producing almost identical manoeuvres.

The reasons for this ill-conditioning was then examined and it was shown to arise due

to the dependence between the coefficient multipliers.

The discussion presented on ill-conditioning also lead to the following related questions:

- Is there a manoeuvre that removes the ill-conditioning and hence will allow the coefficients to be accurately identified?
- Will the 'wrong' identified coefficients reproduce other manoeuvres as accurately or will they only reproduce the test manoeuvres?

To use the non-linear identification technique to answer these questions is possible, but would be extremely time consuming as each test manoeuvre would need to be tested using many different initial estimates of the coefficients and as each test takes a long time to complete the computing power required makes the task a substantial undertaking. Thus, a more appropriate method was required to analyse the problem.

Chapter 8

Converged Coefficient Manoeuvre Prediction

8.1 Introduction

The 50 coefficient sets identified for each submarine, using the non-linear parameter identification procedure reproduced the target manoeuvre remarkably accurately, even though the identified coefficients ($\hat{\boldsymbol{\xi}}^*$) were substantially different from the 'correct' coefficients ($\boldsymbol{\xi}$).

This apparent level of accuracy suggests the question, 'would these identified $\hat{\boldsymbol{\xi}}^*$'s also produce as accurately other 'non-identified' manoeuvres?'. Three possible answers to this question exist, they are:

- *The converged coefficients produce the same accuracy for all possible manoeuvres.*

  If this were the case then the coefficients would be to all intents and purposes the same as the correct values and would be more than capable of being used to model the UVs. The results would also imply that the coupled manoeuvre was sufficiently 'rich' for the $\hat{\boldsymbol{\xi}}^*$'s to captured the essential dynamic characteristics of the UV. However, the Booth et al. (1980) equations would be seen to produce an ill-conditioned system (as defined in Chapter 7) for all manoeuvres.

- *The converged coefficients produce the same accuracy as a set of randomly identified coefficients with the same coefficient error bounds.*

  If randomly generated sets of hydrodynamic coefficients, with the same range of errors as the $\hat{\boldsymbol{\xi}}^*$'s, produced predicted tracks of the same level of accuracy, then the $\hat{\boldsymbol{\xi}}^*$'s would belong to the same population as the randomly generated coefficients. Hence it would be difficult to state that the $\hat{\boldsymbol{\xi}}^*$'s had captured the essential dynamic characteristics of the UV being considered. Therefore the target track ($\boldsymbol{N}$) associated with the manoeuvre might not be considered 'rich'.

- *The coefficients produce the prediction manoeuvres less accurately than the identification manoeuvre but more accurately than randomly generated coefficients.*

  This final case represents the middle ground between the polarized bounds described immediately above. It suggests that some of the dynamics of the UV are captured by the coefficients, but not all, thus a better manoeuvre could be created to capture more of the UV dynamics. It would also imply that all the manoeuvres are ill-conditioned as random coefficients with the same error bounds produce the manoeuvres less accurately. However, the ill-conditioning may not be as great as that shown in the coupled identification manoeuvre.

The ideal method of testing the prediction performance of the $\hat{\boldsymbol{\xi}}^*$'s would be to exhaustively test every possible manoeuvre. However, as there are an infinite number of possible manoeuvres this approach is not feasible. It is thus necessary to examine a subset of possible manoeuvres assuming that this subset is representative of all manoeuvres.

This chapter discusses the testing and analysis of the prediction tests performed by the $\hat{\boldsymbol{\xi}}^*$'s. Of the three test problems used to identify the coefficients ($\hat{\boldsymbol{\xi}}^*$'s) only the coupled manoeuvre coefficients were tested. The $\hat{\boldsymbol{\xi}}^*$'s produced by the horizontal and vertical sub-problems were not tested as the sub-problems were created to build experience in the use of the identification procedure not to produce useful coefficient data.

The chapter first describes the method used to design and produce the manoeuvres used to test the prediction accuracy of the $\hat{\boldsymbol{\xi}}^*$'s. It then discusses in broad terms the

prediction results for the three test submarines. This is followed by an analysis of the effect of the manoeuvre on the prediction accuracy. Thereafter a more detailed study of the results considers the range of prediction accuracies produced by different coefficient sets. The 'best', 'worst' and 'middle' coefficient sets were identified and their converged coefficient values examined to see if there was a correlation between convergence and prediction accuracy. The chapter then concludes by summing up the prediction performance of the $\hat{\boldsymbol{\xi}}^*$'s and outlines the implications for using the technique to identify the correct coefficient values.

8.2 Designing the UV Test Manoeuvres

To test the predictive capabilities of the identified hydrodynamic coefficients it was necessary to use manoeuvres that had not been used in the identification process. The design of an optimum set of manoeuvres to fully test the predictive power of the coefficient is not trivial. This is because the designing of prediction test manoeuvres is, in effect, the same problem as identifying the optimal manoeuvre for the UV identification. As both problems are required to produce 'rich' manoeuvres. Unfortunately no way of determining a rich manoeuvre was available so it was decided to test a large group of random manoeuvres on the basis that the group as a whole would contain suitable richness, and hence would be a reasonable test of the identified coefficients predictive powers.

Creating the random manoeuvres required some consideration. The first idea of using a random number generator to produce a bounded sequence of control plane angles was rejected as these sequences could not necessarily be achieved in real conditions as the approach ignored the control plane dynamics. For example, the δR angle could change from -30° to +30° within 0.1s. This is not realistic. To overcome this shortcoming it was decided to create a model of the control plane dynamics and then specify the control plane demand. The control plane demand could then be randomly generated and passed through the control plane dynamics to produce a reasonably realistic control plane time history. Thus, to produce sensible control plane time histories $\boldsymbol{T_c}$ for a random manoeuvre required the creation of an appropriate control

plane dynamics model.

The control plane dynamics model was based on what was thought to be used in the SubHov simulation. In the setup data for the SubHov simulation it was necessary to define a *control plane constant* and a *control plane rate.* By examining the control plane outputs in detail it was thought that the *control plane rate* described the maximum slew-rate of the control plane. Also, the *control plane constant* described a time constant for an exponential rise to the demanded level. Thus, it appeared that the control plane dynamics were modelled as a rate limited first order system. This seemed a sensible approximation of the control plane dynamics. The response of the control plane to a step input is shown in Figure 70.

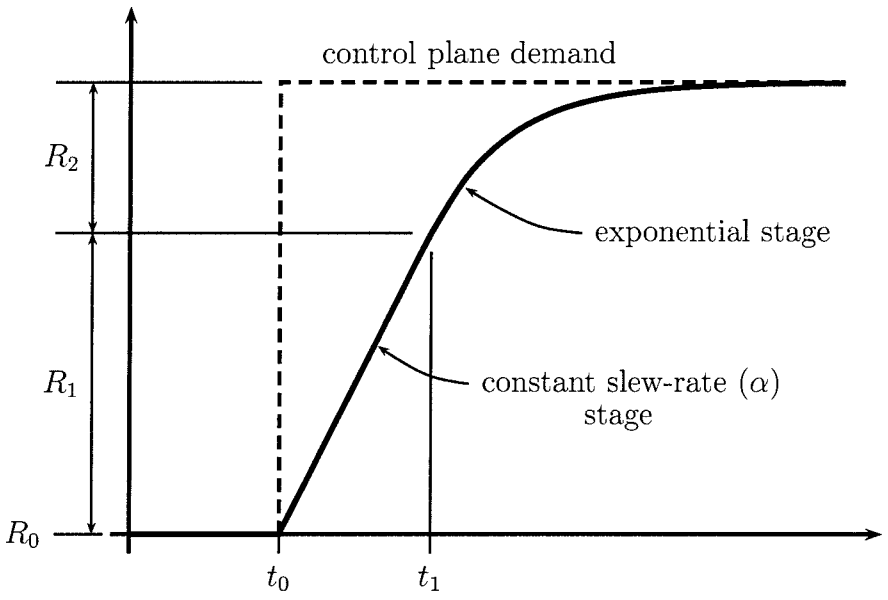

Figure 70: Description of the control plane dynamics.

As can be seen from the figure the control plane response has two parts. In the first stage, the change in control plane angle is at a constant rate, which is defined by the *control plane rate* (α), and in the second stage the change in control plane angle is governed by the first order system with a time constant (τ), the *control plane constant.* The response of the rudder (or any other control plane) can be modelled

mathematically by,

$$\delta R = \begin{cases} R_0 + \alpha(t - t_0), & t \in [t_0, t_1) \\ R_0 + R_1 + R_2(1 - \exp^{-\tau(t-t_1)}), & t \in [t_1, \infty) \end{cases}$$

To determine the model in full it is necessary to calculate the value of R_2. This is chosen so that the initial slope of exponential term is the same as α and hence $R_2 = \alpha/\tau$. If the step change in control plane demand is equal to or less than R_2, then the control plane angle is governed solely by the exponential term.

This model of the control plane dynamics was tested against the output from SubHov and showed remarkably good agreement. Hence, this control plane dynamics model was used in the generation of the random prediction manoeuvres.

Having determined a suitable control plane dynamics model it was necessary to consider how to produce the random prediction test manoeuvres. The first observation was that the bow dive plane angle δB should not be used as an input as the coefficients associated with it had not been identified. The second observation was that if the pitch angle in the model became $\pm 90°$ then the singularities in the Euler angle update ($\boldsymbol{J}_2(\boldsymbol{\eta}_2)$) would make the simulation unreliable and would invalidate the results. To prevent this from occurring the maximum angle of δS was restricted to $\pm 8°$. This value was found through trial and error testing of the three test submarines. These observations meant that the bounds for the control plane angles for the prediction test manoeuvres were set at:

$$\begin{aligned} \delta R &\in [-30°, 30°], \\ \delta B &= 0, \\ \delta S &\in [-8°, 8°]. \end{aligned}$$

Although it would be possible to set a control plane angle demand at every time step it was felt that this could produce less distinct manoeuvres as the demand could rapidly fluctuate above and below zero. This would lead, due to the slew-rate limit of the control planes, to the plane angles not deviating greatly from zero. To remove this possibility and to give the modelled UVs time to establish the new motion it was decided to generate the manoeuvres as a series of steps of random demand angles that were equally spaced and of significant duration.

Following from this, the final specification for the trial manoeuvres was that each manoeuvre would be 610s long. During the first 10s of each manoeuvre there was no control action and so δR and δS were zero. Then at 30s intervals new random control plane demand angles were set for the rudder and stern dive-planes. This led to 12 distinct step changes throughout the manoeuvre. The random demand angles were generated using a random number which produced uniformly distributed demand between the limits described for δR and δS. An example of the first 200s of a test manoeuvre showing the control plane demand and control plane angle is shown in Figure 71.

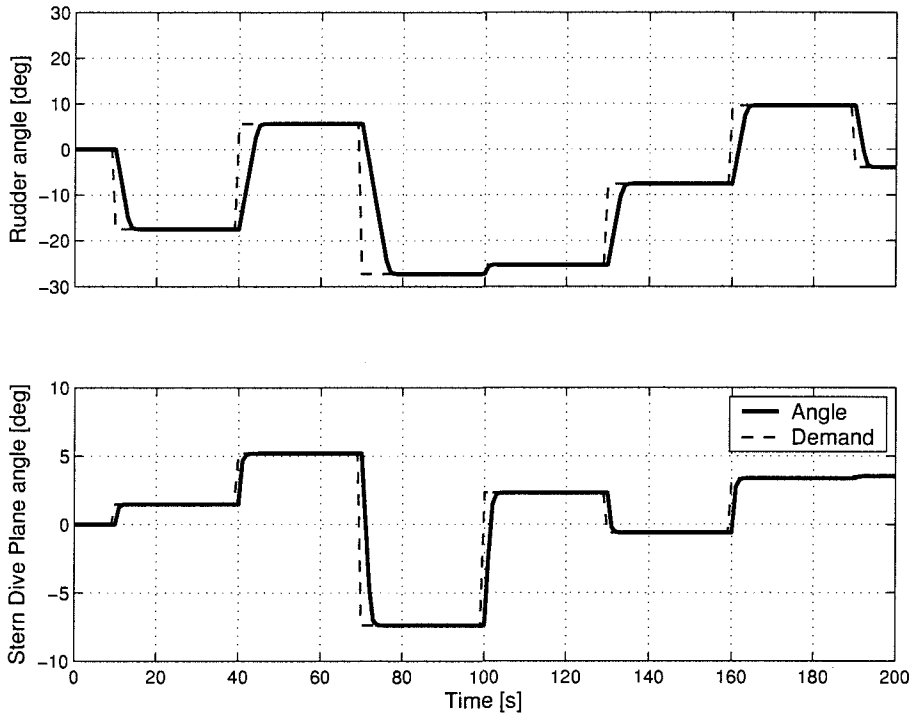

Figure 71: Example of the first 200 seconds of a random test manoeuvre.

8.3 Coefficient Manoeuvre Prediction Test Procedure

It is not possible to test the prediction capabilities of the identified coefficients for every manoeuvre, however, by using a 'suitable number' of manoeuvres some insight

into the prediction capabilities can be gained. What constitutes a 'suitable number' was not obvious. For the purposes of examining the prediction of the 50 $\hat{\boldsymbol{\xi}}^*$'s, 100 random manoeuvres (i.e. 100 random rudder and stern plane control signals) were created. A simple test of the representation of the devised manoeuvres is provided by examining the x-y space covered collectively by the generated manoeuvres.

For submarine 1 the x-y populated as a result of the 100 devised manoeuvres is presented in Figure 72. A 'reasonably' large portion of the area surrounding the manoeuvre start point is covered and consequently the 100 test manoeuvres are viewed collectively as reasonable test bed for examining the prediction accuracy of the $\hat{\boldsymbol{\xi}}^*$'s.

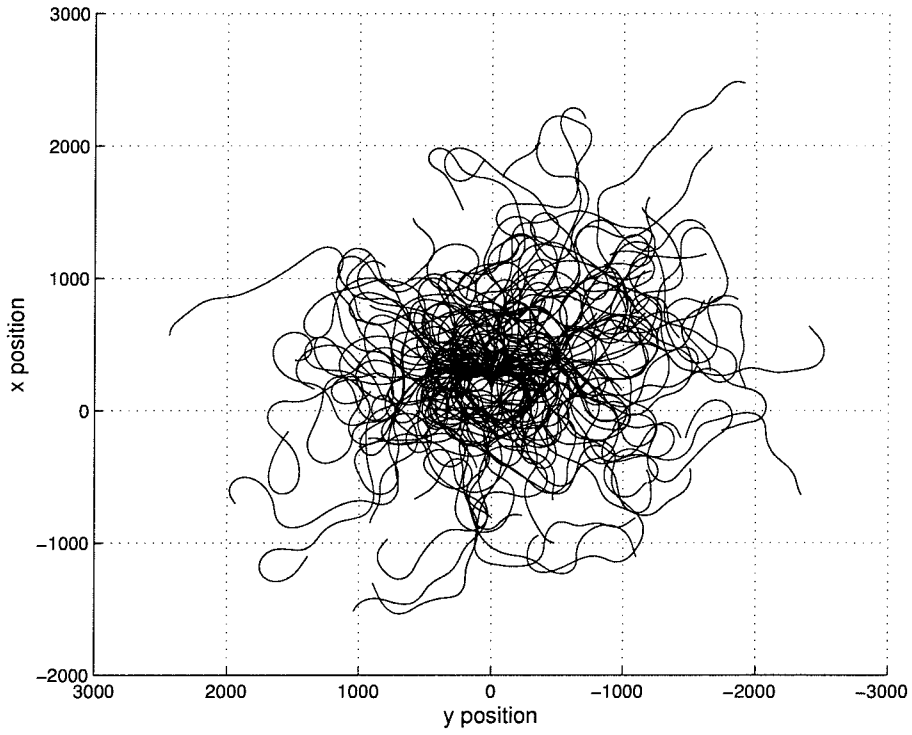

Figure 72: The prediction test manoeuvre produce by submarine 1.

The numerical investigation involves using the 50 $\hat{\boldsymbol{\xi}}^*$'s for each submarine to predict each of the 100 test manoeuvres generated. Thus, 15,000 individual comparisons were performed for the three submarines. For each comparison the cost function ε and maximum positional error was calculated for the predicted path. Although these metrics do not show how the predicted manoeuvres deviate from the correct manoeuvres they do give an estimate of the level of agreement between the two.

The results of the testing are discussed in the following sections.

8.4 Coefficient Manoeuvre Prediction Results

The first level of analysis provided the mean value of the cost function (ε) and the maximum positional error for each submarine together with the overall maximum and overall minimum values. Due to the large peaks in the calculated results the median values were also determined as the median is less affected by the extreme outliers produced by some of the converged coefficients. Table 29 presents for submarine 1 to 3 the indicated cost function and positional error statistics. The positional error statistics (in metres) are given in parentheses underneath the cost function.

	submarine 1	submarine 2	submarine 3
maximum	5.769×10^{7}	1.927×10^{7}	1.079×10^{7}
	(215.6)	(113.7)	(88.56)
mean	8.949×10^{5}	1.922×10^{5}	1.368×10^{5}
	(15.50)	(8.013)	(6.781)
median	1.929×10^{5}	5.960×10^{4}	4.452×10^{5}
	(10.30)	(5.822)	(4.961)
minimum	1.148×10^{3}	3.637×10^{2}	8.721×10^{1}
	(0.731)	(0.394)	(0.234)

Table 29: The manoeuvre prediction summary results for the identified coefficients of submarines 1–3.

The first observation from Table 29 is that the $\hat{\boldsymbol{\xi}}^{*}$ do not predict the 100 test manoeuvres as well as they reproduce the identification manoeuvre. The mean positional errors have increased from 25.4mm, 9.0mm and 19.3mm to 15.50m, 8.01m and 6.78m for submarines 1–3 respectively. Thus, in general the maximum positional error of the predictions are approximately 500 – 1000 times worse than that of the identification manoeuvre. However, the accuracy of the identification manoeuvre was exceptionally high. On the other hand one might consider a predicted positional error of 15m for a manoeuvre exceeding 3.5km in length to be still very good.

The second observation is that the different submarines produce different levels of accuracy in the predictions. Table 29 shows that the $\hat{\boldsymbol{\xi}}^*$'s of submarine 1's lead to substantially worse predictions than those of submarines 2 & 3. The reason for this difference in accuracy is not clear.

The summary results show that there is a considerable spread in the data. To gain a more complete understanding of the generated results the maximum positional error and cost function data are presented as an error surfaces. Displaying the data in this fashion allows comparison between the predictions produced by the different $\hat{\boldsymbol{\xi}}^*$'s for the ensemble of generated manoeuvres.

The positional errors produced by the $\hat{\boldsymbol{\xi}}^*$'s of submarine 1 are presented in Figures 73 & 74 with the associated cost functions (ε) shown in Figure 75.

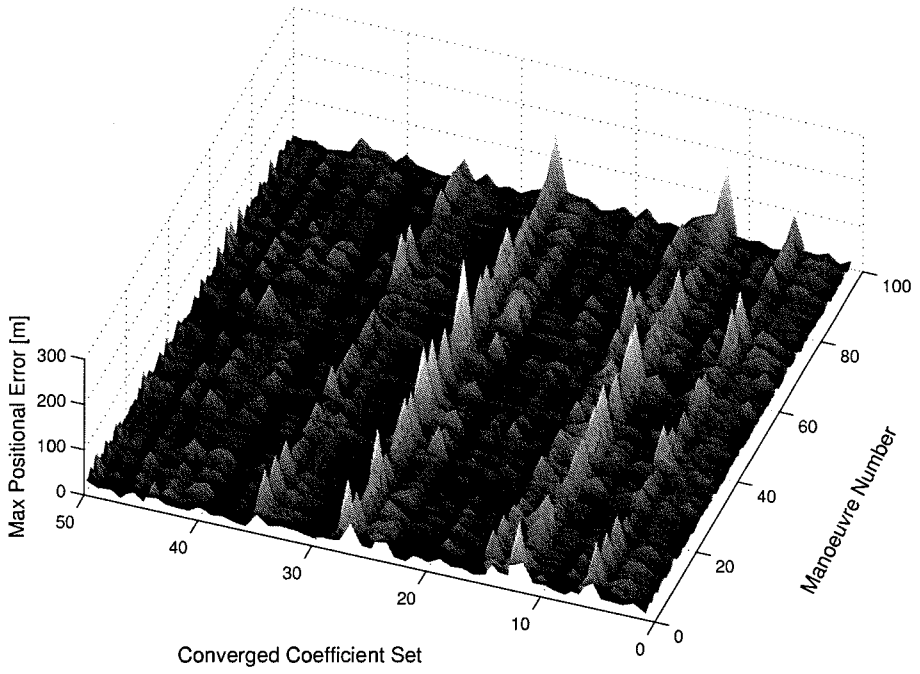

Figure 73: Surface showing the maximum positional error for submarine 1 as a function of $\hat{\boldsymbol{\xi}}^*$ and prediction manoeuvre — coefficient view.

The strong banding of the error peaks shows that some of the converged coefficient sets are poor at predicting the manoeuvres, while others are very good. To a lesser extent the surface variation also suggests that certain manoeuvres tend to be less well predicted than others. This is shown by banding when looking down the manoeuvre

axis in Figure 74.

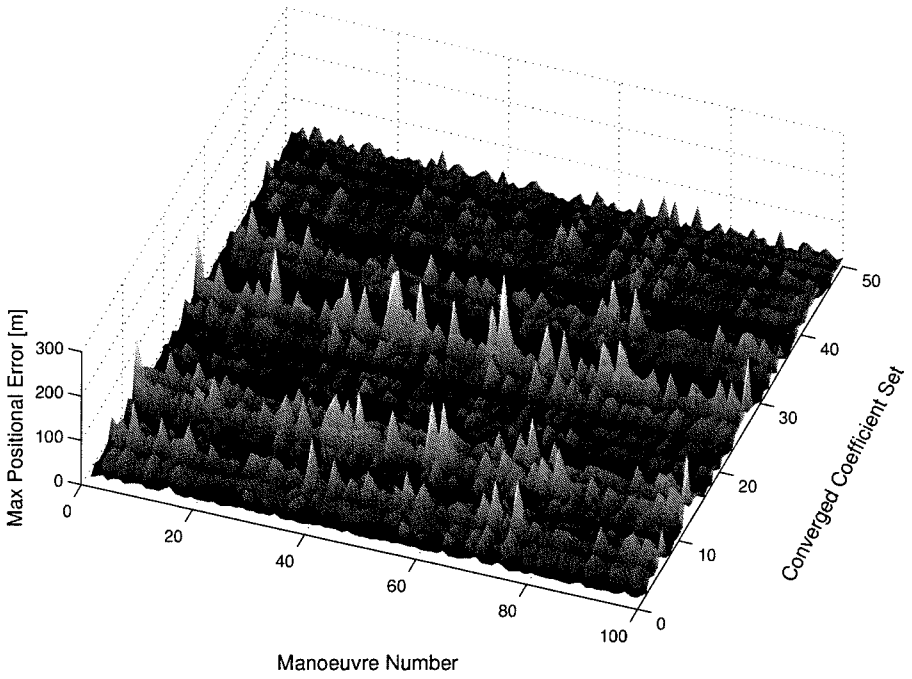

Figure 74: Surface showing the maximum positional error for submarine 1 as a function of $\hat{\boldsymbol{\xi}}^*$ and prediction manoeuvre — manoeuvre view.

In comparison to the positional error the cost function plot of Figure 75 shows a more extreme differences between the predicted manoeuvres. It also shows that the coefficient set has a far larger effect on the prediction performance than the manoeuvre used, as illustrated by the disappearance of the banding relative to the manoeuvre axis.

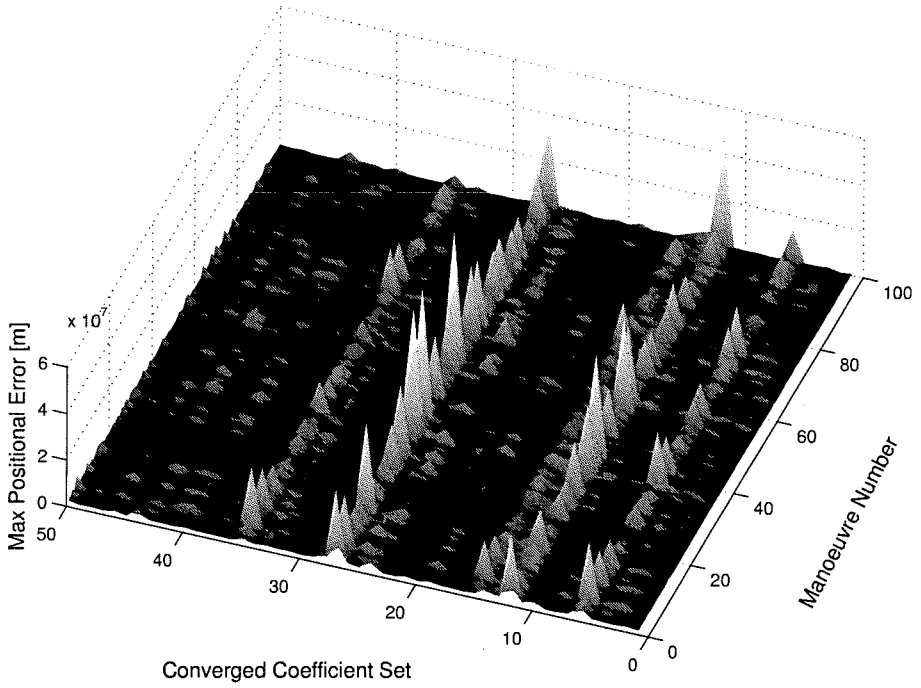

Figure 75: Surface showing the cost functions for submarine 1 as a function of $\hat{\boldsymbol{\xi}}^*$ and prediction manoeuvre — coefficient view.

The corresponding surfaces plots associated with submarines 2 & 3 are provided in Appendix F. Figures 116 and 117 for submarine 3 show more developed banding, that is dependent upon the $\hat{\boldsymbol{\xi}}^*$ and the manoeuvre undertaken.

The surface plots for the submarines give a general view of how the prediction accuracy is affected by the coefficient set and manoeuvre combinations.

The surface plot presented suggest that certain manoeuvres are difficult to predict using the $\hat{\boldsymbol{\xi}}^*$'s. If for each $\hat{\boldsymbol{\xi}}^*$ the variation of the selected statistic (ε or positional error) with manoeuvre number were scaled by the maximum observed error in the particular cut(realization), for each coefficient set in turn, one might expect if some manoeuvre was always poorly predicted irrespective of selected coefficient set. Without necessarily undertaking explicitly the suggested normalization the next section considers this idea in a little more depth.

8.4.1 The Effect of the Manoeuvre on the Prediction Performance

The accuracy with which each test manoeuvre was predicted by all the identified coefficients was investigated. This was done to assess whether all the $\hat{\boldsymbol{\xi}}^*$ badly predicted certain manoeuvres or not. The ε, for each $\hat{\boldsymbol{\xi}}^*$ manoeuvre combination was plotted so that the results could be readily compared.

In particular, the variation of ε with manoeuvre index was produced for each $\hat{\boldsymbol{\xi}}^*$ in turn. Next, the mean value of ε for a given manoeuvre was evaluated. The original manoeuvre index was then mapped onto a sorted manoeuvre index so that the mean value of ε was a monotonically increasing function of the manoeuvre index. Thereafter the value of ε for each $\hat{\boldsymbol{\xi}}^*$ produced when predicting the test manoeuvres was plotted against the sorted manoeuvre index. The results are presented in Figure 76. Similar results were produced for submarines 2 & 3. They are provided in Appendix F.

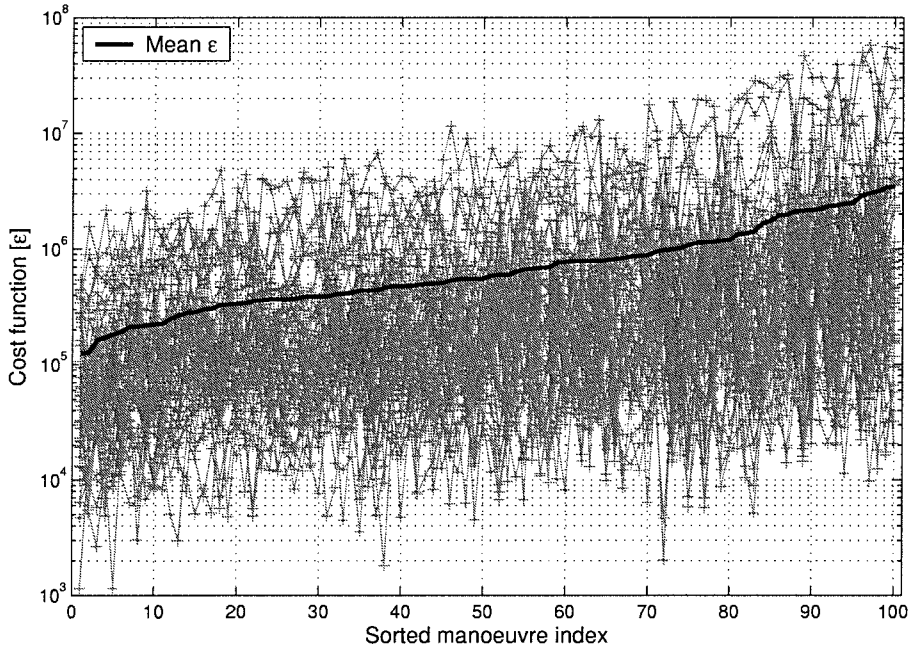

Figure 76: The predicted manoeuvre cost functions (ε's) sorted by average ε — submarine 1.

Figure 76 shows that the manoeuvre does affect the mean ε value produced, but the variation in $bar\varepsilon$ is not large compared to the variability produced by variations of

ε for an individual $\hat{\boldsymbol{\xi}}^*$. The trend in the *bar*ε is not matched by the spikiness of ε variations for each $\hat{\boldsymbol{\xi}}^*$.

To emphasize this differences the coefficient sets $\hat{\boldsymbol{\xi}}^*$ that exhibited the smallest and largest standard deviation of $\log(\varepsilon)$ were identified. It was important to use $\log(\varepsilon)$ as the relative variability of ε was of interest, not the absolute variability. Figures 77 & 78 respectively, illustrate the $\hat{\boldsymbol{\xi}}^*$'s with the largest five identified standard deviations and the smallest five standard deviations. These two figures confirm the earlier observation that the mean value of ε increases with sorted manoeuvres index. However the variation of ε associated with the manoeuvre is less dramatic than that associated with the individual $\hat{\boldsymbol{\xi}}^*$.

The largest five varying $\hat{\boldsymbol{\xi}}^*$s show that the variability between each manoeuvre for a $\hat{\boldsymbol{\xi}}^*$ can be as large as the difference between the maximum and minimum values of mean ε. Thus, the ε value produced by a specific $\hat{\boldsymbol{\xi}}^*$ for any one manoeuvre does not give a good guide as to how well $\hat{\boldsymbol{\xi}}^*$ will predict other manoeuvres.

The lowest five varying $\hat{\boldsymbol{\xi}}^*$s show that for certain $\hat{\boldsymbol{\xi}}^*$ there is almost no upward trend in the ε values when the manoeuvres are sorted by mean ε. Hence, for these $\hat{\boldsymbol{\xi}}^*$ coefficients there does not appear to be any correlation with the values of mean ε. The ε values appear to fluctuate randomly about a mean value.

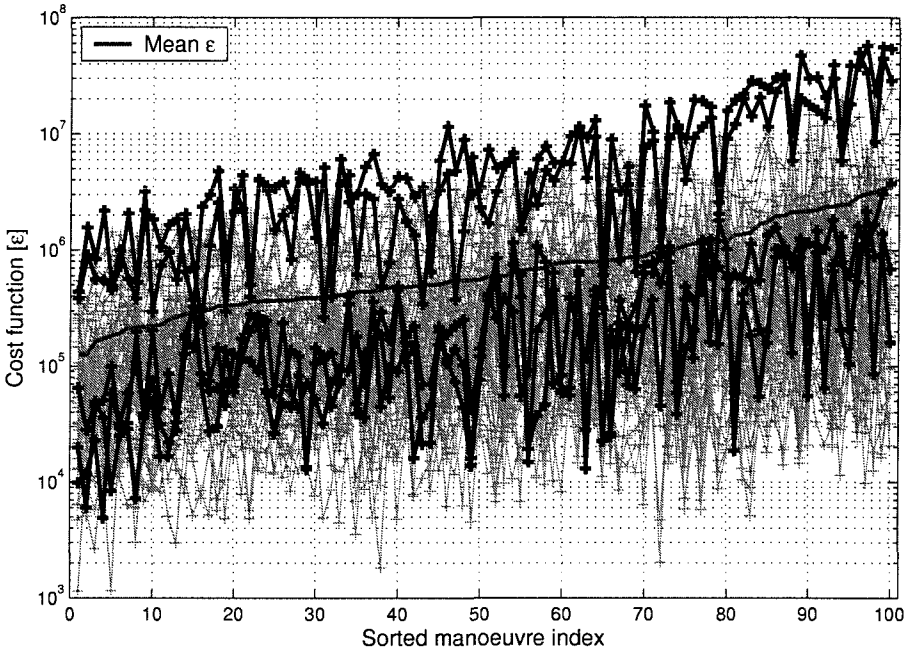

Figure 77: The predicted manoeuvre cost functions (ε's) sorted by average ε, with the five largest varying coefficient sets highlighted — submarine 1.

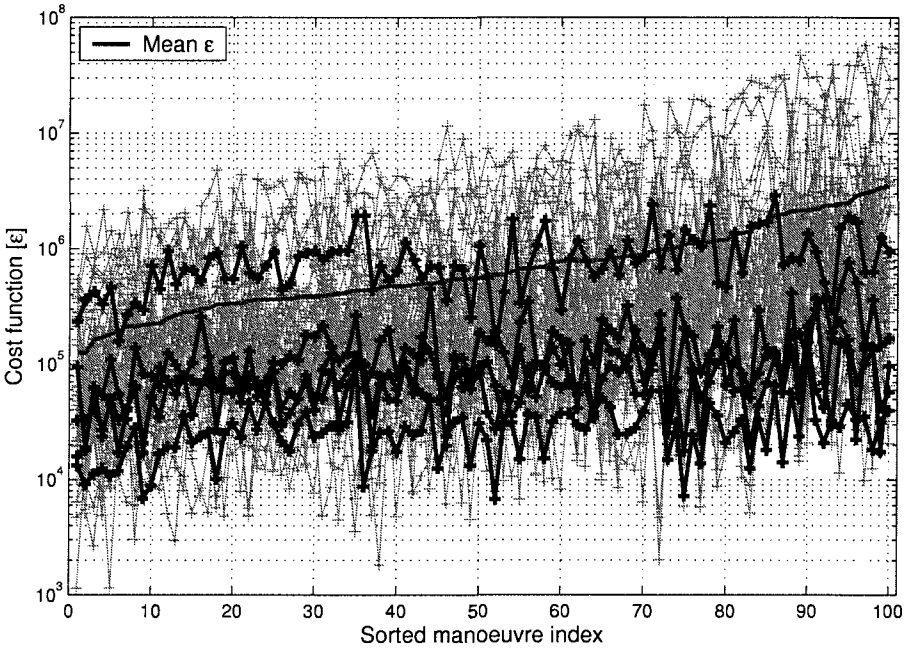

Figure 78: The predicted manoeuvre cost functions (ε's) sorted by average ε, with the five smallest varying coefficient sets highlighted — submarine 1.

The submarine 1 results presented show that although there is an ordering of manoeuvres, from easiest to most difficult to accurately predict, the cost function variation is swamped by the variability produced by the selected $\hat{\boldsymbol{\xi}}^*$. Also, some $\hat{\boldsymbol{\xi}}^*$ do not appear to follow this trend in the worse predicted manoeuvres. Thus, it would appear that identifying features of the manoeuvres that are more challenging to predict is of limited value, as these are only relevant in very broad terms and only have a relatively minor impact on the accuracy of specific $\hat{\boldsymbol{\xi}}^*$. Thus it would appear that all the hydrodynamic coefficient sets ($\hat{\boldsymbol{\xi}}^*$) are not missing a specific part of the UV dynamics but all the $\hat{\boldsymbol{\xi}}^*$ are, in their own way, failing to capturing the complete UV dynamic characteristics. These results have been demonstrated using the $\hat{\boldsymbol{\xi}}^*$ of submarine 1. Similar results are produced using submarines 2 & 3 and these results are collated in Appendix F.

8.5 Analysing the Range in Prediction Accuracy Produced by the Identified Coefficients

The results presented thus far have broadly outlined the absolute accuracy with which the $\hat{\boldsymbol{\xi}}^*$s produce the randomly generated prediction manoeuvres. However, the spread in the accuracy for a specific $\hat{\boldsymbol{\xi}}^*$ has not be analysed in detail. Also, no understanding of the how accurately the predicted manoeuvres are simulated relative to prediction accuracy produce by non-identified sets of coefficients. The presented results show that the $\hat{\boldsymbol{\xi}}^*$ predictions for the test manoeuvres have a higher cost function (ε) and positional error than that of the identified manoeuvre. A particular shortcoming with using the cost function (ε) and positional error, as metrics of manoeuvre accuracy, is that they do not compare directly between submarines and manoeuvres.

Thus, although the prediction manoeuvres are simulated less well than the identification manoeuvre the 'less well' has not been determined. To do this it is necessary to establish 'known accuracy' levels of ε to calibrate the cost function data. One lower calibration level can be produced by calculating the simulation accuracy ε values for all the prediction manoeuvres. An upper calibration level can be produced using the 'correct' hydrodynamic coefficients ($\boldsymbol{\xi}$) to with a random error of known size is added.

These corrupted $\boldsymbol{\xi}$'s can then be used to simulate the prediction manoeuvres and from these simulations cost function values and positional error values can be found. By comparing the ε's produced by the $\hat{\boldsymbol{\xi}}^*$ performing the prediction manoeuvres to the simulation accuracy ε's and the corrupted $\boldsymbol{\xi}$ ε's an appreciation of the prediction accuracy of the $\hat{\boldsymbol{\xi}}^*$'s can be gained.

To perform these comparisons it was necessary to determine the simulation accuracy ε's and the corrupted $\boldsymbol{\xi}$ ε's. This was done for submarines 1 to 3. The simulation accuracy was calculated using the method outlined in Section 5.9 with a time-step of 0.001s considered to produce the 'correct' results. The corrupted $\boldsymbol{\xi}$'s were set to the initial estimates $\hat{\boldsymbol{\xi}}^{(1)}$ of $\boldsymbol{\xi}$ used in the non-linear identification procedure. These coefficients were assigned a uniformly distributed error of up to $\pm 10\%$. However, as all the $\hat{\boldsymbol{\xi}}^*$s had identified X'_{uu} correctly it was decided to set the X'_{uu} value of the corrupted $\boldsymbol{\xi}$'s to the correct value as well. This was done so that the error in X'_{uu} of the corrupted $\boldsymbol{\xi}$'s did not bias the results, as predictions using $\hat{\boldsymbol{\xi}}^{(1)}$ could appear worse than those using $\hat{\boldsymbol{\xi}}^*$ when the difference was solely due to the error in X'_{uu}. These corrupted $\boldsymbol{\xi}$'s will be denoted by $\hat{\boldsymbol{\xi}}^c$.

Since 50 different $\hat{\boldsymbol{\xi}}^{(1)}$ were generated in Chapter 7 and each would be used as one of the corrupted $\boldsymbol{\xi}$'s then a further 5000 tests per submarine were required. The upper calibration level for each prediction manoeuvre was set as the mean value of the ε's produced by the 50 corrupted $\boldsymbol{\xi}$'s simulation that prediction manoeuvre.

Having calculated the upper and lower calibration levels for the 100 prediction manoeuvres, the distributions within given cost function bounds of the manoeuvre ε's produced by the upper lower calibration levels and three different $\hat{\boldsymbol{\xi}}^*$ were calculated. The distributions for the following five situations were considered:

- The lower calibration level (denoting the simulation accuracy) determined using $\boldsymbol{\xi}$ but measuring the difference in manoeuvre between a 0.001s and 0.1s step size.
- The prediction errors produced by $\hat{\boldsymbol{\xi}}^*_{min}$. Where the $\hat{\boldsymbol{\xi}}^*_{min}$ coefficient set gives the minimum value of $\bar{\varepsilon}$ averaged over all prediction manoeuvres.
- The prediction errors produced by $\hat{\boldsymbol{\xi}}^*_{25}$. Where the $\hat{\boldsymbol{\xi}}^*_{25}$ coefficient set is the 25^{th}

coefficient set when $\bar{\varepsilon}$ (averaged over the prediction manoeuvres) is plotted as monotonically increasing function of $\bar{\varepsilon}$ vs. $\hat{\boldsymbol{\xi}}_i^*$.

- The prediction errors produced by $\hat{\boldsymbol{\xi}}_{max}^*$. Where the $\hat{\boldsymbol{\xi}}_{max}^*$ coefficient set gives the maximum value of $\bar{\varepsilon}$ averaged over all prediction manoeuvres.
- The lower calibration level determined using $\boldsymbol{\xi}$ but measuring the difference in manoeuvre between a 0.001s and 0.1s step size.
- The upper calibration level which is defined as the $\bar{\varepsilon}$ averaged over the 50 $\hat{\boldsymbol{\xi}}^c$ coefficients used to simulate the prediction manoeuvres.

The five sets are designated 'simulation accuracy', 'best coefficient', 'middle coefficient', 'worst coefficient', 'mean 10% coefficients' in the figures presented. Figures 79–81 show the relative occurrence of cost functions within specified intervals for each of the five sets of ε's just defined, whereas and a summary of the data statistics is available in Tables 30–32.

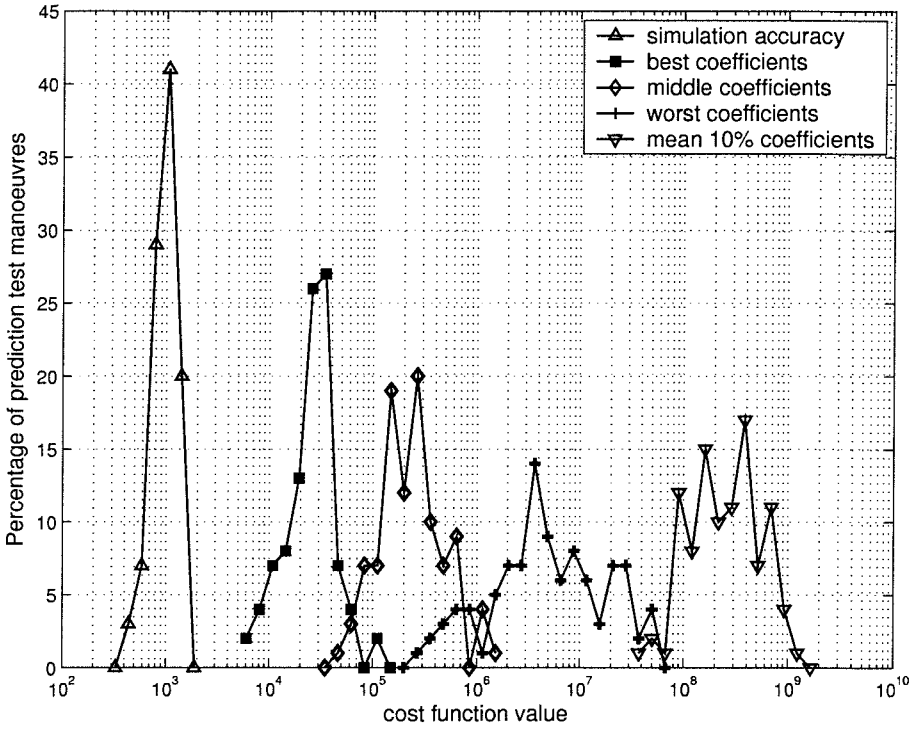

Figure 79: Cost function distribution produced using three selected converged hydrodynamic coefficient sets and the upper and lower calibration levels — submarine 1.

	maximum	mean	median	minimum
Simulation Accuracy	1.628×10^3	1.005×10^3	9.871×10^2	4.360×10^2
	(0.648)	(0.600)	(0.603)	(0.487)
Best Coefficient	1.206×10^5	2.881×10^4	2.683×10^4	6.723×10^3
	(7.207)	(3.711)	(3.718)	(1.770)
Middle Coefficient	1.366×10^6	3.145×10^5	2.444×10^5	4.444×10^4
	(40.89)	(11.90)	(9.184)	(1.914)
Worst coefficient	5.769×10^7	1.026×10^7	4.701×10^6	2.653×10^5
	(215.6)	(64.21)	(52.25)	(10.80)
10% coefficients	1.251×10^9	3.296×10^8	2.666×10^8	4.042×10^7
	(735.51)	(347.42)	(311.16)	(142.40)

Table 30: Spread of the cost function value for the converged coefficient sets — submarine 1, with the corresponding maximum positional error in metres presented within parentheses.

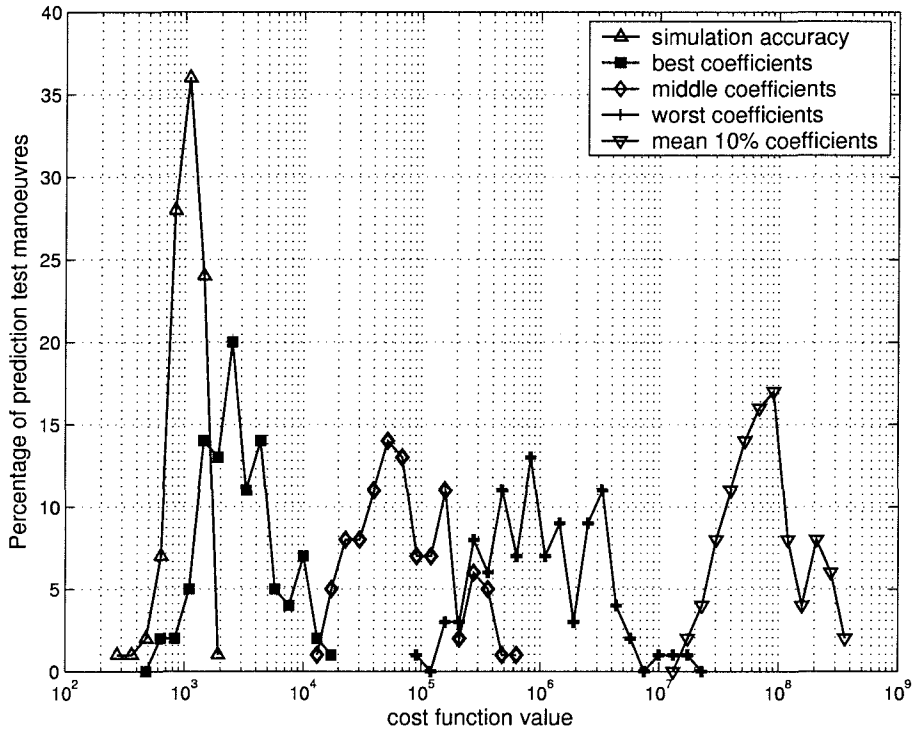

Figure 80: Cost function distribution produced using three selected converged hydrodynamic coefficient sets and the upper and lower calibration levels — submarine 2.

	maximum	mean	median	minimum
Simulation Accuracy	1.771×10^3	1.064×10^3	1.066×10^3	2.897×10^2
	(0.663)	(0.615)	(0.621)	(0.471)
Best Coefficient	1.636×10^4	3.788×10^3	2.759×10^3	5.608×10^2
	(3.093)	(1.343)	(1.192)	(0.557)
Middle Coefficient	5.938×10^5	1.082×10^5	6.696×10^4	1.519×10^4
	(22.16)	(7.091)	(5.760)	(1.303)
Worst coefficient	1.927×10^7	1.828×10^6	8.980×10^5	9.333×10^4
	(113.7)	(28.10)	(24.54)	(7.704)
10% coefficients	3.447×10^8	9.678×10^7	7.153×10^7	1.711×10^7
	(379.3)	(180.3)	(155.0)	(74.10)

Table 31: Spread of the cost function value for the converged coefficient sets — submarine 2, with the corresponding maximum positional error in metres presented within parentheses.

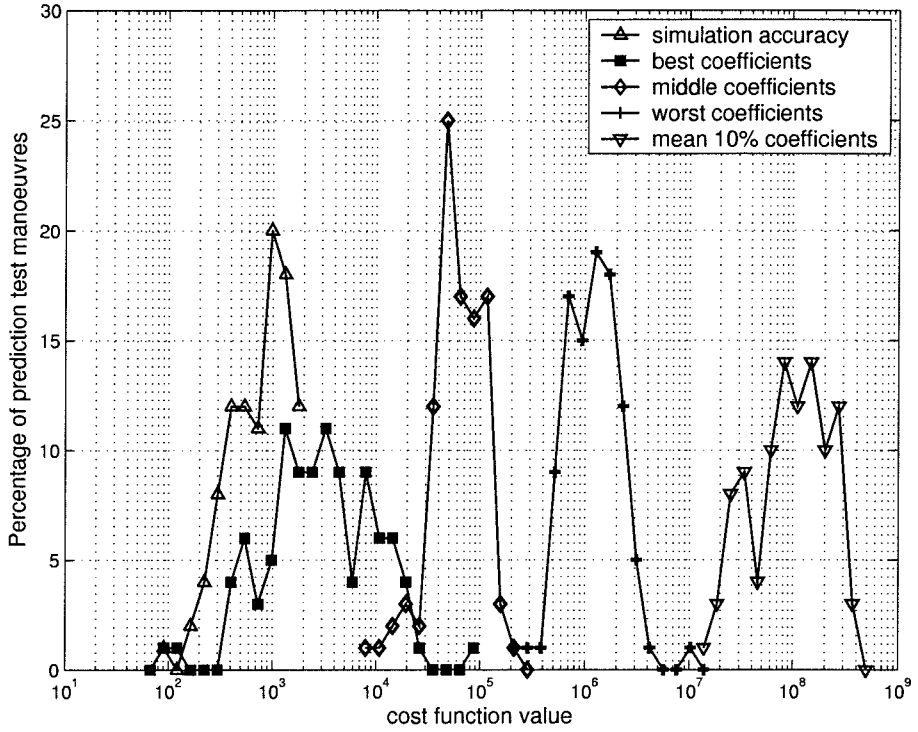

Figure 81: Cost function distribution produced using three selected converged hydrodynamic coefficient sets and the upper and lower calibration levels — submarine 3.

	maximum	mean	median	minimum
Simulation Accuracy	1.754×10^{3}	8.929×10^{2}	8.733×10^{2}	9.865×10^{1}
	(0.652)	(0.546)	(0.582)	(0.262)
Best Coefficient	7.784×10^{4}	5.683×10^{3}	2.955×10^{3}	8.721×10^{1}
	(7.110)	(1.535)	(1.222)	(0.234)
Middle Coefficient	2.203×10^{5}	7.048×10^{4}	6.066×10^{4}	8.888×10^{3}
	(23.74)	(5.941)	(4.879)	(0.686)
Worst coefficient	1.079×10^{7}	1.466×10^{6}	1.257×10^{6}	2.169×10^{5}
	(88.56)	(27.56)	(25.99)	(12.31)
10% coefficients	3.830×10^{8}	1.263×10^{8}	9.759×10^{7}	1.577×10^{7}
	(415.1)	(212.2)	(200.1)	(71.11)

Table 32: Spread of the cost function value for the converged coefficient sets — submarine 3, with the corresponding maximum positional error in metres presented within parentheses.

Considering all the results together, all submarines produce results that are very similar in nature. The simulation accuracy is about the same for all submarines, however, the results for the $\hat{\boldsymbol{\xi}}^*$ and modified $\hat{\boldsymbol{\xi}}^{(1)}$ coefficients of submarine 1 are approximately one order of magnitude higher than those of submarines 2 & 3. The cause of this is not known. The spread of the $\hat{\boldsymbol{\xi}}^*$ results for all submarines is about 2 orders for magnitude and the results overlap. The maximum positional error for the 'middle' $\hat{\boldsymbol{\xi}}^*$ for all three submarines is about 1% of the distance travelled. The results clearly show that the 'best' coefficient very accurately predicts the manoeuvres whereas the 'worst' coefficient predicts the results relatively poorly.

However, to provide some indication of the accuracy of the poorly predicted manoeuvres, the positional time history of the worst $\hat{\boldsymbol{\xi}}^*$ for submarine 1 predicting the worst manoeuvre is shown in Figure 82. Similar results for submarines 2 & 3 are given in Appendix F.

Figure 82 shows the correct path, that should be followed, and the predicted path. Clearly both tracks, although differing considerably at the end of the manoeuvre, have very similar forms. Hence, even though the difference in the tracks at the end of the manoeuvre is large the different in form is not that great. Thus, the dynamics may well be modelled accurately enough for simulation with a control system, as the controller will tend to mask the underlying dynamics of the UV and thus a reasonably realistic simulated output may be achieved.

So even though the 'worst' coefficients predicts the submarine dynamics relatively poorly they may be considered sufficiently accurate for simple simulation purposes.

8.5.1 The Converged Coefficient Results

Having established that some of the 'worst' $\hat{\boldsymbol{\xi}}^*$ coefficient predict the target manoeuvres poorly, compared to 'best' $\hat{\boldsymbol{\xi}}^*$, the possibility of a correlation between the coefficient convergence values outlined in Chapter 7 and the prediction accuracy of $\hat{\boldsymbol{\xi}}^*$ was considered. To investigate this aspect the converged values of the 'best'. 'middle' and 'worst' coefficient sets were compared. The comparison of force and moment coefficients for submarines 1–3 is given in Figures 83–88 respectively.

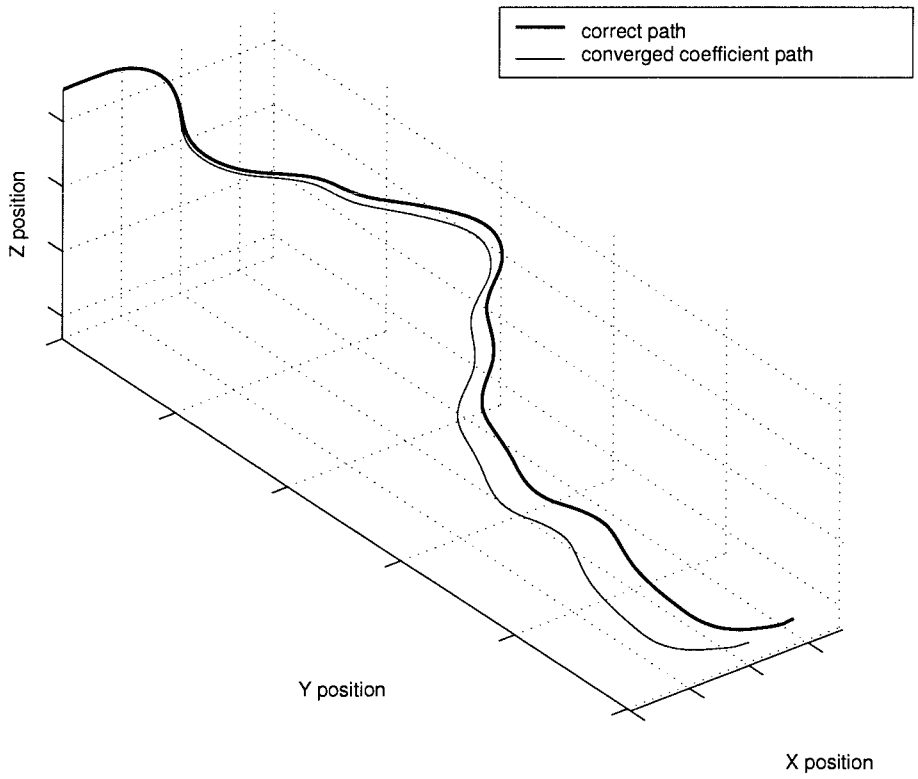

Figure 82: Positional time history of the worst coefficient set performing the worst manoeuvre — submarine 1.

Examination of Figures 83–88 suggests that prediction accuracy is correlated to the level of convergence, as the 'best' $\hat{\boldsymbol{\xi}}^*$ appears to be consistently better converged than the 'middle' and 'worst' $\hat{\boldsymbol{\xi}}^*$ coefficients irrespective of submarine. Thus, the better coefficient convergence seems to produce more accurate predictions. However, it must be remembered that the modified $\hat{\boldsymbol{\xi}}^{(1)}$ coefficients are all within $\pm 10\%$ of the correct value and they produce far worse results. Thus, the test manoeuvres must also be ill-conditioned as the 'poorly' converged 'best' $\hat{\boldsymbol{\xi}}^*$ still predicts all the manoeuvres very accurately.

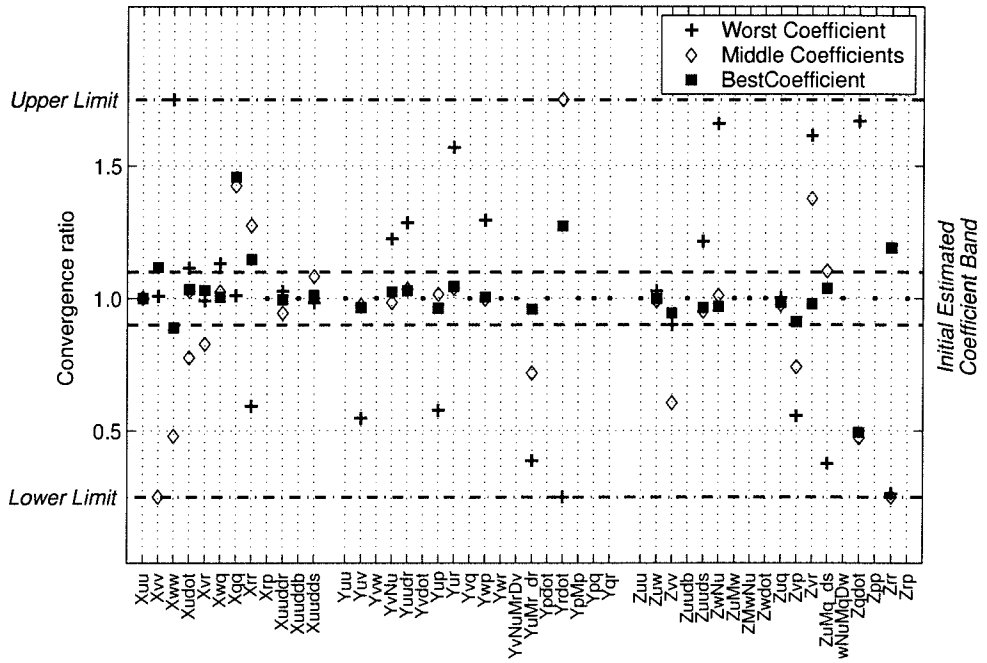

Figure 83: The best, worst and middle performing converged force coefficients — submarine 1.

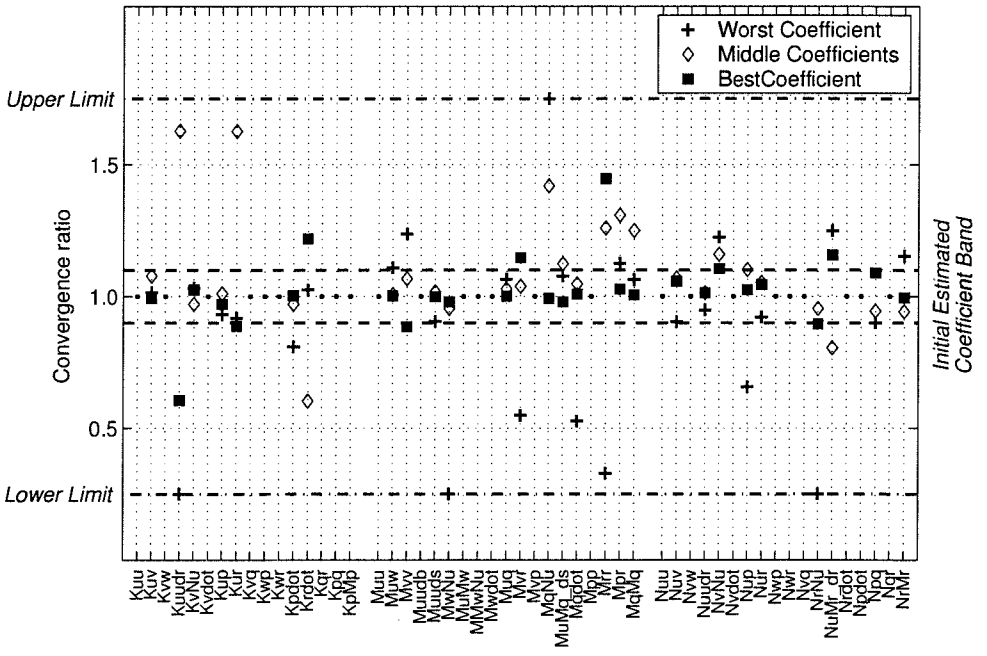

Figure 84: The best, worst and middle performing converged moment coefficients — submarine 1.

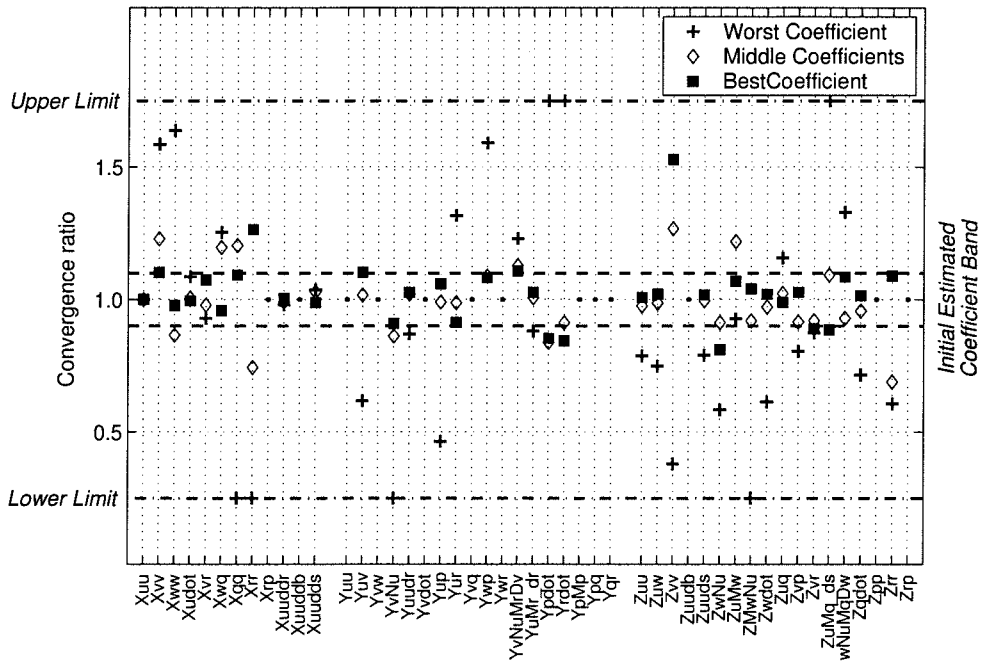

Figure 85: The best, worst and middle performing converged force coefficients — submarine 2.

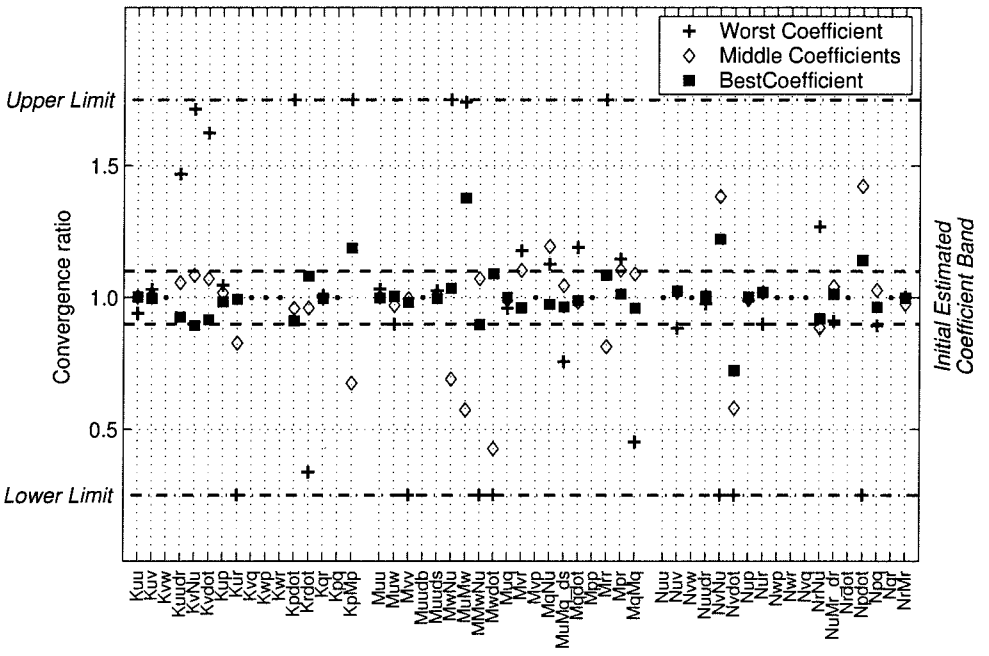

Figure 86: The best, worst and middle performing converged moment coefficients — submarine 2.

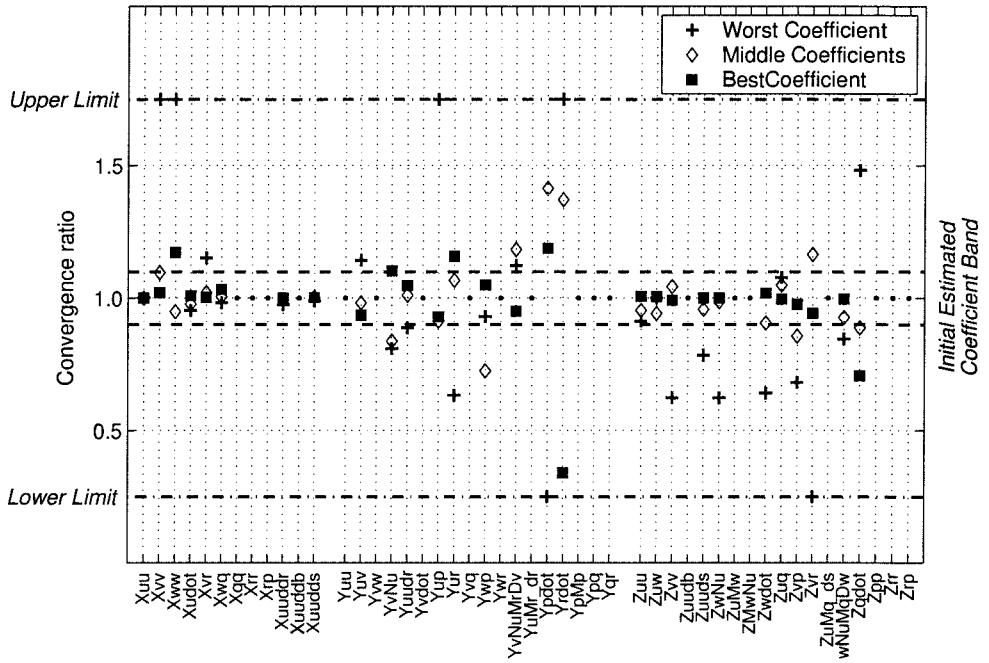

Figure 87: The best, worst and middle performing converged force coefficients — submarine 3.

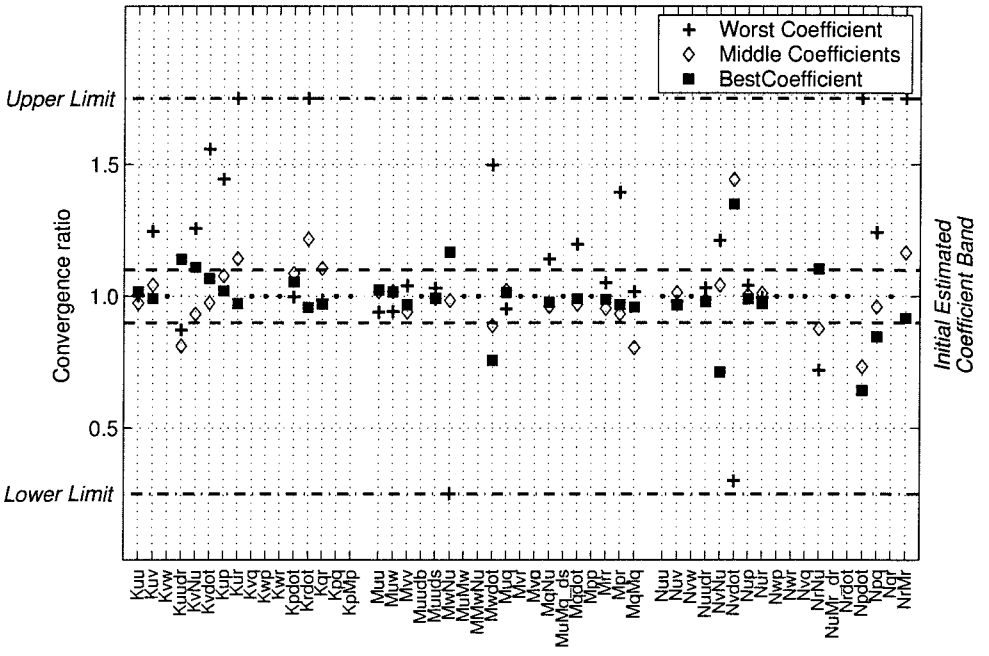

Figure 88: The best, worst and middle performing converged moment coefficients — submarine 3.

8.6 Conclusions

The prediction tests have shown that the $\hat{\boldsymbol{\xi}}^*$ coefficients for the three submarines do not simulate the prediction manoeuvres as accurately as they reproduced the identification manoeuvre. The $\hat{\boldsymbol{\xi}}^*$'s also show considerable variability in prediction accuracy. There is a slight dependence upon the prediction manoeuvre simulated, however, most of the variation comes from the $\hat{\boldsymbol{\xi}}^*$ used. This suggests that some of the identified coefficients poorly capture the UV dynamics. But as all the $\hat{\boldsymbol{\xi}}^*$ reproduced the identified manoeuvre exceptionally accurately this implies that the standard coupled manoeuvre is not ideal for identification purposes, as 'poor' coefficients can still reproduce it exceptionally well. Thus, it suggests that an improved manoeuvre is required.

Although the identified coefficients for all submarines do not reproduce the prediction manoeuvres as accurately as the identification manoeuvre their mean maximum positional error is less than $\frac{1}{3}\%$ of the mean path length of the prediction manoeuvres. However, for the 'worst' coefficient simulating the 'worst' prediction manoeuvre the error is just over 6% of the path length. This level of accuracy may well be acceptable for simulation purposes. However, it is important to remember these results only relate to the prediction manoeuvres tested. Although it is reasonable to extrapolate to all manoeuvres care must be exercised when doing so.

The prediction accuracies reported also show that the coefficient sets for each submarine that produced the minimum $\bar{\varepsilon}$ for all the prediction manoeuvres, and hence had the best prediction accuracy, had in general the best identified coefficients. However, the coefficients were only well identified in the context of the other $\hat{\boldsymbol{\xi}}^*$'s. Many coefficients within the 'best' $\hat{\boldsymbol{\xi}}^*$'s were identified with errors exceeding $\pm 10\%$.

The 'best' coefficient sets for all three submarines all had cost functions and maximum positional errors that were very small for all the prediction manoeuvres. The 'best' coefficient set for submarine 2 was the most accurate of the three while the 'best' coefficient set of submarine 1 was the least accurate. The largest maximum positional error for all the prediction manoeuvres was 3m for the 'best' coefficients of submarine 2 and 7.2m for those of submarine 1. The maximum cost functions were 1.6^4 and 1.2×10^5. Despite these very accurate manoeuvre predictions, the coefficient values

of the 'best' $\hat{\boldsymbol{\xi}}^*$ were still poorly converged.

The 'best' coefficients sets simulate the prediction manoeuvre massively better than the 10% coefficient values. However, the converged coefficient values associated with the 'best' coefficient sets do not appear to be substantially better than would be produce from a set of corrupted coefficients with randomly generated $\pm 10\%$ error. However, as the identified coefficients produce substantially better prediction accuracy it suggests that the all of the 100 prediction manoeuvres are ill-conditioned. This meaning that very small perturbations in the manoeuvre are produced by substantially different hydrodynamic coefficients. If the 100 prediction manoeuvre are ill-conditioned then they could not be used to accurate identify the 'correct' hydrodynamic coefficients.

Chapter 9

The Linear Parameter Identification Procedure

9.1 Introduction

The non-linear identification procedure has been discussed in detail in the previous chapters. As was shown in Chapter 7 the time required to identify the hydrodynamic coefficients from a selected manoeuvre was considerable. Due to the time required to perform one identification and the variable coefficient identification performance of the non-linear identification procedure the linear approach proposed in Section 4.4.1 was reconsidered. It was stated in Section 4.4.1 that determining the UV accelerations and velocities from the positional time history could be problematic when the position and attitude information was subjected to noise. As differentiating the noisy position and attitude data to get the velocity and acceleration information would introduce errors into the calculated values.

During the re-evaluation of the linear approach it was realised that the assumption that only the positional data was available for Autosub was erroneous. To understand why, one needs to consider the nature of the navigation problem for AUVs. On the surface AUVs, such as Autosub, use GPS to measure their position. However, when fully submerged it is not possible to receive the GPS signal. Thus, the position of the AUV must be determined in some alternative manner. A common AUV approach,

used in Autosub, is to use dead reckoning. Dead reckoning requires the vehicle heading and speed to calculate the position. The heading of Autosub is measured using an IXSEA PHINS Inertial Navigation System (INS). This is described in Gaiffe (2002). While the speed of Autosub related to the seabed can be measured using the RD Instruments' Workhorse Navigator fitted to the vehicle. This instrument is a combined Acoustic Doppler Current Profiler (ADCP) and Doppler Velocity Log (DVL). Combining the information from the INS and ADCP gives the vehicles current position. The INS and ADCP are described in more detail in the following sections.

9.1.1 The INS System

IXSEA's PHINS INS comprises three Fibre Optic Gyroscopes (FOG) with a known drift of less than 0.01° per hour. Each gyroscope is mounted at 90° to each other. These measure the vehicles rotation rates. It also contains three orthogonally mounted accelerometers each with a drift of less than $50\mu g$ also mounted at 90° to each other.

The system is designed to calculate the attitude and position of the vehicle as it moves through space. As an indication of the accuracy of the measurements, the system is designed to calculate North from anywhere on the planet (excluding the poles) by measuring the rotation rate of the earth (15° per hour) and the acceleration due to gravity. From these two vectors it is possible to determine the direction of North.

As mentioned the INS directly measures $\boldsymbol{\nu}_2$ and $\dot{\boldsymbol{\nu}}_1$. As the INS produces very accurate noise free measurements of $\boldsymbol{\nu}_2$, it is reasonable to assume that $\dot{\boldsymbol{\nu}}_2$ can be determined through differentiation and $\boldsymbol{\eta}_2$ can be determined through integration of $\boldsymbol{\nu}_2$.

9.1.2 The ADCP

The ADCP measures the speed at which sonar reflecting objects move past its sensor. Furthermore if the ADCP can 'see' the sea floor the it can measure the speed of the ADCP (UV) relative to the bottom. The ADCP measures velocities using sonar reflections either from particulate matter in the water or from the sea bed. Thus, the ADCP can directly measure the translation velocity $\boldsymbol{\nu}_1$ of Autosub.

The ADCP is also used to measure the speed of the water at various distances either above or below the AUV. This is to analyse the variation of water velocity within the water column. These measurements are performed by separating the water column into discrete *bins* and measuring the mean velocity in each bin. One advantage of using the ADCP to measure through water velocity, instead of bottom velocity, is that the effects of currents on the sea trial manoeuvres can be removed.

The ADCP measures the bottom velocity with a error of standard deviation between 0.3–0.6 cm/s (over the operating velocities of Autosub) and resolution of 0.1cm/s. The velocity data can be passed to PHINS and combined internally with the INS data using a Kalman filter to produce a best estimate of the vehicle speed.

9.1.3 Available Autosub State Information

By combining the information from the INS and ADCP sensors the following information is available during an Autosub manoeuver,

Data variable	Determined from
$\boldsymbol{\eta}_1$	Integration of vehicle velocities
z	Depth from the surface, measured from pressure sensor
$\boldsymbol{\eta}_2$	Integration of body rates
$\boldsymbol{\nu}_1$	Measured from ADCP combined INS $\dot{\boldsymbol{\nu}}_1$ data
$\boldsymbol{\nu}_2$	Measured from the INS
$\dot{\boldsymbol{\nu}}_1$	Measured from the INS
$\dot{\boldsymbol{\nu}}_2$	Differentiated of $\boldsymbol{\nu}_2$

Table 33: Manoeuvre data available for Autosub and its source.

This is the data that the linear identification techniques require and it is available without the need to transform and double differentiate the manoeuvre position and attitude time histories.

9.1.4 Applications of INS and ADCP Data

The foregoing observations have shown that the linear approach could be used with the INS and ADCP data recorded by Autosub while manoeuvring rather than through numerical differentiation of noisy positional data as described in Chapter 4. This chapter describes the testing and evaluation of two methods to solve the linear equations. The first considered how the equations can be rearranged into a linear programming (LP) formulation and solved using LP techniques. The second uses linear algebra techniques to find a solution to the over-determined set of linear equations.

The effect of noise on the 'measured' data is then considered to analyse the sensitivity of the hydrodynamic coefficients predictions to measurement errors.

9.2 Linear Form of the Booth et al. Equations

As outlined in Section 4.4.1 the forces and moments in the Booth et al. (1980) submarine equations can be written in a linear form. For example, the X force equation can be expressed in the form

$$\boldsymbol{A}_X \boldsymbol{\xi}_X = \boldsymbol{b}_X. \tag{31}$$

Assuming the following notation:

$\boldsymbol{A}_X$ — The matrix of X force coefficient multiplier.

$\boldsymbol{\xi}_X$ — The X force hydrodynamic coefficients.

$\boldsymbol{b}_X$ — The column vector of 'constant' terms.

Similar equations can be produced for the Y & Z force and the K, M & N moment equations.

Assuming that as a submarine performs a manoeuvre the velocity ($\boldsymbol{\nu}$), acceleration ($\dot{\boldsymbol{\nu}}$) and attitude ($\boldsymbol{\eta}_2$) information is known and recorded at m discrete points in time, then m linear equations can be produced. Each row of $\boldsymbol{A}_X$ and $\boldsymbol{b}_X$ corresponds to a discrete point in time, whereas the column vector $\boldsymbol{\xi}_X$ is of a fixed length and contains the hydrodynamic coefficients. The m linear equations can then be solved. The first

approach to solving the equations, based on linear programming (LP) techniques is discussed next.

9.3 Solving the Linear System Using Linear Programming Techniques

Linear programming is used to find the set of coefficients in a linear expression that minimizes a function subject to a set of linear constraints. It is the simplest form of constrained optimization and has been extensively studied. For more information consult Fletcher (1987). The advantage of the LP approach over the non-linear approach is that there is no need to produce a starting estimate of $\hat{\boldsymbol{\xi}}$. Hence, a manoeuvre can be investigated by identifying the hydrodynamic coefficients once. There is no requirement to repeat the process for many different starting values of $\hat{\boldsymbol{\xi}}$ to build up an appreciation of the suitability of the manoeuvre.

It is also possible to build linear constraints into the LP system of equations so that extra information regarding the coefficients can be used in the identification procedure.

A linear programming problems can be written in the general form,

$$\begin{aligned} &\min_{\boldsymbol{x}} \boldsymbol{f}\boldsymbol{x} \\ \text{subject to:} \quad &\boldsymbol{A}\boldsymbol{x} \leq \boldsymbol{b} \\ &\boldsymbol{A}_{eq}\boldsymbol{x} = \boldsymbol{b}_{eq}, \end{aligned} \tag{32}$$

where $\boldsymbol{f}$ is a row vector premultiplying the unknown column vector $\boldsymbol{x}$. Here, $\boldsymbol{f}\boldsymbol{x}$ represents the function to minimize, $\boldsymbol{A}$ and $\boldsymbol{b}$ represent the inequality constraints and $\boldsymbol{A}_{eq}$ and $\boldsymbol{b}_{eq}$ represent the equality constraints.

Reverting to the linear system for the X-force equation, namely

$$\boldsymbol{A}_X\boldsymbol{\xi}_X = \boldsymbol{b}_X,$$

it appears that this linear algebraic problem ought to be capable of being recast in terms of the general LP problem previously described. One might describe that task

as seeking to find the hydrodynamic coefficient vector $\hat{\boldsymbol{\xi}}_X$ that minimizes the vector $\boldsymbol{c}$ defined as

$$\boldsymbol{c} = \left| \boldsymbol{b}_X - \boldsymbol{A}_X \hat{\boldsymbol{\xi}}_X \right| . \tag{33}$$

Unfortunately, it is not possible to implement this problem formulation directly within the linear programming framework for two reasons. First Equation (33) does not return a scalar value ($\boldsymbol{c}$ is a vector). Second the modulus sign in Equation (33) makes the system non-linear. However, through some subtle manipulation it is possible to recast Equation (33) into a system that can be minimized using Linear Programming.

First the modulus sign in Equation (33) is removed to give,

$$\boldsymbol{c} = \boldsymbol{b}_X - \boldsymbol{A}_X \hat{\boldsymbol{\xi}}_X . \tag{34}$$

The infinity norm of $\boldsymbol{c}$, denoted by $||\boldsymbol{c}||_\infty$, represents the largest absolute value of the elements of $\boldsymbol{c}$. This represents the maximum error produced by the hydrodynamic coefficient estimate $\hat{\boldsymbol{\xi}}_X$. Reducing $||\boldsymbol{c}||_\infty$ is therefore the goal of the minimization process. We shall let $\varepsilon_{lp} = ||\boldsymbol{c}||_\infty$.

We note that each of the m linear equation contained within Equation (34) can be written as

$$\boldsymbol{c}_j = \boldsymbol{b}_{Xj} - \sum_{i=1}^{m} \boldsymbol{A}_{Xj,i} \hat{\boldsymbol{\xi}}_{X_i} \boldsymbol{b}_{Xj} \quad : j = 1, 2, ..., m.$$

As ε_{lp} represents the largest absolute error, in anyone of the m linear equations in Equation (34), then for every equation j the error $\varepsilon_{lp} \geq |\boldsymbol{c}_j|$ or

$$\varepsilon_{lp} \geq \boldsymbol{c}_j \qquad \Rightarrow \qquad -\sum_i \boldsymbol{A}_{Xj,i} \hat{\boldsymbol{\xi}}_{X_i} - \varepsilon_{lp} \leq -\boldsymbol{b}_{Xj}$$

and

$$\varepsilon_{lp} \geq -\boldsymbol{c}_j \qquad \Rightarrow \qquad \sum_i \boldsymbol{A}_{Xj,i} \hat{\boldsymbol{\xi}}_{X_i} - \varepsilon_{lp} \leq .$$

We therefore want to minimize ε_{lp} subject to the constraints just derived. To specify this problem in the linear programming form described in Equation (32) it is necessary to define $\boldsymbol{fx}$ according to

$$\boldsymbol{fx} = \varepsilon_{lp},$$

with

$$\boldsymbol{f} = \begin{bmatrix} 0 & 0 & \dots & 0 & 1 \end{bmatrix}$$

and

$$\boldsymbol{x} = \begin{bmatrix} \hat{\boldsymbol{\xi}}_X^T & \varepsilon_{lp} \end{bmatrix}^T.$$

Next defining enlarged $\boldsymbol{A}_X$ and $\boldsymbol{b}_X$ as

$$\boldsymbol{A}_X^* = \begin{bmatrix} -A_{1,1} & -A_{1,2} & \dots & -A_{1,n} & -1 \\ -A_{2,1} & -A_{2,2} & \dots & -A_{2,n} & -1 \\ \vdots & \vdots & \ddots & \vdots & \vdots \\ -A_{m,1} & -A_{m,2} & \dots & -A_{m,n} & -1 \\ A_{1,1} & A_{1,2} & \dots & A_{1,n} & -1 \\ A_{2,1} & A_{2,2} & \dots & A_{2,n} & -1 \\ \vdots & \vdots & \ddots & \vdots & \vdots \\ A_{m,1} & A_{m,2} & \dots & A_{m,n} & -1 \end{bmatrix} \quad \text{and} \quad \boldsymbol{b}^* = \begin{bmatrix} -b_1 \\ -b_2 \\ \vdots \\ -b_m \\ b_1 \\ b_2 \\ \vdots \\ b_m \end{bmatrix}$$

the linear programming minimization problem can be described as

$$\min_{\boldsymbol{x}} \boldsymbol{f}\boldsymbol{x} \qquad \text{subject to: } \boldsymbol{A}_X^*\boldsymbol{x} \leq \boldsymbol{b}^*.$$

This equation represents the identification of the X force coefficients using linear programming techniques. A similar procedure is used to describe the Y & Z force coefficients and the K, M & N moment coefficients. Therefore 6 different identification sub-problems need to be solved to determine the $\hat{\boldsymbol{\xi}}$ vector.

As linear programming is an extremely common technique there is a large resource of computer code to solve LP problems. In this thesis the Matlab `linprog` routine was used. More information about the routine can be found in MathWorks (2002b).

9.3.1 Testing the Linear Programming Approach

Having identified an appropriate linear programming minimization problem that would identify the unknown hydrodynamic coefficients, the three different submarines

are investigated using data associated with the three standard test manoeuvres (horizontal, vertical and coupled) defined in Chapter 4. However, as already noted in Chapter 6 the hydrodynamic coefficients are not unique as the rank of the associated $\boldsymbol{A}$ matrices are less than the number of unknown hydrodynamic coefficients. Hence, to ensure the LP procedure does not fail too it was necessary to specify certain coefficients to make the remaining coefficients unique. Thus for the horizontal manoeuvre, $\hat{\boldsymbol{\xi}}_Y$ is reduced by one through the specification of $Y'_{\dot{v}}$ and for $\hat{\boldsymbol{\xi}}_N$ the coefficients $N'_{\dot{v}}$ and $N'_{\dot{r}}$ are both specified. For the vertical manoeuvre different submarines require different levels of reduction as reported in Chapter 6. To clarify which coefficients were specified in the testing all the converged coefficient plots presented in this chapter identify the specified coefficients with a vertical grey line.

The first stage of the testing involved specifying the $\boldsymbol{A}^*$ matrices and $\boldsymbol{b}^*$, $\boldsymbol{f}$ and $\boldsymbol{x}$ vectors associated with each manoeuvre and submarine combination. Once this had been done the hydrodynamic coefficient were identified. The time required to determine the coefficient was noted along with the accuracy with which the coefficients converged to the correct value. The predictions generated by the three submarines using the three standard manoeuvres are presented next.

9.3.2 Results of the Linear Programming Investigation

The accuracy of the identified coefficients are presented in Figures 89 to 92. All the coefficients converge exceptionally well, in some ways this came as a surprise given the convergence performance of the non-linear procedure. However, as the problem has been written as a massively over-determined set of linear equations, and formulated so we know it has a solution, perhaps the quality of the results should have been expected. As all the coefficients converged very accurately, the results are presented differently to those of the non-linear identification process. Instead of presenting the *converged ratio* $(\hat{\boldsymbol{\xi}}_i/\boldsymbol{\xi}_i)$ directly the modulus of the convergence ratio minus one is presented. This was necessary as the first 6 significant digits of each coefficient value was correct. Hence plotting the convergence ratio did not indicate the error associated with the coefficients.

The Linear Programming Results — Horizontal Manoeuvre

Figure 89 gives the convergence results for the horizontal manoeuvre. The convergence results for all three tests submarines are shown on the plot. As the convergence ratio gives a relative accuracy it becomes undefined when the correct coefficient value is zero. Therefore, the accuracy with which the zero valued coefficients were identified cannot be displayed in Figure 89. However, the maximum absolute error for all the submarines coefficients used in performing the horizontal manoeuvre was 1.014×10^{-11}. This is 5 orders of magnitude smaller than the smallest coefficient value.

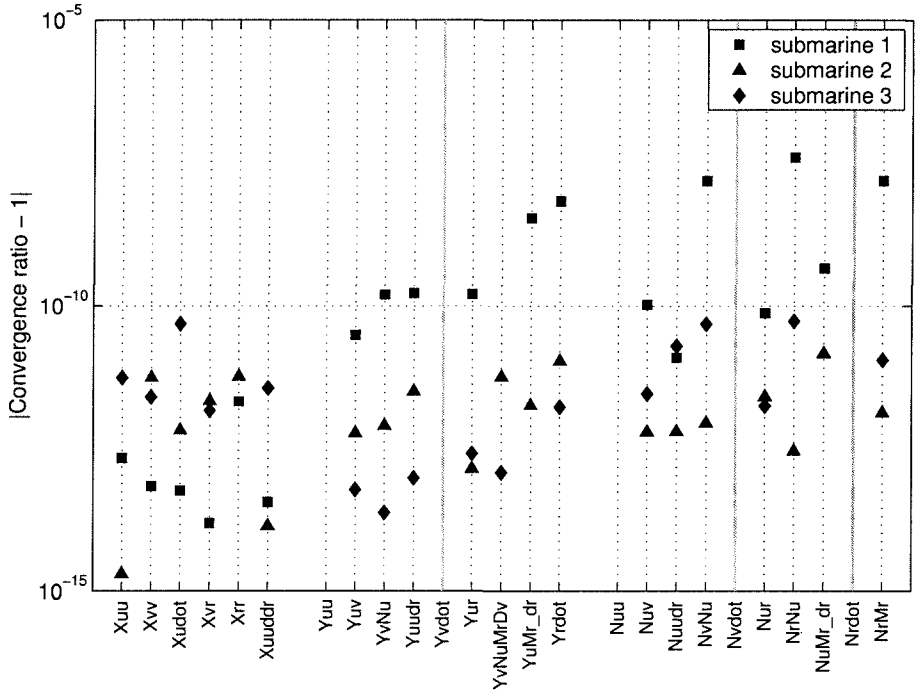

Figure 89: Coefficient convergence results produced using the linear programming procedure — horizontal manoeuvre.

The times taken to identified the X, Y and N coefficients in each linear sub-problem for the three submarines are presented in Table 34. The times show that the LP procedure is significantly quicker than the non-linear procedure, as one would expect. However, there were clearly difficulties in identifying the N coefficients for submarine 1 and 3. This is demonstrated by the long search time required to identify the coefficient values.

	submarine 1	submarine 2	submarine 3
X coefficients	8.36	9.78	8.23
Y coefficients	12.30	14.87	12.26
N coefficients	98.69	16.34	95.56

Table 34: Time in seconds to solve for the different coefficient sets using linear programming techniques — horizontal manoeuvre.

The Linear Programming Results — Vertical Manoeuvre

The converged coefficients produced using the vertical manoeuvre are given in Figure 90. This figure shows similar convergence performance to the horizontal manoeuvre. However, the most striking feature is the consistent, and relatively poor, convergence values for the Z coefficients of submarines 2 and 3. The non-linear results also showed poor convergence as illustrated in Figures 43 & 44 of Section 7.6.2. It was postulated that there was a strong, unidentified coupling between some of the Z coefficient used in the vertical manoeuvre. The results of Figure 90 add weight to this argument. As with the horizontal manoeuvre the accuracy with which the identified coefficient converged to the zero valued coefficients could not be displayed in Figure 90. However the largest absolute error on any of the identified 'zero' coefficient is 1.136×10^{-9}, this is 3 orders of magnitude smaller than the smallest coefficient value.

Note also that submarines 2 & 3 did not have coefficients $Z'_{\dot{w}}$ or $M'_{\dot{w}}$ specified, as illustrated by converged values on these 'specified' coefficients. The $Z'_{\dot{w}}$ and $M'_{\dot{w}}$ coefficients were specified fore submarine 1 and are thus marked as such.

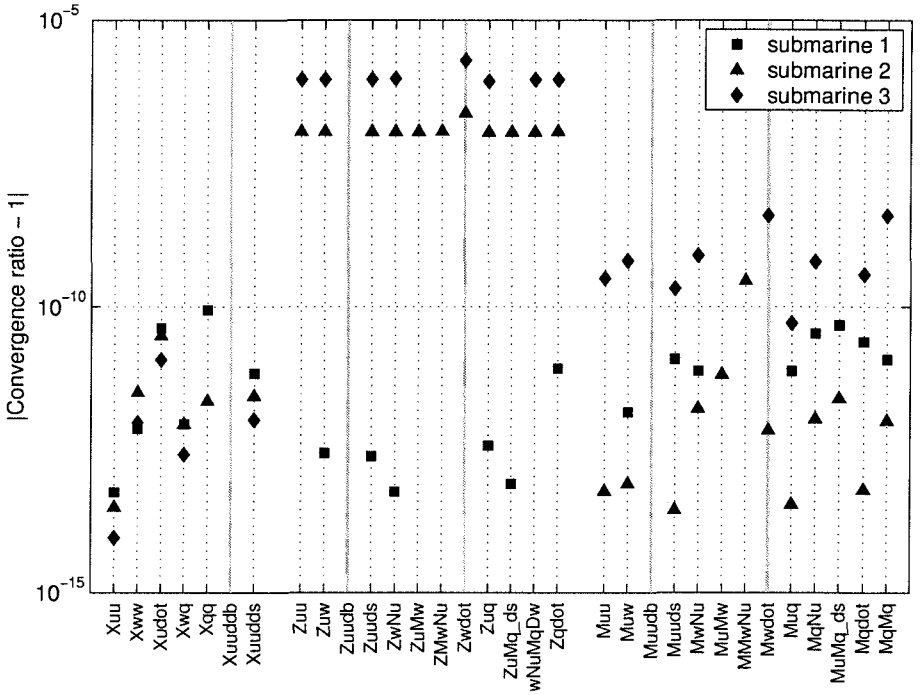

Figure 90: Coefficient convergence results produced using the linear programming procedure — vertical manoeuvre.

The time taken to identify the coefficients in the different coefficient sub-problems of the vertical manoeuvre are shown in Table 35. This table shows that the vertical coefficients are identified considerably faster using the LP method than the non-linear procedure. Also, the increase in the number of coefficients to identify has had no apparent effect upon the convergence time, if anything one could make the erroneous conclusion from the data that increasing the number of coefficients reduces the identification time.

	submarine 1	submarine 2	submarine 3
X coefficients	4.69	4.42	4.45
Z coefficients	7.80	10.41	30.52
M coefficients	11.57	13.96	26.60

Table 35: Time in seconds to solve for the different coefficient sets using linear programming techniques — vertical manoeuvre.

The Linear Programming Results — Coupled Manoeuvre

The accuracy with which the hydrodynamic coefficient converge using the coupled manoeuvre is given in Figures 91 & 92. These figure show a similar level of accuracy to the horizontal and vertical manoeuvres with the largest absolute error on the identified zero valued coefficients was 2.280×10^{-9}. Again this is three orders of magnitude smaller than the smallest non-zero coefficient value.

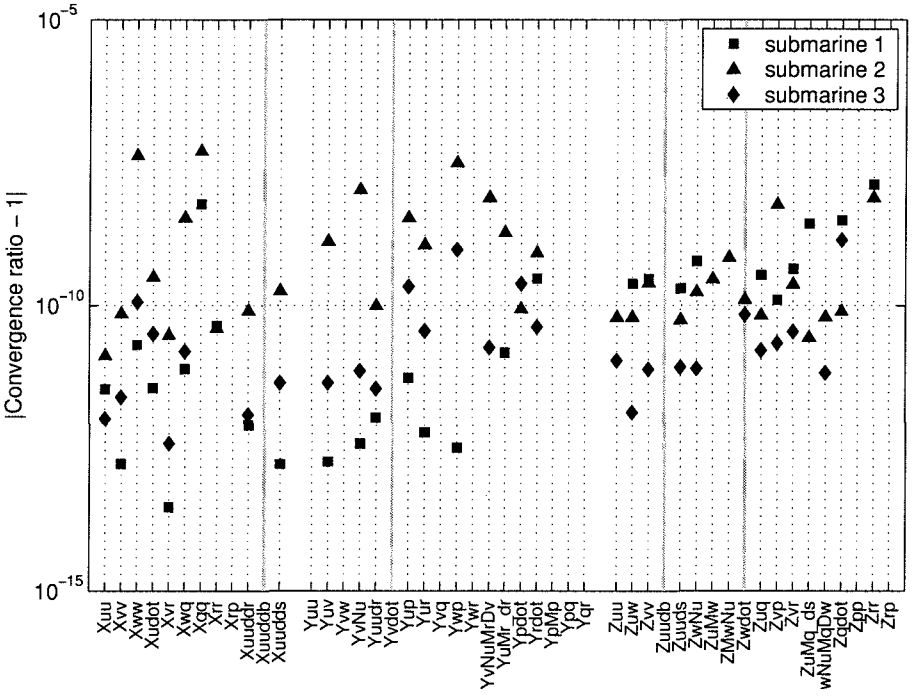

Figure 91: Force coefficient convergence results produced using the linear programming procedure — coupled manoeuvre.

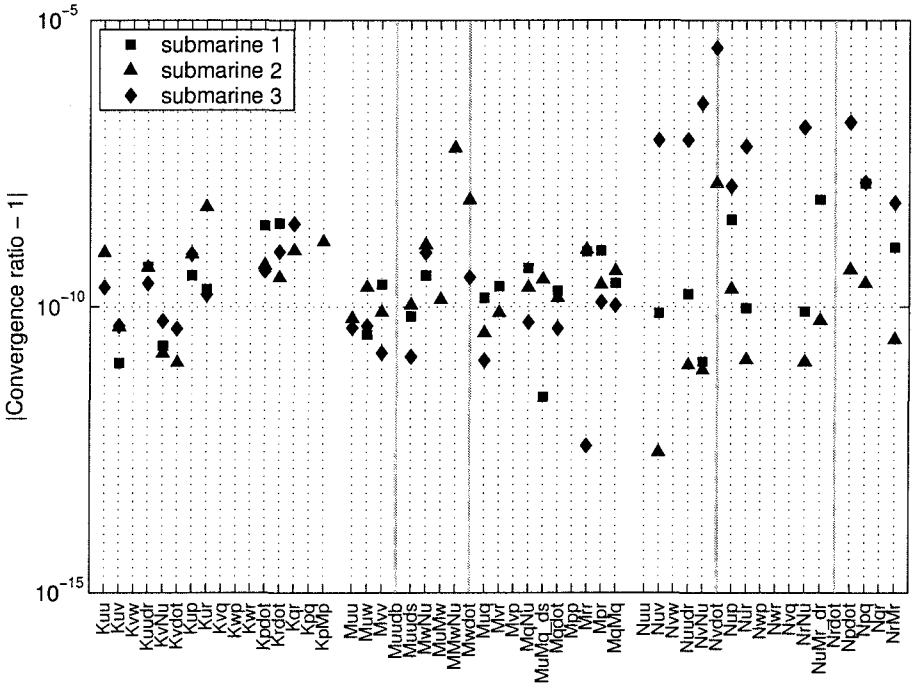

Figure 92: Moment coefficient convergence results produced using the linear programming procedure — coupled manoeuvre.

The time to identify the various coefficient sub-problems using the coupled manoeuvre are given in Table 36. These times show an increase compared to the vertical and horizontal manoeuvres, but the convergence is still, in general, three of four times quicker than the non-linear procedure. The table shows that there were some difficulties in identifying the N coefficients of submarine 3. The cause of this problem was not immediately identifiable.

	submarine 1	submarine 2	submarine 3
X coefficients	15.61	18.22	16.48
Y coefficients	35.94	34.49	33.06
Z coefficients	30.68	47.84	42.76
K coefficients	33.52	33.76	40.62
M coefficients	37.63	42.80	43.45
N coefficients	34.77	54.57	284.91

Table 36: Time in seconds to solve for the different coefficient sets using linear programming techniques — coupled manoeuvre.

The results from all three linear programming tests have shown that the identified hydrodynamic coefficients vector $\hat{\boldsymbol{\xi}}$ has converged accurately to the correct hydrodynamic coefficient $\boldsymbol{\xi}$. This identification process is 3 or 4 times faster than the non-linear identification process and does not require an initial starting estimate of $\hat{\boldsymbol{\xi}}$. It has correctly identified all the coefficients barring the specified added-mass coefficients. Therefore the linear programming method used can be considered better than the non-linear approach.

The performance of the alternative linear algebra based approach of estimating $\hat{\boldsymbol{\xi}}$ is considered next.

9.4 The Linear Algebra Approach

An alternative method of determining $\boldsymbol{\xi}_X$, the solution to Equation (31), is to use linear algebra techniques to solve the equation directly. For a set of linear simultaneous equations it is widely known that provided there is m independent equations and m unknowns then a unique solution vector $\boldsymbol{x}$ exists for the problem. However, if we have n independent equations with $n > m$, then the system is over determined and there is no solution which satisfying all the equations. In the system one linear equation is produced per time-step of the simulation, thus as the time-step is 0.1s and

the identification manoeuvre lasts from 350s to 600s the number of linear equations is very large. However, we know that, for the simulation at least, there is a solution ($\boldsymbol{\xi}_X$) which satisfies all the equations. This is because each row of $\boldsymbol{A}_X$ and $\boldsymbol{b}_X$ when combined with $\hat{\boldsymbol{\xi}}_X$ represents a linear equation which describes the acceleration in the x direction. As this is calculate in the simulation using $\boldsymbol{\xi}_X$ each of the linear equations will be satisfied when $\hat{\boldsymbol{\xi}}_X = \boldsymbol{\xi}_X$ and therefore a solutions exists. However, if noise is added to each of the linear equations, then they will not be satisfied when $\hat{\boldsymbol{\xi}}_X = \boldsymbol{\xi}_X$ and as there are far more linear equations than unknowns the system will be over-determined and have no solution.

Although for $n > m$ there is no determinable solution as such for

$$\boldsymbol{A}_X\boldsymbol{\xi}_X = \boldsymbol{b}_X \tag{35}$$

a best estimate$\hat{\boldsymbol{\xi}}_X$ of $\boldsymbol{\xi}_X$ can be made. This estimate is best in the sense that the sum of the squares of the errors associated with each of the linear equation is minimized.

Calculating the bestestimate involves finding a matrix $\boldsymbol{B}_X$ which is a left inverse for $\boldsymbol{A}_X$ such that,

$$\boldsymbol{B}_X\boldsymbol{A}_X\boldsymbol{\xi}_X = \boldsymbol{I}\boldsymbol{\xi}_X = \boldsymbol{B}_X^*\boldsymbol{b}_X.$$

The common approach to determining the left inverse, which gives the 'least squares' solution $\hat{\boldsymbol{\xi}}_X$ to Equation (35), is to premultiply Equation (35) by the transpose of $\boldsymbol{A}_X$. This leads to,

$$\boldsymbol{A}_X^T\boldsymbol{A}_X\boldsymbol{\xi}_X = \boldsymbol{A}_X^T\boldsymbol{b}_X.$$

Provided $\boldsymbol{A}_X$ is of full rank then it is guaranteed that $\left(\boldsymbol{A}_X^T\boldsymbol{A}_X\right)^{-1}$ exists as shown in Strang (1988), and so

$$\hat{\boldsymbol{\xi}}_X = \left(\boldsymbol{A}_X^T\boldsymbol{A}_X\right)^{-1}\boldsymbol{A}_X^T\boldsymbol{b}_X. \tag{36}$$

This equations gives a solution $\hat{\boldsymbol{\xi}}_X$ which minimizes the sum of the square of the errors in Equation (31).

Having described how to determine a solution to the linear equation, it is clear that provide $\boldsymbol{A}$ and $\boldsymbol{b}$ are known for all the coefficient sub-problems, then the hydrodynamic coefficients can be readily determined using this method.

9.4.1 Applications of the Linear Algebraic Approach

The same manoeuvres used with the linear programming formulation are considered for the linear algebra approach. Again Matlab was used to perform the computations and the Matlab `mldivide` (matrix left divide) command was used to compute $\hat{\boldsymbol{\xi}}$. The Matlab command does not use Equation (36) to determine the solution, this is because any ill-conditioning in $\boldsymbol{A}$ is magnified by using Equation (36). For more information on the implementation of the `mldivide` command, see MathWorks (2002a). The predicted converged coefficients are presented in Figures 93 to 96 and discussed in the following subsections.

The Linear Algebra Results — Horizontal Manoeuvre

The accuracy of the derived coefficients for the three submarines performing the horizontal manoeuvre are presented in Figure 93. The convergence accuracy produced by the linear algebra method is better than that of the LP method shown in Figure 89.

The largest absolute error associated with an identified 'zero' coefficient is 1.068×10^{-14}, this is 3 orders of magnitude smaller than the results produced by the LP method and 8 orders of magnitude smaller than the smallest hydrodynamic coefficient.

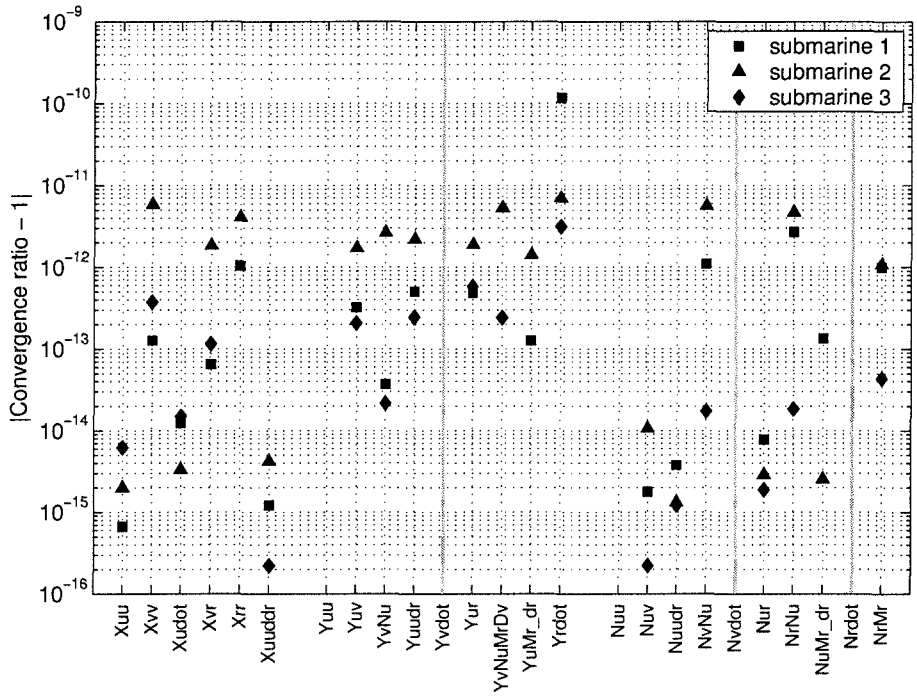

Figure 93: Coefficient convergence results produced using the linear algebra procedure — horizontal manoeuvre.

The times required to identify the coefficients of the associated coefficient sub-problem are given in Table 37. Table 37 shows that the execution times for the linear algebra method are over two orders of magnitude less than the time to compute $\hat{\boldsymbol{\xi}}$ using the LP approach. Thus for the horizontal manoeuvre the linear algebra approach is both faster and more accurate than the LP method.

	submarine 1	submarine 2	submarine 3
X coefficients	0.08	0.12	0.17
Y coefficients	0.16	0.29	0.14
N coefficients	0.15	0.16	0.29

Table 37: Time in seconds to solve for the different coefficient sets using linear algebra techniques — horizontal manoeuvre

The Linear Algebra Results — Vertical Manoeuvre

The convergence results for the vertical manoeuvre are given in Figure 94. During this manoeuvre the largest absolute error on identified 'zero' valued coefficients is 5.423×10^{-15}. As with the horizontal manoeuvre the linear algebra approach identified the coefficients more accurately than the LP method. Interestingly, although the Z coefficients of submarines 2 & 3 are more accurately identified than in the LP method the same basic shape of the identified coefficients still exists.

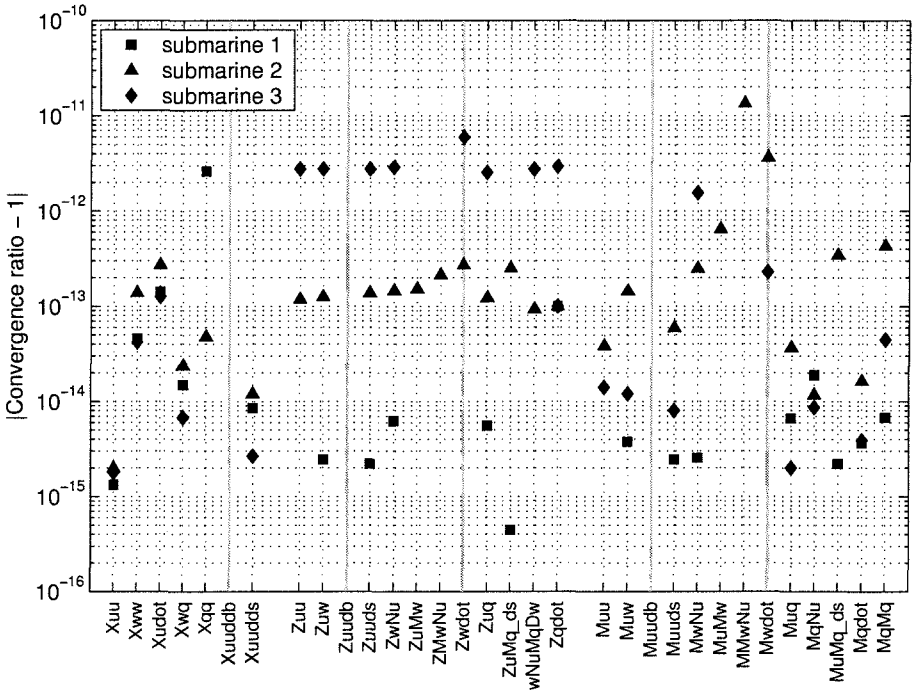

Figure 94: Coefficient convergence results produced using the linear algebra procedure — vertical manoeuvre.

Table 39 provides the time taken to identify the coefficients. The times displayed again show that the linear algebra approach is substantially faster than the LP method.

	submarine 1	submarine 2	submarine 3
X coefficients	0.08	0.07	0.13
Z coefficients	0.10	0.19	0.15
M coefficients	0.39	0.12	0.13

Table 38: Time in seconds to solve for the different coefficient sets using linear algebra techniques — vertical manoeuvre

The Linear Algebra Results — Coupled Manoeuvre

The force and moments coefficient convergence results for the coupled manoeuvre are given in Figures 95 and 96 respectively. Again the coefficients are very well identified and the largest absolute error on identified 'zero' valued coefficients is 6.152×10^{-14} for the coupled manoeuvre.

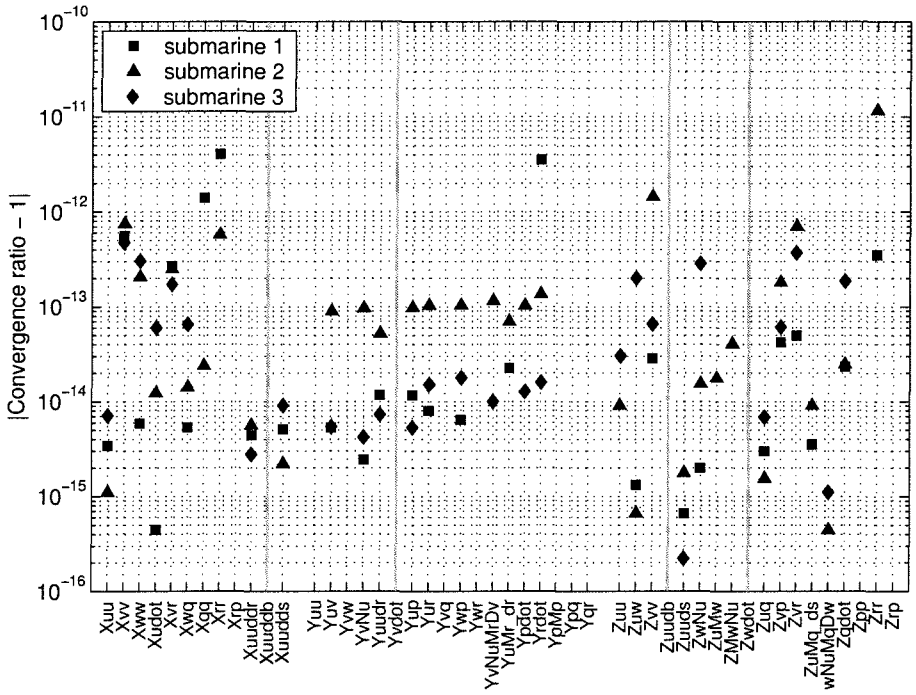

Figure 95: Force coefficient convergence results produced using the linear algebra procedure — coupled manoeuvre.

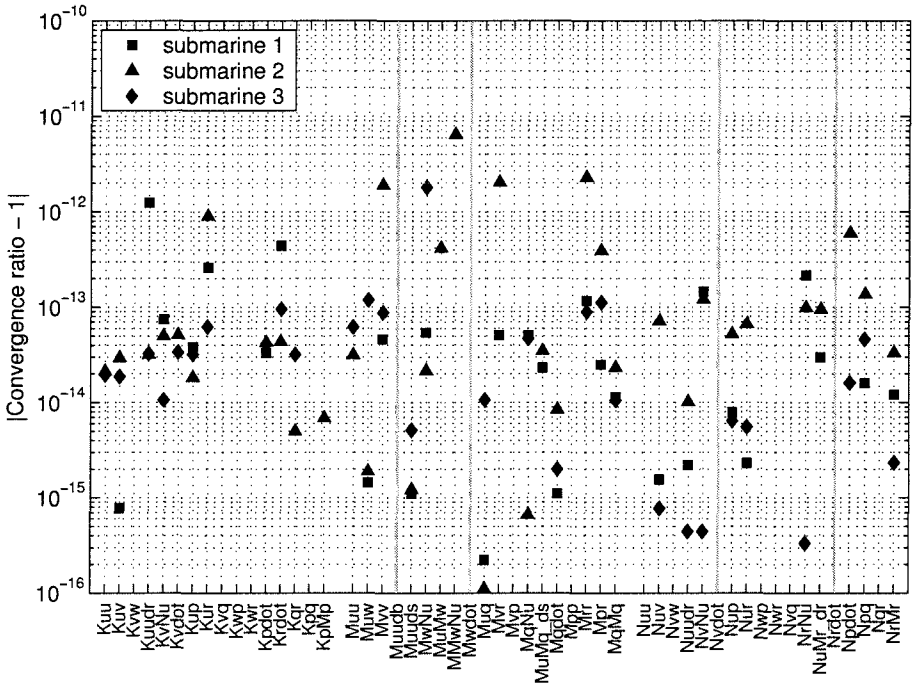

Figure 96: Moment coefficient convergence results produced using the linear algebra procedure — coupled manoeuvre.

Table 39 shows that all the coefficients of $\hat{\boldsymbol{\xi}}$ can be determined in a little over 1s.

	submarine 1	submarine 2	submarine 3
X coefficients	0.09	0.18	0.15
Y coefficients	0.21	0.28	0.17
Z coefficients	0.14	0.34	0.22
K coefficients	0.16	0.15	0.27
M coefficients	0.26	0.27	0.31
N coefficients	0.32	0.24	0.25

Table 39: Time in seconds to solve for the different coefficient sets using linear algebra techniques — coupled manoeuvre

9.5 Comparison of the Two Linear Approaches

The previous sections described, applied and presented the predictions based on both the linear programming (LP) and linear algebra approaches to determining the hydrodynamic coefficients. Both approaches have been shown to be superior to the non-linear approach in that they took less time to converge, produced the 'correct' coefficient values and did not require an initial estimate of $\hat{\boldsymbol{\xi}}$. Thus, reformulating the coefficient identification problem into a system of linear equations hugely improves the identification speed.

Comparing the two approaches, the linear algebra approach is both faster and more accurate than the LP method. Furthermore, it is possible to put additional constraints upon the linear system to try and aid the identification of the correct coefficients. However, this possibility was not explored here and so the linear algebra method was considered to be the best choice of the linear approaches to solve the identification problems.

The fact that the linear algebra method calculated the coefficient values very accurately could lead one to believe that the problem of identification has been solved. However, we know from Chapters 7 and 8 that the manoeuvres produced by the Booth et al. (1980) equations of motion are ill-conditioned. That is almost identical manoeuvres were produced by completely different coefficients. Thus, as both the linear and non-linear approaches represent the same system one suspects that the linear methods will also suffer from this ill-conditioning. Hence, small errors in the measured attitude, linear & angular velocity and linear & angular accelerations will lead to very large errors in the determined coefficients. This aspect of ill-conditioning is considered next.

9.6 Ill-conditioning of the Linear Approach

It was suspected that small measurement errors ($\boldsymbol{\varepsilon}_N$) and slight disturbances ($\boldsymbol{\tau}_d$) would be magnified by the ill-conditioning identified in the non-linear procedure. If true then small errors and disturbances would lead to large errors in the identified

coefficients.

However, the level of ill-conditioning was not known. If the system was very ill-conditioned then it will not be possible to identify the coefficients even if every effort was made to reduce $\boldsymbol{\tau}_d$ and $\boldsymbol{\varepsilon}_N$. This statement does not take into account the 'disturbances' produced by the Booth et al. (1980) equations as a consequence of not precisely describing the loads acting on an UV. Alternatively if the ill-conditioning was not excessive, then it may be possible to produce reasonable estimates of the hydrodynamic coefficients from noisy manoeuvre.

To determine the effect of measurement noise ($\boldsymbol{\varepsilon}_N$) and disturbances ($\boldsymbol{\tau}_d$), experienced in real UV trials, on the accuracy of the coefficient identification it is preferable to have a model of $\boldsymbol{\varepsilon}_N$ and $\boldsymbol{\tau}_d$. Unfortunately no such model exists for Autosub. To overcome this problem, it was decided to test manoeuvres with a noise and disturbance level appreciably less than that expected in reality. A manoeuvre subject to very low noise and disturbance level could indicate the effect it has on coefficient convergence. If the low level noise and disturbances badly affect the coefficient convergence accuracy it could then be surmised that real manoeuvre subject to larger noise and disturbance levels would be even more strongly affected.

In defining the low noise and disturbance levels it was decided for simplicity to assume that the UV was not subject to disturbances and hence $\boldsymbol{\tau}_d = 0$. The measurement noise level was determined from consideration of the sensors on Autosub. As the Fibre Optic Gyros on the PHINS INS are very accurate it was assumed that the UV's attitude and angular velocity & acceleration were measured without error. On the other hand the ADCP does not measure the linear velocity of the vehicle with the same accuracy. It was therefore decided to corrupt only the 'measured' linear acceleration and velocity. The chosen method of corrupting the data was to specify a measurement precision and then to round the 'measured' data to this precision. This was done to make the tests repeatable and to simplify the specification of the 'noise'. In particular, the linear acceleration was assumed to be measured with a precision of 1 $mm{\cdot}s^{-2}$ (based on the PHINS 50μg precision accelerometers) and so the accelerations were rounded to the nearest $mm{\cdot}s^{-2}$. Since the linear velocity was assumed to be measured with a precision of 1 $cm{\cdot}s^{-1}$ and hence the UV linear velocities were rounded

to the nearest cm·s^{-1}.

Having, defined the precision of the errors the 100 prediction manoeuvres described in Chapter 8 were used with the above measurement precision to identify the hydrodynamic coefficients of submarine 1. The results of the coefficient identification tests are shown in Figures 97–98. These figures show that the hydrodynamic coefficients are not well identified with this small noise level. Two coefficients have convergence ratios sufficiently large to not appear within the plotted scale ($K'_{uu\delta R} \in [5,8]$ and $Y'_{\dot{r}} \in [-250,-50]$). Also, the range of X'_{qq} although passing through the plotted range extended from -8 to +5.

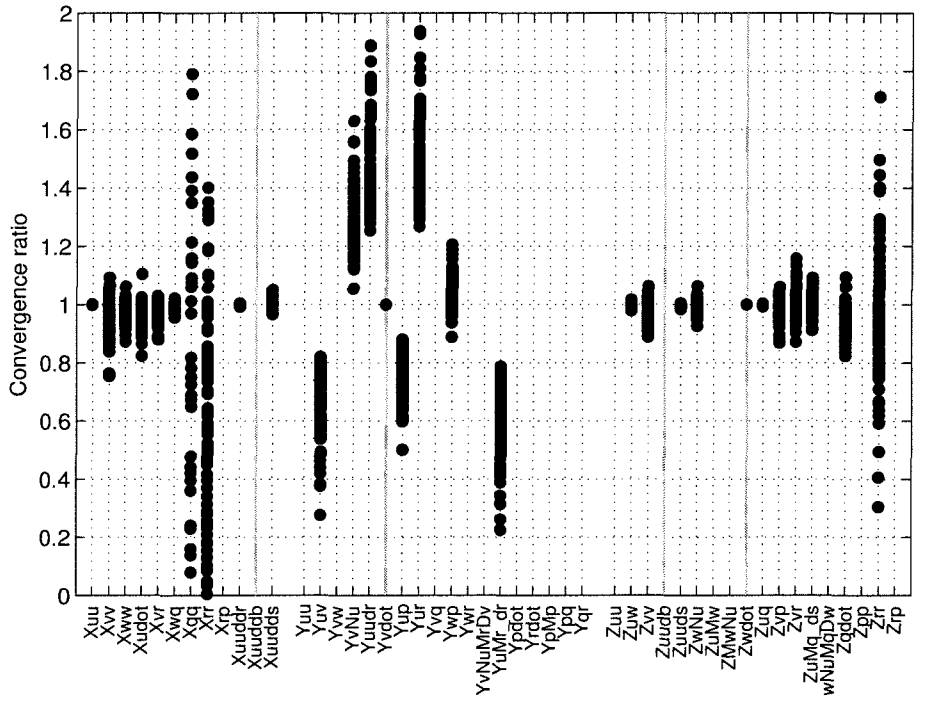

Figure 97: Linear algebra estimated force coefficient values for submarine 1 calculated from the 100 prediction manoeuvres.

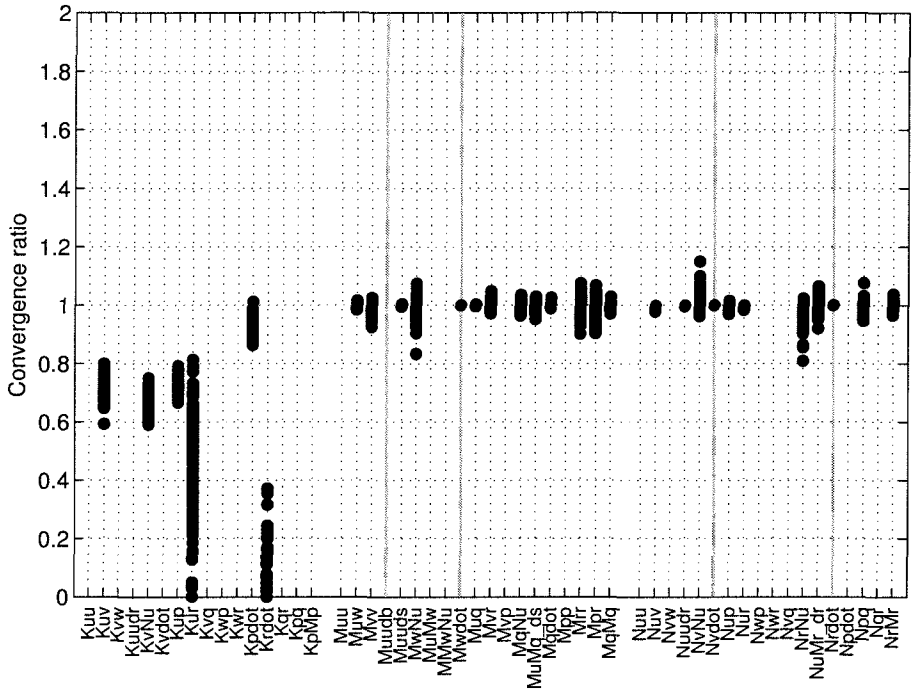

Figure 98: Linear algebra estimated moment coefficient values for submarine 1 calculated from the 100 prediction manoeuvres.

The poor coefficient convergence means that the 'measurement' errors associated with the 100 random prediction manoeuvres have produced coefficients that do not completely match the target track.

However, when these coefficients are used to predict the manoeuvres of the identification process they produce the target manoeuvres with the accuracies shown in Figure 99. Thus, although the individual coefficients are poorly identified the coefficient set still reproduce the target manoeuvre very accurately. This was the definition of an ill-conditioned manoeuvre as set out in Chapter 4.

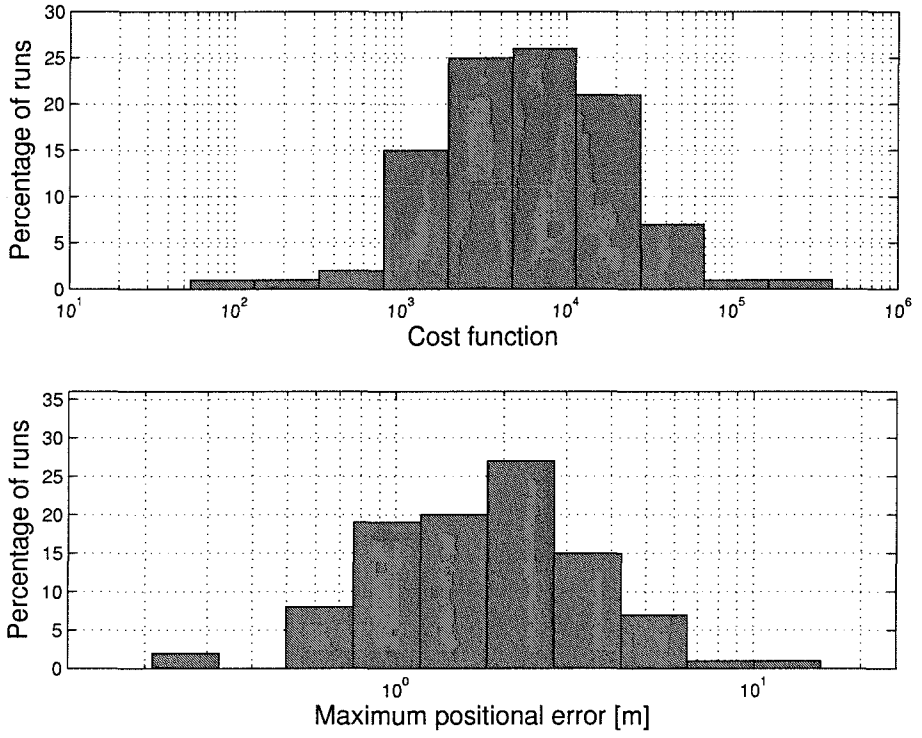

Figure 99: The accuracy with which each identified coefficient set reproduce its identification manoeuvre.

The ill-conditioning testing has shown that very slight errors in the 'measured manoeuvre' data has a profound effect upon the values of the identified coefficients. The 100 random prediction manoeuvres used with the 'noisy' identification process have produced ill-conditioned manoeuvres. This result confirms the hypothesis put forward in Chapter 8 that the 100 prediction manoeuvres were in-conditioned.

9.7 Conclusions

This chapter has described how the initial assumption, posed in the QinetiQ hydrodynamic coefficient identification problem, that only position and attitude data was available during a manoeuvre is not true for Autosub. As Autosub measures velocity and acceleration data directly, linear identification procedures can be easily used. The linear programming technique was describe, implemented and tested. Using this technique the hydrodynamic coefficients were very accurately identified in

considerably less time than using the non-linear identification technique. The linear algebra formulation of the problem was even more successful producing more accurate coefficient values in approximately one hundredth of the time of the LP approach.

Although, the coefficients were exceptionally well identified it was realised that the ill-conditioning exhibited in the non-linear identification testing should also be present in the linear identification process. As the linear algebra approach identifies the coefficient extremely accurately it was suspected that the ill-conditioning would appear when slight errors occurred in the measured data. This was tested by introducing a small rounding error in the 'measured' velocities and accelerations of the 100 prediction manoeuvre (introduced in Chapter 8) performed by submarine 1. The linear algebra technique was then used to identify the hydrodynamic coefficients from this corrupted data. The coefficient values were poorly identified using this corrupted data. However, the coefficients still managed to reproduce the identification manoeuvre with considerable accuracy. Thus, it was concluded that the 100 prediction manoeuvres were ill-conditioned. This supported the conclusions of Chapter 8.

Chapter 10

Conclusions

The motivation for this research was based on a desire to create an accurate motion simulation of Southampton Oceanography Centre's AUV Autosub. This has not been achieved.

The research has investigated whether it is possible to identify the hydrodynamic coefficients used in a non-linear submarine model from free swimming trials data. The results reported in this thesis have demonstrated that this is an extremely challenging, if not impossible, task. The principal difficulties arise from the ill-conditioning of the coefficients identified from manoeuvres time histories and, to a lesser extent, the non-uniqueness of the manoeuvre identified hydrodynamic coefficients.

The research, although not producing a method of identifying the correct coefficient values, has given considerable insight into the equations themselves. The thesis also demonstrated in Chapter 7 a method of identifying the hydrodynamic coefficients using only the UV path data. This non-linear approach determined the coefficients in relatively short order, considering the complexity of the problem being solved, and proved itself eminently suitable for answering the QinetiQ question posed in Chapter 4. Although, the approach was not optimal for the Autosub problem it did provide valuable insight into the ill-conditioning of coefficients in the identification problem. Also, the approach of using a custom coded C based UV motion simulation linked into Matlab and combined with other custom written and off the shelf Matlab tools has proved to be a powerful method of evaluation the system identification

procedure.

The non-uniqueness of the manoeuvre identified hydrodynamic coefficients demonstrated in Chapter 6 showed that the problem arose from the coupling between the inertial and velocity hydrodynamic coefficient terms. Specific added-mass coefficients were identified as being 'associated' with these couplings, and by specifying the value of these coefficients the remaining hydrodynamic coefficients become unique, and hence can, in theory, be identified. It is reasonable to assume that accurate added-mass figures for the UV can be determined using potential flow theory and so the specified added-masses would not introduce errors into the remaining coefficients. So, although the coefficients are not unique, the non-uniqueness can be overcome by specifying the values of the 'associated' added-mass coefficients.

As an aside, this non-uniqueness is a feature of the equations when not subjected to disturbances. If disturbance loads were added to the equations then the coefficients would become unique, but the linear relationship that caused the non-uniqueness would not disappear, and thus would produce ill-conditioning in the system.

So although a method of overcoming the non-uniqueness was available, the thornier problem of the ill-conditioning of the manoeuvres could not be so readily overcome. The ill-conditioning of manoeuvres was discussed in Chapter 4, shown for the standard test manoeuvres in Chapter 7, implied for the 100 prediction manoeuvres in Chapter 8, and demonstrated for the 100 prediction manoeuvres in Chapter 9. In no case was a well-conditioned manoeuvre found.

The ill-conditioned state describes the sensitivity of the hydrodynamic coefficients to small errors in the identification manoeuvre when mapping from the manoeuvre to the coefficients. This ill-conditioning makes it exceptionally difficult to determine the correct coefficient values as a real manoeuvre is always subject to small errors.

The ill-conditioning of all tested manoeuvres poses the question of whether all manoeuvres are ill-conditioned. If all UV manoeuvres are ill-conditioned then it is impossible to determine the correct coefficient values from submarine trials data as all data, as mentioned, will contain small errors which will be magnified to create large errors in the coefficient values.

Also, if all manoeuvres are ill-conditioned there would be sets of coefficients which although substantially different to the correct coefficients values would still reproduce all manoeuvres accurately. This can be demonstrated as follows. If all manoeuvres are ill-conditioned then a manoeuvre can be created that contains all other manoeuvres, and this too will also be ill-conditioned. Any coefficients that can accurately produce this 'super' manoeuvre will also predict all other manoeuvres accurately. So if all manoeuvres are ill-conditioned then although the coefficients may be mathematically unique they will be non-unique for all practical purposes.

Alternatively, if not all manoeuvres are ill-conditioned then there will be a manoeuvre which is well conditioned. If this manoeuvre was used to identify the coefficients then the correct coefficient values should be determined.

The results presented in the thesis suggest that no well-conditioned manoeuvres exist. But proving this is extremely difficult as the only approach which suggests itself is to test every manoeuvre and submarine combination to see if they are all ill-conditioned. Clearly an impractical proposition. However, as all the manoeuvres analysed were ill-conditioned it seems reasonable to extend this and assume that all manoeuvres will be ill-conditioned. From this it would follow that the coefficients of the Booth et al. (1980) submarine equations when identified from a manoeuvre would always be ill-conditioned.

The one caveat to the foregoing analysis is that this is all based on disturbance free motion. There is a possibility that if the UV is subject to disturbances about which information is known, then this extra information may allow for better coefficient identification.

The results of the tested identification process using simulated UV manoeuvre data strongly suggest that the technique will not work when applied to real UVs. The UV motions were simulated under the following idealized conditions, when the linear programming (best identification approach) failed to accurately identify the coefficients:

- The added-mass coefficients were accurately known.
- The manoeuvre data was subject to measurement noise. This took the form of rounding the linear velocities to the nearest $cm{\cdot}s^{-1}$ and the linear accelerations

to the nearest $mm{\cdot}s^{-2}$. These values were as they were significant but less than would be expected with real data.

- The UV was not subject to any external disturbances.
- The UV motions were accurately described by the Booth et al. (1980) submarine equations.
- All the UV 'mechanical' coefficients were known (e.g. I_{XX}).
- The error of the simulation in approximating the Booth et al. (1980) submarine equations was ignored.

Thus, even when the manoeuvre data is subject to very small levels of error the linear programming approach failed to identify the correct hydrodynamic coefficient values. This demonstrates the ill-conditioning of the manoeuvre identified coefficient values.

Thus, using the tested it is not possible to accurately determine the hydrodynamic coefficients with the tested identification techniques.

It is important for the identification procedure to identify the correct coefficient values as first it would validate the procedure was working correctly and would guarantee that all manoeuvres would be the same as those generated from captive model testing. Second, although it maybe possible to determine a set of coefficient which albeit different will always produce acceptable manoeuvre accuracy for all simulated disturbances free manoeuvres, the approach may well fail when disturbances are added to the simulation.

Finally, although the coefficients appear to be non-unique and ill-conditioned when considered in the Booth et al. (1980) equations, this is a feature of the equations not the coefficients. The coefficients themselves represent the loads associated with physical motions of an UV, and as such are unique and well-conditioned. If the coefficients were not unique and well-conditioned then they could not be derived in captive model testing. This begs the question of why the coefficients are non-unique and ill-conditioned when within the Booth et al. (1980) equations.

The cause of the ill-conditioning is thought to arise from the fact that free swimming UVs can only produce a subset of all possible motions when manoeuvring, and so the

manoeuvring UV cannot produce a rich enough motion set to allow the hydrodynamic coefficients to be accurately identified. An example of the limited possible motion occurs when a UV is turning; it is not possible to generate a yaw-rate (r) without producing an associated sway velocity (v). This coupling of sway and yaw-rate restricts the UV motion to a band in the $v - r$ plane (as illustrated by Figure 68). Thus, any set of identified hydrodynamic coefficient that accurately reproduces the hydrodynamic loads in this band will accurately reproduce all free-swimming UV manoeuvres. It is thought that there are many such coefficients sets which accurately model an UV's loads in this restricted motion band and this fact causes the ill-conditioning noted when attempting to identifying the hydrodynamic coefficients from manoeuvring data.

10.1 Further Works

First to strengthen the hypothesis that the Booth et al. (1980) equations always generate ill-conditioned manoeuvre, and hence cannot be used to determine the correct coefficient values, the following tests could be performed.

- Test manoeuvres where the buoyancy of the UV changes during the manoeuvre.
- Test manoeuvres where there are propeller rpm changes during the manoeuvre.

One possible method of speeding up the manoeuvre evaluation would be to use the concepts of matrix conditioning numbers with the matrices generated in the linear identification procedure. This method could potentially produce an estimate of how well conditioned the manoeuvre is without exhaustively testing it. This would speed up the manoeuvre evaluation.

The approach to determining the hydrodynamic coefficients laid out in the research could also be applied to other set of non-linear UV equations to see if they also produced non-unique ill-conditioned coefficients.

Finally, a more interesting line of enquiry would be to evaluate whether a set of 'wrong' valued coefficients can reproduce all other manoeuvres accurately. If they

can then the identification manoeuvre may well prove suitable for determine such a set.

REFERENCES

Abkowitz, M. A. (1969). *Stability and motion control of ocean vehicles.* M.I.T. Press, Cambridge (Mass.) ; London.

Åström, K. J. and Källström, C. G. (1976). Identification of ship steering dynamics. *Automatica*, 12(1):9 – 22.

Bertram, V. (2000). *Practical ship hydrodynamics.* Butterworth-Heinemann, Oxford.

Blevins, R. D. (1993). *Formulas for natural frequency and mode shape.* Krieger Publishing Company, Malabar, Florida.

Bø, H. (2004). *Hydrodynamic estimation and identification.* Master's thesis, NTNU.

Booth, T. B., Randall, J. W., and Hirom, C. P. J. (1980). Dynamic characteristics of submarines [second edition]. Technical report, AMTE Haslar, UK.

Breslin, J. P. and Andersen, P. (1994). *Hydrodynamics of ship propellers.* Cambridge ocean technology series ; 3. CUP, Cambridge. Includes bibliographical references and index.

Chou, J. (1992). Quaternion kinematic and dynamic differential equations. *Robotics and Automation, IEEE Transactions on*, 8(1):53–64.

Clarke, D., Gedling, P., and Hine, G. (1983). Application of manoeuvring criteria in hull design using linear theory. *Naval Architect*, pages 45 – 68.

Cooke, J. M., Zyda, M. J., Pratt, D. R., and McGhee, R. B. (1992). Npsnet: Flight simulation dynamic modeling using quaternions. *Presence: Teleoperators and Virtual Environments*, 1(4):404–420.

Craig, J. J. (1986). *Introduction to robotics mechanics and control.* Addison-Wesley, Reading, Mass.

Duman, I. (1999). *Design, Implementation, and Testing of a Real-Time Software System for a Quaternion-Based Attitude Estimation Filter.* Masters thesis, Naval Postgraduate School.

Feldman, J. (1979). DTNSRDC revised standard submarine equations of motion. Technical Report DTNSRDC/SPD-0393-09, David W. Taylor Naval Ship Research And Development Center, Bethesda, MD.

Fjellstad, O.-E. and Fossen, T. (1994). Singularity-free tracking of unmanned underwater vehicles in 6 dof. In *Decision and Control, 1994., Proceedings of the 33rd IEEE Conference on*, volume 2, pages 1128–1133 vol.2.

Fletcher (1987). *Practical methods of optimization.* Wiley, Chichester, 2nd ed edition. B8732879.

Fossen, T. (1994). *Guidance and control of ocean vehicles.* Wiley, Chichester.

Fossen, T. and Blanke, M. (2000). Nonlinear output feedback control of underwater vehicle propellers using feedback form estimated axial flow velocity. *Oceanic Engineering, IEEE Journal of*, 25(2):241–255.

Furlong, M. E., Hearn, G. E., Veres, S. M., and Rogers, E. (2003). Nonlinear system identification tools applied to the modelling of submarine dynamics. In *First IFAC Workshop on Guidance and Control of Underwater Vehicles, GCUV2003.* Newport, South Wales, UK.

Gaiffe, T. (2002). U-PHINS: A fog-based inertial navigation sysem developed specifically for auv navigation and control. In *Underwater Intervention, Inertnational Conference*, New-Orleans, USA.

Haddara, M. R. and Wang, Y. (1999). Parametric identification of manoeuvring models for ships. *International Shipbuilding Progress*, 46(445):5 – 27.

Healey, A. and Lienard, D. (1993). Multivariable sliding mode control for autonomous diving and steering of unmanned underwater vehicles. *Oceanic Engineering, IEEE Journal of*, 18(3):327–339.

Källström, C. G. and Åström, K. J. (1981). Experiences of system identification applied to ship steering. *Automatica*, 17(1):187 – 198.

Kuipers, J. B. (2002). *Quaternions and rotation sequences : a primer with applications to Orbits, Aerospace and Virtual Reality.* Princeton University Press, Princeton, N.J. ; Oxford. Includes bibliographical references and index.

Lamb, H. (1932). *Hydrodynamics.* C.U.P., Cambridge, 6th ed edition.

Lewis, E. V. (1989a). *Principles of naval architecture*, volume III. Motion in Waves and Controllability. Society of Naval Architects and Marine Engineers, Jersey City, N.J., 2nd rev. ed edition.

Lewis, E. V. (1989b). *Principles of naval architecture*, volume Vol 2: Resistance, propulsion and vibration. Society of Naval Architects and Marine Engineers, 2nd revision edition.

Marco, D. B. and Healey, A. J. (1998). Surge motion parameter identification for the nps phoenix auv. In *Proceedings International Advanced Robotics Program IARP '98*, pages 197 – 210, University of South Louisiana.

MathWorks (2002a). *MATLAB Function Reference Volume 1: A - E.* MathWorks.

MathWorks (2002b). *Optimization Toolbox Version 2.2 — for use with MATLAB — User's Guide.* Mathworks.

McGhee, R. B., Bachmann, E. R., and Zyda, M. J. (2000). Rigid body dynamics, inertial reference frames, and graphics coordinate systems: A resolution of conflicting conventions and terminology. MOVES Academic Group Technical Report NPS-MV-01-002, Naval Postgraduate School.

Millard, N., McPhail, S., Pebody, M., Perrett, J., Stevenson, P., and Webb, A. (1997). Autosub-1. from test-tank to autonomy and the science beyond. In *Electronic Engineering in Oceanography, 1997. 'Technology Transfer from Research to Industry'., Seventh International Conference on*, pages 1–8.

Munk, M. M. (1923). The drag of Zepplin airships. Technical Report 117, N.A.C.A.

Newman, J. N. (1977). *Marine hydrodynamics.* M.I.T. Press, Cambridge, Mass.; London.

Norrbin, N. H. (1970). Theory and observations on the use of a mathematical model for ship manoeuvring in deep and confined waters. In *Eighth Symposium on Naval Hydrodynamics.* Pasadena, CA.

Pankajakshan, R., Remotigue, M. G., Taylor, L. K., Jiang, M., Briley, W. R., and Whitfield, D. L. (2002). Validation of control-surface induceed submarine maneuvering simulations using UNCLE. In *Twenty-Fourth Symposium on Naval Hydrodynamics*, pages 624 – 629, Fukuoka, Japan.

Press, W. H., Teukolsky, S. A., Vetterling, W. T., and Flannery, B. P. (1992). *Numerical recipes in C : the art of scientific computing.* CUP, Cambridge, 2nd ed edition.

Prestero, T. (2001a). Development of a six-degree of freedom simulation model for the remus autonomous underwater vehicle. In *OCEANS, 2001. MTS/IEEE Conference and Exhibition*, volume 1, pages 450–455 vol.1.

Prestero, T. (2001b). *Veritication of a Six-Degree of Freedom Simulation Model for the Remus Autonomous Underwater Vehicle.* Master's thesis, M.I.T.

Ridao, P., Batlle, J., and Carreras, M. (2001). Model identification of a low-speed uuv. In *Proceedings of Conference on Control Applications in Marine Systems, 18-20 July 2001*, Control Applications in Marine Systems 2001 (CAMS 2001) Proceedings volume from the IFAC Conference, pages 395–400, Glasgow, UK. Elsevier Sci.

Sharpe, R. (1996). *Jane's fighting ships 1996-1997.* Jane's Information Group, London.

Strang, G. (1988). *Linear algebra and its applications.* Harcourt, Brace, Jovanovich, Publishers, San Diego, 3rd ed edition.

Veres, S. (2003). Grey box identification of large dynamic models. Technical Note 4/2003, University of Southampton, Tizard library.

Yoon, H. K. and Rhee, K. P. (2003). Identification of hydrodynamic coefficients in ship maneuvering equations of motion by estimation-before-modeling technique. *Ocean Engineering*, 30(18):2379 – 2404.

APPENDICES

Appendix A

Calculating the Euler Angle Update Matrix

From Section 2.1.3 it was shown that,

$$\begin{bmatrix} p \\ q \\ r \end{bmatrix} = \begin{bmatrix} 1 & s\phi \cdot t\theta & c\phi \cdot t\theta \\ 0 & c\phi & -s\phi \\ 0 & s\phi/c\theta & c\phi/c\theta \end{bmatrix} \begin{bmatrix} \dot{\phi} \\ \dot{\theta} \\ \dot{\psi} \end{bmatrix}.$$

Thus,

$$p = \dot{\phi} + (\sin\phi \tan\theta)\,\dot{\theta} + (\cos\phi \tan\theta)\,\dot{\psi}, \tag{37}$$

$$q = (\cos\phi)\,\dot{\theta} - (\sin\phi)\,\dot{\psi}, \tag{38}$$

$$r = (\sin\phi/\cos\theta)\,\dot{\theta} + (\cos\phi/\cos\theta)\,\dot{\psi}\,. \tag{39}$$

Now multiplying equations (38) and (39) by $\cos\phi$ and $-\sin\phi$ respectively and adding gives

$$
\begin{aligned}
q\cos\phi - r\sin\phi &= \left(\cos^2\phi\right)\dot{\theta} + \left(\sin\phi\cos\phi\cos\theta\right)\dot{\psi} \\
&\quad + \left(\sin^2\phi\right)\dot{\theta} - \left(\sin\phi\cos\phi\cos\theta\right)\dot{\psi}, \\
&= \left(\sin^2\phi + \cos^2\phi\right)\dot{\theta}, \\
&= \dot{\theta}\,.
\end{aligned}
\tag{40}
$$

Substituting for $\dot{\theta}$ from equation (40) into equation (39) leads to

$$
\begin{aligned}
r &= -\sin\phi\left(q\cos\phi - r\sin\phi\right) + \left(\cos\phi\cos\theta\right)\dot{\psi}, \\
&= -q\sin\phi\cos\phi + r\sin^2\phi + \left(\cos\phi\cos\theta\right)\dot{\psi}\,.
\end{aligned}
$$

Rearranging then yields

$$
\begin{aligned}
\left(\cos\phi\cos\theta\right)\dot{\psi} &= q\sin\phi\cos\phi - r\left(\sin^2\phi - 1\right), \\
&= q\sin\phi\cos\phi + r\cos^2\phi,
\end{aligned}
$$

and so

$$
\dot{\psi} = q\frac{\sin\phi}{\cos\theta} + r\frac{\cos\phi}{\cos\theta}\,. \tag{41}
$$

Substituting $\dot{\psi}$ from equation (41) into equation (37), yields

$$
\begin{aligned}
p &= \dot{\phi} - \sin\theta\left(q\frac{\sin\phi}{\cos\theta} + r\frac{\cos\phi}{\cos\theta}\right), \\
&= \dot{\phi} - q\sin\phi\tan\theta - r\cos\phi\tan\theta\,.
\end{aligned}
$$

Thus

$$
\dot{\phi} = p + q\sin\phi\tan\theta + r\cos\phi\tan\theta\,.
$$

The three governing equations are then,

$$
\begin{aligned}
\dot{\phi} &= p + q\sin\phi\tan\theta + r\cos\phi\tan\theta\,, \\
\dot{\theta} &= q\cos\phi - r\sin\phi\,, \\
\dot{\psi} &= q\frac{\sin\phi}{\cos\theta} + r\frac{\cos\phi}{\cos\theta}\,.
\end{aligned}
$$

Written in matrix form this becomes,

$$\begin{bmatrix} \dot{\phi} \\ \dot{\theta} \\ \dot{\psi} \end{bmatrix} = \begin{bmatrix} 1 & \sin\phi\tan\theta & \cos\phi\tan\theta \\ 0 & \cos\phi & -r\sin\phi \\ 0 & \sin\phi/\cos\theta & \sin\phi/\cos\theta \end{bmatrix} \begin{bmatrix} p \\ q \\ r \end{bmatrix}.$$

Or written in Fossen's notation, this becomes,

$$\dot{\boldsymbol{\eta}}_2 = \boldsymbol{J}_2(\boldsymbol{\eta}_2)\boldsymbol{\nu}_2,$$

as required.

Appendix B

Quaternion Representation of Rotation

Due to the singularities associated with Euler angles, quaternions have been proposed as an alternative method of defining the body rotations required in UV simulations. The quaternion definition was created by William Rowan Hamilton in 1856 and is a forerunner to vector notation. As quaternions were more complex to use than vectors they fell from use. However, interest in them has resurged, as they are capable of representing rotations without the singularity problems associated with Euler angles and discussed in Section 2.1.2.

The following appendix briefiy describe how quaternions can be used to represent the rotations required in simulating UVs. For a fuller description of quaternions see Chou (1992) and Kuipers (2002).

B.1 Quaternion Fundamentals

Quaternions are an extension of complex numbers known as *hyper-complex* numbers, where 3 different variables represent the purely imaginary number $\sqrt{-1}$. Thus the imaginary part of the number is represented by a vector in $\mathbb{R}^3$. The three variables

are defined as $\boldsymbol{i}$, $\boldsymbol{j}$ & $\boldsymbol{k}$. By definition multiplication of these bases proceeds as follow,

$$\boldsymbol{i}^2 = -1, \qquad \boldsymbol{j}^2 = -1 \qquad \text{and} \quad \boldsymbol{k}^2 = -1.$$

Similarly, when any two of the bases are multiplied together, they produce:

$$\begin{aligned} \boldsymbol{ij} &= -\boldsymbol{ji} = \boldsymbol{k} \\ \boldsymbol{jk} &= -\boldsymbol{kj} = \boldsymbol{i} \\ \boldsymbol{ki} &= -\boldsymbol{ik} = \boldsymbol{j} \end{aligned} .$$

Furthermore, triple products satisfy the cyclic relationship:

$$\boldsymbol{ijk} \equiv \boldsymbol{jki} \equiv \boldsymbol{kij} \equiv -1.$$

Quaternion Representation

A quaternion can be defined geometrically as a point in a four dimensional space with one dimension represented by the real component and three dimensions represented by the imaginary components. The 'directions' of the space are represented here as 1, $\boldsymbol{i}$, $\boldsymbol{j}$ & $\boldsymbol{k}$ with associated magnitudes (q_0, q_1, q_2, q_3). Two quaternions are said to be equal if their corresponding components are equal. Thus,

$$\mathfrak{q} = \mathfrak{p} \implies \quad q_0 = p_0,\ q_1 = p_1,\ q_2 = p_2 \text{ and } q_3 = p_3.$$

Quaternions are usually represented in one of the following ways.

1. A linear combination of the four components (q_0, q_1, q_2, q_3) in the directions 1, $\boldsymbol{i}$, $\boldsymbol{j}$ & $\boldsymbol{k}$. Thus,
$$\mathfrak{q} = q_0 + q_1\boldsymbol{i} + q_2\boldsymbol{j} + q_3\boldsymbol{k}.$$
2. A vector of four coefficients, written as
$$\mathfrak{q} = [q_0, q_1, q_2, q_3].$$
3. A scalar representing the real part and a vector representing the imaginary terms, written as
$$\mathfrak{q} = (w, \boldsymbol{q}) \qquad \text{where} \quad \boldsymbol{q} = [q_1, q_2, q_3].$$

Quaternion Addition

Quaternion addition works in the same fashion as vector addition, that is, corresponding elements are added so that,

$$\mathbf{q} + \mathbf{p} = [(q_0 + p_0), (q_1 + p_1), (q_2 + p_2), (q_3 + p_3)].$$

It follows from this definition of quaternion addition that the algebraic rules governing quaternion addition are the same as those for real numbers, thus:

$\mathbf{q} + \mathbf{p} = \mathbf{p} + \mathbf{q}$	- Quaternion addition is commutative
$\mathbf{q} + (\mathbf{p} + \mathbf{r}) = (\mathbf{q} + \mathbf{p}) + \mathbf{r}$	- Quaternion addition is associative
$\mathbf{q} + 0 = 0 + \mathbf{q} = \mathbf{q}$	- Quaternion addition has an additive identity
$\mathbf{q} + (-\mathbf{q}) = (-\mathbf{q}) + \mathbf{q} = 0$	- Quaternion addition has an additive inverse

Scalar Multiplication

Quaternion scalar multiplication is defined in the same fashion as that for vectors, thus:

If $\mathbf{q} = (q_0, \boldsymbol{q})$ then $s\mathbf{q} = (sq_0, s\boldsymbol{q})$.

Quaternion Multiplication

Quaternion multiplication is defined as follows:

$$\begin{aligned}\mathbf{qp} = &(q_0p_0 - q_1p_1 - q_2p_2 - q_3p_3) \\ &+ (q_1p_0 + q_0p_1 - q_3p_2 + q_2p_3)\boldsymbol{i} \\ &+ (q_2p_0 + q_3p_1 + q_0p_2 - q_1p_3)\boldsymbol{j} \\ &+ (q_3p_0 - q_2p_1 + q_1p_2 + q_0p_3)\boldsymbol{k}\end{aligned}$$

Alternatively quaternion multiplication can be written using the concepts of vectorial dot and cross products as follows:

With $\mathfrak{q} = (q_0, \boldsymbol{q})$ and $\mathfrak{p} = (p_0, \boldsymbol{p})$ then

$$\mathfrak{q}\mathfrak{p} = \Big((q_0 p_0 - \boldsymbol{q} \cdot \boldsymbol{p}), (q_0 \boldsymbol{p} + p_0 \boldsymbol{q} + \boldsymbol{q} \times \boldsymbol{p}) \Big).$$

Quaternion multiplication is associative but not commutative, consequently,

$$(\mathfrak{q}_1 \mathfrak{q}_2)\mathfrak{q}_3 = \mathfrak{q}_1(\mathfrak{q}_2 \mathfrak{q}_3)$$

but

$$\mathfrak{q}_1 \mathfrak{q}_2 \neq \mathfrak{q}_2 \mathfrak{q}_1, \quad \text{since} \quad \boldsymbol{q}_1 \times \boldsymbol{q}_2 \neq \boldsymbol{q}_2 \times \boldsymbol{q}_1.$$

Quaternion Conjugate

If $\mathfrak{q} = q_0 + q_1 \boldsymbol{i} + q_2 \boldsymbol{j} + q_3 \boldsymbol{k}$ then the quaternion conjugate of $\mathfrak{q}$ is defined as:

$$\begin{aligned} \mathfrak{q}^* &= q_0 - q_1 \boldsymbol{i} - q_2 \boldsymbol{j} - q_3 \boldsymbol{k} \\ &= (q_0, -\boldsymbol{q}). \end{aligned}$$

Quaternion Norm

The Norm of a quaternion $N(\mathfrak{q})$ is defined by Kuipers (2002) as,

$$N(\mathfrak{q}) = \sqrt{\mathfrak{q}\mathfrak{q}^*}$$

however as,

$$\begin{aligned} \mathfrak{q}\mathfrak{q}^* &= (q_0, \boldsymbol{q})(q_0, -\boldsymbol{q}) \\ &= q_0^2 - (\boldsymbol{q}) \cdot \boldsymbol{q} + q_0 \boldsymbol{q} \ + (-\boldsymbol{q}) q_0 + (-\boldsymbol{q}) \times \boldsymbol{q} \\ &= q_0^2 + \boldsymbol{q} \cdot \boldsymbol{q} \\ &= q_0^2 + q_1^2 + q_2^2 + q_3^2 \end{aligned}$$

Thus the quaternion norm can be written in terms of the Euclidean norm, that is

$$N(\mathfrak{q}) = ||(q_0, q_1, q_2, q_3)||_2.$$

Thus, using this definition, the quaternion norm is equivalent to the Euclidean norm of the vector of the quaternion component values in four dimensional space.

A quaternion whose norm is 1 is known as a unit quaternion.

Quaternion Inverse

The quaternion inverse is defined as:

$$\mathbf{q}^{-1} = \frac{\mathbf{q}^*}{N(\mathbf{q})^2}.$$

Thus for unit quaternions where $N(\mathbf{q}) = 1$,

$$\mathbf{q}^{-1} = \mathbf{q}^*.$$

B.2 Rotation Using Quaternions

It is shown in Kuipers (2002) that the 3-dimensional rotation of a vector can be computed using the quaternion product,

$$\mathbf{p}' = \mathbf{q}\mathbf{p}\mathbf{q}^*.$$

The rotation of a point p about a unit vector $\boldsymbol{u}$ through an angle α to a point p' with the rotation direction determined by the right hand screw rule, can be achieved using quaternions as follows:

$$\mathbf{p}' = \mathbf{q}\mathbf{p}\mathbf{q}^*$$

where $\mathbf{q}$ is the unit quaternion

$$\mathbf{q} = (q_0, \boldsymbol{q})$$

defined by

$$q_0 = \cos\left(\tfrac{\alpha}{2}\right)$$
$$\boldsymbol{q} = \boldsymbol{u}\sin\left(\tfrac{\alpha}{2}\right).$$

Also $\mathfrak{p}$ is the vector quaternion with a zero scalar component and the $\boldsymbol{i}$, $\boldsymbol{j}$ & $\boldsymbol{k}$ components corresponding to the x, y & z position of the point p to be rotated. Therefore $\mathfrak{p}$ is defined as,

$$\mathfrak{p} = (0, [x, y, z]).$$

The new quaternion $\mathfrak{p}'$ is also a vector quaternion with a zero real component and with $\boldsymbol{i}$, $\boldsymbol{j}$ & $\boldsymbol{k}$ components corresponding to the rotated coordinate values of p' designated x', y' & z'. Thus,

$$\mathfrak{p}' = (0, [x', y', z']).$$

This operation is illustrated in Figure 100(a) by the rotation of point p about the x axis by an angle ϕ. The rotation of a coordinate system is shown in Figure 100(b), again using the right hand convention. This operation is performed using the quaternion product,

$$\mathfrak{p}' = \mathfrak{q}^* \mathfrak{p} \mathfrak{q}$$

where the $\mathfrak{p}$ and $\mathfrak{q}$ are defined as above.

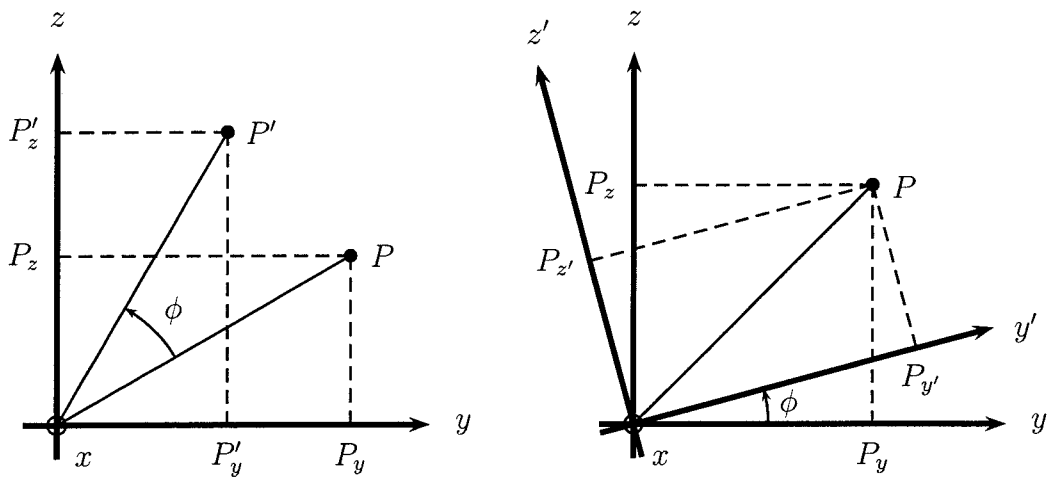

Figure 100: Vector and reference frame rotation about the x-axis by angle ϕ.

Performing the Body to Inertial Coordinate Frame Rotation

The orientation of the body fixed coordinate system is defined by a rotation from the inertial coordinate frame. This rotation is described using quaternions by the axis $\boldsymbol{u}$ and angle α. The rotations from the inertial to the body fixed coordinate frame are performed using the quaternion product,

$$\mathfrak{p}' = \mathfrak{q}^* \mathfrak{p} \mathfrak{q}.$$

However, rotations from the body fixed to the inertial reference frame, as required in the UV modelling, required a rotation angle of $-\alpha$. We shall use $\mathfrak{q}^-$ to describe the quaternion governing this negative rotation. Where,

$$\mathfrak{q}^- = (q_0^-, \boldsymbol{q}^-)$$

with

$$q_0^- = \cos\left(\frac{-\alpha}{2}\right) = \cos\left(\frac{\alpha}{2}\right) = q_0$$

and

$$\boldsymbol{q}^- = \boldsymbol{u}\sin\left(\frac{-\alpha}{2}\right) = -\boldsymbol{u}\sin\left(\frac{\alpha}{2}\right) = -\boldsymbol{q}.$$

Therefore,

$$\mathfrak{q}^- = (q_0, -\boldsymbol{q}) = \mathfrak{q}^*.$$

By noting the $(\mathfrak{q}^*)^* = \mathfrak{q}$, the body fixed to inertial coordinate system rotation can thus be described as,

$$\begin{aligned} \mathfrak{p}' &= \mathfrak{q}^{-*} \mathfrak{p} \mathfrak{q}^- \\ &= \mathfrak{q} \mathfrak{p} \mathfrak{q}^*. \end{aligned}$$

Thus, the point rotation quaternion product is used to calculate the rotation from the body fixed to the inertial reference frame when modelling UVs.

Matrix Representation of the Body Fixed to Inertial Coordinate Frame Quaternion Rotation

It is desirable to use the quaternion rotation product to compute a rotation matrix that could be used to rotate the associated vectors so that,

$$\begin{bmatrix} x' \\ y' \\ z' \end{bmatrix} = \boldsymbol{M}_{\mathfrak{q}} \begin{bmatrix} x \\ y \\ z \end{bmatrix}.$$

Where $\boldsymbol{M}_{\mathfrak{q}}$ is calculated from the quaternion product.

This can be achieved by multiplying out and manipulating the quaternion product

$$\mathfrak{p}' = \mathfrak{q}\mathfrak{p}\mathfrak{q}^*$$

written equivalently as

$$(0 + \boldsymbol{p}') = (q_0 + \boldsymbol{q})(0 + \boldsymbol{p})(q_0 - \boldsymbol{q})$$

to give,

$$\mathfrak{p}' = 0 + (2q_0^2 - 1)\boldsymbol{p} + 2(\boldsymbol{q} \cdot \boldsymbol{p})\boldsymbol{q} + 2q_0(\boldsymbol{q} \times \boldsymbol{p}).$$

This product can then be converted to the rotation matrix $\boldsymbol{M}_{\mathfrak{q}}$ which multiplies $\boldsymbol{p}$ to form $\boldsymbol{p}'$. The rotation matrix $\boldsymbol{M}_{\mathfrak{q}}$ is given by

$$\boldsymbol{M}_{\mathfrak{q}} = \begin{bmatrix} q_0^2 + q_1^2 - q_2^2 - q_3^2 & 2(q_1q_2 - q_0q_3) & 2(q_1q_3 + q_0q_2) \\ 2(q_1q_2 + q_0q_3) & q_0^2 - q_1^2 + q_2^2 - q_3^2 & 2(q_2q_3 - q_0q_1) \\ 2(q_1q_3 - q_0q_2) & 2(q_2q_3 + q_0q_1) & q_0^2 - q_1^2 - q_2^2 + q_3^2 \end{bmatrix}. \tag{42}$$

Updating Quaternion Rotation Using Body Rates

The purpose of performing rotations in the context of modelling UVs is to transform the vehicle linear velocities from the body fixed to the inertial coordinates system. As the vehicle's orientation changes with time so must the unit quaternion $\mathfrak{q}$. Therefore,

$$\mathfrak{q}(t) = \mathfrak{q}_0 + \int \dot{\mathfrak{q}} dt.$$

As the UVs orientation is changed only by body rotation rates there must be some relationship between $\dot{\mathbf{q}}$ and $[p, q, r]$. It has been shown by Duman (1999) and Fossen (1994) that this relationship is,

$$\dot{\mathbf{q}} = \frac{1}{2}\mathbf{q}(0, [p, q, r]).$$

Using the quaternion product defined earlier, this becomes,

$$\begin{aligned}\dot{\mathbf{q}} =& \frac{1}{2}(q_0, [q_1\boldsymbol{i} + q_2\boldsymbol{j} + q_3\boldsymbol{k}])(0, [p\boldsymbol{i} + q\boldsymbol{j} + r\boldsymbol{k}]) \\ =& -\frac{1}{2}(q_1 p + q_2 q + q_3 r) \\ &+ \frac{1}{2}(q_0 p + q_2 r - q_3 q)\boldsymbol{i} \\ &+ \frac{1}{2}(q_0 q + q_3 p - q_1 r)\boldsymbol{j} \\ &+ \frac{1}{2}(q_0 r + q_1 q - q_2 p)\boldsymbol{k}\end{aligned}$$

or in matrix notation this can be written as,

$$\begin{bmatrix}\dot{q}_0 \\ \dot{q}_1 \\ \dot{q}_2 \\ \dot{q}_3\end{bmatrix} = \frac{1}{2}\begin{bmatrix}-q_1 & -q_2 & -q_3 \\ q_0 & -q_3 & q_2 \\ q_3 & q_0 & -q_1 \\ -q_2 & q_1 & q_0\end{bmatrix}\begin{bmatrix}p \\ q \\ r\end{bmatrix} = \boldsymbol{Q}(\mathbf{q})\begin{bmatrix}p \\ q \\ r\end{bmatrix}. \tag{43}$$

Due to computer numerics integrating $\mathbf{q}$ over a period of time will lead to it drifting from a unit quaternion. It is therefore necessary to normalize the quaternion periodically as described in Fossen (1994) and Cooke et al. (1992).

B.3 Using Quaternions for UV Modelling

Quaternions can be used in a very similar way to Euler angles described in Section 2.1.4. The key difference is in the method of calculating the rotation matrix $\boldsymbol{M}_{\mathbf{q}}$ and the method of defining the vehicle's attitude. By combining Equations (42) and (43) the general approach becomes,

$$\begin{bmatrix} \dot{\boldsymbol{\eta}}_1 \\ \dot{\mathfrak{q}} \end{bmatrix} = \begin{bmatrix} \boldsymbol{M}_{\mathfrak{q}} & \mathbf{0}_{3\times 3} \\ \mathbf{0}_{4\times 3} & \boldsymbol{Q}(\mathfrak{q}) \end{bmatrix} \begin{bmatrix} \boldsymbol{\nu}_1 \\ \boldsymbol{\nu}_2 \end{bmatrix}$$

This completes the description of how quaternions can be used in the modelling of UV motions.

Appendix C

Alternative Propulsion Models

This appendix reviews different propulsion models found within the literature of AUV modelling and attempts to describe how the model the thrust coefficient (K_T) and the torque coefficient (K_Q) in terms of the advance coefficient (J). The coefficients just specified are described in terms of the following equations,

$$J = \frac{V_a}{nD} \tag{44}$$

$$K_T(J) = \frac{T}{\rho n^2 D^4} \tag{45}$$

$$K_Q(J) = \frac{Q}{\rho n^2 D^5}. \tag{46}$$

These equations are used in subsequent sections.

C.1 The NPS AUV II propulsion model

Healey and Lienard (1993) give the equations used to model the motion of the Naval Postgraduate School (NPS) AUV II. The NPS AUV II is a twin propeller AUV designed and tested in the early to mid 1990s. Within the NPS AUV governing equations the propulsion system as modelled both produces a force and moment on the vehicle and also influences the certain of the coefficient values. Only the direct

forces and moments are considered here. The load vector is described by,

$$\boldsymbol{\tau}_n = [X_n, 0, 0, K_n, 0, N_n]^T,$$

However, the NPS AUV II coefficient values of K_n and N_n are zero so only an X force in modelled.

It is supposed that the $K_n = 0$ because the two propellers rotate in opposite directions and develop the same torque. Similarly it is assumed that N_n is zero because the two propellers are positioned symmetrically about the central vertical $x - z$ plane and develop the same thrust.

The X force component generated by the propulsion system (X_n) is combined with the X force viscous damping term ($\boldsymbol{d}(\boldsymbol{\nu})_X$) in the modelled expression. This expression is,

$$X_n - \boldsymbol{d}(\boldsymbol{\nu})_X = \frac{1}{2}\rho l^2 u^2 C_{d0}\,(\eta|\eta| - 1)$$

where,

$$\begin{aligned} C_{d0} &= 0.00385 \qquad \text{(drag coefficient)} \\ \eta &= 0.012\frac{n}{u} \equiv \gamma\frac{n}{u} \\ u &= \text{forward speed } (\text{m}\cdot\text{s}^{-1}) \\ n &= \text{propeller speed (rpm)} \end{aligned}$$

Thus,

$$\boldsymbol{d}(\boldsymbol{\nu})_X = \frac{1}{2}\rho l^2 u^2 C_{d0} \qquad \text{— viscous drag in the } x\text{-direction.}$$

$$X_n = \frac{1}{2}\rho l^2 u^2 \gamma^2 \frac{n}{u}\left|\frac{n}{u}\right| \qquad \text{— propulsion system thrust.}$$

with

$$\gamma = 0.012.$$

Provided that $n > 0$ and $u > 0$, as would be the case for Autosub then the thrust equation becomes,

$$X_n = \frac{1}{2}\rho l^2 \gamma^2 n^2. \tag{47}$$

As the only force generate by the propulsion system is X_n then $T = X_n$. From Equation (45) it can be seen that,

$$X_n = \rho n^2 D^4 K_T. \tag{48}$$

Substituting equation (47) into equation (48) gives,

$$\frac{1}{2} l^2 \gamma^2 = D^4 K_T.$$

By inspecting the thruster model it can be seen that the γ term has dimensions of $[L]$, thus the constant γ is non-dimensional hence scaling the vehicle will also scale the value of γ.

The value of K_T in the NPS AUV II model can be determined from,

$$K_T = \frac{\frac{1}{2}\rho l^2 \gamma^2 n^2}{\rho n^2 D^4} = \frac{\frac{1}{2} l^2 \gamma^2}{D^4}.$$

Hence, K_T is a constant in this model and so,

$$K_T(J) = \alpha_1$$
$$K_Q(J) = 0$$

for this twin screw AUV.

C.2 The Fossen Two Parameter Propulsion Model

Fossen and Blanke (2000) used a linear mapping to model K_T and K_Q. This provides a two parameter description of the thruster model with K_T defined in the form

$$K_T(J) = \alpha_1 + \alpha_2 J, \tag{49}$$

with

$$\alpha_1 > 0 \quad \text{and} \quad \alpha_2 < 0.$$

Thrust for the four quadrant thruster is defined by,

$$T = \rho D^4 K_T(J)|n|n. \tag{50}$$

Combining equations (49) and (50) the thrust (T) can be expressed as,

$$T(n, V_A) = T_{|n|n}|n|n + T_{|n|V_A}|n|V_A$$

where

$$T_{|n|n} = \rho D^4 \alpha_1$$
$$T_{|n|V_A} = \rho D^3 \alpha_2$$

Similarly, describing K_Q as a linear function of J, namely

$$K_Q(J) = \beta_1 + \beta_2 J,$$

the propeller torque (Q) may also be described in the form,

$$Q(n, V_A) = Q_{|n|n}|n|n + Q_{|n|V_A}|n|V_A. \tag{51}$$

Expressions for $Q_{|n|n}$ and $Q_{|n|V_A}$ are readily derived from $T_{|n|n}$ and $T_{|n|V_A}$ by multiplying by D and substituting β for *alpha*.

To use this model within an AUV it would be necessary to transform the thrust (T) and torque (Q) vectors into the body fixed axis system.

C.3 The Booth et al. Propulsion Model

The details of the Booth et al. (1980) propulsion model are presented in Appendix D.1.1 so that all the Booth et al. (1980) modelling information is contained within the same appendix. It is shown in Appendix D.1.1, that the models used for $K_T(J)$ and $K_Q(J)$ are,

$$K_T(J) = \alpha_1 + \alpha_2 J + \alpha_3 J^2$$
$$K_Q(J) = \beta_1 + \beta_2 J,$$

when $n \geq 0$ and $J \geq 0$.

Appendix D

The Booth et al. Submarine Equations

This appendix reproduces the submarine equations of motion reported in Booth et al. (1980). The equations are non-linear and fully coupled. They use the aerospace Euler angle sequence to model the attitude of the submarine. Hence, the rotation matrix and Euler angle update matrix described in Chapter 2 are used in the model. The equations combine the rigid body dynamics equations, a rotation method, a vehicle loads model and a propulsion model to form a complete package for modelling submarines.

This appendix initially describes the full equations and thereafter develops the modified general submarine equations the horizontal and vertical sub-problems described in Chapter 4 of this thesis. The assumptions made in developing the cited sub-problems are stated and their use in producing the modified equations is illustrated.

D.1 The Booth et al. Submarine Equations

The fully coupled 6 degrees of freedom rigid body dynamics equations described in Chapter 2 are represented here to aid clarity. There general form is:

$$
\begin{aligned}
m\left[\dot{u} - vr + wq - x_G(q^2 + r^2) + y_G(pq - \dot{r}) + z_G(pr + \dot{q})\right] &= X \\
m\left[\dot{v} - wp + ur - y_G(r^2 + p^2) + z_G(qr - \dot{p}) + x_G(qp + \dot{r})\right] &= Y \\
m\left[\dot{w} - uq + vp - z_G(p^2 + q^2) + x_G(rp - \dot{q}) + y_G(rq + \dot{p})\right] &= Z \\
I_{XX}\dot{p} + (I_{ZZ} - I_{YY})qr - (\dot{r} + pq)I_{ZX} + (r^2 - q^2)I_{YZ} + (pr - \dot{q})I_{XY} & \\
+m\left[y_G\left(\dot{w} - uq + vp\right) - z_G\left(\dot{v} - wp + ur\right)\right] &= K \\
I_{YY}\dot{q} + (I_{XX} - I_{ZZ})rp - (\dot{p} + qr)I_{XY} + (p^2 - r^2)I_{ZX} + (qp - \dot{r})I_{YZ} & \\
+m\left[z_G\left(\dot{u} - vr + wq\right) - x_G\left(\dot{w} - uq + vp\right)\right] &= M \\
I_{ZZ}\dot{r} + (I_{YY} - I_{XX})pq - (\dot{q} + rp)I_{YZ} + (q^2 - p^2)I_{XY} + (rq - \dot{p})I_{ZX} & \\
+m\left[x_G\left(\dot{v} - wp + ur\right) - y_G\left(\dot{u} - vr + wq\right)\right] &= N
\end{aligned}
$$

The right hand sides of the above rigid body dynamics equations express the forces (X, Y, Z) and the moments (K, M, N) acting on the submarine. These external forces and moments are expressed as the sum of the hydrostatic, control, propulsion and hydrodynamic forces and moments. The constituent forces and moments are modelled by the Booth et al. (1980) as follows:

The X, Y and Z forces assume ther respective forms:

$$\begin{aligned}
X = & \frac{1}{2}\rho l^2 \left(X'_{uu}u^2 + X'_{vv}v^2 + X'_{ww}w^2\right) \\
& + \frac{1}{2}\rho l^3 \left(X'_{\dot{u}}\dot{u} + X'_{vr}vr + X'_{wq}wq\right) \\
& + \frac{1}{2}\rho l^4 \left(X'_{qq}q^2 + X'_{rr}r^2 + X'_{rp}rp\right) \\
& + \frac{1}{2}\rho l^2 u^2 \left(X'_{uu\delta\delta R}\delta R^2 + X'_{uu\delta\delta B}\delta B^2 + X'_{uu\delta\delta S}\delta S^2\right) \\
& + (B - mg)\sin\theta \\
& + X_n,
\end{aligned}$$

$$\begin{aligned}
Y = & \frac{1}{2}\rho l^2 \left(Y'_{uu}u^2 + Y'_{uv}uv + Y'_{vw}vw + Y'_{v\nu}v\nu + Y'_{uu\delta R}u^2\delta R\right) \\
& + \frac{1}{2}\rho l^3 \left(Y'_{\dot{v}}\dot{v} + Y'_{up}up + Y'_{ur}ur + Y'_{vq}vq + Y'_{wp}wp + Y'_{wr}wr\right) \\
& + \frac{1}{2}\rho l^3 \left(Y'_{v\nu|\frac{r}{v}|}v\nu\left|\frac{r}{v}\right| + Y'_{u|r|\delta R}u|r|\delta R\right) \\
& + \frac{1}{2}\rho l^4 \left(Y'_{\dot{p}}\dot{p} + Y'_{\dot{r}}\dot{r} + Y'_{p|p|}p|p| + Y'_{pq}pq + Y'_{qr}qr\right) \\
& + (mg - B)\sin\phi\cos\theta \\
& + Y_n
\end{aligned}$$

and

$$\begin{aligned}
Z = & \frac{1}{2}\rho l^2 \left(Z'_{uu}u^2 + Z'_{uw}uw + Z'_{vv}v^2 + Z'_{uu\delta B}u^2\delta B + Z'_{uu\delta S}u^2\delta S\right) \\
& + \frac{1}{2}\rho l^2 \left(Z'_{w\nu}w\nu + Z'_{u|w|}u|w| + Z'_{|w\nu|}|w\nu|\right) \\
& + \frac{1}{2}\rho l^3 \left(Z'_{\dot{w}}\dot{w} + Z'_{uq}uq + Z'_{vp}vp + Z'_{vr}vr\right) \\
& + \frac{1}{2}\rho l^3 \left(Z'_{u|q|\delta S}u|q|\delta S + Z'_{w\nu|\frac{q}{w}|}w\nu\left|\frac{q}{w}\right|\right) \\
& + \frac{1}{2}\rho l^4 \left(Z'_{\dot{q}}\dot{q} + Z'_{pp}p^2 + Z'_{rr}r^2 + Z'_{rp}rp\right) \\
& + (mg - B)\cos\phi\cos\theta \\
& + Z_n,
\end{aligned}$$

whereas the moments are expressed in the form:

$$
\begin{aligned}
K = & \frac{1}{2}\rho l^3 \left(K'_{uu}u^2 + K'_{uv}uv + K'_{vw}vw + K'_{uu\delta R}u^2\delta R\right) \\
& + \frac{1}{2}\rho l^3 \left(K'_{v\nu}v\nu\right) \\
& + \frac{1}{2}\rho l^4 \left(K'_{\dot{v}}\dot{v} + K'_{up}up + K'_{ur}ur + K'_{vq}vq + K'_{wp}wp + K'_{wr}wr\right) \\
& + \frac{1}{2}\rho l^5 \left(K'_{\dot{p}}\dot{p} + K'_{\dot{r}}\dot{r} + K'_{qr}qr + K'_{pq}pq + K'_{p|p|}p|p|\right) \\
& + (mgY_G - BY_B)\cos\phi\cos\theta - (mgZ_G - BZ_B)\sin\phi\cos\theta \\
& + K_n,
\end{aligned}
$$

$$
\begin{aligned}
M = & \frac{1}{2}\rho l^3 \left(M'_{uu}u^2 + M'_{uw}uw + M'_{vv}v^2 + M'_{uu\delta B}u^2\delta B + M'_{uu\delta S}u^2\delta S\right) \\
& + \frac{1}{2}\rho l^3 \left(M'_{w\nu}w\nu + M'_{u|w|}u|w| + M'_{|w\nu|}|w\nu|\right) \\
& + \frac{1}{2}\rho l^4 \left(M'_{\dot{w}}\dot{w} + M'_{uq}uq + M'_{vr}vr + M'_{vp}vp\right) \\
& + \frac{1}{2}\rho l^4 \left(M'_{q\nu}q\nu + M'_{u|q|\delta S}u|q|\delta S\right) \\
& + \frac{1}{2}\rho l^5 \left(M'_{\dot{q}}\dot{q} + M'_{pp}p^2 + M'_{rr}r^2 + M'_{pr}pr + M'_{q|q|}q|q|\right) \\
& - (mgX_g - BX_B)\cos\phi\cos\theta - (mgZ_G - BZ_B)\sin\theta \\
& + M_n
\end{aligned}
$$

and

$$
\begin{aligned}
N = & \frac{1}{2}\rho l^3 \left(N'_{uu}u^2 + N'_{uv}uv + N'_{vw}vw + N'_{uu\delta R}u^2\delta R\right) \\
& + \frac{1}{2}\rho l^3 \left(N'_{v\nu}v\nu\right) \\
& + \frac{1}{2}\rho l^4 \left(N'_{\dot{v}}\dot{v} + N'_{up}up + N'_{ur}ur + N'_{wp}wp + N'_{wr}wr + N'_{vq}vq\right) \\
& + \frac{1}{2}\rho l^4 \left(N'_{r\nu}r\nu + N'_{u|r|\delta R}u|r|\delta R\right) \\
& + \frac{1}{2}\rho l^5 \left(N'_{\dot{r}}\dot{r} + N'_{\dot{p}}\dot{p} + N'_{pq}pq + N'_{qr}qr + N'_{r|r|}r|r|\right) \\
& + (mgX_G - BX_B)\sin\phi\cos\theta + (mgY_G - BY_B)\sin\theta \\
& + N_n.
\end{aligned}
$$

The component, X_n, Y_n ... N_n represent the forces and moment produced by the propulsion system and ν represents the cross-flow velocity defined by,

$$\nu = \sqrt{v^2 + w^2}.$$

D.1.1 The Propulsion Model

The propulsion model described by Booth et al. (1980) is largely empirical and is based on a fit to experimental results. The model assumes 'Propulsion is...provided by a single shaft in the plane of symmetry and parallel to the X-axis'. Thus, for this case,

$$Y_n = Z_n = N_n = 0.$$

The force X_n and moments K_n & M_n are calculated in the following fashion.

The model uses a shaft rpm ratio that is defined as,

$$n' = \frac{n}{k_o u} \tag{52}$$

where,

n' = rpm ratio

n = instantaneous rpm

k_o = ratio of rpm to speed at self propulsion

u = forward speed.

Assuming that k_o is constant, it can be seen that $k_o u$ gives the rpm necessary to maintain the forward speed. From this it is clear that

$$\frac{n}{k_o} = u_{req}$$

where u_{req} is the speed at which the current rpm (n) will produce a thrust that matches the drag of the vehicle, ie produce a steady forward speed. Thus, equation (52) can be written as

$$n' = \frac{u_{req}}{u}$$

Definition of X_n

The propulsion system thrust is developed according to:

$$X_{prop} = \begin{cases} \frac{1}{2}\rho l^2 u|u| \left(b'_1 + b'_2 n' + b'_3 (n')^2\right) & \text{if} \quad \infty > n' \geq 1 \\ \frac{1}{2}\rho l^2 u|u| \left(b'_4 + b'_5 n' + b'_6 (n')^2\right) & \text{if} \quad 1 > n' \geq 0 \\ \frac{1}{2}\rho l^2 u|u| \left(b'_7 + b'_8 n' + b'_9 (n')^2\right) & \text{if} \quad 0 > n' \geq -\infty \end{cases}$$

As the propeller is in-line with the x-axis the thrust from the propeller (T) equals the propeller force X_n. Thus, the propeller thrust equation can be written as,

$$T = \frac{1}{2}\rho l^2 u^2 \left(b_i + b_{i+1} n' + b_{i+2} n'^2\right)$$

where,

$$i = \begin{cases} 1 & \text{if} \quad \infty > n' \geq 1 \\ 4 & \text{if} \quad 1 > n' \geq 0 \\ 7 & \text{if} \quad 0 > n' \geq -\infty \end{cases}$$

Substitution for n' into T leads to,

$$\begin{aligned} T &= \frac{1}{2}\rho l^2 \left(b'_i u^2 + b'_{i+1} \frac{nu}{k_o} + b'_{i+2} \frac{n^2}{k_0^2}\right) \\ &= \frac{1}{2}\rho l^2 n^2 D^2 \left(b'_i \frac{u^2}{n^2 D^2} + \frac{b'_{i+1}}{k_o D} \frac{u}{nD} + \frac{b'_{i+2}}{k_o^2 D^2}\right) \\ &= \frac{1}{2}\rho l^2 n^2 D^2 \left(b'_i J^2 + \frac{b'_{i+1}}{k_o D} J + \frac{b'_{i+2}}{k_o^2 D^2}\right) \\ &= \rho n^2 D^4 K_T. \end{aligned}$$

Here the equations are dimensionally correct because k_o has dimensions of $[T^{-1} \cdot (LT^{-1})^{-1} = L^{-1}]$ and becomes non-dimensional when multiplied by D. The value of K_T can thus be calculated from,

$$K_T = \frac{l^2}{2D^2} \left(b'_i J^2 + \frac{b'_{i+1}}{k_o D} J + \frac{b'_{i+2}}{k_o^2 D^2}\right).$$

Alternatively writing

$$K_T = \alpha_1 + \alpha_2 J + \alpha_3 J^2$$

it follows that,

$$\alpha_1 = \frac{l^2}{2D^4 k_o^2} b'_{i+2} \,.$$
$$\alpha_2 = \frac{l^2}{2D^3 k_o} b'_{i+1}$$
$$\alpha_3 = \frac{l^2}{2D^2} b'_i$$

A similar quadratic model of K_T is used in Feldman (1979). However, in that case the value of K_T also depends, to a small measure, on the submarine drag coefficient.

Definition of M_n

The pitching moment M_n can be calculated from the propulsion system thrust X_n and the vertical distance (Z_p) between the thrust vector and the origin of the body fixed axis. That is,

$$M_n = X_n Z_p \,.$$

This equation is simply the pitching moment produced by the propeller not thrusting through the X-y plane of the body fixed axis.

Definition of K_n

The rolling moment produced by the torque on the propeller is modelled as,

$$K_n = K_{n1} n^2 + K_{n2} nu \equiv Q,$$

subject to,

$$K_{n2} = 0 \quad \text{if } u \text{ is negative}$$
$$K_{n1} = K_{n2} = 0 \quad \text{if } n \text{ is negative.}$$

From Appendix C.2 the equation give by Fossen for torque was,

$$Q(n, V_A) = Q_{|n|n}|n|n + Q_{|n|V_A}|n|V_A.$$

Comparing Fossen's torque equation with the Booth et al. (1980) torque equation it can be seen that apart from different notation, provided $n \geq 0$ and $u = V_A \geq 0$ the equations are the same. Therefore as with Fossen's torque equation, K_T for the Booth et al. (1980) equations can be written as,

$$K_T = \beta_1 + \beta_2 J,$$

when $J \geq 0$ and $n \geq 0$.

For the simulations performed in this thesis no data was available for the test submarines on the values of K_{n1} and K_{n2}. Thus for the thesis K_{n1} and K_{n2} were assumed to be zero. Hence, roll was generated by the torque from the propeller. Although this is unrealistic the roll generated by the propeller on Autosub is only a few degrees so it was felt acceptable to make this simplification.

D.2 The Modified Booth et al. Equations — Horizontal Sub-problem

D.2.1 Assumptions Used in the Horizontal Motion Model

The horizontal subproblem only considers the submarine motions to take place in the horizontal $x - y$ plane. The only non-zero velocities are the surge, sway and yaw components u, v and r. The remaining velocity components w, p and q are ignored. In this case the cross-flow velocity $\nu = |v|$ as the heave motion is identically zero.

The subset of motions to be modelled thus become:

	Modelled motions	Zero valued motions
Accelerations	$\dot{u}$, $\dot{v}$, $\dot{r}$	$\dot{w}$, $\dot{p}$, $\dot{q}$
Velocities	u, v, r	w, p, q

In this case the only control inputs come from the rudder. Hence the coefficients associated with the dive-planes (δB and δS) are assumed to be zero.

D.2.2 Equations of Motion — Horizontal Case

Using the stated assumptions of D.2.1 the fully coupled 6 degree of freedom rigid body dynamics model reduce to:

$$\begin{aligned} m\left[\dot{u} - vr - x_G r^2 - y_G \dot{r}\right] &= X, \\ m\left[\dot{v} + ur - y_G r^2 + x_G \dot{r}\right] &= Y, \\ I_{ZZ}\dot{r} + m\left[x_G\left(\dot{v} + ur\right) - y_G\left(\dot{u} - vr\right)\right] &= N. \end{aligned}$$

Noting that $\nu = |v|$ the horizontal plane loads on the submarine simplify as follows:

$$\begin{aligned} X = &\frac{1}{2}\rho l^2\left(X'_{uu}u^2 + X'_{vv}v^2 + X'_{uu\delta\delta R}u^2\delta R^2\right) \\ &+ \frac{1}{2}\rho l^3\left(X'_{\dot{u}}\dot{u} + X'_{vr}vr\right) \\ &+ \frac{1}{2}\rho l^4 X'_{rr}r^2 \\ &+ X_n, \\ Y = &\frac{1}{2}\rho l^2\left(Y'_{uu}u^2 + Y'_{uv}uv + Y'_{v\nu}v|v| + Y'_{uu\delta R}u^2\delta R\right) \\ &+ \frac{1}{2}\rho l^3\left(Y'_{\dot{v}}\dot{v} + Y'_{ur}ur\right) \\ &+ \frac{1}{2}\rho l^3\left(Y'_{v\nu|\frac{r}{v}|}v|r| + Y'_{u|r|\delta R}u|r|\delta R\right) \\ &+ \frac{1}{2}\rho l^4\left(Y'_{\dot{r}}\dot{r}\right), \end{aligned}$$

and

$$\begin{aligned} N = &\frac{1}{2}\rho l^3\left(N'_{uu}u^2 + N'_{uv}uv + N'_{uu\delta R}u^2\delta R\right) \\ &+ \frac{1}{2}\rho l^3\left(N'_{v\nu}v|v|\right) \\ &+ \frac{1}{2}\rho l^4\left(N'_{\dot{v}}\dot{v} + N'_{ur}ur\right) \\ &+ \frac{1}{2}\rho l^4\left(N'_{r\nu}r|v| + N'_{u|r|\delta R}u|r|\delta R\right) \\ &+ \frac{1}{2}\rho l^5\left(N'_{\dot{r}}\dot{R} + N'_{r|r|}r|r|\right). \end{aligned}$$

Since $Y_n = 0$ and $Z_n = 0$ as discussed in D.1.1.

D.3 The Modified Booth et al. Equations — Vertical Sub-problem

D.3.1 Assumptions Used in the Vertical Motion Model

The vertical sub-problem UV motions are constrained to the vertical x-z plane. Thus, the only non-zero velocities are the surge, heave and pitch components u, w and q. The velocities v, p and r are all identically zero. As $v = 0$ the cross-flow velocity is in this case $\nu = |w|$.

The subset of motions to be modelled in this case are:

	Modelled motions	Zero values motions
Accelerations	$\dot{u}$, $\dot{w}$, $\dot{q}$	$\dot{v}$, $\dot{p}$, $\dot{r}$
Velocities	u, w, q	v, p, r

In the vertical sub-problem only the stern dive-planes (δS) was used during the test manoeuvres. However, for completeness the bow dive-plane (δB) was included in the model. As the rudder induced motions that would not be simulated, the rudder related coefficients were not modelled.

D.3.2 Equations of Motion — Vertical Case

The fully coupled 6 degrees of freedom rigid body dynamics equations reduce for the vertical plane motion to:

$$\begin{aligned} m\left[\dot{u} + wq - X_G q^2 + Z_G \dot{q}\right] &= X, \\ m\left[\dot{w} - uq - Z_G q^2 - X_G \dot{q}\right] &= Z, \\ I_{YY}\dot{q} + m\left[Z_G\left(\dot{u} + wq\right) - X_G\left(\dot{w} - uq\right)\right] &= M. \end{aligned}$$

Also the UV load equations become,

$$
\begin{aligned}
X = & \frac{1}{2}\rho l^2 \left(X'_{uu}u^2 + X'_{ww}w^2 + X'_{uu\delta\delta B}u^2\delta B^2 X'_{uu\delta\delta S}u^2\delta S^2\right) \\
& + \frac{1}{2}\rho l^3 \left(X'_{\dot{u}}\dot{u} + X'_{wq}wq\right) \\
& + \frac{1}{2}\rho l^4 X'_{qq}q^2 \\
& + (B - mg)\sin\theta \\
& + X_n, \\
Z = & \frac{1}{2}\rho l^2 \left(Z'_{uu}u^2 + Z'_{uw}uw + Z'_{uu\delta B}u^2\delta B + Z'_{uu\delta S}u^2\delta S\right) \\
& + \frac{1}{2}\rho l^2 \left(Z'_{w\nu}w|w| + Z'_{u|w|}u|w| + Z'_{|w\nu|}w^2\right) \\
& + \frac{1}{2}\rho l^3 \left(Z'_{\dot{w}}\dot{w} + Z'_{uq}uq\right) \\
& + \frac{1}{2}\rho l^3 \left(Z'_{u|q|\delta S}u|q|\delta S + Z'_{w\nu|\frac{q}{w}|}w|q|\right) \\
& + \frac{1}{2}\rho l^4 \left(Z'_{\dot{q}}\dot{q}\right) \\
& + (mg - B)\cos\theta,
\end{aligned}
$$

and

$$
\begin{aligned}
M = & \frac{1}{2}\rho l^3 \left(M'_{uu}u^2 + M'_{uw}uw + M'_{uu\delta B}u^2\delta B + M'_{uu\delta S}u^2\delta S\right) \\
& + \frac{1}{2}\rho l^3 \left(M'_{w\nu}w|w| + M'_{u|w|}u|w| + M'_{|w\nu|}w^2\right) \\
& + \frac{1}{2}\rho l^4 \left(M'_{\dot{w}}\dot{w} + M'_{uq}uq\right) \\
& + \frac{1}{2}\rho l^4 \left(M'_{q\nu}q|w| + M'_{u|q|\delta S}u|q|\delta S\right) \\
& + \frac{1}{2}\rho l^5 \left(M'_{\dot{q}}\dot{q} + M'_{q|q|}q|q|\right) \\
& - (mgX_G - BX_B)\cos\theta - (mgZ_G - BZ_B)\sin\theta.
\end{aligned}
$$

since Y_n and M_n are zero.

Appendix E

Inputs to the Matlab Submarine Simulation

E.1 The UV Mechanical Coefficient Vector — $\boldsymbol{m}$

The submarine mechanical coefficient input vector designated $\boldsymbol{m}$ has dimensions defined as:

$$\boldsymbol{m} \in \mathbb{R}^{15}.$$

In particular, the components of $\boldsymbol{m}$ are:

$$\boldsymbol{m} = \Big[\rho, B, l, I_{XX}, I_{YY}, I_{ZZ}, I_{XY}, I_{YZ}, I_{ZX}, x_G, y_G, z_G, x_B, y_B, z_B\Big]^T.$$

E.2 The UV Propulsion Coefficient Vector — $\boldsymbol{n}$

The submarine propulsion coefficient input vector designated $\boldsymbol{n}$ has dimensions defined as:

$$\boldsymbol{n} \in \mathbb{R}^{9}.$$

The components of $\boldsymbol{n}$ are:

$$\boldsymbol{n} = \Big[b_1, b_2, b_3, b_4, b_5, b_6, b_7, b_8, b_9\Big]^T.$$

E.3 The UV Hydrodynamic Coefficient Vector – $\boldsymbol{\xi}$

The submarine hydrodynamic coefficient vector designated $\boldsymbol{\xi}$ has dimensions,

$$\boldsymbol{\xi} \in \mathbb{R}^{101}.$$

The components of $\boldsymbol{\xi}$ can be partitioned into the form:

$$\boldsymbol{\xi} = \left[\boldsymbol{\xi}_X{}^T, \boldsymbol{\xi}_Y{}^T, \boldsymbol{\xi}_Z{}^T, \boldsymbol{\xi}_K{}^T, \boldsymbol{\xi}_M{}^T, \boldsymbol{\xi}_N{}^T\right]^T,$$

with,

$$\boldsymbol{\xi}_X = \left[X'_{uu}, X'_{vv}, X'_{ww}, X'_{\dot{u}}, X'_{vr}, X'_{wq}, X'_{qq}, X'_{rr}, X'_{rp}, X'_{uu\delta\delta R}, X'_{uu\delta\delta B}, X'_{uu\delta\delta S}\right]^T,$$

$$\boldsymbol{\xi}_Y = \Big[Y'_{uu}, Y'_{uv}, Y'_{vw}, Y'_{v\nu}, Y'_{uu\delta R}, Y'_{\dot{v}}, Y'_{up}, Y'_{ur}, Y'_{vq}, Y'_{wp}, Y'_{wr}, Y'_{v\nu|\frac{r}{v}|}, Y'_{u|r|\delta R}, Y'_{\dot{p}}, Y'_{\dot{r}}, Y'_{p|p|}, Y'_{pq}, Y'_{qr}\Big]^T,$$

$$\boldsymbol{\xi}_Z = \Big[Z'_{uu}, Z'_{uw}, Z'_{vv}, Z'_{uu\delta B}, Z'_{uu\delta S}, Z'_{w\nu}, Z'_{u|w|}, Z'_{|w\nu|}, Z'_{\dot{w}}, Z'_{uq}, Z'_{vp}, Z'_{vr}, Z'_{u|q|\delta S}, Z'_{w\nu|\frac{q}{w}|}, Z'_{\dot{q}}, Z'_{pp}, Z'_{rr}, Z'_{rp}\Big]^T,$$

$$\boldsymbol{\xi}_K = \Big[K'_{uu}, K'_{uv}, K'_{vw}, K'_{uu\delta R}, K'_{v\nu}, K'_{\dot{v}}, K'_{up}, K'_{ur}, K'_{vq}, K'_{wp}, K'_{wr}, K'_{\dot{p}}, K'_{\dot{r}}, K'_{qr}, K'_{pq}, K'_{p|p|}\Big]^T,$$

$$\boldsymbol{\xi}_M = \Big[M'_{uu}, M'_{uw}, M'_{vv}, M'_{uu\delta B}, M'_{uu\delta S}, M'_{w\nu}, M'_{u|w|}, M'_{|w\nu|}, M'_{\dot{w}}, M'_{uq}, M'_{vr}, M'_{vp}, M'_{q\nu}, M'_{u|q|\delta S}, M'_{\dot{q}}, M'_{pp}, M'_{rr}, M'_{pr}, M'_{q|q|}\Big]^T,$$

$$\boldsymbol{\xi}_N = \Big[N'_{uu}, N'_{uv}, N'_{vw}, N'_{uu\delta R}, N'_{v\nu}, N'_{\dot{v}}, N'_{up}, N'_{ur}, N'_{wp}, N'_{wr}, N'_{vq}, N'_{r\nu}, N'_{u|r|\delta R}, N'_{\dot{r}}, N'_{\dot{p}}, N'_{pq}, N'_{qr}, N'_{r|r|}\Big]^T.$$

E.4 Comparison Between SubHov and the Matlab Simulations

In Chapter 5 some discussion of the predictions based on the QinetiQ SubHov simulation package and the Matlab simulation was presented. This appendix presents a number of comparative plots to demonstrate the relatively good agreement between the two alternative simulations performing the fully coupled comparison manoeuvre.

Figure 101–112 provide comparisons and measures of error for the x, y & z components of the track, the roll, pitch and yaw rotations, the translational velocities u, v, & w and the rotational velocities p, q, & r.

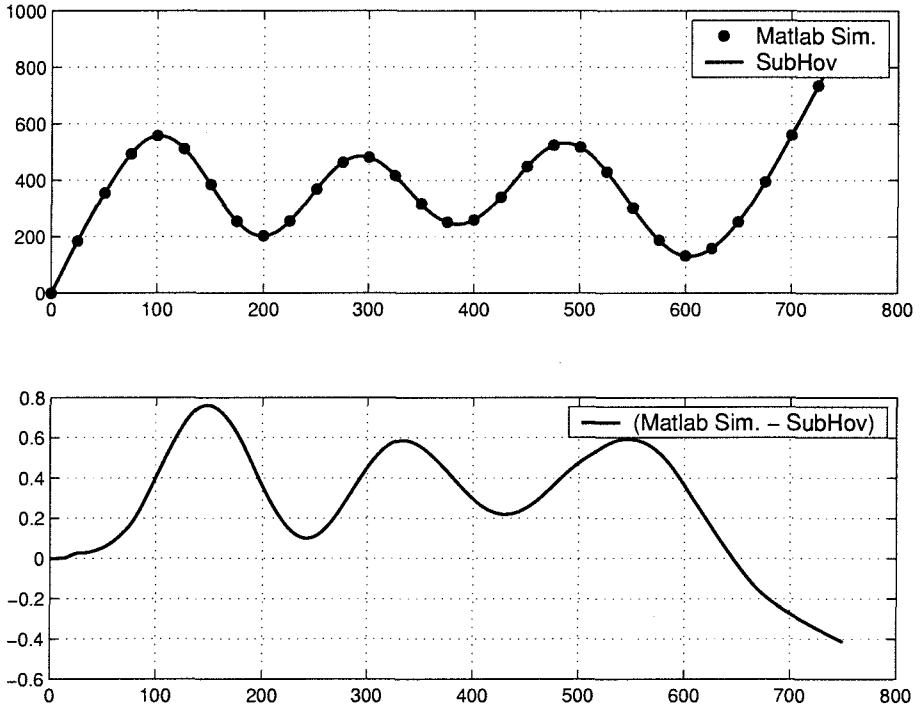

Figure 101: Plot of the errors associated with the x value.

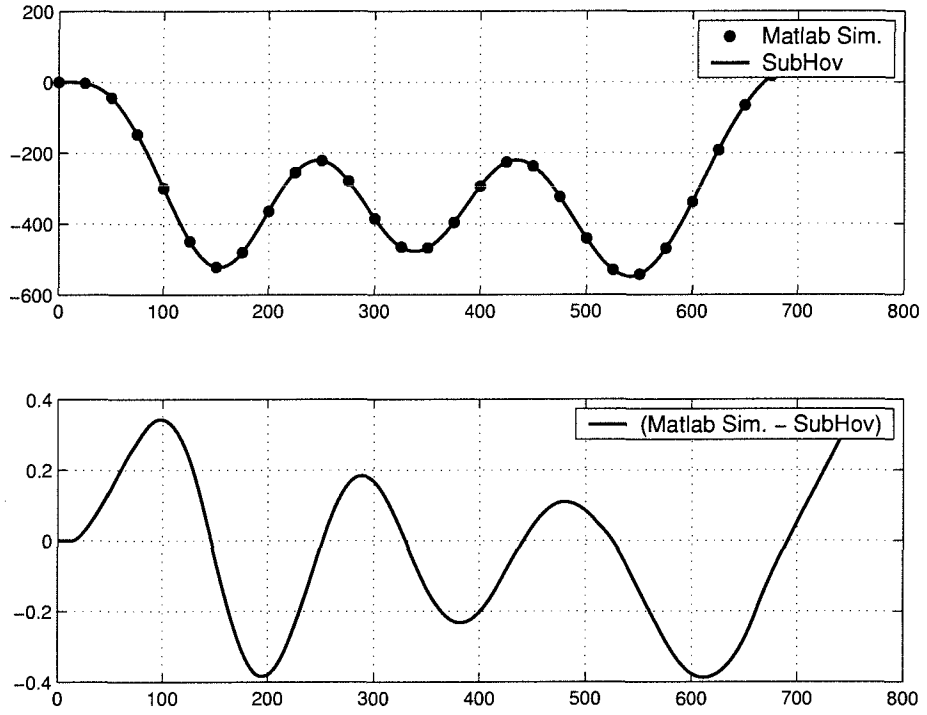

Figure 102: Plot of the errors associated with the y value.

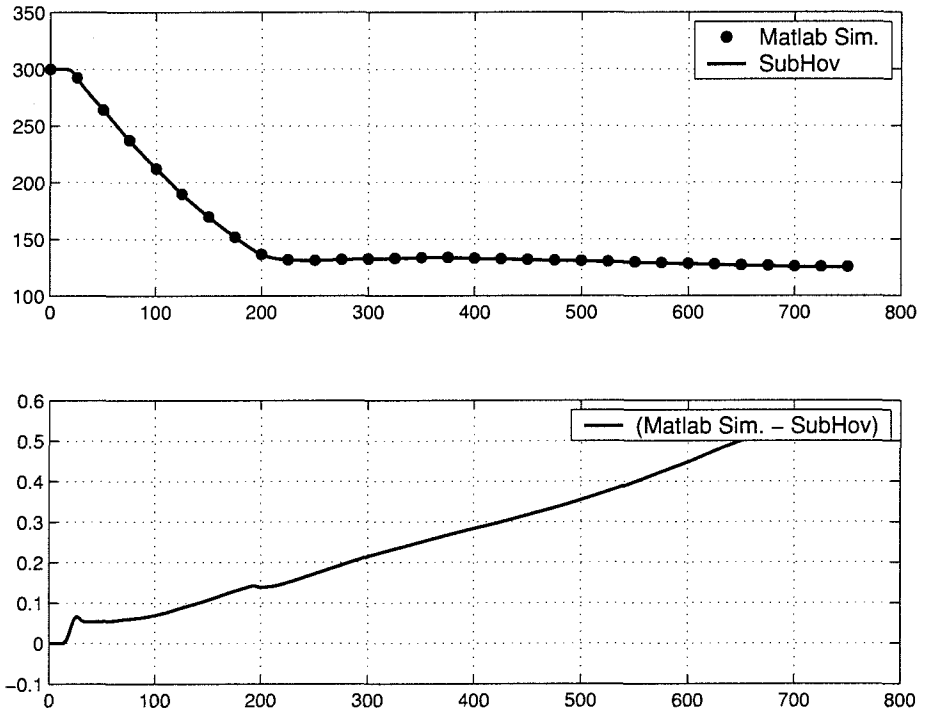

Figure 103: Plot of the errors associated with the z value.

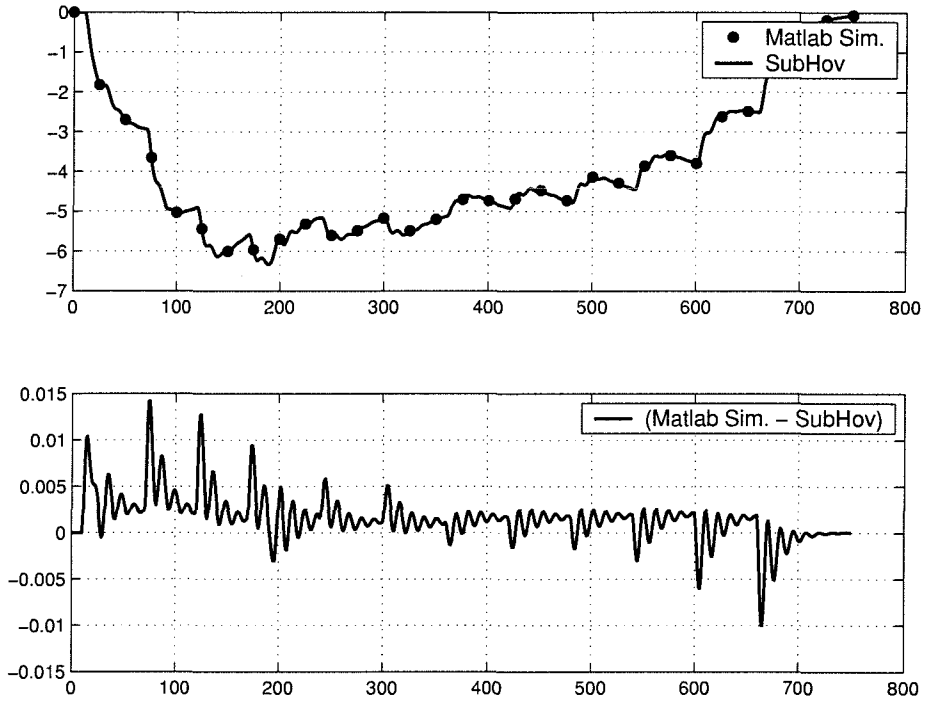

Figure 104: Plot of the errors associated with the ϕ value (roll).

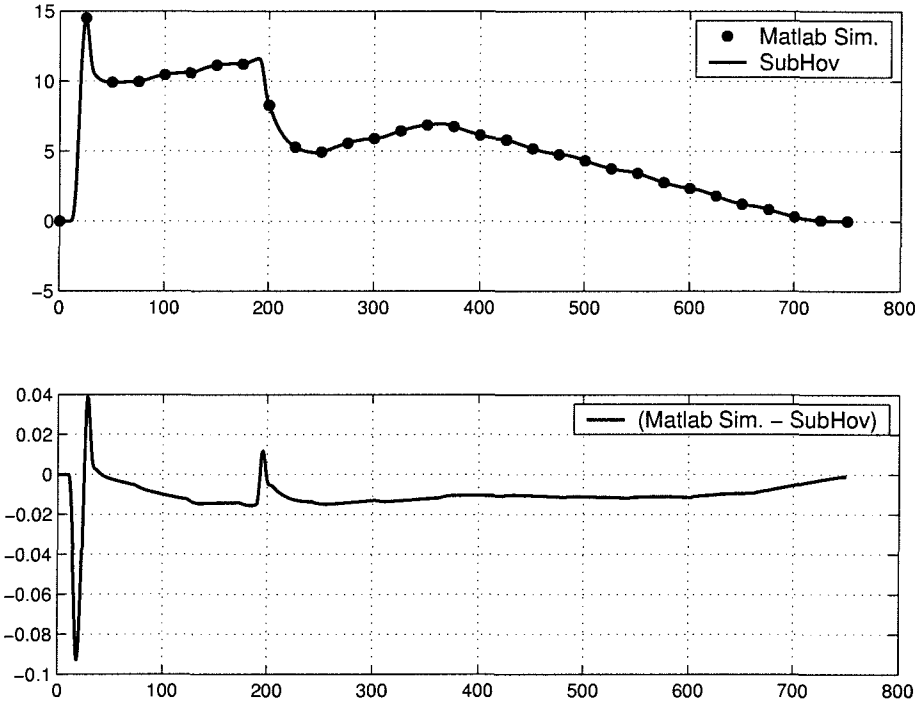

Figure 105: Plot of the errors associated with the θ value (pitch).

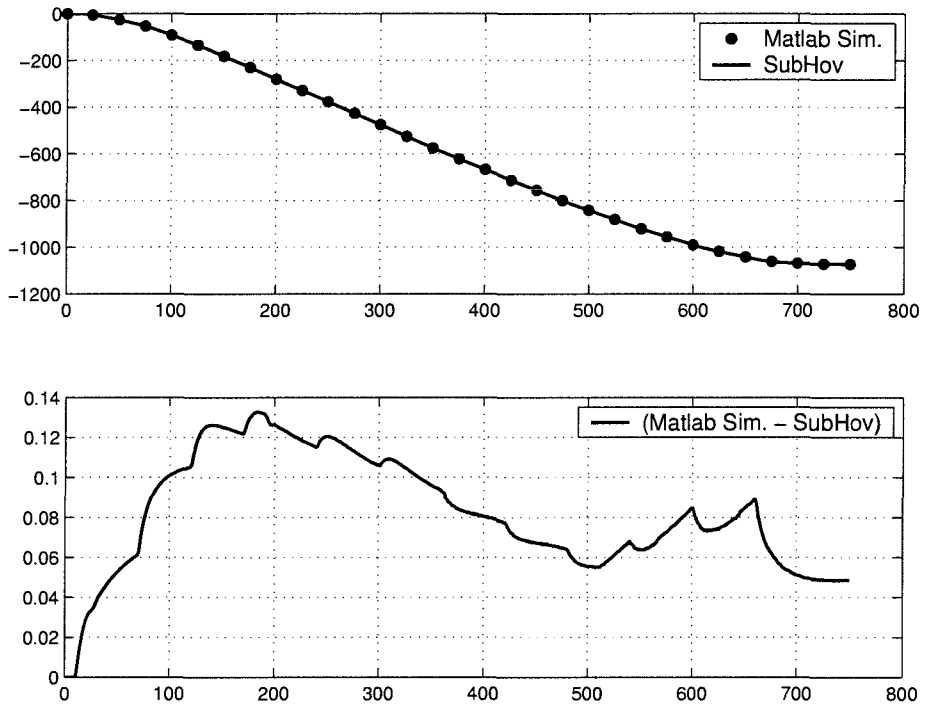

Figure 106: Plot of the errors associated with the ψ value (yaw).

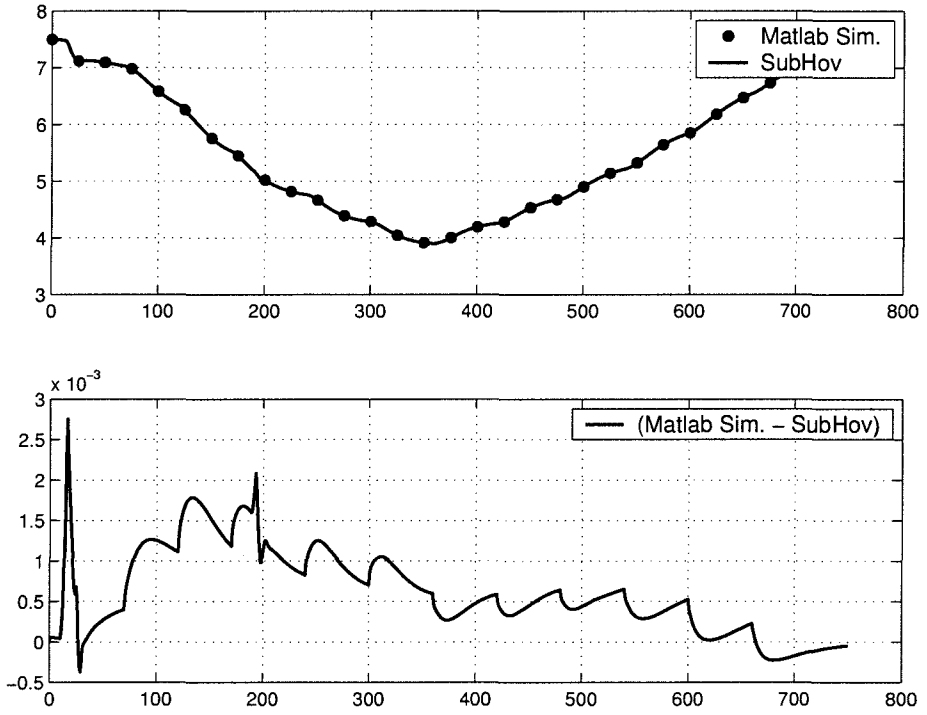

Figure 107: Plot of the errors associated with the u value.

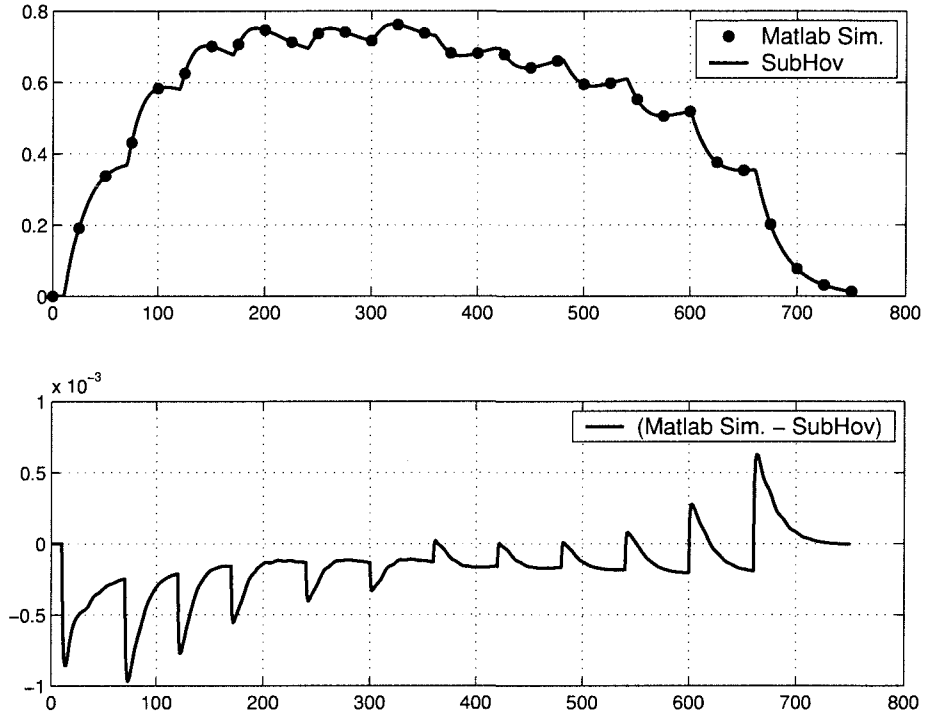

Figure 108: Plot of the errors associated with the v value.

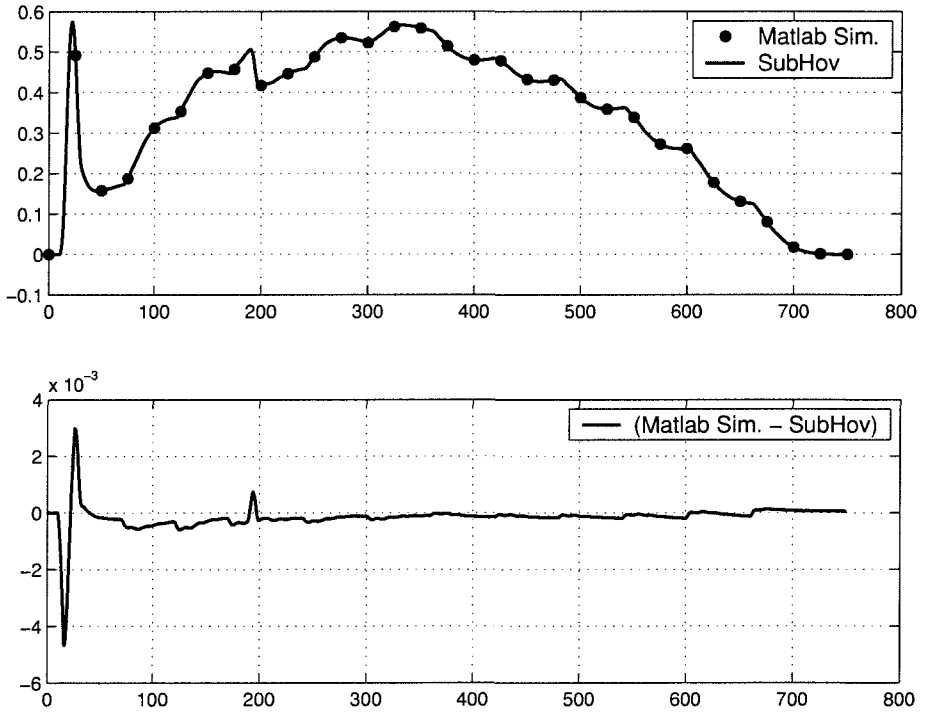

Figure 109: Plot of the errors associated with the w value.

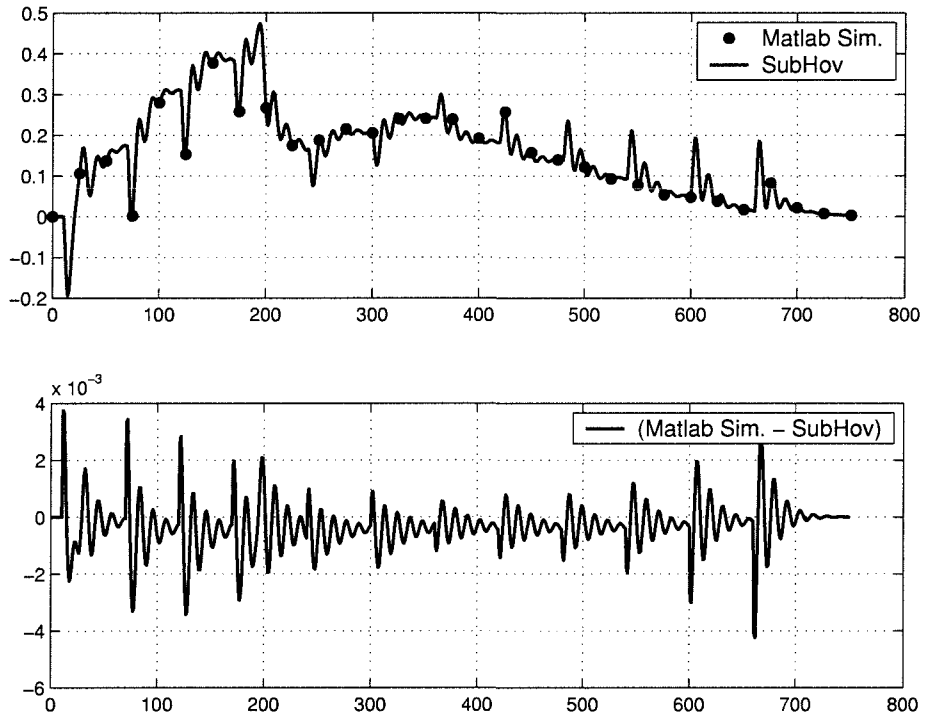

Figure 110: Plot of the errors associated with the p value.

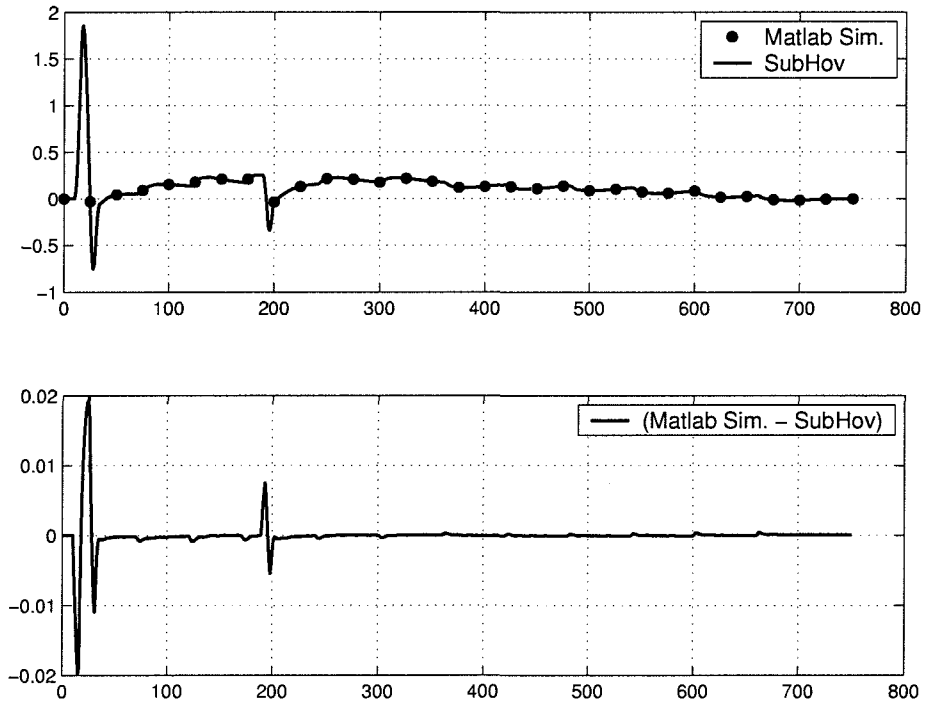

Figure 111: Plot of the errors associated with the q value.

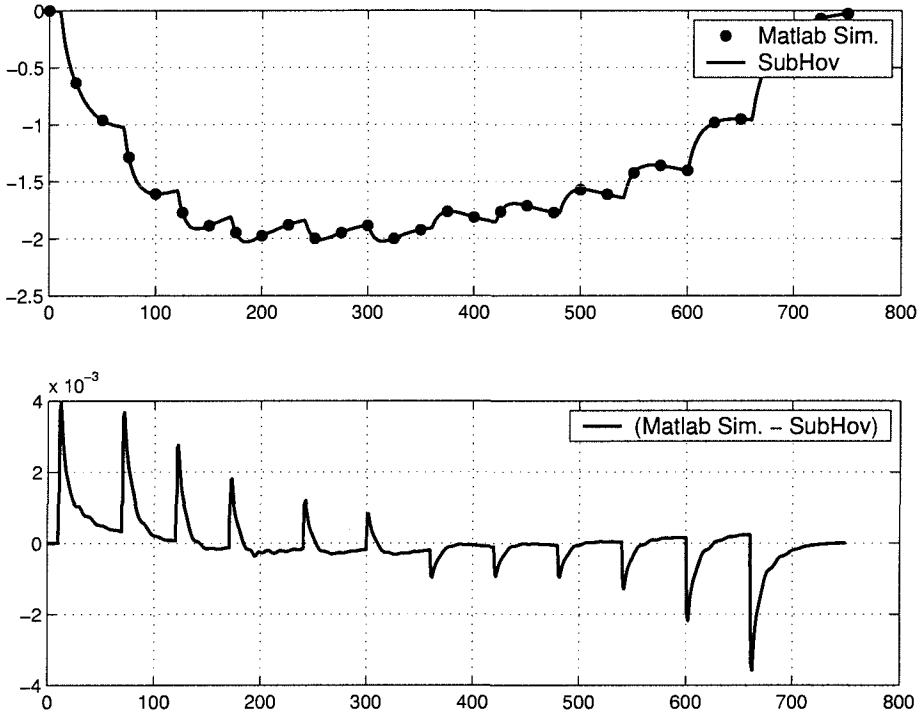

Figure 112: Plot of the errors associated with the r value.

Appendix F

Coefficient Prediction Results

This appendix presents the converged coefficient prediction plots for submarines 2 & 3 not shown in Chapter 8. The following plots are presented:

1. The maximum positional error and cost function surfaces generated by using the 50 identified coefficient sets ($\hat{\boldsymbol{\xi}}^*$'s) predicting the 100 test manoeuvres;
2. The predicted manoeuvre cost functions (ε) sorted by the average ε, with the five highest and five lowest varying coefficient sets highlighted;
3. The worst identified coefficients predicting the worst manoeuvre.

These three sets of plots are presented in the following sections.

F.1 The Manoeuvre Prediction Surfaces

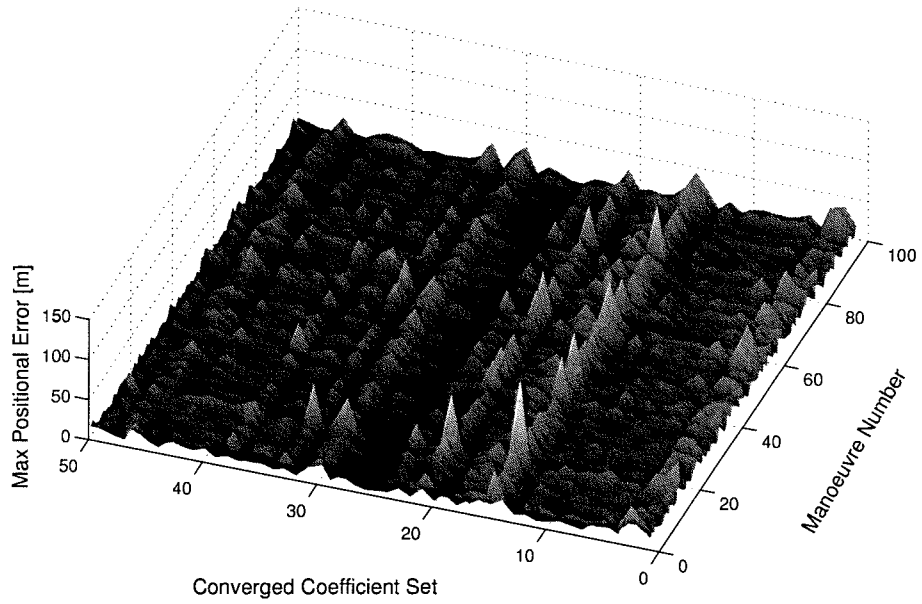

Figure 113: Surface showing the maximum positional error for submarine 2's as a function of $\hat{\boldsymbol{\xi}}^*$ and prediction manoeuvre — coefficient view.

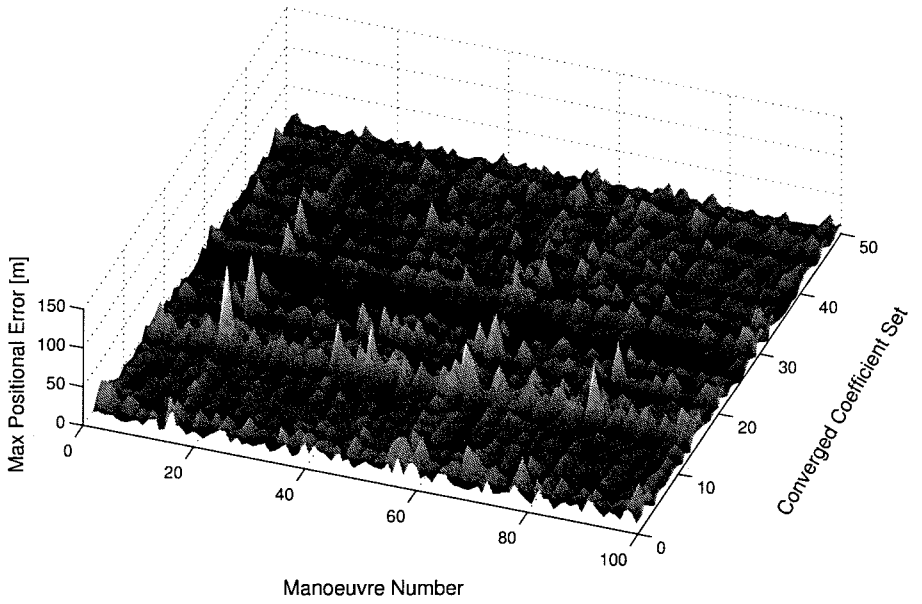

Figure 114: Surface showing the maximum positional error for submarine 2' as a function of $\hat{\boldsymbol{\xi}}^*$'s and prediction manoeuvre — manoeuvre view.

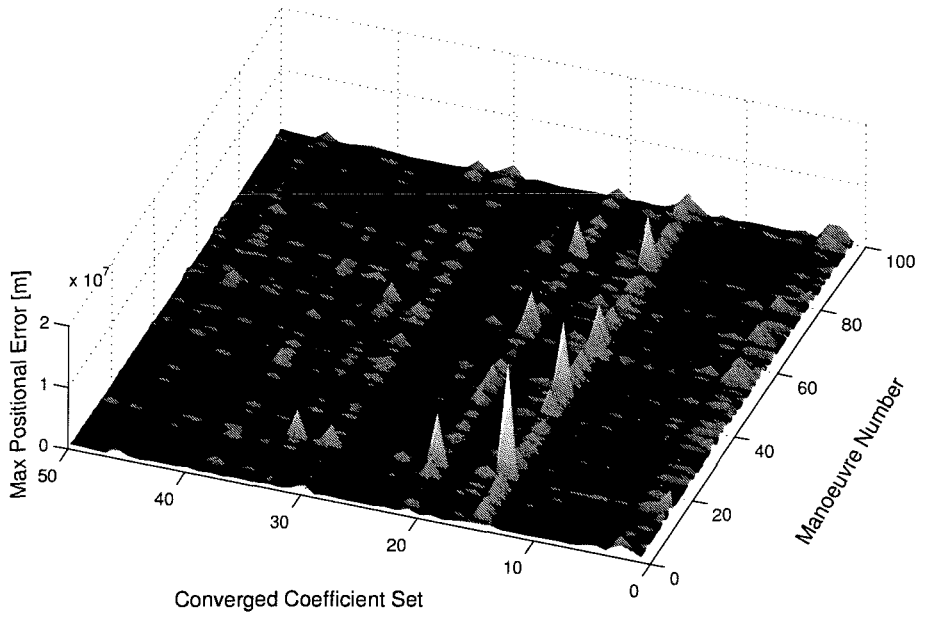

Figure 115: Surface showing the cost functions for submarine 2's as a function of $\hat{\boldsymbol{\xi}}^*$'s and prediction manoeuvre — coefficient view

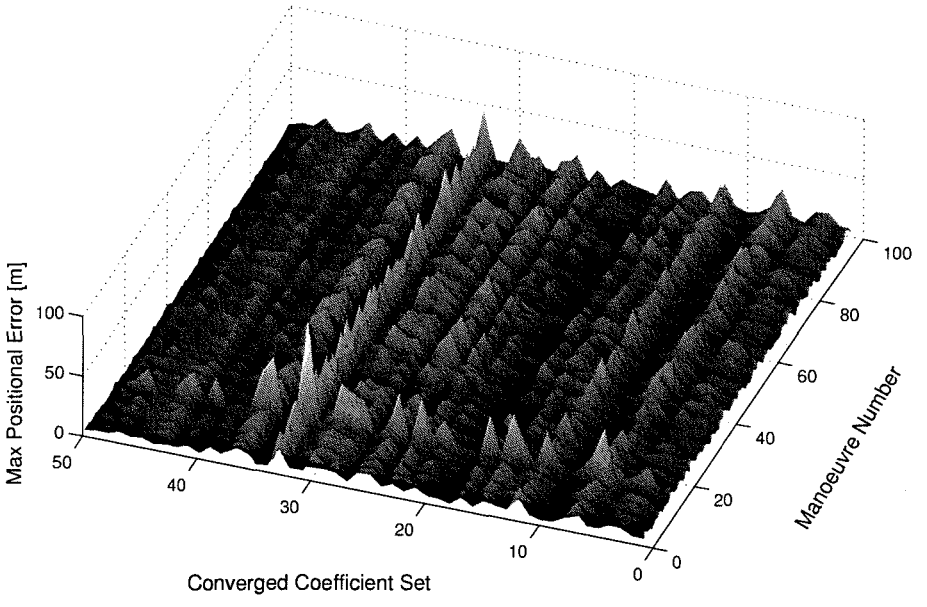

Figure 116: Surface showing the maximum positional error for submarine 3's as a function of $\hat{\boldsymbol{\xi}}^*$ and prediction manoeuvre — coefficient view.

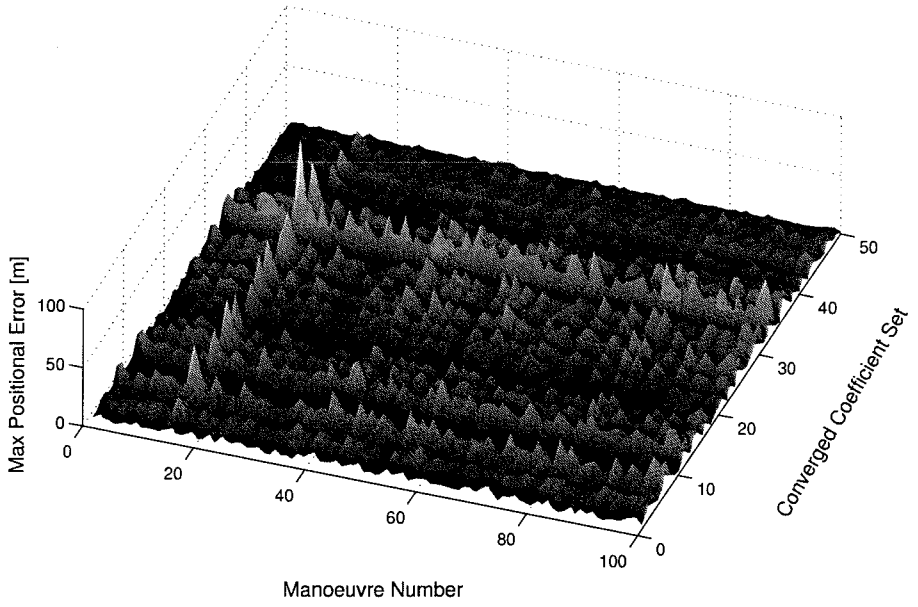

Figure 117: Surface showing the maximum positional error for submarine 3' as a function of $\hat{\boldsymbol{\xi}}^*$'s and prediction manoeuvre — manoeuvre view.

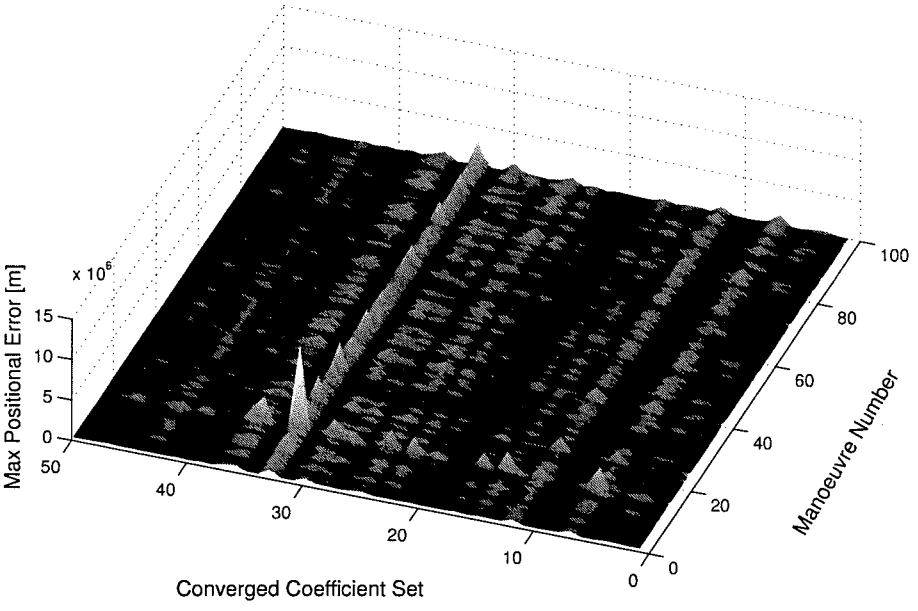

Figure 118: Surface showing the cost functions for submarine 3's as a function of $\hat{\boldsymbol{\xi}}^*$'s and prediction manoeuvre — coefficient view

F.2 The Predicted Manoeuvre Cost Functions

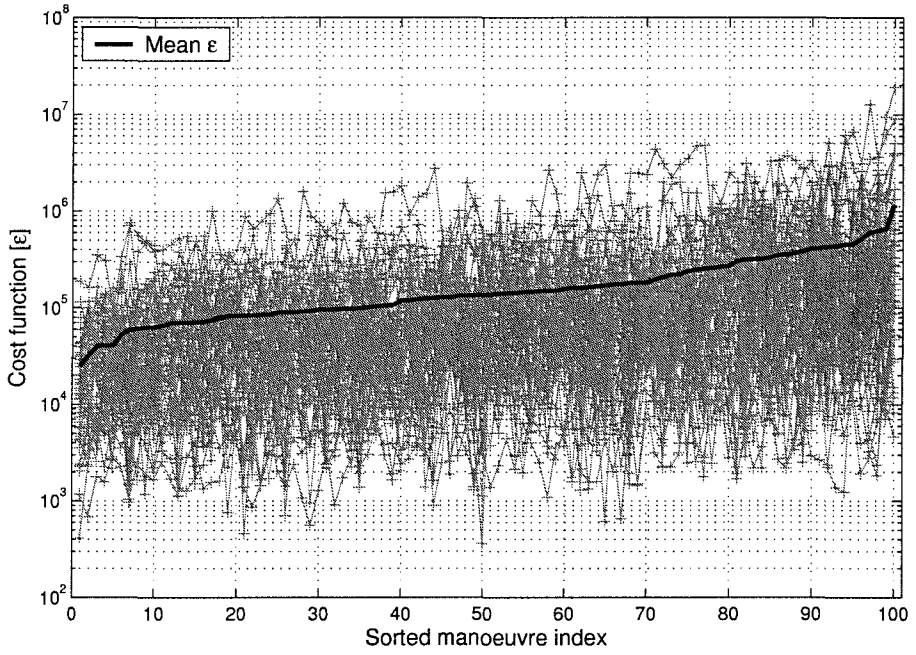

Figure 119: The predicted manoeuvre ε's sorted by average ε — submarine 2.

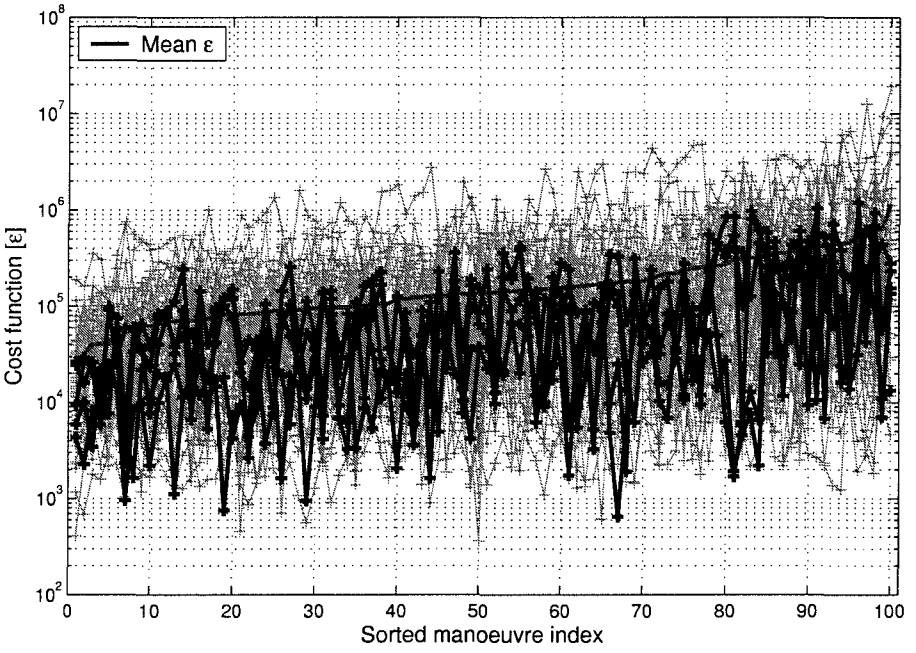

Figure 120: The predicted manoeuvre ε's sorted by average ε, with the five highest varying coefficient sets highlighted — submarine 2.

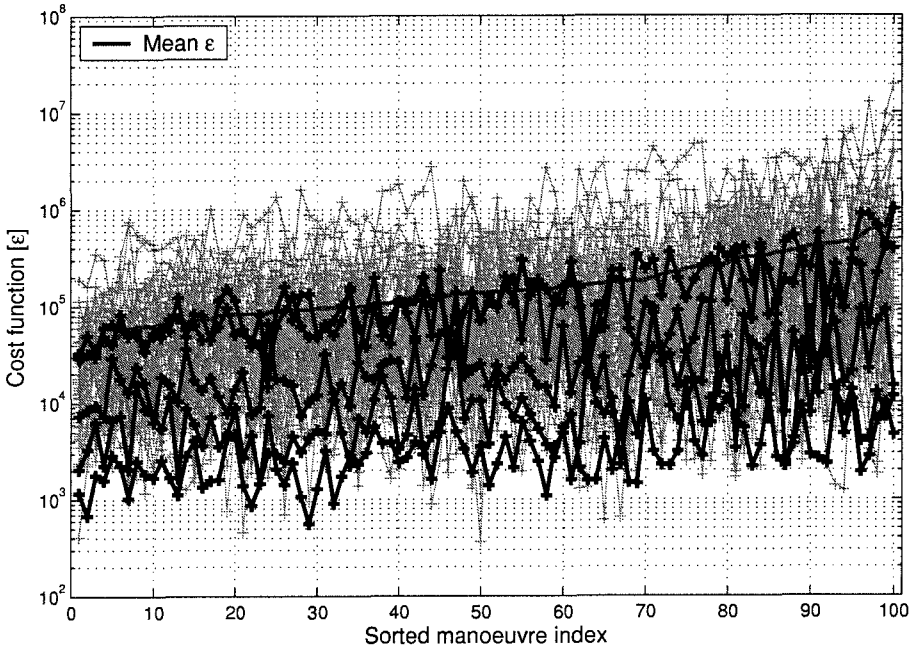

Figure 121: The predicted manoeuvre ε's sorted by average ε, with the five lowest varying coefficient sets highlighted — submarine 2.

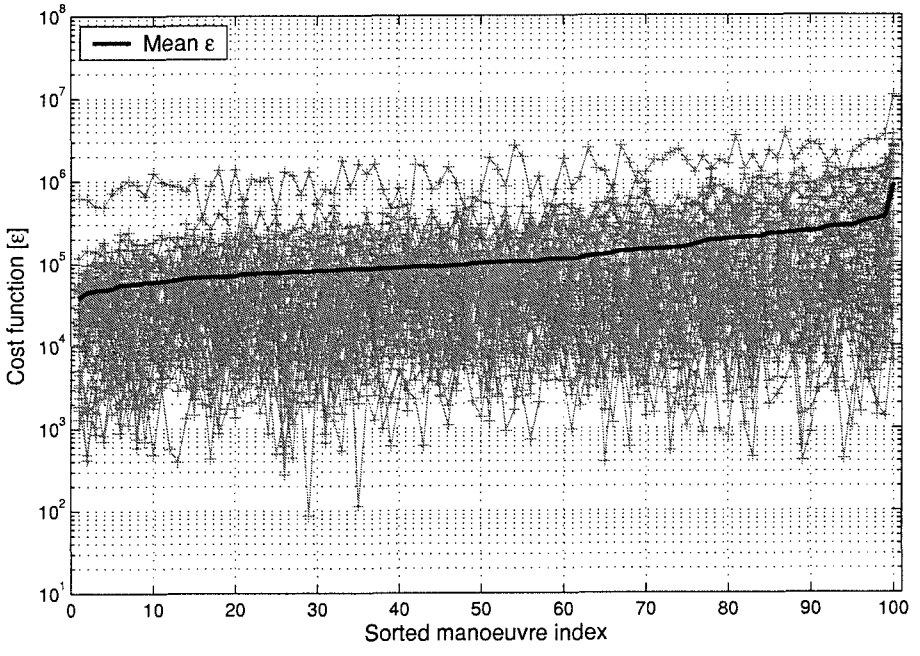

Figure 122: The predicted manoeuvre ε's sorted by average ε — submarine 3.

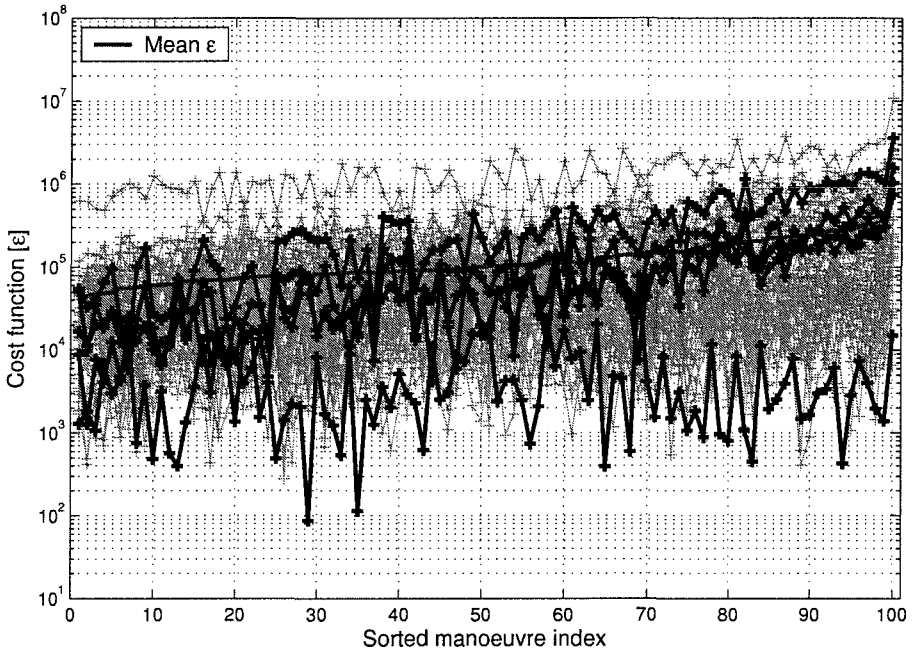

Figure 123: The predicted manoeuvre ε's sorted by average ε, with the five highest varying coefficient sets highlighted — submarine 3.

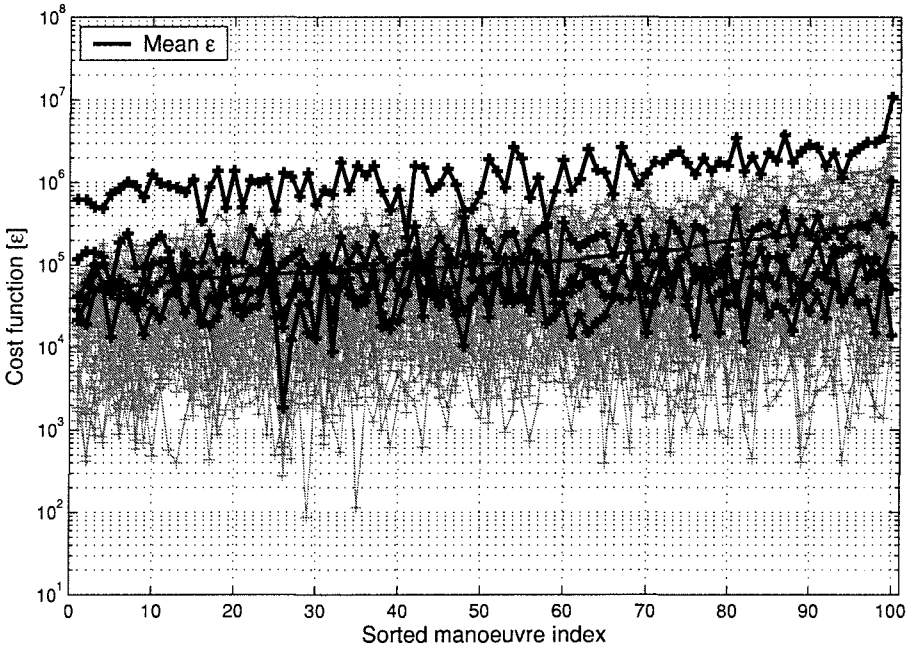

Figure 124: The predicted manoeuvre ε's sorted by average ε, with the five lowest varying coefficient sets highlighted — submarine 3.

F.3 The Worst Predicted Manoeuvres

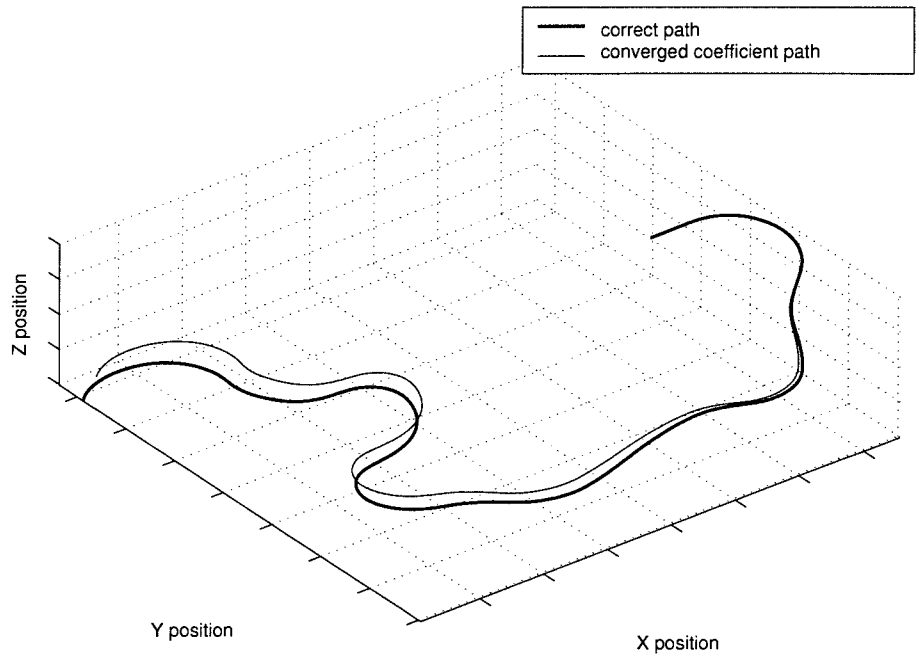

Figure 125: Positional time history of the worst coefficient set performing the worst manoeuvre — submarine 2.

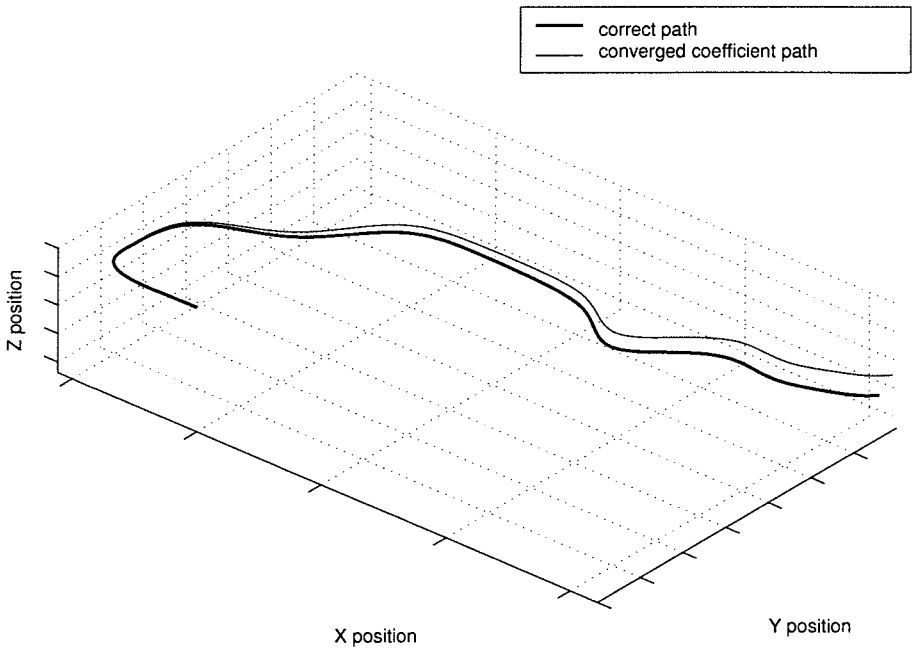

Figure 126: Positional time history of the worst coefficient set performing the worst manoeuvre — submarine 3.

Appendix G

Presented Paper

The following paper was presented in April 2003 by the Author at the *1st IFAC workshop on guidance and control of underwater vehicles (GCUV2003)*, Newport, Wales.

NONLINEAR SYSTEM IDENTIFICATION TOOLS APPLIED TO THE MODELLING OF SUBMARINE DYNAMICS

M. E. Furlong *,** **G. E. Hearn** *,** **S. M. Veres** *
E. Rogers ***

* *School of Engineering Sciences, University of Southampton, UK*
** *Ocean Engineering Division, Southampton Oceanography Centre, UK*
*** *Department of Electronics and Computer Science, University of Southampton, UK*

Abstract: This paper presents initial results on the use of nonlinear systems identification algorithms to estimate the hydrodynamic coefficients in fully coupled, non-linear submarine motion equations. Parameter identification algorithms rely on the sequential quadratic programming technique. The paper briefly describes the form of the non-linear equations used in the submarine simulation, describes the system identification algorithms developed and then illustrates their application to three test cases of interest. These are based on horizontal motion only and aim to identify the model coefficients in the cases when these are completely unknown, partially known, and partially known but with an error on the known values respectively.

Keywords: system identification,sequential quadratic programming, submarine/AUV hydrodynamic coefficients, motion simulation.

1. INTRODUCTION

The motivation for this on going research programme is the development of a representative simulation of the AUV AUTOSUB (McPhail, 1996). Modelling the behaviour of an AUV or a submarine requires the calculation of the time-depend hydrodynamic forces and moments. These forces and moments are usually calculated using the hydrodynamic coefficient method, see, for example, (Fieldman, 1979). However, a large number of coefficients relating hydrodynamic loads to vehicle geometry must be known. Moreover, the values of these coefficients are commonly determined from extensive captive model testing using planar motion mechanism equipped towing tanks and rotating arm test facilities. This experimental process is expensive and time consuming and hence determination of all the hydrodynamic coefficients for an AUV by this route would almost certainly be outside the financial budget for AUV development.

An alternative method of establishing the hydrodynamic coefficients is to us a free running model and system identification (SI) techniques. Several approaches using this starting point have been described in the literature where some of these aim to identifying the coefficients for decoupled motion (Marco *et al.*, 1998; Ridao and Carreras, 2001) and others the identification of the linear damping coefficients (Kim *et al.*, 2002). These approaches are based upon extended Kalman filtering techniques. To-date, however, application of SI to determine the coefficients of the fully coupled non-linear equations has not been attempted.

This paper describes the development of an SI based approach to this last problem as part of on-going research programme in the general area of identifying the coefficients for a fully coupled nonlinear model of submarine dynamics. One immediate application area is to identify the model coefficients to enables the construction of a dynamic simulation of the AUTOSUB dynamics. In contrast to previously reported approaches, here we use the positional time history of the vehicle as a target track and the control plane position and propeller rpm as the system input. The procedure then simulates an estimated track from a starting set of estimated hydrodynamic coefficients. This estimated track is then compared to the target track to produce a cost function, which is then minimised using sequential quadratic programming techniques to force the tracks to converge.

The equations of motion used to model hydrodynamic loads on the submarine and how they are included in the submarine simulation is described in Section 2. This simulation is used by the SI procedure and for target track generation. The relevant details of the SQP approach are given in a later section of this paper.

By way of results, Section 4 details three cases studies of the application of the SI procedure developed in this work. These all relate to the identification of the coefficients in the model of the dynamics of a submarine whose motion is restricted to the horizontal plane (the simplest practically relevant case). The first of these (denoted by Case 1) concerns the case when all model coefficients are required, and the second (Case 2) treats the case when some of the coefficients are known and the rest are to be estimated. The third (Case 3) treats identification of the same subset of coefficients as in Case 2 but with the known coefficients being subject to an error of up to 1%.

2. MODELLING SUBMARINE DYNAMICS

The submarine motion equations are formulated with the following simplifying assumptions:

- The vehicle can be modelled as a rigid body.
- The vehicles motion exists in an unbounded homogeneous fluid.
- There are no memory effects, that is, current state vectors are not explicitly dependent upon knowledge of all previous state vectors.
- The rate of change of control surface position has no effect upon the hydrodynamic loading of the submarine.

2.1 Formulation of Motion Equations

The equations used to simulate the motion of the submarine are described in the classified report (Booth *et al.*, 1980). However, they are suitably similar to those developed at the David Taylor Research Basin (Fieldman, 1979) to be relevant.

The equations use the standard fixed and body reference frames and rotation from global to local co-ordinates is undertaken using the XYZ Euler angle representation. The motion equations used are expressed here as:

$$
\begin{aligned}
&m[\dot{u} - vr + wq - \\
&\quad x_g(q^2 + r^2) + y_g(pq - \dot{r}) + Z_g(pr + \dot{q})] \\
&\qquad = X \\
&m[\dot{v} - wp + ur - \\
&\quad y_g(r^2 + p^2) + z_g(qr - \dot{p}) + x_g(qp + \dot{r})] \\
&\qquad = Y \\
&m[\dot{w} - uq + vp - \\
&\quad z_g(p^2 + q^2) + x_g(rp - \dot{q}) + y_g(rq + \dot{p})] \\
&\qquad = Z \\
&I_{xx}\dot{p} + (I_{zz} - I_{yy})qr - (\dot{r} + pq)I_{xz} \\
&\qquad + (r^2 - q^2) + (pr - \dot{q})I_{xy} \\
&\quad + m[y_g(\dot{w} - uq + vp) - z_g(\dot{v} - wp + ur)] \\
&\qquad = K \\
&I_{yy}\dot{q} + (I_{xx} - I_{xx})rp - (\dot{p} + qr)I_{xy} \\
&\qquad + (p^2 - r^2)I_{zx} + (qp - \dot{r})I_{yz} \\
&\quad + m[z_g(\dot{u} - vr + wq) - x_g(\dot{w} - uq + vp)] \\
&\qquad = M \\
&I_{zz}\dot{r} + (I_{yy} - I_{xx})pq - (\dot{q} + rp)I_{yz} \\
&\qquad + (q^2 - p^2)I_{xy} + (rq - \dot{p})I_{zx} \\
&\quad + m[x_g(\dot{v} - wp + ur) - y_g(\dot{u} - vr + wq)] \\
&\qquad = N
\end{aligned}
\tag{1}
$$

The forces and moments $[X, Y, Z, K, M, N]^T$ are composed of the following components:

$$
\begin{bmatrix} X \\ Y \\ Z \\ K \\ M \\ N \end{bmatrix} = \begin{bmatrix} X_{prop} \\ Y_{prop} \\ Z_{prop} \\ K_{prop} \\ M_{prop} \\ N_{prop} \end{bmatrix} + \begin{bmatrix} X_{static} \\ Y_{static} \\ Z_{static} \\ K_{static} \\ M_{static} \\ N_{static} \end{bmatrix} + \begin{bmatrix} X_{dynamic} \\ Y_{dynamic} \\ Z_{dynamic} \\ K_{dynamic} \\ M_{dynamic} \\ N_{dynamic} \end{bmatrix} \tag{2}
$$

where X, Y, Z are the forces on the submarine in the body axes and K, M, N are the moments about the body axes (x, y, z).

The hydrostatic forces are readily determined, see (Fossen, 1994, pages 45–46) but the propulsive forces require a number of coefficients that have to be determined from experimental sea trials, and

the hydrodynamic forces and moments are calculated from the hydrodynamic coefficient approach.

2.2 Simulation of the Submarine Motion

The system identification procedure (next section) requires a simulation of the submarine dynamics that would produce a positional time history from a sequences of control inputs. Also, the target track required by the SI procedure needs to be generated by a submarine simulation

To simulate submarine motion the equations of motion described (1), (2) need to be transformed. The approach used, based on (McGhee *et al.*, 2000), was to convert the 6-coupled second-order differential equations into 12-coupled first-order differential equations. Thereafter, the resulting 12-coupled equations could be integrated with respect to time. The coupled first-order equations can be expressed in the general vector form:

$$\dot{S_n} = f(S_n, U_n) \tag{3}$$

Where S_n is the state vector of the system with:

$$S_n = \begin{bmatrix} S_{nu} \\ S_{nl} \end{bmatrix} \quad \text{where} \quad \begin{matrix} S_{nu} = [x, y, z, \phi, \theta, \psi]^T \\ S_{nl} = [u, v, w, p, q, r]^T \end{matrix}$$

Consistent with the original equations (x, y, z) denote global positions, (ϕ, θ, ψ) represent the Euler angles, (u, v, w) are the linear velocity vectors in body-fixed co-ordinate system and (p, q, r) are the angular velocity vector in body-fixed co-ordinate system.

The vector U_n denotes the system input and is defined as:

$$U_n = [\delta r, \delta b, \delta s]^T$$

With δr, δb and δs describing the angles of the rudder, horizontal bow plane and horizontal stern plane respectively.

The relationship between $\dot{S}_{nu}$ and S_{nu} was determined as described in (McGhee *et al.*, 2000).

The relationship between $\dot{S}_{nl}$ and S_{nl} was defined by rearranging the motion equations (1), (2) to the following form:

$$A \cdot \dot{S}_{nl} = g(S_{nl}, U_n) \tag{4}$$

This was achieved by moving all the acceleration terms to the left hand side and all the remaining terms to the right hand side. Then the equation were rearranged to form the required relationship, as follows:

$$\dot{S}_{nl} = A^{-1} \cdot g(S_{nl}, U_n) \tag{5}$$

Having defined the relationship between S_n and $\dot{S}_n$. The state vector S_n was updated using the 4th order Runge-Kutta (RK) integration method.

3. ESTIMATION OF DYNAMIC PARAMETERS

The cost function used here is:

$$V(\rho) = \Delta x + \Delta y + \Delta z + \Delta \phi + \Delta \theta + \Delta \psi$$

$$\Delta x = \sum_{i=1}^{n} (x_{\text{target}_i} - x_{\text{estimated}_i})^2$$

$$\Delta y = \sum_{i=1}^{n} (y_{\text{target}_i} - y_{\text{estimated}_i})^2$$

$$\cdots$$

$$\Delta \psi = \sum_{i=1}^{n} (\psi_{\text{target}_i} - \psi_{\text{estimated}_i})^2$$

where ρ is the model parameter vector whose entries correspond to the hydrodynamic coefficients to be identified,and i denotes the sample times at which values are taken from the continuous time simulation of the submarine dynamics.

The parameter vector ρ is estimated by minimization of the criterion $V(\rho)$. Since some a priori bounds are known on the dynamical parameters, sequential quadratic programming (SQP, see for example, (Gill *et al.*, 1981)), is used to find a local minimum of $V(\rho)$. SQP is a Lagrange-Newton method which is widely known to have excellent adaptation properties to achieve fast convergence to a local minimum. For the SI problem considered here there are two main points to be considered when applying SQP.

(1) The method only finds a local minimum of the criterion function with regard to the dynamical parameters. It is possible that other local minima exist away from the physically meaningful one. To avoid finding meaningless minima, initial bounds must be used for ρ.
(2) Although SQP is one of the most reliable methods currently available, it still can happen that it spends too much time on case diagnostics which, in turn, depends on the numerical implementation used. Monitoring of the main activities of the SQP procedure has therefore been implemented to make the percentage of line-search, Hessian updating, quadratic programming sub-problem solution and other activities available for inspection during an optimization run. This

modification makes the SI process more reliable and practical.

4. SIMULATED TEST CASES

The simulated trials presented here only considered horizontal motion. Thus, all the coefficients relating to velocities in w, p and q were considered to be zero and all the coefficients relating to the force Z and the moments K and M were also considered to be zero. Therefore when the general 6 degree of freedom simulation was run only motion in the horizontal plane was generated. That is, only positional changes in x, y, and ψ occurred. This simplification was used to speed development of the technique.

The trials described are all based on the same input vector time history U_n. This time history covers 10 minutes of simulated time and produces a spiral type manoeuvre and is shown in Figure 1. The coefficients used to generate the manoeuvre are based on those for a large naval submarine. In all the tests described the initial estimates of these coefficients were within $\pm 10\%$ of their correct values. Also, each coefficient estimate was constrained to lie within a certain range, hence limiting the search space. In Case 1 this range was $\pm 10\%$ of the starting coefficient value while in Case 2 & 3 the range was $\pm 25\%$ of the correct coefficient value. This change occurred to allow for different testing and does not affect the results presented.

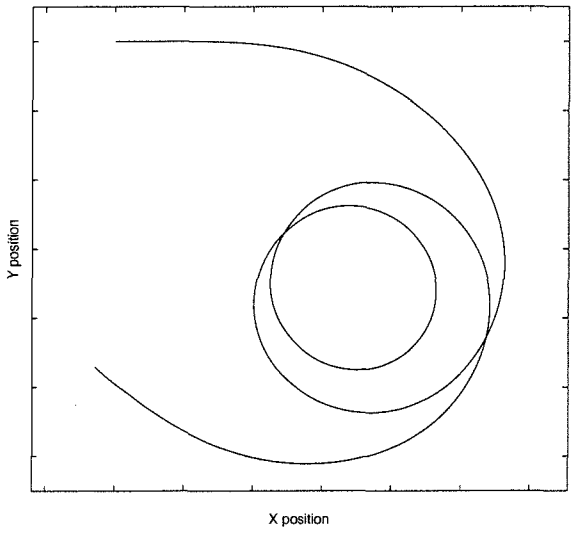

Fig. 1. X-Y Plot of the Spiral Manoeuvre

Three different identification cases are presented. The first (Case 1) is based on full identification of all the hydrodynamic coefficients. As the results will show, the coefficients did not accurately converge to the correct values. The second case (Case 2) is an attempt to improve convergence by specifying the coefficient values that could be easily obtained from a towing tank without the use of a planar motion mechanism. Therefore less coefficients need to be identified and as the results will show improved convergence will result. The final case (Case 3) is identical to Case 2 but it was assumed that there will be measurement error of up to $\pm 1\%$ on the known coefficients. The results from this test show that the measurement error has a marked effect on the identified coefficients.

4.1 Convergence to the Target Track

The SI procedure identified a set of coefficients, in all cases, that produced an estimated track that was almost identical to the target track. It was not possible to see the difference in the tracks from a X-Y plot of both as they appeared to be identical. The horizontal displacement between the estimated track and the target track for the three cases is shown in Figure 2. The ordinate scale of the traces vary as the difference in magnitude prevent display on one plot. Case 1 has a maximum positional error of less than 2mm. Case 2 has a maximum positional error of less than 1mm. Case 3 has a maximum positional error of less than $0.5m$. Clearly, Case 1 & 2 converged more accurately than Case 3, however, even Case 3 converged well.

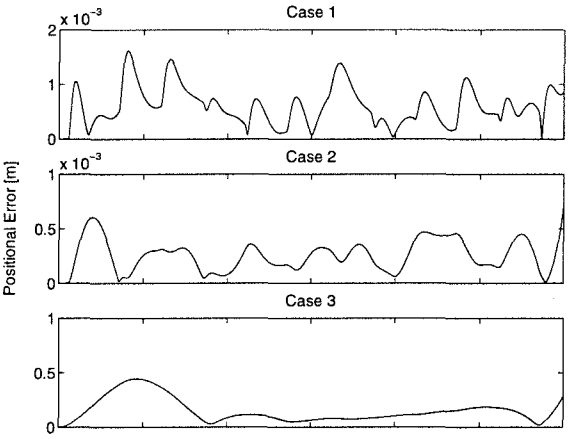

Fig. 2. Positional error of track generated by the converged coefficients

The values of the cost function at the start and end of the identification process are shown in Table 1. This table shows a large drop in the cost function between the initial and converged coefficient values and also shows the inferior convergence obtained in Case 3.

4.2 Convergence of the Hydrodynamic Coefficients

The convergence of the hydrodynamic coefficients for Cases 1–3 are shown in Figures 3–5.

	Starting Cost Function	Converged Cost Function
Case 1	3.3e+8	2.0e−2
Case 2	1.1e+8	1.0e−3
Case 3	1.3e+8	2.3e+2

Table 1. Cost Function Values for Cases 1–3

The ordinate gives the ratio of the estimated coefficient value to the real coefficient value. Thus, an ordinate value of 1 indicates the estimated coefficient is equal to the real coefficient value.

The coefficients on the abscissa are divided into three groups. These groups show the coefficients used in the X force calculation, the Y force calculations and the N moment calculations respectively.

Each Figure has circular, square and cross markers on it. The squares represent the initial estimate of the coefficient values and the circles represent the converged coefficient values. The crosses represent coefficients that were either zero or known and hence were not identified.

Convergence of the Coefficients in Case 1. These results shown in Figure 3 demonstrate improvement in many of the estimated coefficient values. However, it was a surprise that the coefficients were not more accurately identified as the cost function had reduced to approximately zero thus implying an almost identical manoeuvre. The N coefficients were particularly poorly identified.

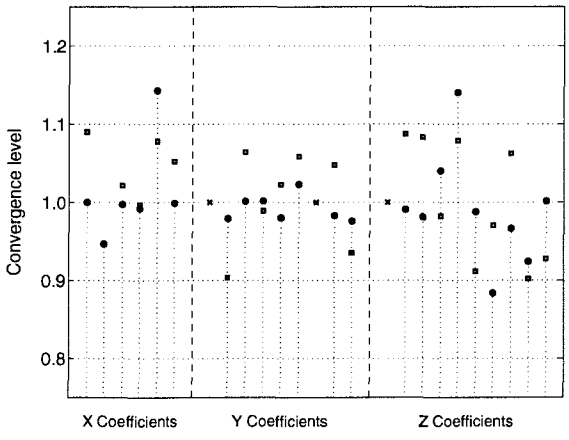

Fig. 3. Coefficient Convergence Results for Case 1

The reasons for this poor coefficient convergence was analysed. It was found that this arose from several sources. These were:

(1) The spiral manoeuvre used was not 'rich' enough to stimulate all the dynamics of the model. This was seen when the identified coefficient set was used to predict other manoeuvre. If the manoeuvre was similar in form to the spiral reasonable prediction occurred, however, if a more unusual manoeuvre was used the prediction accuracy deteriorated. Thus, by combining manoeuvres it may be possible to converge more closely to the real coefficient values.

(2) It was found that in certain circumstances some of the Y and N coefficients could be described as linear combinations of the remaining coefficients. Thus, it is impossible to fully determine all the coefficients.

(3) Some of the coefficients have a very small effect upon the total force or moment generated. Thus, a large error in one of these coefficients produces an insignificant effect on the total force or moment than a small error associated with a larger force. This made these small coefficients difficult to identify.

(4) Close coupling between the sway velocity v and the yaw-rate r was observed in the simulation. As several of the coefficients used to generate the forces X, Y and N are related to either rr, vr, or vv errors between the coefficients can be partially cancelled. Thus, large errors in several of these coefficients when summed produce a small resultant error in the final force.

Convergence of the Coefficients in Case 2. The results for Case 2 are shown in Figure 4. This shows the number of coefficients to be identified was greatly reduced. The identified coefficients showed improved convergence to the correct value over that of Case 1. However, some of the coefficients still converged very poorly.

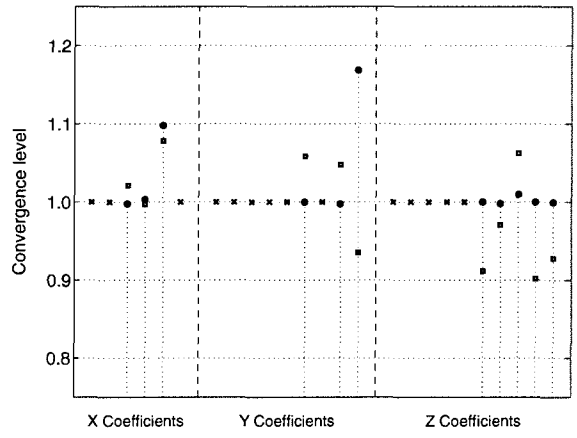

Fig. 4. Coefficient Convergence Results for Case 2

The Case 2 results reduce the impact of the problems seen in Case 1 by removing the redundant terms in Y and N. Also, the cancellation effect of the coefficients is reduced as the vv coefficients are known. However, the poorly converged X coefficient is due to the cancellation effect between $X_{vr}{}'$ and $X_{rr}{}'$ and the stray Y coefficient is due to its small effect on the total Y force.

Convergence of the Coefficients in Case 3. The results of the convergence for Case 3 are shown in Figure 5. Here the error on the 'known' coefficients can be seen in the slight offset of some of the 'x's. The convergence to the correct coefficient values for this case is very poor. Five of the coefficients deviated by ±25% from the correct value and thus hit either the upper of lower tolerance bound.

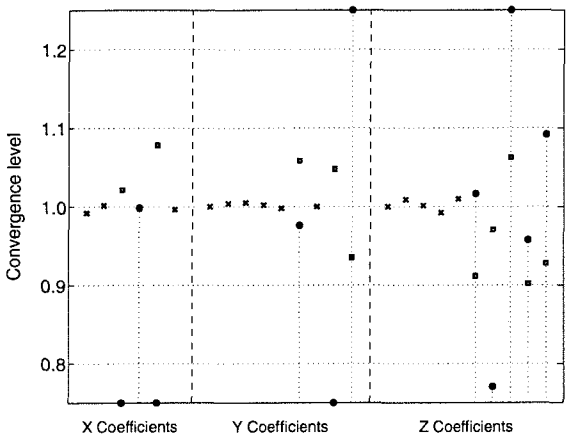

Fig. 5. Coefficient Convergence Results for Case 3

These results are interesting as it shows that errors in the 'known' coefficient have a marked effect on the identified coefficient values.

It was found that when the correct values of the coefficients to be identified were used with the 'known' coefficients the cost function value was $1.3e+5$. This is approximately 500 times larger than that of the 'incorrect' identified coefficients. Thus, the SI process generated a coefficient set that minimises the cost function but did not converge to the 'correct' coefficient values. This occurred as the errors in the 'known' coefficients produced a system minima that did not correspond to the correct hydrodynamic coefficient values.

5. DISCUSSION OF RESULTS

The system identification procedure has shown that it is very adept at producing a set of coefficients which will produce a track that is almost identical to that of the target track. However, the results suggest that there are a wide variety of widely different coefficient sets which produced almost identical manoeuvres. Thus identification of the real coefficients is challenging. The tests have also shown the sensitivity of the identified coefficients to errors in specified coefficients. The data showed that it was not possible to converge to the correct coefficient values if errors of 1% are applied to the towing tank derived coefficients.

6. CONCLUSIONS

This paper has briefly described the non-linear equations of motion used to model submarine motions. It has explained the problems associated with determine the coefficients required in these equations. Then an alternative method of determining these methods has been considered where the coefficients can be determined via a system identification method. It has then shown results from three simulated test cases. These Cases have shown how the system identification procedure can produce a coefficient set that will generate an estimated track which very closely matches the target track. However, the estimated coefficients in this set do not accurately correspond to the coefficient used in the target manoeuvre. The reasons for this have then been discussed.

REFERENCES

Booth, T. B., J. W. Randell and C. P. J. Hirom (1980). *Dynamical characteristics of submarines [second edition] [U].* Technical Report. AMTE Hasler, UK.

Fieldman, J. (1979). *DTNSRDC revised standard submarine equations of motion.* Technical Report SPD-0393-09. David W. Taylor Naval Research and Development Center, USA.

Fossen, T. I. (1994). *Guidance and Control of Ocean Vehicles.* John Wiley.

Gill, P. E., W. Murray and M. H. Wright (1981). *Practical Optimization.* Academic Press.

Kim, J., K. Kim, H. S. Choi, W. Seong and K-Y Lee (2002). Estimation of hydrodynamic coefficients for an auv using nonlinear observers. **27**, 830–840.

Marco, D. B. M., M. Alfredo and A. J. Healy (1998). *Surge motion parameter identification for the nps phoenix auv.* In Proceedings of International Advanced Robotics Programme IARP 98.

McGhee, R. B., R. E. Bachmann and M. J. Zyda (2000). *Rigid body dynamics, inertial reference frames and graphical co-ordinate systems: resolution of conflicting conventions and terminology.* Technical Report NPS-MV-01-002, Naval Postgraduate School, Monterey, California.

McPhail, S. (1996). *AUTOSUB-1 an AUV to demonstrate data gathering in the World's ocean's.* IEE Colloquium on Autonomous Underwater Vehicles and their Systems—Recent Developments and Future Prospects, London, UK.

Ridao, P. J. and B. M. Carreras (2001). *Model identification of a low-speed UUV.* Proceedings of IFAC Conference CAMS'2001, Control Applications in Marine Systems, Glasgow, UK.